THE UNIVERSITY *of* EDINBURGH

This thesis has been submitted in fulfilment of the requirements for a postgraduate degree (e.g. PhD, MPhil, DClinPsychol) at the University of Edinburgh. Please note the following terms and conditions of use:

This work is protected by copyright and other intellectual property rights, which are retained by the thesis author, unless otherwise stated.
A copy can be downloaded for personal non-commercial research or study, without prior permission or charge.
This thesis cannot be reproduced or quoted extensively from without first obtaining permission in writing from the author.
The content must not be changed in any way or sold commercially in any format or medium without the formal permission of the author.
When referring to this work, full bibliographic details including the author, title, awarding institution and date of the thesis must be given.

Neutron Diffraction of Hydrogen Inclusion Compounds Under Pressure

Mary-Ellen Donnelly

Doctor of Philosophy
The University of Edinburgh
July 2016

Abstract

When ice is compressed alongside a gas, crystalline 'host - guest' inclusion compounds known as gas clathrate hydrates form. These compounds are of interest not only for their environmental and possible technological impact as gas storage and separation materials, but also for their ability to probe networks not readily adopted by the pure 'host' water molecules, and to study the interactions between water and gas molecules. Despite the pressure dependent crystal structures being fully determined for a large variety of 'guest' gas species there is still relatively little known about the crystal structures in small guest gas systems such as H_2 hydrate. The majority of structural studies have been done with x-ray diffraction and report a number of conflicting structures or hydrogen contents for the four known stable phases (sII, C_0, C_1 and C_2). As this is a very hydrogen rich system the most ideal method to study the structure is neutron diffraction, which is able to fully determine the location of the hydrogen atoms within the structure and would allow a direct measurement of any hydrogen ordering within the host structure and the H_2 content.

In this work the phase diagram of the deuterated analogue of the H_2-H_2O system is explored at low pressures (below 0.3 GPa) with neutron diffraction. In the pressure/temperature region where the sII phase is known to be stable, two metastable phases were observed between the formation of sII from ice Ih and that this transition sequence occurred in line with Ostwald's Rule of Stages. One of these metastable phases was the C_0 phase known to be stable in the H_2-H_2O system above 0.5 GPa, and the other is a new structure not previously observed in this system and is dubbed in this work as C_{-1} . Prior to this work the C_0 phase has been reported with various structures that were determined with x-ray diffraction, and here the crystal structure and H_2 content at low pressure are determined with neutron diffraction. The C_0 phase was found to form a similar host structure to those of the previous studies with spiral guest sites but

is best described with highly mobile H_2 guests and a higher symmetry space group which make it the same structure as the spiral hydrate structure (s-Sp) recently observed in the CO_2 hydrate system. In addition to this structure being determined at pressure a sample of C_0 was also recovered to ambient pressure at low temperature and its structure/H_2 content is presented as it was warmed to decomposition. The crystal structure of the C_{-1} phase was determined to be similar to ice Ih and a sample was recovered to ambient pressure to study its decomposition behaviour. Evidence for a similar structure in the helium hydrate system at low pressure is also reported here.

This work was then extended to higher pressures with the recent developments of a hydrogen-compatible gas loader and large-volume diamond anvil cells. Several test experiments on gas-loaded Paris-Edinburgh presses are described on systems that are similar to hydrogen-water like urea-hydrogen and neon-water. And a further preliminary high pressure study on the deuterated analogue of the H_2-H_2O system in a diamond anvil cell between 3.6 and 28 GPa shows decomposition behaviour as pressure was increased.

Lay Summary

When ice is compressed alongside a gas, crystalline 'host - guest' inclusion compounds known as gas clathrate hydrates form. In these compounds the 'host ice molecules form 'cage-like structures around the 'guest gas molecules and the arrangement and structure of these cage is pressure dependent. These compounds are of interest not only for their environmental and possible technological impact as gas storage and separation materials, but also for their ability to probe networks not readily adopted by the pure 'host' ice molecules, and to study the interactions between ice and gas molecules. Although much research has been done on how the structure of these host-guest compounds evolve with pressure for large guest gas species such as methane or nitrogen, there is still relatively little known about the pressure dependence of the structures formed with small sized guest gases such as hydrogen or helium.

Using a technique that allows the positions of light atoms such as hydrogen and helium to be determined, alongside recent advances in high pressure apparatus for this technique, the pressure dependence of the host-guest structures formed between hydrogen-ice and helium-ice are examined. In the hydrogen-ice system a number of metastable structures were found to form between 2000 and 3000 times atmospheric pressure (atmospheres). The transitions between these structures was also found to be in order of increasing stability. In addition to this transition sequence, the temperature dependence of the structures and their behaviour on recovery from 3000 atmospheres to ambient pressure is also examined. The full structural details are also presented for one of the metastable structures is given. One of the metastable structures formed is also believed to be a new clathrate hydrate structure and a candidate structure is proposed based on evidence from both the hydrogen-ice and helium-ice systems.

In addition to the above work, a preliminary study found the hydrogen-ice material compressed as expected above 30000 atmospheres. This work also

presents a study on the hydrogen-urea system that suggests no host-guest inclusion compounds are formed under the conditions studied.

Declaration

I declare that this thesis was composed by myself, that the work contained herein is my own except where explicitly stated otherwise in the text, and that this work has not been submitted for any other degree or professional qualification except as specified.

Parts of this work have been published in M.Donnelly, C.L.Bull, R.J.Husband, A.D.Frantzana, S.Klotz & J.S.Loveday, J.Chem.Phys. 142 (12), 124503, 2015.

(*Mary-Ellen Donnelly, July 2016*)

Acknowledgements

First and foremost, I would like to thank my supervisor Dr John Loveday for all of his support over the years. Thanks for always being available to answer any of my questions and for your help and guidance on the work in this thesis. I would also like to thank Dr Craig Bull for all of his teachings and support on experiments at ISIS, for all the favours and for sharing his coffee/tea stash on beamtime. Thank-you to Dr Malcolm Guthrie for all of his support with all things neutron diamond cell related, and thanks to Dr Daniel Amos for the lending of books, the answering of all my questions and for the great late night playlists on beamtime.

I would like to thank several people for their help on experiments and who aided in the preparation of samples. Thanks to Cip Pruteanu, Athina Frantzana and Dr Rachel Husband for all of their help and company on beamtime. I would also like to thank Prof Stefan Klotz, Chris Goodway, Prof Eugene Gregoryanz, Dr Ross Howie, Dr Phillip Dalladay-Simpson, Dr Mungo Frost and Robin Turnbull for giving up their time to gas load various samples. Thanks to Jamie Molaison, Dr Chris Tulk and Dr Antonio dos Santos for all of their help on experiments at the SNS and thanks to Dr Reini Boehler for the preparation of diamond anvil cells. Further thanks goes to Dr Andreas Hermann and Pat Teeratchanan for sharing their work on the stability of various gas hydrates.

I would also like to thank all of my friends and family for their support and for keeping me sane. A special thanks goes to office mates Charlotte, Duncan, Keith, Martin and Veronika for the chats (both the science-based and the random ones) and for the thesis games. Thanks to my wee brother James for answering all of my chemistry related questions and for the funny cartoons. Finally I would like to thank my parents for their support and for putting up with the ‘eternal student’.

Contents

List of Figures

List of Tables

Chapter 1

Introduction

Gas clathrate hydrates, from now on referred to simply as clathrates, are a type of crystalline host-guest inclusion compound formed between water and gas. In these compounds the 'host' H_2O molecules form hydrogen-bonded cage-like structures around the 'guest' gas atoms or molecules. The host and guest interact via the relatively weak van der Waals force and are generally stabilised by elevated pressures or low temperatures [1, 2]. Clathrates are particularly known for their impact on the oil and gas industry due to either the formation of methane (CH_4) clathrate in pipelines or the vast quantities of this clathrate present on the ocean floor [3, 4, 5]. However, research on clathrates is not only of industrial and environmental interest, but also of academic interest.

Much of the early research on clathrates was driven by the need to stop the formation of clathrates in natural gas pipelines. However, now there is a drive to use clathrates as energy storage materials. For example, CH_4 clathrates found at the bottom of the ocean have been proposed as a source of natural gas [6]. Carbon dioxide clathrate has also been researched as a possible carbon capture and storage material [7]. Hydrogen hydrate was proposed as a candidate material for the storage of hydrogen as a clean energy source such as fuel for mobile transport [8]. However, in both of the latter cases (carbon capture and hydrogen storage) other materials, such as metal organic frameworks (MOFs), are capable of storing larger quantities of gas at lower pressures than the clathrates discovered in these systems [9, 10]. Clathrates are also found to occur in nature, for example methane clathrate at the bottom of the ocean and air clathrates locked in the polar ice caps [11]. However, the natural occurence of clathrates is not only

incident on our planet but also in the outer solar system [12]. For example, the source of methane in the atmosphere on Titan is thought to be due to the decomposition of methane clathrate [13]. Clathrates are also useful to study the bonding of water molecules by probing H_2O networks not readily adopted by the pure host ice material. In addition to this, clathrates are also of interest to study the interactions between not only confined gas atoms/molecules but also interactions between gas and water molecules.

The pressure dependency of the crystalline structures formed by clathrates have been well studied [2]. However, little is known about the crystalline structures of clathrates formed with the most basic molecule, hydrogen (H_2). Though this system has been well studied with x-ray diffraction prior to this work, the full structural details for any phase present above 0.2 GPa are unknown. Any structural details reported above this pressure have been inferred from crystal structures observed in other clathrate forming systems, such as helium hydrate, or from pure ice. However, there is some evidence to suggest that these inferred crystal structures are not correct, and that the clathrates formed in the hydrogen hydrate system differ from those observed in helium hydrate [14].

This thesis covers work done to expand the structural details of hydrogen hydrate at high pressures with the recent developments in neutron diffraction. Chapter 2 gives an overview of the pressure dependent structural behaviour of gas clathrates as a whole, the research done prior to this work on hydrogen hydrate that highlights where further information is needed, and a discussion of other materials where hydrogen is known to, or has been proposed to, form clathrates. Chapter 3 gives a brief introduction to crystallography and time-of-flight neutron diffraction before an overview of the various high pressure apparatus and instrument beamlines used given in chapter 4. The remaining chapters consist of an overview of transitions in the low pressure D_2-D_2O system (chapter 5), and a discussion of the possible crystal structures of the C_0 phase (chapter 6) and the new C_{-1} phase observed (chapter 7). Following this a summary of further high pressure studies are presented of the urea-deuterium and D_2-D_2O systems (chapter 8) are shown before a summary of the whole thesis (chapter 9).

Chapter 2

Gas Clathrates and Hydrogen Inclusion Compounds

Since the discovery of clathrates in 1811 many different gases have been known to form clathrate or clathrate-like crystal structures [2, 15]. This variety of gases range in size from 'larger' type guest gas species such as methane (CH_4) or carbon dioxide (CO_2) to 'mid-size' guests such as molecular oxygen (O_2) or nitrogen (N_2) to 'smaller' gas species like helium (He) and hydrogen (H_2). The different crystal structures formed are generally dependent on guest size with larger gas species more likely to form the 'traditional' clathrate structures and smaller gas species generally forming filled ices. The differences between these two types of structures are discussed in section 2.1. Though elevated pressures are required to form clathrates the application of further pressure gives rise to structural changes between different clathrate structures and, if enough pressure is applied filled ices will sometimes form. These transitions are discussed further in section 2.1.1.

Over the past two centuries, since the first discovery of clathrates, the behaviour of these inclusion compounds at high pressures has been well explored [2]. However, the full structural details of many crystal structures formed at high pressures in the hydrogen hydrate system are unknown. Hydrogen inclusion compounds, such as hydrogen hydrate, are of interest as possible hydrogen storage materials due to their ability to contain large quantities of gas and they are also generally made from environmentally benign materials such as water. A brief summary of the structures formed and high pressure behaviour of the H_2-H_2O system are given in section 2.2. Though not much is known about the crystalline structures

formed in the hydrogen hydrate system, even less is known about other hydrogen inclusion compounds of other simple hydrogen-bonded materials such as urea or hydroquinone. These are discussed in section 2.3.

2.1 Crystal Structures of Gas Clathrates

The majority of all gas clathrates crystallise into one of two cubic structures at low pressures denoted as 'sI' for 'cubic structure - I', or 'sII' for 'cubic structure - II'. These structures are both formed of cages consisting of pentagonal and hexagonal faces made up of 5 or 6 hydrogen-bonded H_2O, respectively. Examples of these pentagonal/hexagonal cages are shown at the top of figure 2.1. The sI clathrate is generally found in larger sized gas species hydrate systems such as those with CO_2 and CH_4 as the guest. The sI structure comprises two different types of cages[1], 5^{12} and $5^{12}6^2$ (shown in figure 2.1) that are arranged to give a crystal structure described by the cubic space group $Pm3n$ with $a \sim 11.9$ Å and a gas:H_2O ratio of 1:5.75. The mid-size and smaller gas species such as O_2, Kr and H_2, generally form sII at low pressures. The sII clathrate is also made up of two different types of pentagonal/hexagonal faced cages (5^{12} and $5^{12}6^4$) that are arranged to form the structure shown in figure 2.1 that can be described by the cubic space group $Fd\bar{3}m$ with $a \sim 17.3$ Å and a gas:H_2O ratio of 1:5.66. Although the majority of gases either form sI or sII exclusively, krypton hydrate has been observed to form sII at low pressures and then transform in to sI with the application of pressure [2]. However, no other gas species to date have been observed to follow this behaviour, and it is generally accepted that the majority of gas species will form either one or the other. The gas:H_2O ratios given above are assuming single occupancy of the cages within the structure, however, this is known not to be the case. A large number of gas species are known to have multiple occupancy of the cages in clathrates which increases with pressure or lowering temperatures [16, 17, 18].

As pressure is applied to clathrates other 'high pressure structures' are formed. One of these is the hexagonal structure (shown in figure 2.2) and is denoted as 'sH', which is described by space group $P6/mmm$ with $a \sim 12.2$ Å , $c \sim 10.1$ Å

[1]The notation used to describe the cage, for example '$5^{12}6^2$', is used for convenience. In this notation a cage is described as 'S^{N_f}' where S describes the type of face, for example pentagonal (5) or hexagonal (6), and N_f is the number of that type of face that make up the cage. In the example here, $5^{12}6^2$ describes a cage that has 12 pentagonal faces and 2 hexagonal faces.

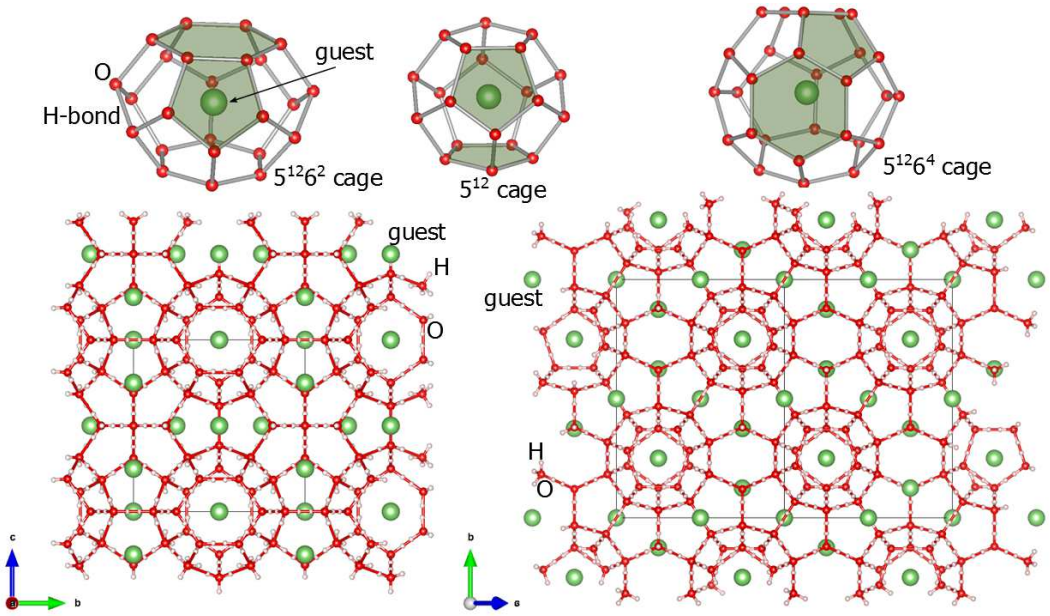

Figure 2.1 *The images across the top of the figure show the types of cages present in the sI and sII clathrate structures. Below these on the left is the cubic sI structure, and on the right is the cubic sII crystal structure. Red and pink spheres indicate the positions of oxygen and hydrogen atoms of the host H_2O. Green spheres indicate the guest gas atom/molecule positions.*

and a gas:H_2O ratio of 1:3.5 [2]. It is composed of one large cage which is the length of the c-axis ($\sim$ 10.1 Å), and two smaller cages that are shown on the left hand side of figure 2.2. Unlike the sI and sII structures that are generally found in either large or mid-size/small guest gas clathrates respectively, sH is found to occur within the mid-size to large guest range such as those with N_2 and CH_4 as the guest. This is due to the large cage in sH requiring large guests for stability [2]. However, not all large guests gas species form sH under pressure. In the CO_2 hydrate system there have been no observations of sH at pressures up to 4 GPa [19, 20]. Another 'cage-like' clathrate structure found at higher pressures is the tetragonal structure denoted as 'sT', which is described by the space group $P4_2/mnm$ and lattice parameters $a \sim 6.3$ Å and $c \sim 10.6$ Å (shown in figure 2.3). Similarly to sH, sT has also only been observed to form in systems with mid-to-large range sized guests. Unlike sH, sT has only been observed to form in systems that have adopted the sII structure at low pressures.

At higher pressures, or in systems with small guest gases such as helium or hydrogen, channel-containing 'filled ices' are generally more preferred over the 'cage-like' clathrate structures described above. These filled ice structures (FIS) are where the host H_2O molecules adopt a similar network to one that is readily

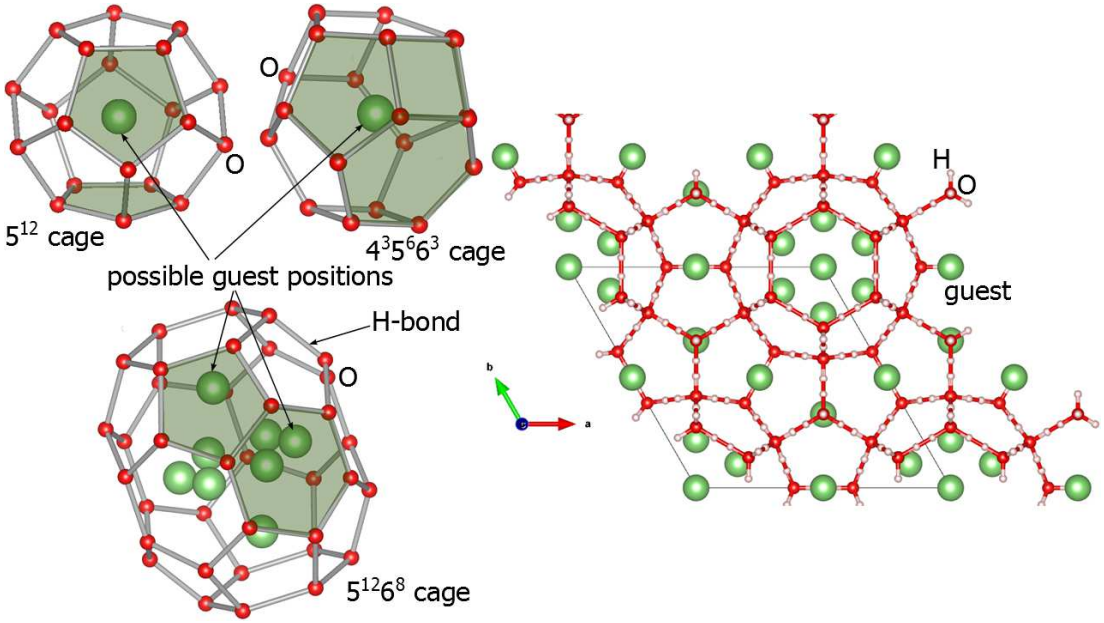

Figure 2.2 *On the left are the cages formed in sH clathrate. On the right is the hexagonal sH crystal structure. Red and pink spheres indicate the positions of oxygen and hydrogen atoms of the host H_2O. Green spheres indicate the guest gas atom/molecule positions.*

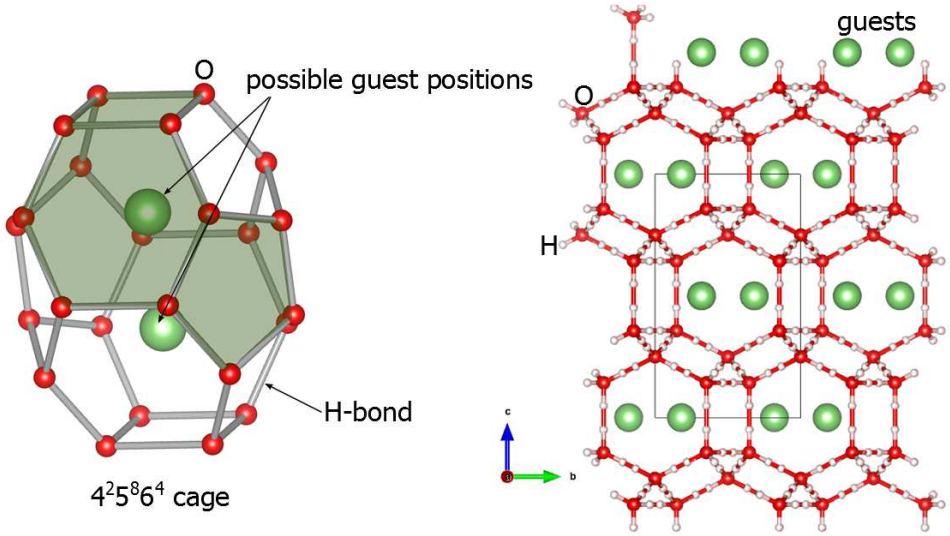

Figure 2.3 *On the left is the cage that makes up sT clathrate. On the right is the tetragonal sT crystal structure. Red and pink spheres indicate the positions of oxygen and hydrogen atoms of the host H_2O. Green spheres indicate the guest gas atom/molecule positions.*

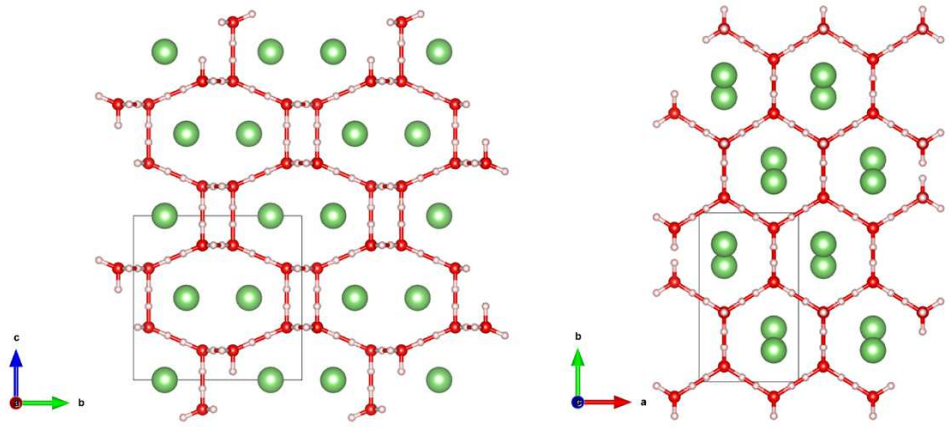

Figure 2.4 *Crystal structure of filled ice Ih (FIS-Ih). Red and pink spheres indicate the positions of oxygen and hydrogen atoms of the host H_2O. Green spheres indicate the guest gas atom/molecule positions.*

formed by pure ice, such as ice Ih or ice II, and the gas atoms/molecules occupy the channels within this framework. Though the term 'FIS' is usually reserved solely for the ice-Ih based structure found in methane or krypton hydrates at high pressure, here the filled ices shall be denoted as FIS-t where t describes which phase of pure ice it is related to such as Ih or Ic. The FIS-Ih is the most common filled ice in gas clathrates. The H_2O molecules form an ice Ih network and the inclusion of the guest gas gives rise to a slight distortion in the H_2O network which transforms the symmetry from hexagonal to orthorhombic. It is described by space group $Imcm$ and lattice parameters $a \sim 4.7$ Å , $b \sim 8.1$ Å and $c \sim 7.8$ Å (shown in figure 2.4). Other filled ices such as FIS-II and FIS-Ic are less common and have only been found with small guest species such as helium, neon and hydrogen. These other filled ice structures are described in more detail in section 2.2.

2.1.1 At High Pressures

As pressure is increased, gas clathrates go through a series of structural transitions that are highly dependent on the guest species. Though the high pressure transitions are gas species dependant, there are some generalisations that can be made based on the low pressure clathrate structure that a gas species adopts

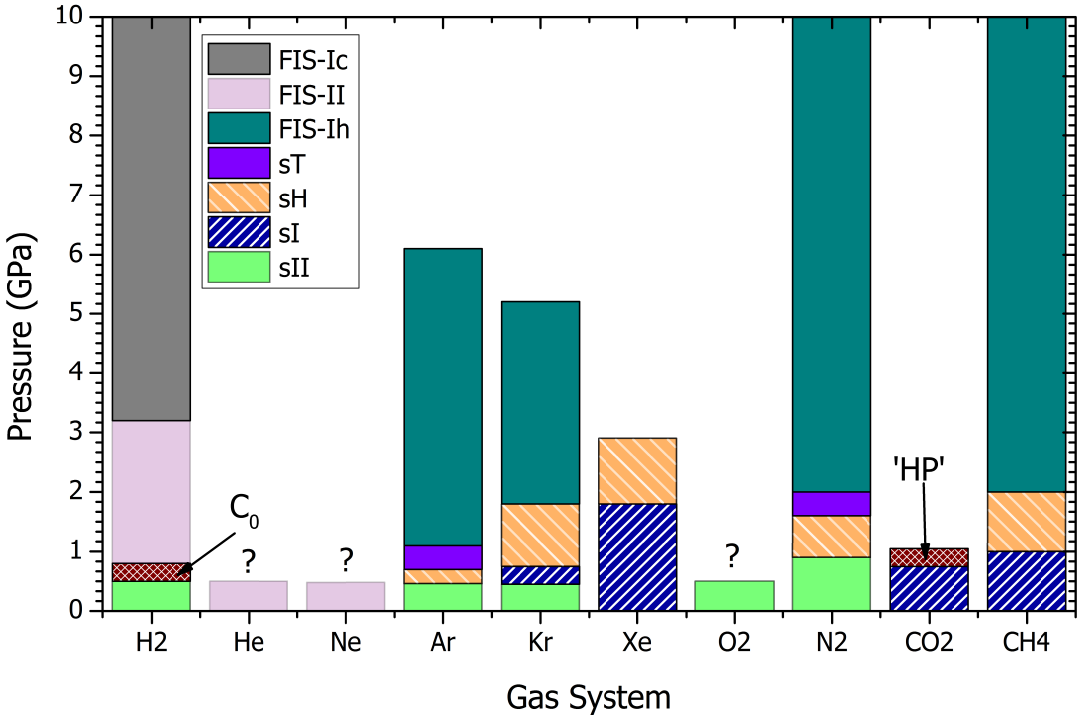

Figure 2.5 *Pressure dependence of the clathrate/filled-ice structures for various guest gas species.*

(either sI or sII). In general as pressure is increased the observed transitions are sI or sII → sH → sT (if sII was formed at low pressure) → FIS-Ih → decompose. A summary of these transitions is shown in figure 2.5 for various guest gas species [2]. There are notable exceptions from this general transition such as CO_2 hydrate which forms sI clathrate at low pressures before transforming into 'HP' hydrate before decomposition just above 1 GPa [19, 20]. This HP phase was orginally thought to have a structure similar to FIS-Ih but has recently been shown to have a spiral-like structure similar to the C_0 phase found in H_2 hydrate (see section 2.2 and chapter 6 for more details on C_0) [19, 20, 21].

In addition to changes in the host framework at increasing pressure, there are also changes within the guest occupancy. For example in Ar hydrate the occupancy of the large cages in sII increases as pressure is increased [22]. There are also transitions in occupancy of the large cage of sH clathrate such as in Kr or CH_4 [2]. Temperature has also been found to have an impact on the occupancy of the cages. For example, in the FIS-II of Ne hydrate there is a decrease in the occupancy of the channel guest sites from 0.8 around 70 K to 0.3 at 260 K at 0.48 GPa [23].

2.1.2 Ordered Hydrogen Bonds

To date there have been seventeen experimentally found crystalline phases of pure ice (these differ from those of amorphous ice which are similar to a glass in that there is no long range order like that found in crystalline systems)[24]. All of the ice networks formed in these structures obey the 'Bernal-Fowler ice rules'. These say that the oxygen atom within a water molecule is bonded to four other oxygen atoms via hydrogen bonding with the water molecule forming two of these bonds with its own hydrogen atoms, and 'accepting' the bond formed by the hydrogen atoms of two other water molecules [25]. Within these ice frameworks there are two types of ordering. The first of these is where the hydrogen bonds between neighbouring water molecules are ordered. This is usually referred to as 'hydrogen ordered' or 'proton ordered' and is shown in figure 2.6. The other type of ordering is where the hydrogen bonds formed by the water molecules in crystalline ice are disordered (shown in fig 2.6) and this is referred to as 'hydrogen disordered' or 'proton disordered'. In hydrogen disordered forms an oxygen atom is thought of as being bonded to 4 hydrogen atoms, but with each of these hydrogen sites having an occupancy of 0.5. All phases of pure ice, with the exception of phases II and XVI, exist in both hydrogen-ordered and hydrogen-disordered forms. For example the hydrogen ordered form of ice Ih is ice XI and is found by cooling to low temperatures (below 72 K) [26, 27]. In addition to ordered/disordered hydrogen bonds there is also the possibility of partial ordering where some of the bonds within the structure are disordered and some are ordered. For example ice III is partially ordered before it is cooled to form its H-ordered counterpart ice IX [28, 29]. As ice II has no known hydrogen disordered counterpart, the FIS-II clathrate is also the only known clathrate to form with ordered hydrogen bonds [23, 30].

In addition to hydrogen bond ordering, another type of transition that is important to the hydrogen bond is 'centering'. This is where the hydrogen atom occupies the centre of the bond between the two oxygen atoms. In low pressure ice, such as ice Ih, the covalent O-H bond is around 1 Å in length and the overall O-H...O hydrogen bond distance[2] is around 2.8 Å . This makes the hydrogen atom closer to one oxygen than the other. At high pressures (above 100 GPa) the hydrogen atom is predicted to occupy the centre of the hydrogen bond formed between neighbouring oxygen atoms [31]. However, the exact nature of how this

[2]This is the distance between the oxygen atoms along the hydrogen bond.

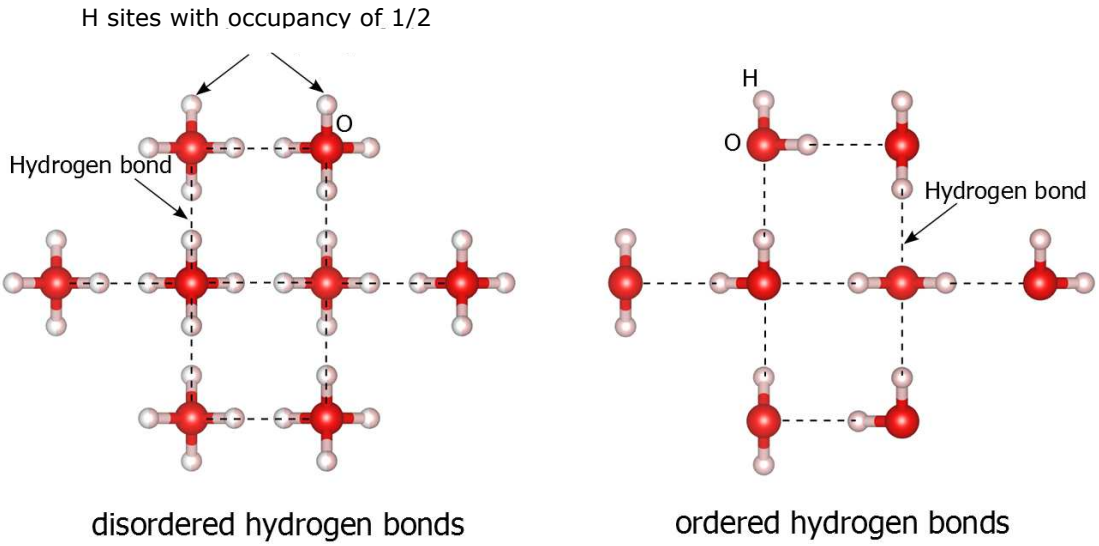

Figure 2.6 *Disordered and ordered hydrogen bonds.*

transition occurs is currently unknown. The centering of the O-H...O bond is not really an issue for clathrates as most dissociate at pressures much lower than the pressure where centering is expected to occur.

2.2 The H_2–H_2O System

As seen in figure 2.5 hydrogen hydrate behaves very differently from the majority of other clathrates. As pressure is increased the resultant transition sequence (sII $\rightarrow$ C_0 $\rightarrow$ FIS-II $\rightarrow$ FIS-Ic) differs from the transitions observed in clathrates with guest gases species of a similar size such as helium or neon. Though the H_2–H_2O system has been well studied with x-ray diffraction and spectroscopic methods, there are still some unknowns about the structures formed and these are highlighted in the discussion below.

2.2.1 sII

The formation of sII at low pressures and temperatures in H_2 hydrate was first observed by Mao *et al.* [38]. However, there were hints observed earlier by Dyadin *et al.* in melt curve data [33, 39]. Its crystal structure is the traditional clathrate structure exhibited by systems such as Ar and N_2 hydrates. More details of sII are

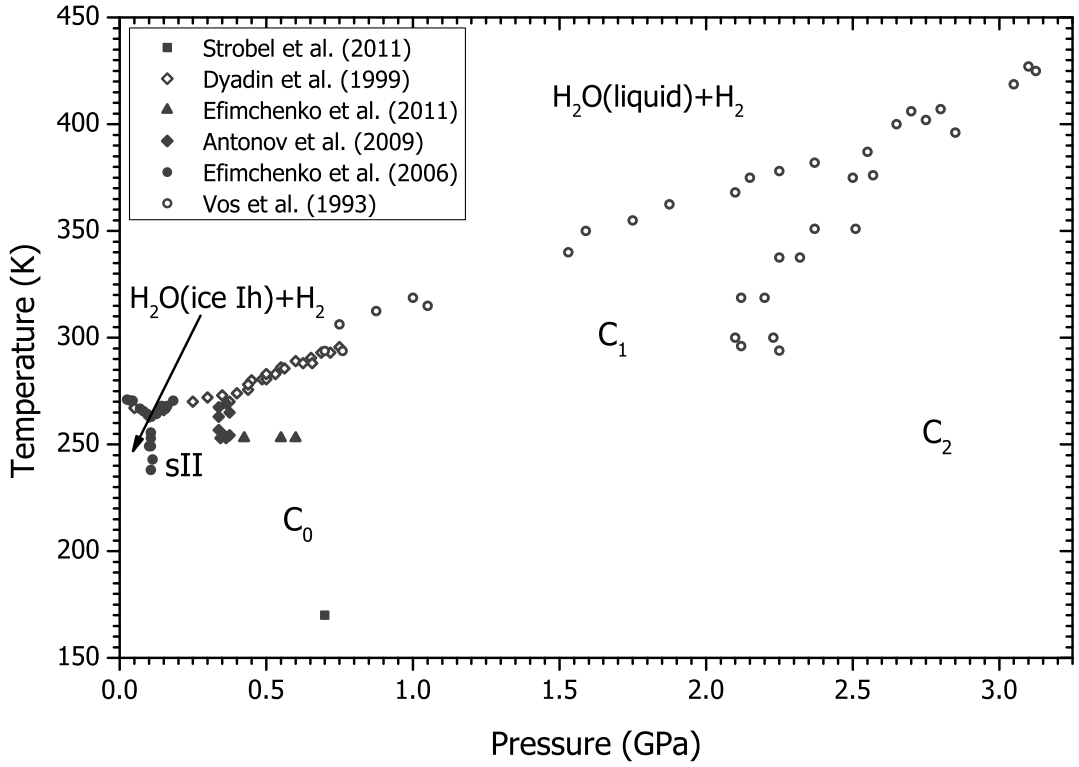

Figure 2.7 *The phase diagram of the H_2–H_2O system. The points are those found in references [32, 33, 34, 35, 36, 37].*

described in section 2.1. As the hydrogen molecule is very small when compared to typical sII-forming guest species such as N_2, multiple H_2 are required to occupy both the large and small sII cages for stability. Based on the size of the large and small cages there were initially four H_2 proposed to occupy the large cages and two molecules in the small cages on the basis of hydrogen molecule cluster sizes [38]. This would give sII a maximum H_2:H_2O ratio of approximately 1:2.1, and an overall hydrogen content of 5.56 wt% [3] [38]. This was later shown to be overestimated by a neutron diffraction study that showed a maximum hydrogen content of 3.77 wt % with a maximum of four H_2 molecules in the large cage and one in the small cage [18]. This neutron study also showed that there is an ordering transition in the H_2 molecules below 50 K. Above 50 K the H_2 are randomly distributed and mobile in an approximately spherical shape in the large cage, and below 50 K the H_2 form an ordered tetrahedron. Due to the possible high hydrogen content of this phase and its stability at relatively low pressure, the hydrogen hydrate sII phase has been well studied as a hydrogen storage material (more details given in 2.2.6).

[3] wt% is weight percent, or mass percent, and is the mass of a solute expressed as a percentage of the total mass of the solution.

2.2.2 The C_0 Phase

The C_0 phase is the most recent structure to be observed in the H_2–H_2O system. Originally found by Efimchenko *et al.*, and subsequently in another experiment by Strobel *et al.* using x-ray diffraction the crystal structure has not yet been fully determined [32, 34, 40]. Efimchenko *et al.* proposed a structure with a trigonal space group $P3_112$ with lattice parameters $a = 6.33$ Å and $c = 6.20$ Å, and a spiral H_2O host network that had never been observed in either pure ice or clathrate systems (see C_0-I in figure 2.8). In the centre of the channels formed by the H_2O network are partially occupied H_2O positions and guest H positions. The presence of these partially occupied H_2O positions is unconventional. A revised C_0 structure was proposed by Smirnov *et al.* who reported that the partially occupied H_2O positions could instead be occupied by N_2 that had been substituted for guest species during storage of the sample in liquid nitrogen [41]. This revised structure proposed the unconventional H_2O molecule positions to instead be guest H_2 positions. Two other candidate structures were proposed by Strobel *et al.*. The first of these is with the same space group as the structure proposed by Efimchenko *et al.*, $P3_112$, and lattice parameters to that of C_0-I but with a molecular structure based on α-quartz (C_0-quartz in figure 2.8) [32, 41, 42]. The other structure proposed was a tetragonal structure sT shown in 2.8 (marked as C_0-T) and details given in section 2.1.

In addition to the experimental studies several computational studies have also determined the stability of the C_0 structure. Smirnov *et al.* compared the stability of the modified C_0 with the stability of an sT hydrogen clathrate and found both to be stable. A structure search also found an ordered C_0 structure. This structure has the same H_2O network as the modified C_0 but was reported with ordered hydrogen bonds (a consequence of the structure search) and is shown as C_0-II in figure 2.8 [43].

2.2.3 The C_1 Phase

The C_1 phase was the first phase to be found in the hydrogen hydrate system. At room temperature C_1 is stable from around 0.9 GPa to 3 GPa (with coexistence with C_2 from around 2.3 GPa) [37]. It is a 'filled-ice' structure based on ice II (the same structure is found in He hydrate) with a hexagonal unit cell, an ordered hydrogen bond H_2O network and freely rotating H_2 located in the channel

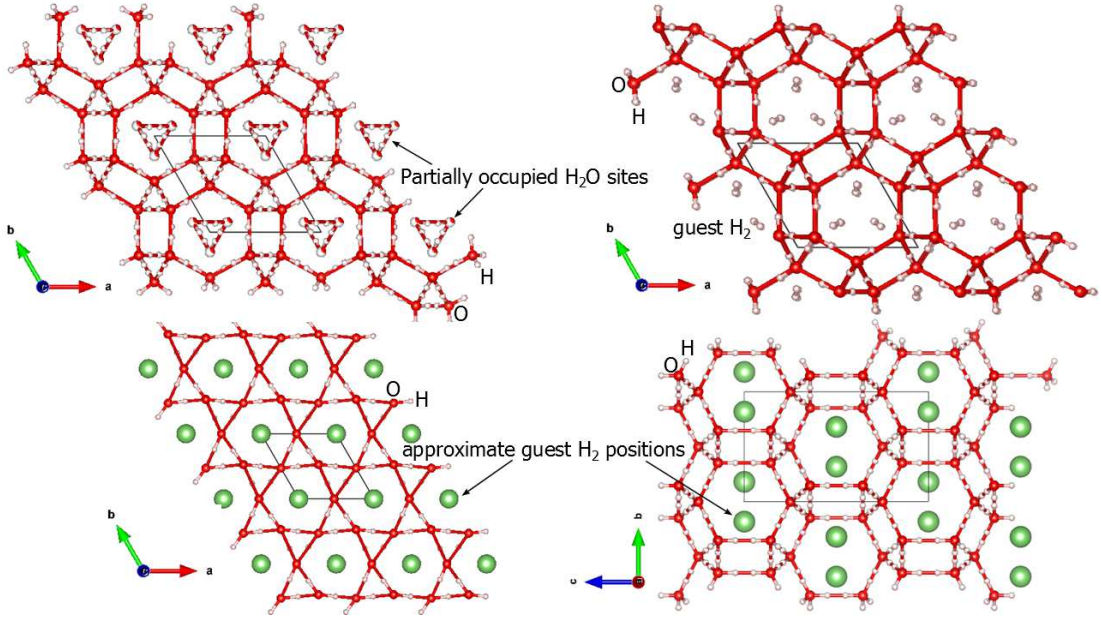

Figure 2.8 *Crystal structures proposed for the C_0 phase of hydrogen hydrate. Top left shows the original crystal structure proposed by Efimchenko et al. [34, 40]. Top right shows the structure found in a structure search by Qian et al. [43]. Bottom left shows an approximate structure proposed by Strobel et al. based on α-quartz [32, 41, 42]. Bottom right shows another structure proposed by Strobel et al. which is the tetragonal structure discussed in 2.1 [32]. Red and pink spheres indicate the positions of oxygen and hydrogen atoms. Green spheres indicate approximate guest H_2 position.*

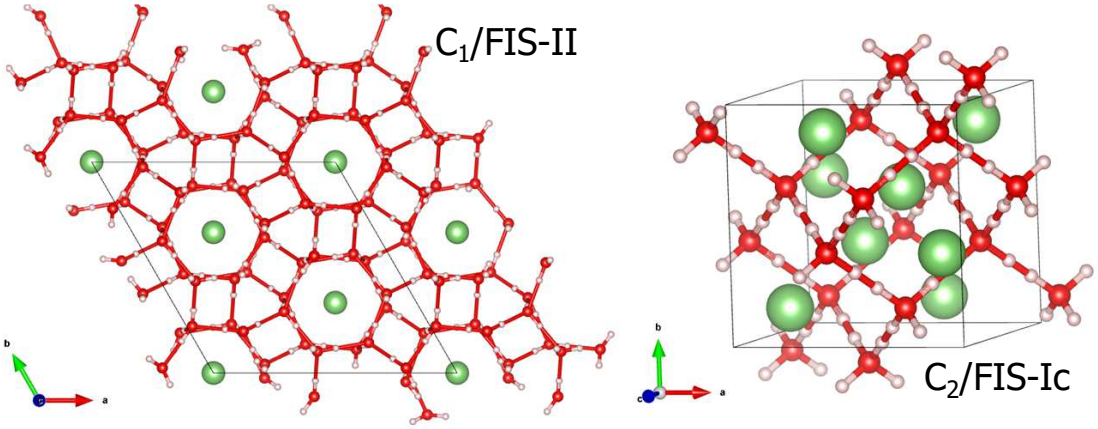

Figure 2.9 *On the left is the crystal structure of the C_1 phase of hydrogen hydrate (filled ice II) and on the right is the C_2 phase of hydrogen hydrate (filled ice Ih) [30, 37]. Red and pink spheres indicate the positions of oxygen and hydrogen atoms of the host H_2O. Green spheres indicate the guest gas atom/molecule positions.*

(see figure 2.9) [30]. Given the presence of the hydrogen molecules the lattice parameters of C_1 are slightly expanded compared to ice II with $a = 12.736(2)$ Å and $c = 5.968(2)$ Å around 2 GPa [37]. The C_1 phase is reported as having a structure exactly like that of the filled ice phase found in neon and helium clathrate, however there has been some evidence to suggest the hydrogen bond ordering may be different in the hydrogen clathrate than that of the FIS-II structure found in helium or neon clathrates [14].

2.2.4 The C_2 Phase

The C_2 phase is also found at room temperatures and requires pressures above 2.3 GPa to be stable. Currently, hydrogen is the only known gas to form this clathrate structure with H_2O. However, computational studies have suggested that it may also be found in helium and neon hydrate systems, but there has been no experimental confirmation of this yet [43, 44]. The C_2 structure is a filled ice described by cubic space group $Fd\bar{3}m$ with $a \sim 6.43$ Å and a H_2O network similar to ice Ic with H_2 molecules occupying the voids (see figure 2.9). The FIS-Ic can also be described as ice VII-like with one of the interpenetrating

Ic networks replaced entirely with H_2 molecules [4] giving a H_2:H_2O ratio of 1:1 (10 wt%) [37].

The replacement of one of the H_2O Ic networks with a H_2 network gives rise to an interesting property: the C_2 structure has a compressibility twice that of pure ice VII [37, 45]. This is of interest as it is thought to lower the pressure at which the hydrogen bond is centered (see 2.1.2). In ice VII this is expected to occur around 100 GPa when ice VII transforms into ice X, however in C_2 this transition is expected to occur somewhere around 40-60 GPa [37, 45]. Vos *et al.* originally reported the O-H...O bond centered at $\sim$ 60 GPa in a study that combined both Raman spectroscopy and x-ray diffraction [37, 45]. This was based on the assumption that C_2 remains cubic and the atomic structure does not change with pressure. However, more recent work suggests that the hydrogen bond centering occurs around 38 GPa based on slight changes to the guest H_2 vibron in a Raman spectroscopy study and changes in the pressure - volume curve determined from x-ray diffraction measurements [46, 47]. A recent theoretical study on the stability of hydrogen hydrates proposed that the transitions observed around 38 GPa are attributed to the formation of a different structure, C_3, (see 2.2.5) and that the symmetrisation of the hydrogen bond occurs around 120 GPa [43].

At lower pressures (between 10 and 20 GPa) another change in the C_2 structure is expected to occur. A Raman spectroscopic study observed solid hydrogen at 19 GPa upon compression of C_2 at room temperature [47]. This transition occurs reversibly and is thought to aid in stabilising the structure. As the rotational motion of the H_2 molecules within the structure become increasingly damped up until 19 GPa due to increasing confinement, some of the hydrogen is expulsed from the structure. Following this, the rotational motion is recovered [47]. However, it is currently not known how much hydrogen is lost from the C_2 structure during this. An x-ray diffraction study also observed the C_2 phase transform from cubic to tetragonal at 19 GPa and that this transition occurs as H_2 is extracted from the structure [48]. The cubic to tetragonal transition was observed to be highly dependent on temperature and was observed to occur as low at 10 GPa at 100 K [48]. The cubic C_2 structure was determined to not be stable above 10 GPa in a DFT study and that its existence in experiments is purely metastable [43].

[4] Ice VII is a cubic form of ice that is formed at high pressures (above 2.1 GPa) at room temperature. It is described by space group $Pn\bar{3}m$ with lattice parameter $a \sim 3.3$ Å. In ice VII the H_2O molecules form two inter-penetrating Ic-like networks.

2.2.5 Other Phases

Partially-filled ice Ic

Given the small size of the hydrogen molecule it is not unexpected that H_2 could be filled into ice Ic at pressures of a few megapascals [49]. Pure ice Ic is a proposed ambient pressure form of ice that the C_2 structure's host H_2O network is based upon. Although the formation of ice Ic has been well reported within the literature, recent work has shown that these ice Ic observations were actually ice Isd - a type of mixture of ice Ic and ice Ih [50]. A combined x-ray and neutron diffraction study with Raman spectroscopy and NMR reported that upon the pressurisation of amorphous ice with H_2 gas, the C_2 structure was formed. However, this was a depleted C_2 with considerably less H_2 than in standard C_2 where the H_2 content is around 10 wt% [49]. Though this was reported as a partially-filled C_2 structure it is most likely an H_2 filled ice Isd due to the presence of ice Ih within the diffraction pattern [49, 50].

Ice Ih-C_0

A recent computational structure search predicted a new structure to be stable in the hydrogen-water system at low pressures (below 1.1 GPa) [43]. This structure called 'Ih-C_0' is predicted to have a similar pressure stability region as C_0, with the Ih-C_0 structure becoming more stable than C_0 at higher pressures. Its crystal structure is similar to ice Ih and there are two hydrogen molecules located in the hexagonal channels with a H_2:H_2O ratio of 2:1. This basis on ice Ih means that it is similar to the FIS-Ih structure observed in a large majority of the other hydrate systems such as CH_4, Ar and H_2 at high pressure (section 2.1). This phase has not previously been observed experimentally.

The C_3 Phase

Another structure found in a structure search of the hydrogen-water system is the C_3 phase predicted to be stable from 38 GPa. It is similar to the C_2 structure but with the H_2 molecules not only occupying the voids in the structure but also occupying sites in the 'faces' made by the Ic H_2O network. This occupation of the faces allows for an increase in the H_2:H_2O ratio to 2:1 resulting

in a hydrogen content of 18 wt%. Although this phase has not been observed directly experimentally, it has been proposed as the resultant structure observed in experiments on C_2 when changes in the vibrons and x-ray diffraction patterns occurred around 40 GPa (see section 2.2.4). The C_3 phase is predicted to remain stable up to 120 GPa where the symmetrisation of the hydrogen bond is expected to occur [43].

2.2.6 Possibility as a Hydrogen Storage Material

Molecular hydrogen (H_2) has been proposed as a clean energy source with some of the benefits including clean combustion and ready availability [51]. Another benefit being H_2 having the largest energy density by mass than any known fuel; though H_2 has an extremely low energy density by volume, which causes the current H_2 storage problems [51]. A seemingly simple solution would be to liquefy H_2, though this requires either extremely low temperatures (20K) or high pressures (5GPa), both of which are costly or dangerous on board a vehicle [52]. Storing hydrogen within a compound such that the hydrogen density be comparable with that of liquid H_2 is a possible solution, with the current aim of at least 5.5 wt% H_2 content and an ultimate long-term goal of upwards of 7.5 wt% [10, 53]. Some progress has been made using compounds such as: metal organic frameworks (MOFs), metal hydrides and carbon nano-tubes/nano-fibers[10]. Though the reported hydrogen content for each material is extremely varied, few meet the requirements or are impractical for use either physically or financially [10, 53].

Clathrates are known for their ability to store large quantities of gas and given the high quantity of hydrogen within the H_2-H_2O system it was considered to be of interest as a hydrogen strorage material [8]. Ice would also make an ideal host material to store hydrogen as water is cheap, readily available and environmentally benign. However, the known stable phases in the H_2-H_2O system are either too low in H_2 (sII and C_1) or require extremely high pressures to form (C_2). Despite the low H_2 content, focus has been concentrated on the sII structure and much research has attempted to stabilise sII at more favourable conditions by the inclusion of larger guest species such as tetrahydrafuron (THF) [8]. These have had some success in achieving low-pressure stability but come at a cost of reduced H_2 content. Though the H_2 content of C_2 would be ideal (10 wt %) there are problems with low pressure synthesis and stability. Attempts to form C_2 at

lower pressure are accompanied by a dramatic decrease in the H_2 content to ∼2.5 wt% around 16 MPa. However, there is the possibility that hydrogen content can increase with the application of pressure [49].

2.3 Other Hydrogen Inclusion Compounds

Whilst water has been very widely studied for its ability to take up hydrogen, less is known about the formation of hydrogen inclusion compounds with other simple hydrogen-bonded organic materials such as hydroquinone or urea. The former of these two materials, hydroquinone, is known to form a hydrogen inclusion compound at high pressure [54]. Urea on the other hand has been proposed to form an inclusion compound with hydrogen but it is not known whether this is the case [8]. These compounds may also be of interest for hydrogen storage applications as the host material is also organic, environmentally benign and cheap.

2.3.1 Hydroquinone

Hydroquinone ($C_6H_4(OH)_2$) is a crystalline solid at ambient conditions. It is a well known clathrate former with not only 'large' gas species such as carbon dioxide and methane but also with simple organic solvents and acids [55, 56, 57, 58, 59]. Recently it has been shown to form inclusion compounds with hydrogen [54, 60]. One of these is the inclusion of hydrogen into the channels present in the ambient pressure form α-hydroquinone at slightly elevated pressures ($\sim$ 12 MPa) [60]. In addition to hydrogen being able to occupy the channels in α-hydroquinone, H_2-hydroquinone has also been found to form the cage-like clathrate β-hydroquinone structure typically found to form with larger gas guest species, simple solvents and acids [1, 56, 59]. This structure is stable above 200 MPa at room temperature and was found to have one hydrogen molecule located in the cage [54]. As pressure is increased the occupancy of the cage increases to have triple H_2 occupancy at 3 GPa [61].

Despite the low H_2 content, the hydroquinone-hydrogen system has also been considered as a possible hydrogen storage material. It has been shown possible to synthesise an 'empty' guest-free β structure by allowing a guest molecule such as CO_2 to diffuse out of the host. It has also been shown that this pre-

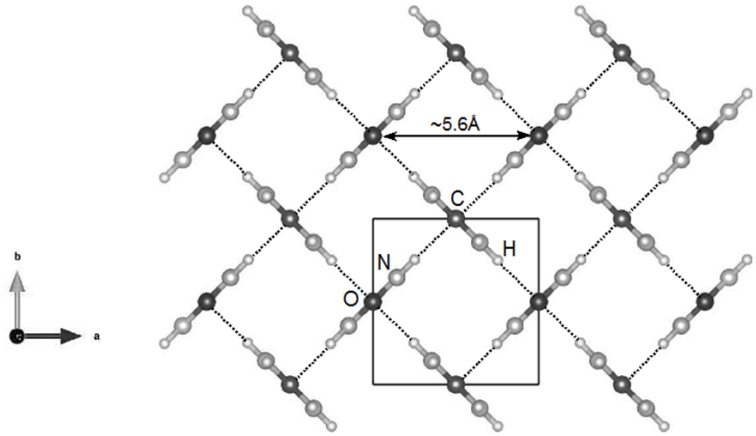

Figure 2.10 *The crystal structure of the tetragonal phase I of urea ($P\bar{4}2_1m$) showing the channels running along the c direction. Dotted lines mark the hydrogen bonds between the urea molecules.*

formed structure can uptake and release gas within a few seconds [62]. Although the occupancy of the β-hydroquinone cages is low below 0.5 GPa (with one H_2 molecule in the cage the content is $\sim$ 0.6 wt%) there is the possibility to increase the hydrogen storage capacity by almost 300 % to 2.4 wt% by utilising the hydrogen within the host hydroquinone framework also as a source of hydrogen by chemically breaking up the host material [54].

2.3.2 Urea

Urea (CH_4N_2O) is known to form inclusion compounds with long-chain hydrocarbons but currently, little is known about its ability to take up simple gases such as hydrogen [63, 64]. Urea however is a potentially valuable inclusion compound former as it is readily available in nature as a major component of *Avian Stercore* and hence is cheap. Urea's structure at ambient pressure which is tetragonal (space group $P\bar{4}2_1m$, $a = b = 5.589$ Å, $c = 4.680$ Å) has square channels formed from hydrogen bonded planar urea molecules running along the tetragonal c-axis (see figure 2.10). These channels, which are 5.6 Å across, are large enough to accommodate a simple molecule [65, 66, 67].

Furthermore, neutron and x-ray diffraction studies of pure urea have identified

three high-pressure phases at room temperature. The ambient pressure form transforms to an orthorhombic structure above 0.5 GPa known as phase III ($P2_12_12_1$, a = 8.272 Å, b = 3.624 Å, c = 8.844 Å). At around 2.8 GPa, phase III of urea transforms to another orthorhombic structure known as phase IV ($P2_12_12$, a = 3.414 Å, b = 7.360 Å, c = 4.606 Å) and then transforms above 7.2 GPa into a further orthorhombic phase V ($Pmcn$) [65, 66, 67]. These transformations indicate that pressure has strong effects on the network bonding and thus may access new inclusion compounds. However, despite hydrogen-urea being suggested as a potential system to form such inclusion compounds, to date, there have been no searches for hydrogen-urea inclusion compounds [8].

2.4 Aims of Thesis

This thesis aims to expand the structural details of the phases found in high pressure hydrogen hydrate with the use of neutron diffraction. These include determining the structure of the C_0 phase, confirming whether the C_1 structure is the same one found in the helium hydrate system, and studying the C_2 phase at high pressure to determine the structure and how the hydrogen bond of the host ice framework evolves with pressure. In addition to studying the hydrogen hydrate system, this thesis aims to study the possibility of forming hydrogen inclusion compounds in other hydrogen-bond forming materials such as urea.

Chapter 3

Crystals & Neutron Diffraction

Neutron diffraction is the best tool for investigating the crystalline structures of hydrogen-rich systems such as those described in the previous chapter. This chapter gives a brief overview of crystal structures and the space group notation used in later chapters. Following this, the basic theory of neutron diffraction and the methods used for structural refinement are presented. The last section of the chapter focuses on the practical aspects of neutron diffraction including a summary of neutron sources and brief explanation of the time-of-flight method. All of this chapter is based on the explanations given in references [68, 69, 70, 71] unless otherwise stated.

3.1 Crystals

Crystalline materials are solid state matter that exhibit long range order. This long-range order originates from the fact that crystals can be reduced down to a single block that is repeated a large number of times to build the entire crystal. In a crystal this block is called a 'unit cell' which can be split into two parts; the lattice and the basis. The lattice is related to the shape, size and symmetry of the unit cell. The basis describes the atomic/molecular positions in the unit cell and this is repeated at every lattice point. Together these two components can describe the whole crystal structure.

A lattice is a collection of points that represent the points of repeating symmetry within a crystal that are related by translation (shown in two dimensions in the

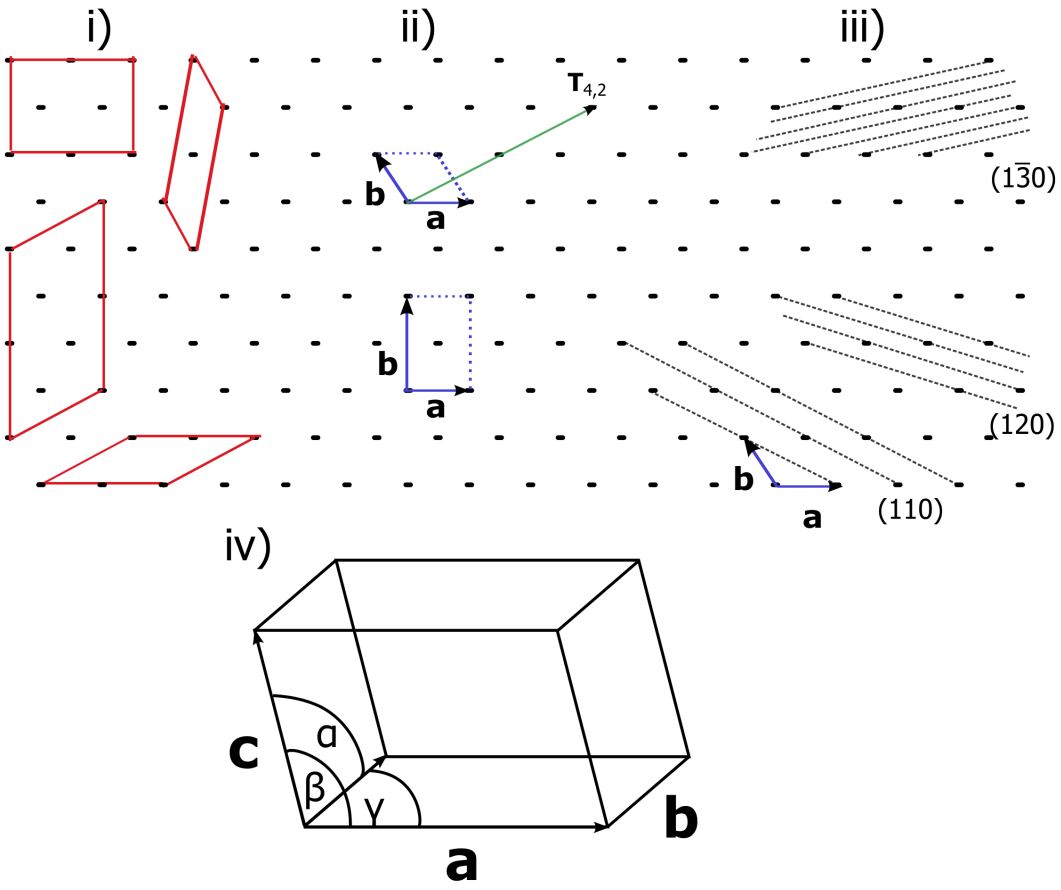

Figure 3.1 *In (i) is a selection of possible unit cells that could describe the symmetry of the lattice shown. In (ii) two of the smallest cells that describe this lattice. At the top is a primitive cell with a centered cell below that could be used instead. In (iii) various planes (represented here as lines in two dimensions) for the smallest primitive unit cell shown in (ii). In (iv) a three dimensional unit cell showing the relationship between the lattice parameters* $\boldsymbol{a}$, $\boldsymbol{b}$, $\boldsymbol{c}$, *and angles* α, β *and* γ *between them.*

Crystal System	Length Restrictions	Angle Restrictions	Cell Types
triclinic	$a \neq b \neq c$	$\alpha \neq \beta \neq \gamma$	*P*
monoclinic	$a \neq b \neq c$	$\alpha = \gamma = 90°$	*P C(I)*
orthorhombic	$a \neq b \neq c$	$\alpha = \beta = \gamma = 90°$	*P C(A) I F*
tetragonal	$a = b$	$\alpha = \beta = \gamma = 90°$	*P I*
trigonal	$a = b = c$	$\alpha = \beta = \gamma \neq 90°$	*R (P)*
hexagonal	$a = b$	$\alpha = \beta = 90°$, $\gamma = 120°$	*P*
cubic	$a = b = c$	$\alpha = \beta = \gamma = 90°$	*P I F*

Table 3.1 *The different crystal systems with the unit cell restrictions and types of cell types present in that system.*

top part of figure 3.1). A unit cell describes the relationship between the lattice points (represented in 3.1(i) as a box). Although any unit cell/box could be chosen to describe the relationship between the points, such as those shown in part (i) of 3.1 . It is conventional to choose the smallest box such as those shown in figure 3.1(ii) that consists of one lattice point. This is known as a primitive cell. However, sometimes it is more convenient to describe the system with a larger centered cell depending on the symmetry present (also shown in figure 3.1(ii)). In three dimensions this unit cell is described by the translation vectors **a**, **b** and **c** known as the lattice parameters that define a parallelepiped. All lattice points can then be reproduced by combinations of these vectors via the translation vector **T**:

$$\mathbf{T} = n_a\mathbf{a} + n_b\mathbf{b} + n_c\mathbf{c} \tag{3.1}$$

Where n_a, n_b and n_c are integer values. An example in two dimensions is shown in 3.1(ii) for $T_{4,2}$ with $n_a = 4$ and $n_b = 2$ in this case. All basic crystals (those that are not incommensurate or quasicrystals) can be broken down into one of the 7 unit cells shown in table 3.1, that range from the most general triclinic unit cell to the highest symmetry cubic unit cell. If these 7 cells are then combined with the type of lattice, whether primitive (denoted as P or R for rhombohedral lattices) or centered (denoted as either C, I, A or F depending on the type of centering), they give a group of 14 that are known as the Bravais lattices that can describe all three dimensional crystals.

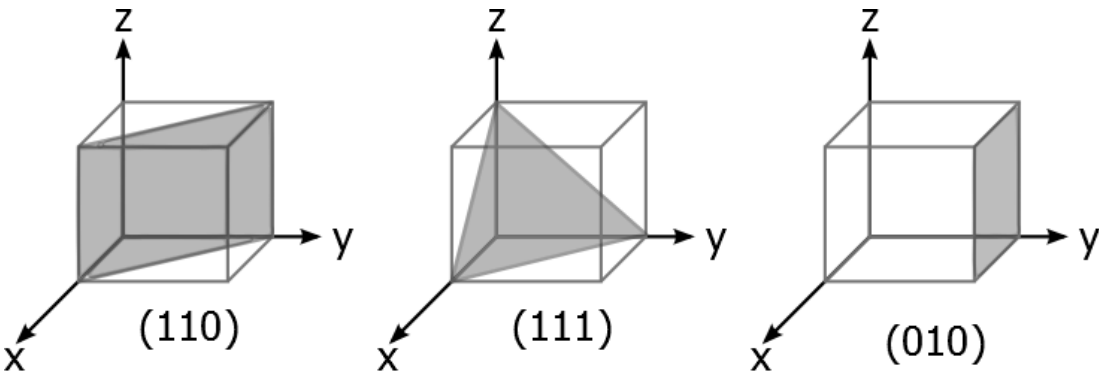

Figure 3.2 *A selection of planes with the Miller indices that describe those planes for a cubic unit cell.*

3.1.1 Miller Indices

Miller indices provide a way of referring to the planes of atoms within a crystal. Three points on a lattice can define a plane through a crystal, such as those represented by lines in two dimensions in figure 3.1. The Miller indices h, k and l are used to describe these planes and relate where the plane intercepts the unit cell axes a, b and c, respectively. This is done by taking the coordinate of where a plane intercepts the axes and the reciprocal of those coordinates provides the index (h, k or l) for that plane. For example, the (110) plane in 3.1(iii) intercepts the crystallographic axes $\mathbf{a}, \mathbf{b}$ at a and b respectively, whereas the (120) plane intercepts the $\mathbf{a}, \mathbf{b}$ axes at a and $b/2$. Any negatives are denoted by a bar above the index. The planes are marked in regular brackets and directions are described in terms of the Miller indices of the plane normal to the direction with square brackets [hkl]. For example the [110] direction would be 'looking' normal to the (110) plane. Parallel planes are separated by a specific spacing known as d_{hkl} which is simply referred to as d-spacing in the work presented here. A selection of planes are shown in three dimensions for a cubic unit cell in figure 3.2. Dependent on the symmetry present a group of planes may be 'symmetry equivalent'. For example in 3.2 the (010) plane is equivalent to the (100) and the (001) due to the cubic symmetry. In this case the group of planes are denoted with curly brackets {100}.

3.1.2 Space Groups and Notation

In addition to the translational symmetry described above there are other types of symmetry such as rotational or rototranslational, that can be used to describe the constituents of a unit cell. These other symmetries can be combined in certain combinations to create the 32 crystallographic point groups[1] that are compatible with translational symmetry. If these 32 point groups are combined with the 14 Bravais lattices the result is 230 space groups that are capable of describing the symmetry present in all basic crystals.

The 230 space groups are conventionally described by Hermann-Mauguin symbols. For example, in a primitive lattice, one which only has one lattice point/unit cell, is described by P, or R in the case of a rhombohedral cell. Pure rotational axes, are noted purely as a number n, which describes an n-fold rotation axis. A screw axis, also known as a rototranslational axis, is noted by a subscript on the rotation axis. For example, a 3_2 axis acting on an object would repeat that object at 120° around the axes and then shift the object two thirds of the way up the unit cell. The symbols m, n, a, b, c, d indicate mirror or glide planes. An inversion centre is indicated by the symbol $\bar{n}$, e.g. $\bar{1}$ or $\bar{3}$. However, as all of the inversions with n greater than 1 can be explained by combinations of other types of symmetries it is conventional to describe these inversions as the other symmetries. For example, a $\bar{6}$ inversion can be explained by a combination of a threefold rotation followed by a reflection in the plane perpendicular to it so this symmetry can be denoted by the symbol $3/m$.

3.1.3 Atomic Coordinates

The above descriptions of the lattice and space groups only describe the size, lattice type and symmetry operators present within a unit cell. In order to fully describe the unit cell the 'basis' is needed. This describes the location of the atoms within the unit cell. Instead of listing all of the atomic positions within the unit cell only a collection of atoms known as the 'asymmetric unit' are needed. The asymmetric unit describes the position of a few atoms (usually given in fractional coordinates of the lattice parameters) and the symmetry operators given by the space group then produce the rest of the atoms within the cell from this

[1] A point group is a set of symmetry elements, for example a mirror plane or rotation axis, that are grouped together to describe the symmetry present at a point.

collection. The use of the symmetry operators and asymmetric unit to describe the unit cell results in two types of positions. The first of these is when atoms are located exactly on the point group symmetry elements. These are called 'special positions'. All others are known as 'general' positions. Therefore to describe the entire crystal only the lattice parameters, space group and asymmetric unit are needed.

3.2 Diffraction

The repetitive nature of crystals allows for the study of their structure with a technique known as a diffraction. This is done by probing the crystalline materials with x-rays, neutrons or electrons that have a wavelength with a similar order of magnitude as the spacing between atoms. Neutrons have many advantages over x-rays and electrons, however, these are also accompanied with many disadvantages too. The main advantage is that neutrons do not have an interaction that has a simple dependency on the atomic number of an atom (such as Z^2 in the case of x-rays) and so, interact just as strongly, if not stronger, with light elements such as hydrogen or oxygen. For this reason neutron diffraction is the method used for the work presented in this thesis and is the only one described here. However, the same principles can be applied to x-ray or electron diffraction with some differences. Some of the disadvantages and how they impact neutron diffraction experiments are discussed in section 3.4.4.

There are a number of ways neutrons can interact with nuclei and elastic scattering is the most important when it comes to diffraction. This is where there is no energy transfer between the sample nuclei and incoming neutron. Other types of interactions are either inelastic, which involves a transfer of energy between the neutron and nuclei, or absorption where the neutron is captured by the nuclei. The two main mechanisms that cause elastic scattering of neutrons are either scattering by the strong nuclear force, or by electromagnetic interaction of the magnetic dipole moment of the incoming neutron and the unpaired electrons of the atom. As neutrons mainly interact via the nuclear force and not the electromagnetic like x-rays or electrons, neutron scattering is the preferred method for investigating the crystal structures of materials rich in light elements (low Z) such as hydrogen, carbon or oxygen. However, the strong nuclear force is weak compared to the electromagnetic force which gives rise to some of the major disadvantages when it comes to the practical aspects of

Isotope	σ_{coh}	σ_{inc}	σ_{scatt}	σ_{abs}
^{1}H	1.7583	80.27	82.03	0.3326
D (^{2}H)	5.592	2.05	7.64	0.000519
^{12}C	5.559	0	5.559	0.00353
^{16}O	4.232	0	4.232	0.0001
^{10}B	0.144	3	3.1	3835
^{56}Fe	12.42	0	12.42	2.59
^{187}Re	10.9	1	11.19	76

Table 3.2 *Cross sections of various isotopes for coherent scattering (σ_{coh}), incoherent scattering (σ_{inc}), total scattering (σ_{scatt}) and absorption (σ_{abs}) of thermal neutrons. All values are in units of 'barn' (1 barn = $10^{-24}cm^2$) and are from the NIST database [74].*

performing neutron diffraction experiments (discussed further in 3.4.4).

The scattering length b governs the strength of the interaction between a nucleus and an incoming neutron, and can be viewed as the effective radius that a neutron 'sees' a nucleus. For neutrons the scattering length is dependent on a number of factors, and is generally a constant for a specific isotope at the neutron energies used in typical diffraction experiments, and in some cases can be both complex or negative. This property of negative and complex values for the scattering length mean that 'null' scattering materials can be constructed by balancing the values of b to give an overall scattering length of zero [72]. Unlike x-rays the scattering length generally does not vary with the wavelength of the incoming neutrons or the scattering angle θ. Instead the scattering length depends on the spin of the nuclei, is isotope specific and do not have a simple dependency on increasing atomic number like x-rays have. This dependency on spin contributes to incoherent scattering[2]. Though the scattering length governs the strength of the interaction a more useful quantity is often used to describe this that is related to b via equations of the form: $\sigma_{coh} = 4\pi|b_{coh}|^2$ and $\sigma_{inc} = 4\pi|b_{inc}|^2$ [73]. The scattering cross section σ_{scatt} quantifies the probability that a neutron will be scattered or absorbed (a selection of cross sections for various isotopes are shown in table 3.2). This quantity is measured in 'barns' where 1 barn = 10^{-24}cm^2.

[2]Incoherent scattering is where the incoming neutrons interact independently with each nucleus causing random changes in the relative phases of each neutron, and the resultant waves do not interfere constructively as they all have random phases. Coherent scattering is where the neutrons interact in a way that they are scattered in-phase and contribute to Bragg scattering. Coherent scattering is described further in section 3.2.2.

3.2.1 Scattering from One Atom

Here the interaction between a single neutron and nucleus is described before the case for many neutrons and multiple nuclei are considered. An incoming neutron travelling in the z direction can be described by a plane wave with wavefunction $\psi_i = \psi_0 e^{ikz}$. This plane wave/neutron will then interact with the nucleus of an atom with scattering length b. As the only type of interaction considered here is elastic, no energy is transferred in the interaction and the deflected neutron will have the same magnitude of wavevector, $|\mathbf{k'}| = |\mathbf{k}|$, as the incoming neutron. However, the direction of this outgoing wavevector, **k'**, will be different to that of the incoming neutron. After the neutron/plane wave interacts with the nucleus, the deflected neutron is then described by a spherical wavefunction:

$$\psi_f = -\psi_0 b \frac{e^{ik'r}}{r} \tag{3.2}$$

The minus sign before the scattering length b is a matter of convention.

3.2.2 Scattering from Multiple Atoms

Similarly to the interaction described above for a single nucleus, incoming neutrons with wavevector **k** are described as plane waves (figure 3.3). These are then deflected when they interact with the sample nuclei forming spherical waves. These spherical waves then interfere and either add constructively or deconstructively depending on their phase relative to each other and the Bragg condition is satisfied. This results in the plane wave **k'** shown in figure 3.3. This is coherent scattering. The scattered spherical waves only add to give constructive interference/plane waves in certain directions which are related to the symmetry and spacing of the lattice which is in turn related to the unit cell.

$$n\lambda = 2d_{hkl} sin\theta \tag{3.3}$$

The condition that needs to be satisfied for the spherical waves to interfere in this way and result in a diffracted neutron beam (often referred to as a reflection) is known as Bragg's Law. This law can be described by two different formulations that give identical results. The first of these is derived by considering the path

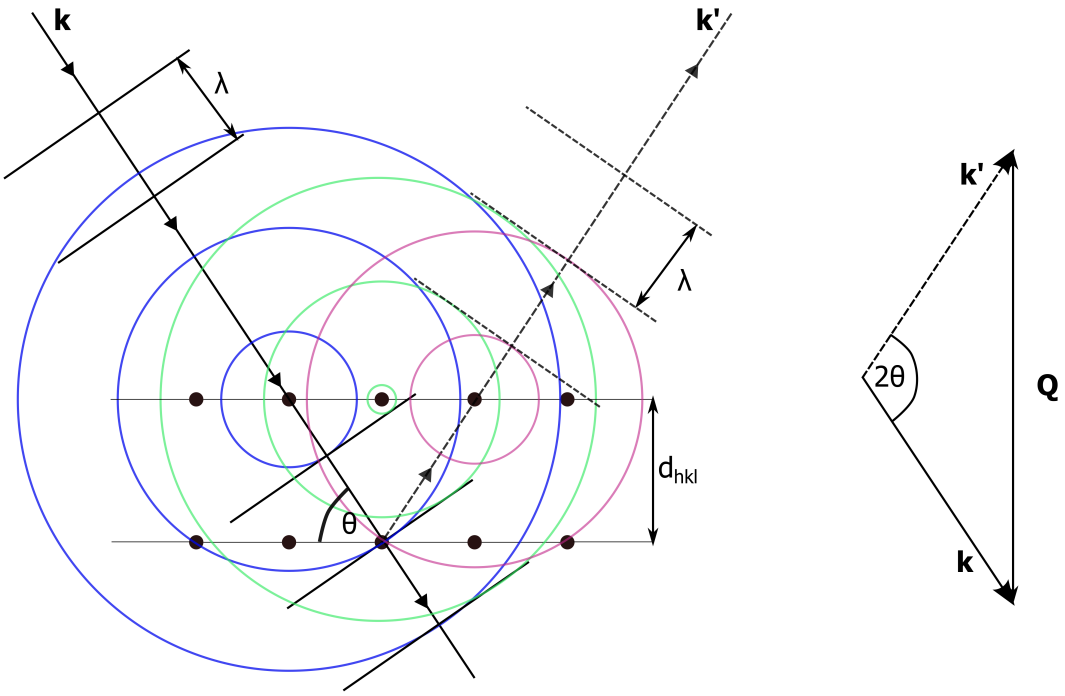

Figure 3.3 *On the left is a basic schematic showing how incoming neutrons are scattered from planes to give an outgoing plane wave in 2D. An incoming neutron wave, described by a plane wave with wavevector* ***k*** *and wavelength* λ*, scatters from the nuclei (black circles). As the plane waves are scattered from the nuclei they form spherical waves (shown here as grey circles) with different phases. These scattered spherical waves then interfere to produce the outgoing plane wave* ***k'****. Note: lines representing the planar wave nature in* ***k*** *and* ***k'****, and the scattered spherical waves for the second plane of nuclei have been omitted for clarity. On the right is the resultant scattering vector* ***Q*** *which must be perpendicular to the scattering planes. This diagram is based on one by Pynn [71].*

length difference between the scattered waves of neighbouring planes and is shown in equation 3.3. This relates the wavelength of the incoming neutron (λ) and angle with which it comes into contact with the plane (θ), to the interplanar spacing (d_{hkl}). The second of these formulations is explained in terms of the wavevectors of the incoming and outgoing neutrons (**k** and **k'** respectively) and their relation to the scattering vector **Q** as seen in figure 3.3. For constructive interference **Q** must be perpendicular to the scattering planes of atoms/nuclei. This requires that the magnitude of Q then be that shown in equation 3.5 via arguments from geometry and due to the scattering considered here being solely elastic so $|k'| = |k|$.

$$\mathbf{Q} = \mathbf{k} - \mathbf{k'} \tag{3.4}$$

$$Q = 2ksin\theta = \frac{4\pi}{\lambda}sin\theta \tag{3.5}$$

3.2.3 Structure Factors and Intensities

The above description of scattering determines where a reflection is observed but not the intensity of that reflection. The effect of the basis on the intensity of a reflection, I_{hkl}, needs to be considered as this is where the neutron is actually scattered from. This is done by summing together all of the scattered neutrons that satisfied the Bragg condition. If a crystal has only one atom in its basis then scattering would be directly from the planes containing these atoms. However, if the basis contains two or more nuclei then the phase difference between the scattering from these nuclei need to be considered. As an example a basis of two nuclei is considered here, with one nucleus located on a lattice site and the other located at (x, y, z) away from the lattice point. If the Bragg condition for a plane (hkl) is satisfied for this crystal then the points located at lattice points will scatter in phase, and those also located at (x, y, z) will scatter in phase. Due to interference this introduces a phase difference ϕ between the scattering from these two points which causes a change in intensity of the (hkl) reflection. This phase difference is given by:

$$\phi = 2\pi(hx + ky + lz) \tag{3.6}$$

If all of the n nuclei within the unit cell are considered and the contribution from each of them added together then this leads to the general equation:

$$F_{hkl} = \sum_n b_n e^{i2\pi(hx_n+ky_n+lz_n)} = \sum_n b_n e^{i\phi}, \tag{3.7}$$

where F_{hkl} is known as the 'structure factor'. The structure factor can be thought of as the Fourier transform of the scattering density as sampled at each (hkl) of the crystal. In a diffraction experiment it is not the structure factor that is measured but the intensity (I_{hkl}) which is related to the structure factor via:

$$I_{hkl} \propto |F_{hkl}|^2 \tag{3.8}$$

There are other factors which contribute to the intensity observed in diffraction experiments such as the thermal motion of the atoms or the incident flux of neutrons are a few examples.

In a diffraction experiment intensity (I_{hkl}) is measured. This is a square of a quantity that can be complex which means that the information in the phase is lost. This results in the 'phase problem' which means that the measured intensities cannot be directly related to the atomic positions in Bragg diffraction. However, there are ways around this to determine the structural information on the atomic positions. One of these is discussed further in section 3.3.

The case described above is only for that of diffraction of a single crystal. However, the same principles still apply when extending the above description to crystalline powders. If a powder is made up of an extremely large number of similarly sized crystallites that are randomly oriented (this is known as a 'good' non-textured powder) then instead of individual 'spots' of intensity for a given (hkl) reflection being observed as is the case for single crystal diffraction, a 'ring' of intensity is observed for that (hkl) at a given d-spacing or 2θ.

3.3 Structural Refinement

As the phase cannot be determined there are other ways that can determine the structural details of the crystal from the observed intensities.

3.3.1 Rietveld Refinement

The Rietveld method works by trying to match calculated intensities to the observed intensities [75]. However, this method relies on having a 'starter' structural model (unit cell, space group and atomic positions) to input. The Rietveld method works by first determining the d-spacings of the expected reflections from the starter unit cell parameters and space group. Then the intensity of each of these reflections are calculated by the structure factor shown in 3.7. This intensity is then modified with scaling factors to account for, for example, multiplicity, instrumental factors, preferred orientation and a temperature dependent factor that depends on the vibrational displacement of the atoms. These intensities then have a profile function applied to them such as a Gaussian or Lorentzian function, or some combination of these to describe the peak shape. A background is also fitted to the data that is usually by a polynomial function or sum of cosines that is built into the software used. Parameters such as unit cell dimensions, profile function parameters, and positions/thermal parameters[3] of the atoms are then varied to try to best match the observed full pattern. This is done via an iterative least squares approach.

A figure of merit is used to describe how well a model describes/fits the data. In least squares fitting, the quantity χ^2 is normally used (equation 3.9). In the work described in latter chapters the weighted profile R-factor (R_{wp}) is used for comparisons of the fits to the same data of different models (equation 3.10). This is used over a non-weighted R-factor as it gives a more equal merit to intensities observed that may not have as many counts. This is done to ensure that the model best fits all of the reflections and not just those with the largest intensities.

$$\chi^2 = \sum_n \frac{(I_n(obs) - I_n(exp))^2}{I_n(exp)}, \tag{3.9}$$

$$R_{wp} = \left\{ \frac{\sum_n w_n (I_n(obs) - I_n(exp))^2}{\sum_n w_n (I_n(obs))^2} \right\}^{\frac{1}{2}} \tag{3.10}$$

To analyse the neutron diffraction data presented in later chapters with Rietveld refinement the General Structure Analysis System (GSAS) is used [76].

[3]The thermal parameter describes the vibrational motion of an atom around its mean position. It has more of an effect on the intensities at lower d-spacings.

3.3.2 Le Bail Extraction

Unlike the Rietveld method described above the Le Bail extraction method does not require a full starter model and only the unit cell dimensions and symmetry are required [77]. Le Bail extraction works by the same initial procedure as the Rietveld refinement method does; calculating the positions of the reflections from the unit cell and space group symmetry. Then a 'guess' of the possible intensity for each peak is made by the software. These intensities are then varied over several iterations to minimise the difference between the observed and calculated intensities. Unlike in the Rietveld method, only the lattice parameters and profile shapes can be refined with the Le Bail method. Thus this method also produces the best possible fit of a unit cell to the data. This method can extract values for the intensities of the observed peaks if matched up well and can then be used for *ab-initio* methods such as charge flipping [78]. In the work presented here Le Bail extraction is also used within the GSAS software suite.

3.4 Neutron Sources

Neutrons can be produced in two types of nuclear reactions, either by nuclear fission or by spallation of nuclei by charged particles such as protons. Both of these methods are used to make neutrons that can be used for diffraction, meaning that there are two types of neutron sources either reactor sources or spallation sources. These sources are sometimes referred to as 'continuous' or 'pulsed' sources, respectively. At reactor and spallation sources different quantities in Bragg's Law are varied to study the crystal structures of materials and these are discussed below.

3.4.1 Reactor Sources

Reactor sources are those in which neutrons are produced as a result of the nuclear fission process. This provides a large flux of neutrons (typically around 10^{15} neutrons/cm^2 s or above for some of the more powerful reactors such as the ILL) which is one of the benefits of reactor sources[4]. Neutrons are produced

[4]This flux is extremely small when compared to typical synchrotron fluxes which are in the range 10^{13} - 10^{23} photons/ cm^2 s [70].

in the reactor core by the fission of ^{235}U and this process typically produces neutrons with kinetic energies of around 2 MeV which is much larger than the typical energies needed to produce neutrons with wavelengths that can be used in diffraction experiments on crystalline solids ($\sim$ 20 meV). To lower the energy of the neutrons (and thus lengthen the wavelength) down to those of use for diffraction, the neutrons pass through a moderator which slows them down. These are typically made from light elements such as hydrogen. The moderator produces a Maxwellian distribution of neutrons with various wavelengths with the peak of that distribution dependent on the temperature of the moderator that the neutrons pass through. For example, the neutrons could pass through a cold moderator such as liquid hydrogen at 20 K, or a hot moderator at 2000 K such as graphite which would cause the peak wavelength of the Maxwellian distribution to be either 3.5 Å or 0.5 Å, respectively [70]. After the neutrons pass through the moderator, they are then guided to the instrument beamlines located around the reactor before being passed through a crystal monochromator to select a single (or a few) wavelength(s) and then diffracted by the sample. For diffraction experiments these are constant wavelength sources where the Bragg condition is satisfied by probing different 2θ.

3.4.2 Spallation Sources

At spallation sources neutrons are produced by accelerated charged particles, such as protons, impacting a target made from a heavy metal. To produce protons, bunches of H^- ions are accelerated in a linac before being stripped of the electrons. The resulting protons are then accelerated to high speeds in a synchrotron before hitting the heavy-metal target made from materials such as tungsten, tantalum, or mercury. Spallation sources are often referred to as 'pulsed' sources as bunches of protons hit the target a certain number of times (anywhere between 10 and 60 times) in a second, creating pulses of neutrons. For example, at the Spallation Neutron Source at the Oak Ridge National Lab in the USA, bunches of protons hit the target 60 times per second giving pulses of 60 Hz [79]. This gives spallation sources one of their benefits in that they can be modified to accommodate more targets (and hence instrument beamlines). For example, at the ISIS neutron source the synchrotron accelerates 50 bunches of protons per second, with 40 of these sent to one target station giving it a pulse rate of 40 Hz, and the other 10 are sent to a secondary target station that has a lower pulse rate of 10 Hz.

When the protons hit the target there are two types of neutrons produced, 'epithermal' and 'thermal' neutrons. Epithermal neutrons are those that are produced on impact of the protons on the target. As a result of this, these neutrons are extremely high in energy and are too fast to be effectively moderated to the desired λ range. Thermal neutrons are made after the nuclei within the target have been excited by the protons and then decay via β-decay to produce neutrons. The neutrons produced in this way have a range of wavelengths (see section 3.4.3 for details) and can be effectively moderated to shift the peak wavelength to the desired Maxwellian profile (figure 3.4). This is done in the similar way to the moderation process described for reactors. After neutrons are produced they pass through a moderator and the shift of the peak wavelength varies with the temperature of the moderator. For example, at the ISIS spallation source there are several moderators such as hydrogen at 20 K, methane at 111 K and water at room temperature. Following moderation the neutrons are guided down the beamlines to different instruments and during this can be 'chopped' into specific λ ranges if required. The neutrons are then scattered off the sample and collected at constant angles as Bragg's Law at these sources is probed by using different wavelengths. This gives spallation sources another benefit being that they use all of the neutrons produced whereas reactor sources tend to discard most of incident flux on monochromatisation. Another benefit of spallation sources for samples that require numerous sample environment, such as high pressure devices, is that as the detectors are fixed the neutrons scattered from the sample environment can be effectively screened.

3.4.3 Time-of-Flight Diffraction

Time-of-flight (ToF) diffraction relies on the property that high-energy, fast-moving neutrons have shorter wavelengths than those that are lower in energy and slower moving. This means that neutrons with shorter wavelengths will arrive faster at a detector than those with longer wavelengths over the same distance. Therefore if the origin and destination of the neutrons are fixed, and the flight time of the neutron recorded then it is possible to determine the wavelength of that neutron via a modified de Broglie equation (3.11). This can then be converted into d-spacing by recording the angle at which the neutron arrives (equation 3.12), where h is Planck's constant, m the mass of the neutron, θ is half of the 2θ where the neutron arrives after it is diffracted and t, L are the total total flight time and path from the moderator to the detectors respectively. The

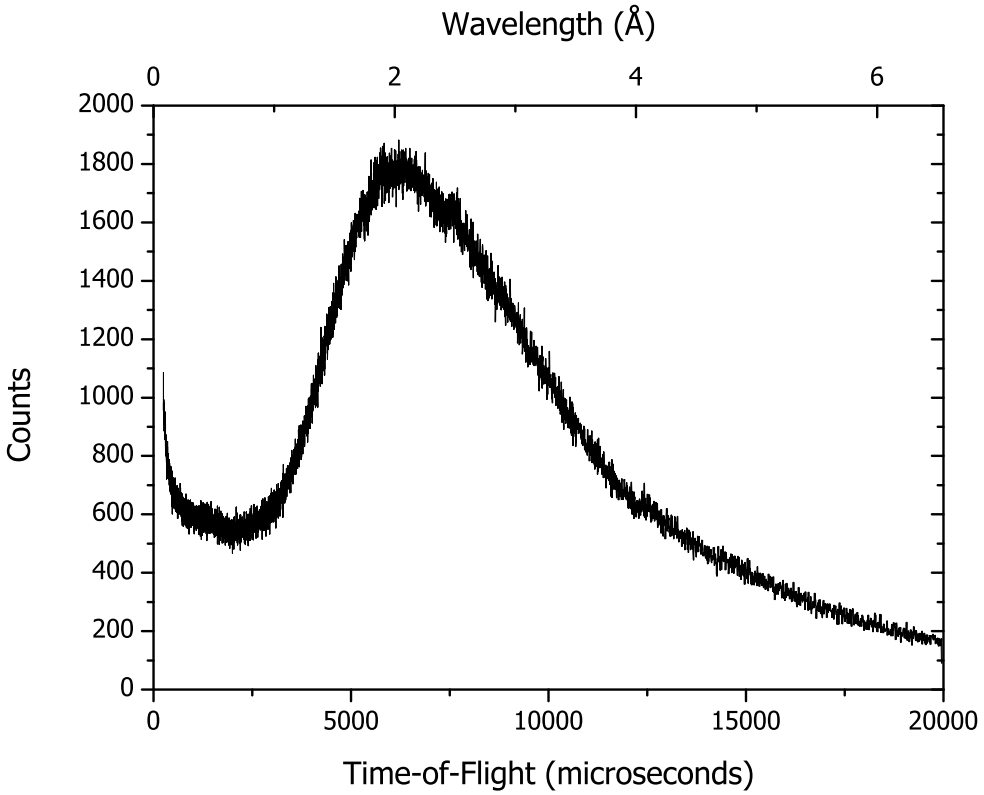

Figure 3.4 *Incident neutron flux profile on the PEARL instrument at the ISIS neutron source after the neutrons pass through the methane moderator held at ∼ 111 K. The reference spectrum shown here is noisy due to the data collection time of less than 10 minutes.*

ToF and wavelengths of the incident flux on the PEARL instrument can be seen in figure 3.4.

$$\lambda = \frac{ht}{mL} \tag{3.11}$$

$$d = \frac{ht}{2mLsin\theta} \tag{3.12}$$

This is one of the benefits of spallation sources as more of the incident flux is used compared to reactor sources where most of the flux is lost through monochromatisation. This is due to there being no other way, apart from monochromatisation, to tell the wavelength of an incoming neutron at a reactor source as there is no way to determine origin, or how long the neutron has been travelling. At spallation sources this is possible as the neutrons have a fixed origin and destination, and therefore a known path length. This path length is usually accurately calibrated with use of a sample with well known d-spacings such as silicon. The discrete pulses of neutrons produced by the bunches of protons also mean the start and arrival time can be accurately recorded. However, this relies on there being no overlap between the slow neutrons of one pulse and the fast neutrons of the next. This can be fixed with the use of choppers.

Another benefit of using the ToF technique for diffraction experiments is the resolution ($\Delta d/d$) which is governed by equation 3.13 [69]. From equation 3.13 it can be seen that the factors controlling the resolution of a ToF diffractometer are the uncertainties in scattering angle θ, timing and the path length L. As the systems for timing the pulse start and detection are so precise the contribution from the t term is essentially zero. From equation 3.13 it can also be seen that as 2θ increases from 0 to 180° the contribution of θ to the resolution decreases to near 0. For this reason back-scattering detector banks are used for high resolution work if allowed by the sample environment. However, the opposite is true for banks located at small angles which have low resolution and tend not to be used in the work presented here.

$$\frac{\Delta d}{d} = \left[\Delta\theta^2 cot^2\theta + \frac{\Delta t^2}{t^2} + \frac{\Delta L^2}{L^2}\right]^{\frac{1}{2}} \tag{3.13}$$

One of the best ways to improve resolution is to increase the path length. As neutrons could originate from any position in the moderator, the uncertainty

in the flight path is mainly due to the thickness of the moderator ΔL. By increasing the path length, the arrival times of the neutrons are more spread out giving a higher resolution. However, this comes with a loss of intensity so may not be suitable for extremely small samples such as those used in high pressure experiments.

3.4.4 Practicalities of Neutron Diffraction Experiments

The basics of ToF neutron diffraction are covered in the previous sections, however, there are some issues that come with the practicalities of carrying out a neutron diffraction experiment such as collection times, the deuteration of samples and how to get reliable intensities/structure factors.

Reliable Intensities

Reliable intensities are required to obtain reliable structural information. As can be seen from figure 3.4, the intensity of the incident neutron flux varies across the range of wavelengths which would result in unreliable diffracted intensities. To account for this the collected diffraction pattern is usually normalised to the flux profile such as the one shown in 3.4. In addition to this normalisation, attenuation effects need to be considered, such as the incident neutrons absorbed in the sample environment or by the sample. Beam can also be lost at specific wavelengths through significant diffraction of the sample environment. How these issues were dealt with are discussed for each high pressure apparatus used in chapter 4.

Peak Shapes

In general the profiles of the peaks in diffraction patterns collected at reactor sources are easier to model than those collected in the ToF geometry. This is because at reactor sources the peak shapes tend to be described by Gaussian or Lorentzian functions whilst data collected at spallation sources also have this shape but include some of the 'spallation profile' (flux profile) superimposed on to it. This superposition of the flux profile onto the peak shape is due to the moderation of the neutrons and results in an asymmetric peak shape. This means that specialised software is often needed even when fitting a single peak. This is

done in the work presented in this thesis in GSAS which can fit the 'Jorgensen' function needed for the ToF profile shape. However, unlike data collected at reactor sources where the peak shape may vary over the range of data collected, the profile of ToF collected data is generally constant for the whole pattern within a given 2θ range.

Data Collection Times and Backgrounds

In addition to the factors mentioned above there are other issues to consider like backgrounds and data collection times. The first of these, the background can be minimised by reducing the incoherent signal coming from the sample. For example, using certain isotopes that have smaller incoherent scattering lengths/cross sections can minimise the background such as the use of deuterated samples instead of hydrogenous samples as hydrogen is a strong incoherent scatterer (table 3.2). To reduce the background signal from sample environments, shielding made with materials that are strongly neutron absorbing such as cadmium, boron or gadolinium, are used.

One of the reasons that so much care has to be given to improve the sample signal to background noise ratio is that the strong nuclear force is much weaker than the electromagnetic force which governs the interaction of x-rays and matter. This combined with the fact that neutron sources are generally not as bright as modern synchrotrons results in low sample signal to background ratios. This can be improved by collecting data for longer timescales to improve statistics or by increasing the size of samples. This is a problem for high pressures where small sample sizes are generally needed.

Chapter 4

Neutron Diffraction At High Pressures

Due to the combination of the weak interaction of the nuclear force and the low neutron flux produced at neutron sources, large sample volumes are needed in neutron diffraction experiments to improve the sample signal to background ratio. This is an issue when performing neutron scattering measurements at high pressure as pressure is generally applied to the sample by reducing the volume available to it. For neutron diffraction experiments 'large-volume' apparatus have been developed to generate pressure such as the Paris-Edinburgh press (with sample volumes larger than 25 mm^3) and more recently, large volume diamond anvil cells that have volumes between 0.06 and 0.2 mm^3 [80]. This chapter gives an overview of each of the high pressure devices used (gas cells, Paris-Edinburgh presses and diamond anvil cells) and the experimental beamlines on which they are used, any specialist loading techniques used in conjunction with them and a brief description of any data preprocessing for the data discussed in chapters 5 - 8.

4.1 Gas Cells

In a gas cell the pressure is generated on a sample by a compressed gas such as helium or hydrogen. As can be seen in figure 4.1, a gas cell is composed of a cylindrical body with a sample chamber located in the centre that is connected

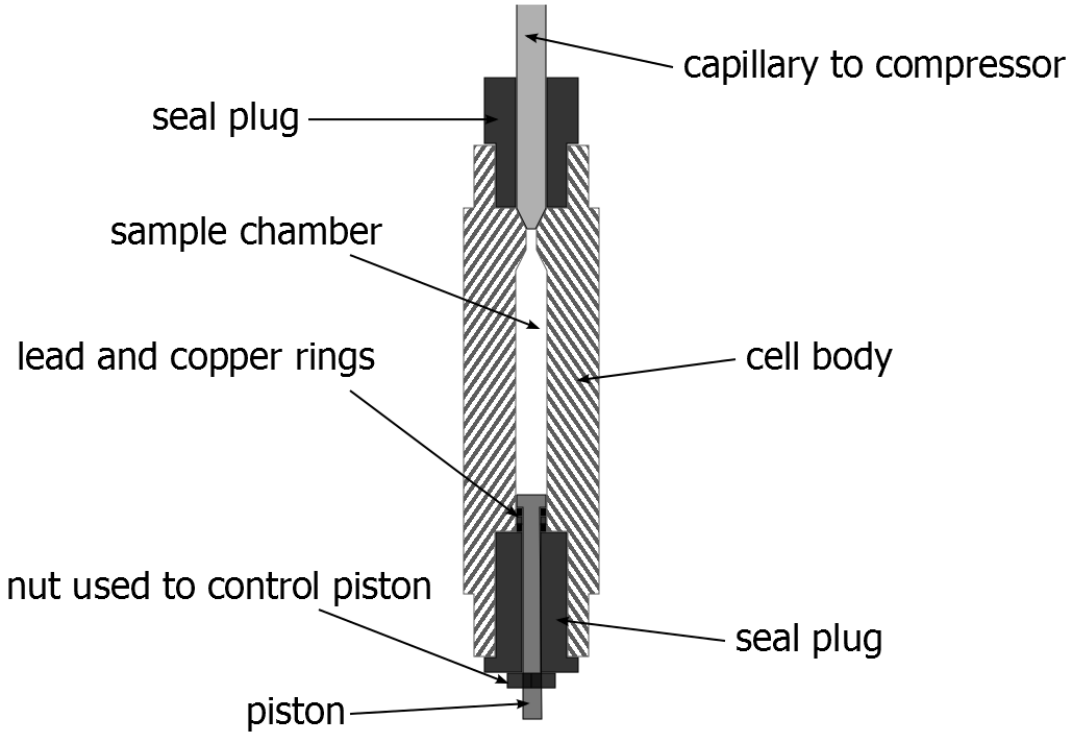

Figure 4.1 *A schematic of a gas cell. The piston and lead/copper rings located at the bottom form a Bridgman seal.*

to a capstan compressor pump via a capillary at one end and is sealed by a Bridgman seal at the other [81]. The gas is compressed by the pump and the sample pressure is taken as being the pressure of the compressed gas. In the work presented in later chapters two gas cells are used with one made of the null neutron scattering alloy titanium zirconium (TiZr) and the other of aluminium. Though both of these gas cells are constructed in the same way the aluminium gas cell is used for experiments on the D_2-D_2O system due to the reactivity of TiZr with hydrogen [72]. To prepare a sample, pre-powdered D_2O ice or deuterated water is loaded into the sample chamber before the cell is sealed and attached on to the bottom of a 'stick' which the capillary is fed through. The whole set up (compressor-capillary-cell) is then checked for leaks via a helium pressure test. This is where pressure is applied to the system with compressed helium at the maximum pressure allowed and the pressure monitored to ensure there are no leaks within the connections between compressor, capillary and the cell. The gas cell is then mounted into a cryostat on a diffraction instrument and data collected at various pressures and temperatures.

Gas cells have many advantages over other high pressure techniques such as

shorter data collection times due to the large sample volume, good control of the sample pressure and easy adaptability to many instruments. One of the main disadvantages to gas cells are that they have a very limited pressure range. For example the TiZr and aluminium cells used in the work presented in the later chapters, the maximum pressures allowed are 0.5 and 0.3 GPa, respectively.

4.1.1 Instrument Beamlines

As stated above, the gas cell can be easily used on many different instruments. Here an overview of the GEM and PEARL instrument beamlines used at the ISIS spallation neutron source at the Rutherford Appleton Laboratory are given. Both of these instruments have fixed (constant θ) ZnS scintillator detector banks consisting of multiple modules and make use of the time-of-flight method discussed in 3.4.3. The detector modules span several 2θ and data are collected as ToF spectra in each pixel of these modules. Following this collection the data are then put through a preprocessing procedure known as 'focussing'. This is where the ToF spectra for each pixel in a detector module are converted into d-spacing via the modified Bragg's Law (3.12) and summed together. This results in a complete diffraction pattern for each module that can be checked to ensure that the sample diffraction pattern is consistent throughout before the diffraction patterns for all modules in the detector bank are combined together to give the final diffraction pattern that can then be used for analysis with Rietveld refinement or with the Le Bail extraction method. The error in the number of counts detected in each pixel (N) for a given ToF (the intensity) is given by $\sqrt{N}$ and is carried through the focussing procedure. This is a standard procedure and is not tested further in this work. During this process an attenuation correction may be applied if needed (section 4.1.2). All of this is done with use of the Mantid software before the data is analysed by Rietveld or Le Bail refinement within the GSAS crystallographic software suite [76, 82].

GEM

The GEM instrument is a general purpose materials diffractometer [83]. It has a primary flight path of 17 metres (distance between moderator and sample) and secondary flight paths between 1.0 and 2.9 m (distance between sample and detectors)[84]. Six large detector banks covering from 1.1° to 169.3° are arranged

around a central sample tank that can accomodate the OC100 cryostat used in the gas cell experiments [84]. This large detector coverage is of good use for not only diffraction of crystalline materials but also disordered materials.

PEARL

The PEARL instrument is a specialised high-pressure diffraction beamline and is optimally designed to be used with Paris-Edinburgh presses (see section 4.2 for more details). As PEARL is located closer to the methane moderator than the GEM diffractometer it has a shorter primary flightpath of 12.8 m. The ZnS scintillator detectors that surround the large sample tank are either at distances of 0.8 m or 1.2 m [85]. Unlike the GEM diffractometer, the detectors on PEARL do not give a large angular coverage but instead are concentrated at specific 2θ that best suit the use of Paris-Edinburgh presses. These fixed detector banks are located at 90° ($81.2° < 2\theta < 98.8°$), a low angle bank covering a range of $20° < 2\theta < 60°$, and a back-scattering bank covering a range of $100° < 2\theta < 160°$ (see figure 4.2). Though this may seem like a large area of detector coverage in the standard Paris-Edinburgh press geometry only some of these detectors can be accessed at any one time. In transverse mode (through-anvil) the banks at 90° are the only ones that can be accessed. In longitudinal mode (through-gasket) the other banks can be accessed, with the 90° bank being shielded by the press itself.

4.1.2 Attenuation Correction for the Gas Cell

When the neutron beam passes through the sample environment (such as the gas cell body or anvils of a Paris-Edinburgh press) there can be significant amounts of neutrons either absorbed or diffracted out of the beam resulting in a significant loss of intensity at specific d-spacings. To correct for this and determine accurate intensities an attenuation correction has to be applied. This is done by determining how much of the beam is lost through the sample environment. Usually if certain sample environments are used on a regular basis on an instrument, such as a Paris-Edinburgh press on the PEARL instrument, an attenuation correction has been pre-determined and is applied in the focussing procedure. However, no attenuation correction for the aluminium gas cell used on the PEARL instrument had been determined prior to this work. In the case

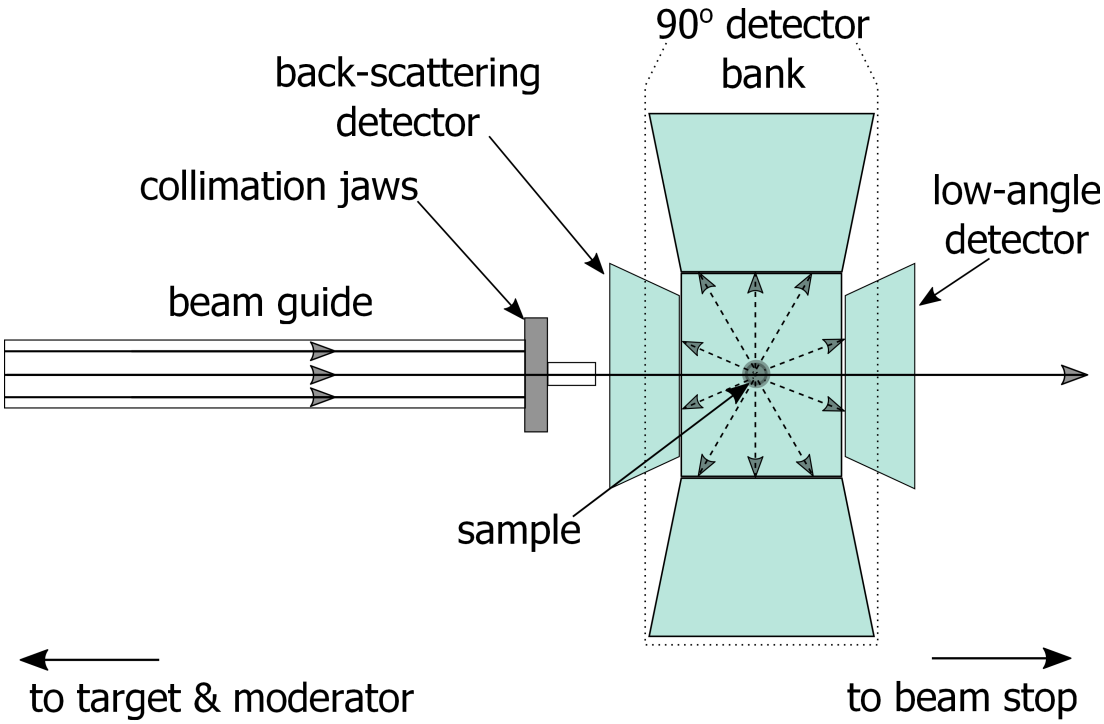

Figure 4.2 *A schematic of the PEARL instrument at the ISIS neutron source at the Rutherford Appleton Laboratory showing the path the neutrons take once they enter the experimental hutch. The 90° detector bank consists of 9 modules that are arranged in an arc around the sides and underneath the sample position. Solid lines mark the path of incoming neutrons and dashed lines path of neutrons diffracted from sample.*

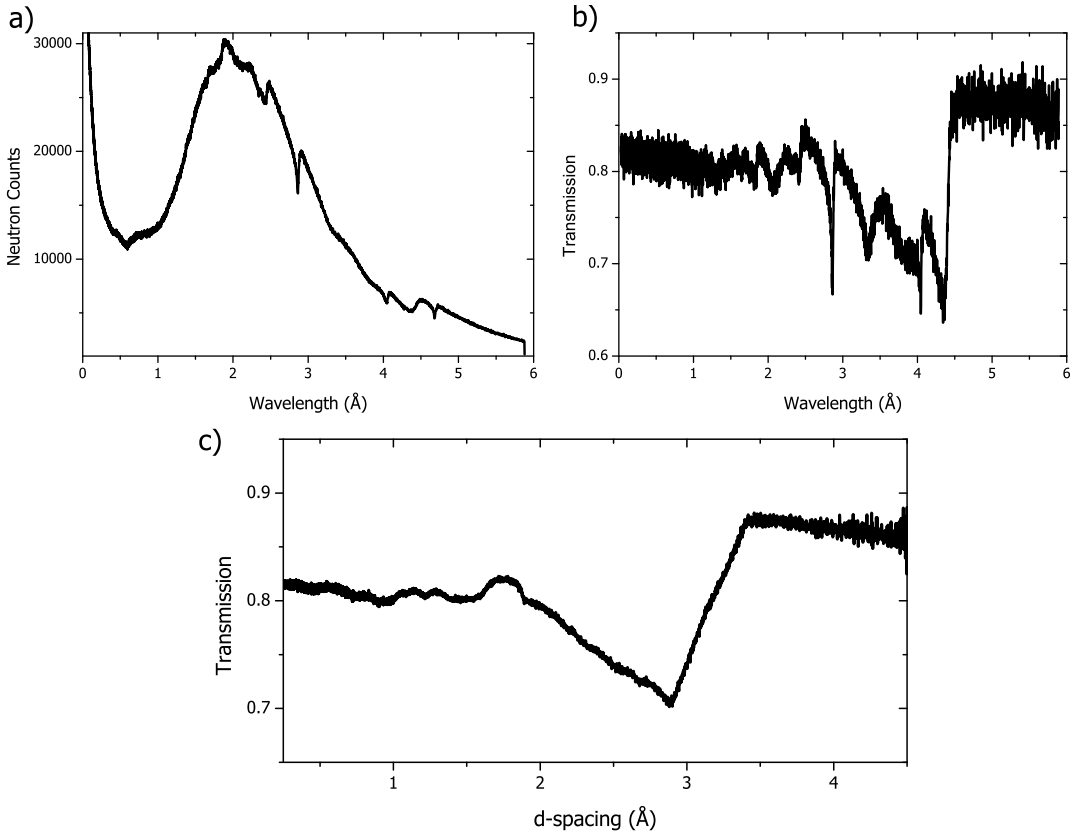

Figure 4.3 *Figure (a) shows the transmission of the aluminium gas cell and cryostat. Figure (b) shows the transmission shown in figure (a) normalised to the neutron flux profile like the one shown in figure 3.4. Figure (c) shows the transmission function of (b) 'smeared' out as a function of d-spacing.*

of the null scattering TiZr gas cell used on the GEM instrument the attenuation correction is applied during the Rietveld refinement as this is a purely linear function of neutron wavelength and is discussed later [72].

To determine the attenuation correction the empty aluminium cell (without powdered D_2O ice and the D_2 gas) was placed in a cryostat and transmission of the neutron beam monitored (figure 4.3a). Afterwards a measurement of the transmission was taken without the cryostat and gas cell to determine the neutron flux profile (similar to the one shown in figure 3.4). These two measurements of the transmission are then divided one by the other and the resulting plot shows the 'Bragg edges' in the transmission for the combination of cell and cryostat where there is significant beam lost at wavelengths between 2.5 and 4.5 Å (figure 4.3b). At this point the correction could be applied to the data as a function of wavelength in the focussing procedure described in 4.1.1 prior to conversion to

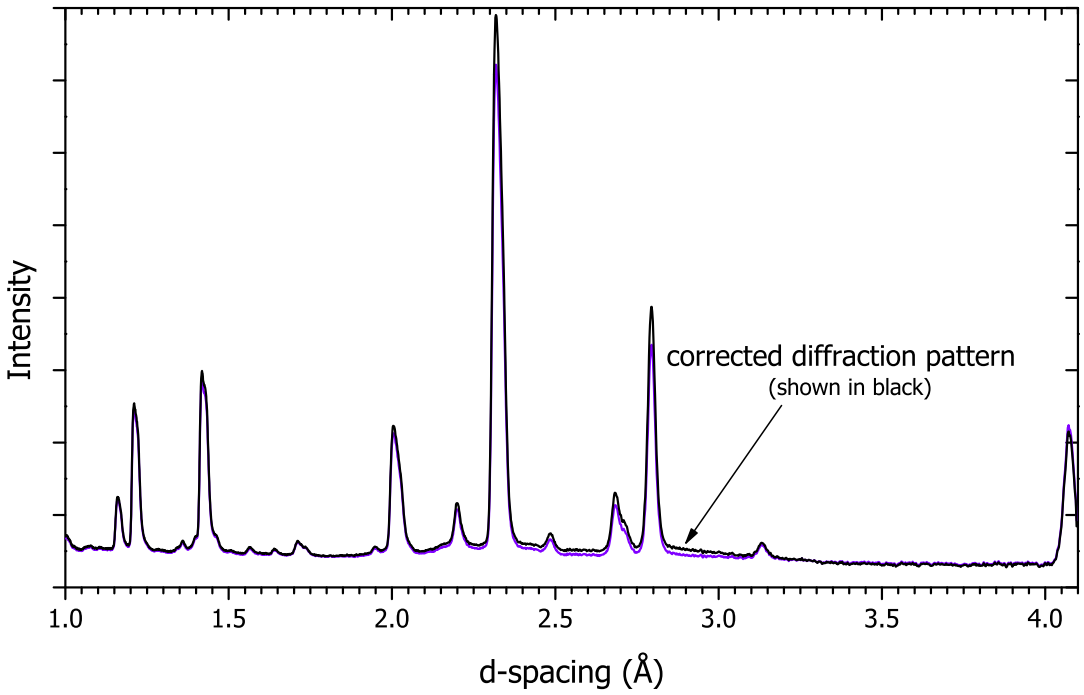

Figure 4.4 *Comparison of the attenuation corrected and uncorrected diffraction patterns collected on a sample of D_2–D_2O. The corrected pattern is shown in black and the uncorrected in purple.*

d-spacing. However, here the attenuation correction is converted into d-spacing before being applied to the data. To do this the 90° detector banks which span angles 81.2° to 98.8°, were split up into 0.88° degree intervals (ie. angles at 82.08, 82.96°) and the attenuation correction converted to d-spacing for each of these angles. The transmission spectra for all of the angles are then merged together to create the spectrum shown in figure 4.3c. This is then applied to the data before Rietveld refinement. As can be seen in figure 4.4 this can have the effect of changing the ratio of the observed reflection intensities.

4.2 Paris–Edinburgh Press

The Paris-Edinburgh press (PE press) is a large-volume opposed anvil device usually used for high pressure neutron diffraction. In this type of device the pressure is generated in the sample by restricting the volume that is available. Depending on the anvil material and gasket design the PE press can reach sample pressures above 25 GPa. Though there are a variety of different types of PE presses used the only PE press used in this work is a VX-type press as it can be used in conjunction with a loading clamp used for gases. There are three main

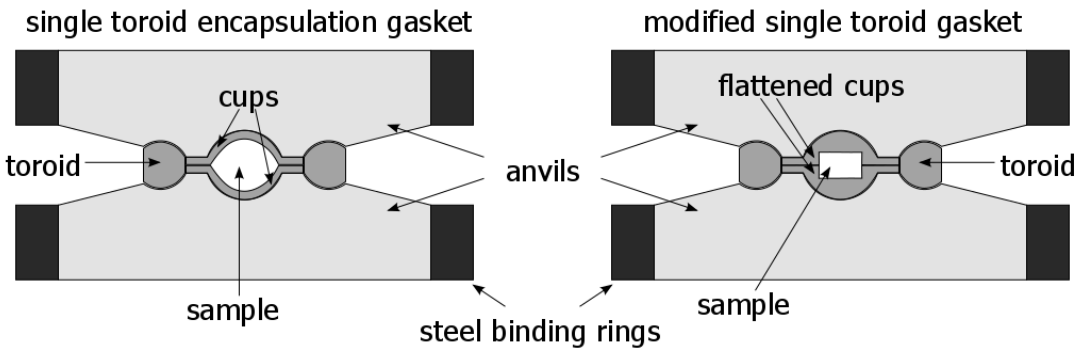

Figure 4.5 *On the left is a standard single toroid encapsulation gasket and on the right the modified single toroid encapsulation gasket used in the D_2 loading of a PE press.*

parts to the press used in this work; the press body, the loading clamp and the anvil/gasket set up. The anvil/gasket set up is shown in figure 4.5. The anvils are usually made from a hardened material such as sintered diamond or, used in this work, tungsten carbide (WC). The type of gasket used in this work (on the neon-water system) to hold the sample between the two anvils is a 'single toroid encapsulation gasket' that consists of two cups made from the null scattering alloy TiZr surrounded by a toroidal ring that is sealed with the application of load to the anvils (shown on the left in figure 4.5) [65, 86]. Another gasket that is a modified version of this single toroid gasket is used for deuterium loaded PE presses. This modified gasket, made from a deuterium-proof copper beryllium alloy has flattened cups to reduce the volume needed to fill with D_2 and thus increasing the applied load to sample pressure ratio. This modified gasket reduces the sample volume from ~ 100 mm^3 (standard single encapsulation gasket) to ~ 27 mm^3.

In a standard set up the anvil/gasket set up is placed directly into a PE press. However, as the gasket and anvils are required to contain the gas in the work here, they are placed in a specially designed loading clamp that allows high density gases to be loaded into the sample chamber (shown in figure 4.6). This clamp has a locking mechanism that means once load has been applied to the anvils to seal the gasket the locking mechanism can hold this load on the clamp [87, 88]. Once loaded the clamp is then placed inside a VX-type press (shown in figure 4.6). This type of press has two tie-rods giving it large windows that mean it is normally used for single crystal measurements or for use with long detector banks at reactor source [89]. Pressure is increased in the sample by load being applied to the piston with hydraulic fluid.

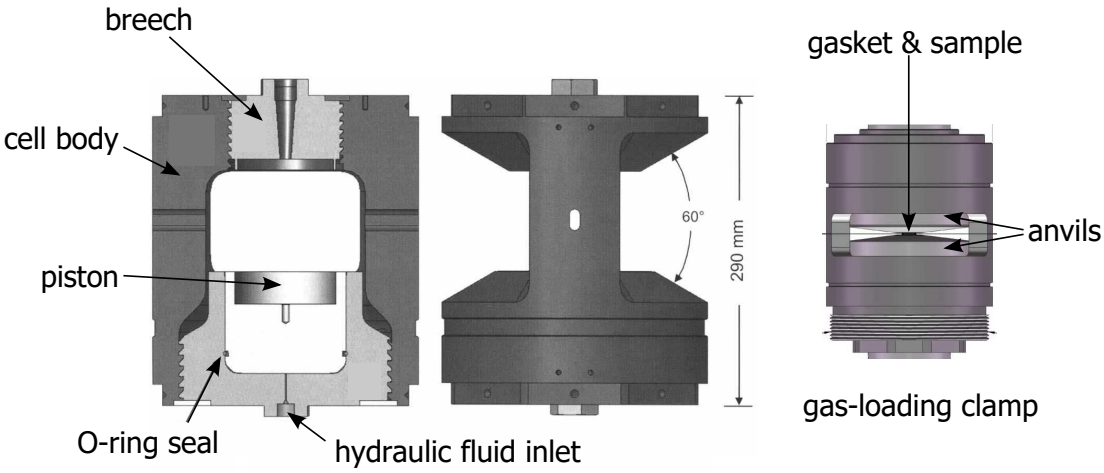

Figure 4.6 *Schematic of a VX-type Paris-Edinburgh press (two leftmost) and the gas loading clamp that fits into the VX press. Image is modified from references [87, 89]*

4.2.1 Loading Procedure

As gases such as neon or hydrogen are extremely compressible they need to be loaded at pressure to reduce the loss of sample volume upon compression. This is done with use of a hydrogen compatible gas-loader for PE presses [87]. This gas-loader is of a similar design to other gas loaders previously made for Paris-Edinburgh presses, however comes with an interior copper beryllium alloy liner to make it suitable to load hydrogen [87]. It is designed to accommodate the gas-loading clamp shown in figure 4.6. Prior to the work presented here there were several successful loadings of pure deuterium and one successful loading of a mixed D_2-hydroquinone system all at 0.2 GPa. All of these sample loadings failed to be compressed however as they 'blew out' immediately on compression from the initial loading pressure of 0.2 GPa. More details of the gas loader can be found in [87].

In the work presented in chapter 8 two different systems make use of this gas loading technique; the deuterium-urea system and the neon-water system. The type of gasket used is dependent on which gas is loaded. The standard encapsulation gasket is used for neon and the modified gasket is used for deuterium (figure 4.5). First the anvils and gasket are set up in the gas-loading clamp and powdered deuterated urea or liquid D_2O is placed in the lower half of the gasket, and a gap of a few millimetres left between the lower and upper encapsulation cups. The gas loading clamp is then sealed inside the gas loader. For the D_2-urea loading the gas-loading vessel was evacuated, however this was

not done in the Ne-D_2O loading to avoid the loss of the liquid D_2O. Prior to a loading with deuterium, the whole system is taken up to 0.2 GPa with helium and left for one hour to test the seals and check for leaks. Following this, the gas loader is taken up to 0.2 GPa with neon/D_2 before the clamp is sealed with the application of load and the locking mechanism tightened to retain the high density neon/D_2 gas in the sample volume. This process has been fully described elsewhere [87]. The sealed clamp is then placed in a VX3 variant PE press and mounted on the PEARL instrument in transverse mode (section 4.1.1) for data collection.

4.2.2 Data Preprocessing and Attenuation

Both of the experiments on the neon-D_2O and D_2-urea system were done on the PEARL instrument and the data-processing protocol is outlined in 4.1.1. Just as the gas cell data needed to be corrected for attenuation of the beam, the data here had to be corrected for attenuation of the beam through both the upstream anvil and the gasket. In the case of the anvils, both samples used tungsten carbide and the attenuation correction for these is built into the focussing routine used in Mantid on PEARL. The attenuation of the gasket was not treated for different reasons for each sample. In the case of the D_2-urea system, the gasket used is a copper beryllium alloy that is known to attenuate the beam strongly. As the sample signal was so weak and the urea was precompressed into pellets to ensure that the sample would not blow away which resulted in a highly textured (bad) powder that would give unreliable intensities. In the case of the Ne-D_2O sample, this resulted in an unsuccessful loading so was not corrected.

4.3 Diamond Anvil Cells

Diamond anvil cells (DAC) are an opposed anvil device that consists of two diamonds which are pressed together and between them sits the sample of interest held in place by a thin metal gasket. An example of the type of DAC used in this work can be found in figure 4.7. Unlike the gasket for a PE press the gasket used for a DAC is made from a thin sheet of metal that is pre-indented by forcing the diamonds together, and then a small sample hole is drilled with use of an electro-discharge machine. This type of apparatus has long been used for structural

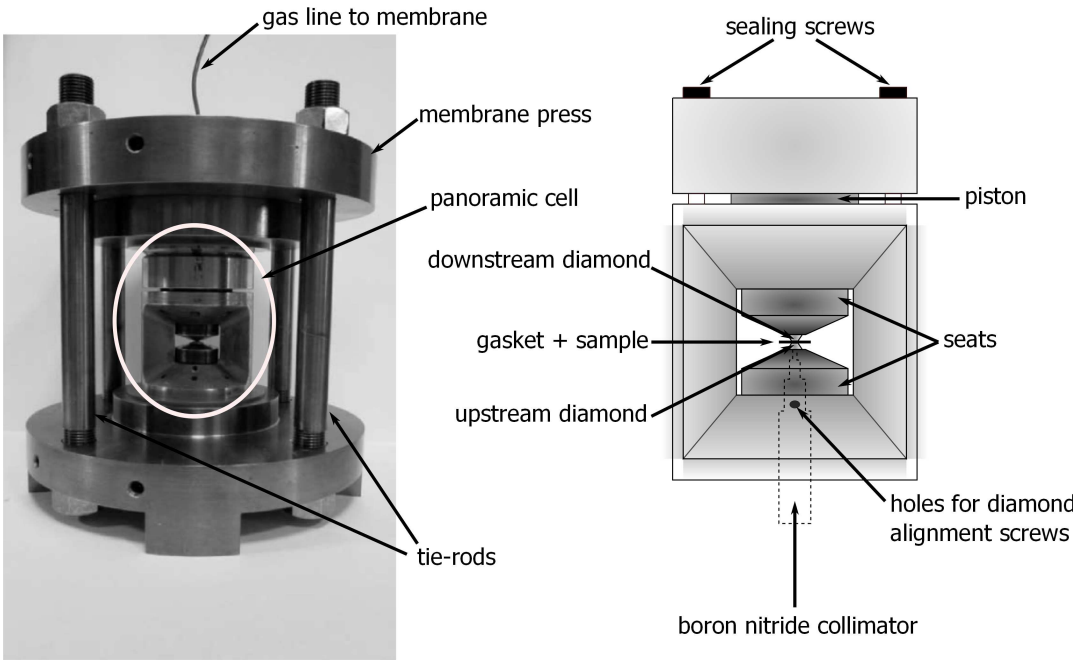

Figure 4.7 *On the left is the panoramic cell in the membrane press. Image modified from [80]. On the right is a schematic of the panoramic diamond anvil cell.*

studies at high pressures with x-ray diffraction [90]. However they have only been used in the past in combination with neutron diffraction on very rare occasions [91, 92, 93]. This is due to a combination of the small sample sizes conventionally used in DACs, the weakness of neutron sources and the expensiveness of large single crystal diamonds. Only recently have the use of diamond anvil cells with neutron diffraction become more routine [80, 94, 95, 96]. .

There are a variety of different designs of the large-volume diamond cells that are capable of reaching different pressure regimes [80]. Here a 'panoramic' type cell with a modified seat design is used [80, 97, 98]. This modified seat design is a WC seat with a bore in the centre to allow optical access to the cell and neutrons to be collimated to the back of the diamond, this WC seat is then pressed into

a steel ring for support. A similar support ring is used in large volume opposed anvil cells such as the PE press (4.2). One seat is attached to the piston and pressure can be applied by tightening the four screws (2 left-handed and 2 right-handed) that drive the piston (and hence top diamond in figure 4.7) towards the bottom diamond. As the diamonds used for neutron diffraction have much larger culet sizes (>1 mm) than those typically used in a conventional DAC, the forces required to seal the gasket and generate pressure in the sample, are much greater than those in a conventional DAC [80]. The maximum pressure that can be reached purely on the screws by hand is usually $\sim$ 6 GPa, but this is entirely dependent on the quality of the sample loading and the type of loading (liquid or solid etc.). To increase sample pressure further a secondary press is required. This secondary press is shown in figure 4.7. This press consists of a membrane filled with helium gas which then drives the piston resulting in an increase in sample pressure. With this set up and 1.6 mm culets the sample can be compressed to pressures just above 30 GPa. If optical access is available to the cell then pressure calibration is with the ruby fluorescence scale, if there is no optical access to the cell (for example the cell is placed in a cryostat) then pressure determination is from the sample equation of state [99].

4.3.1 D_2 - D_2O Loading Procedure

In chapter 8 a loading of D_2-D_2O is studied. A small circle of T301 stainless steel with initial thickness 300 μm was used for the gasket. This circle was polished to a mirror finish to ensure that a seal would be made when gas-loading with deuterium. Diamond culets of size of 1.6 mm then pre-indented the gasket to $\sim$ 175 μm before a gasket hole of 1.1 mm was drilled. A ruby sphere is placed on the piston side diamond and D_2O was placed in the gasket on the bottom diamond and left to evaporate until about a third of the gasket volume remained. This was then sealed and opened only when under a D_2 atmosphere of 0.2 GPa in a gas loader. The cell was then sealed at 0.2 GPa and unloaded from the gas loader. The sample was then increased in pressure to $\sim$ 3 GPa to freeze it into the desired phase before data collection on the SNAP instrument.

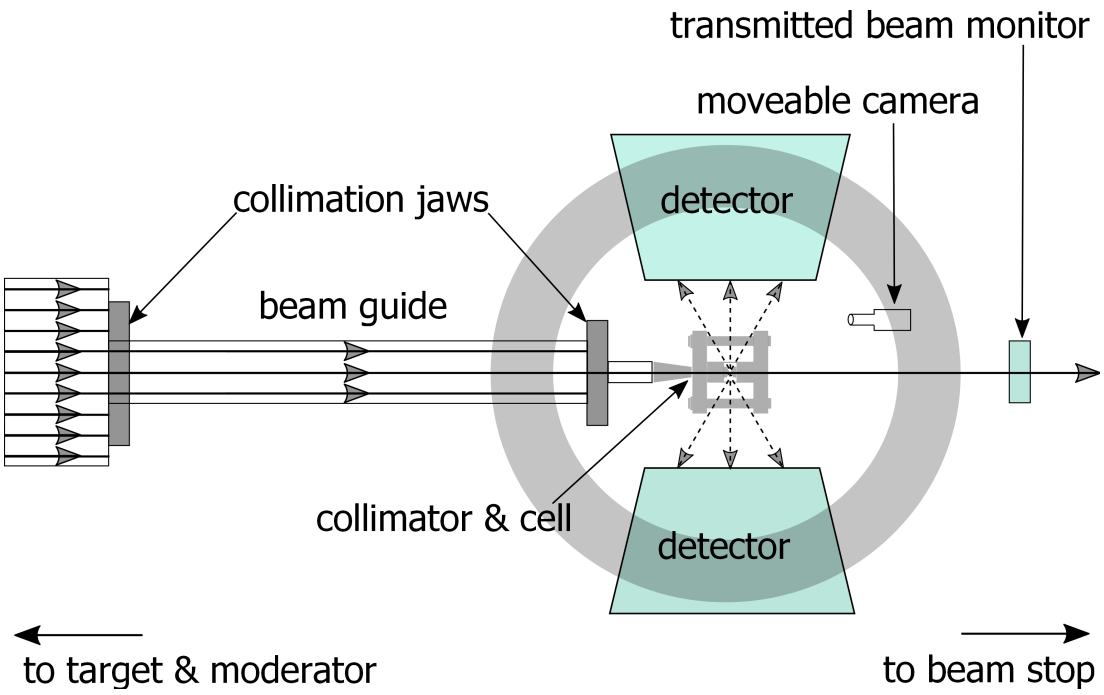

Figure 4.8 *A schematic of beamline 3 (Spallation Neutrons and Pressure - SNAP) at the Spallation Neutron Source (SNS) showing the path the neutrons take once they enter the experimental hutch. Solid lines mark the path of incoming neutrons and dashed lines path of neutrons diffracted from sample.*

4.3.2 Spallation Neutron Source - SNAP

The SNAP beamline (Spallation Neutrons and Pressure) is located at the Spallation Neutron Source at the Oak Ridge National Laboratory in the USA. At this facility the protons impact on a liquid mercury target creating neutrons that pass through a hydrogen moderator on their way to the sample [100]. There is a primary flight path of 15 m from the moderator to the sample position. The sample and sample environment used such as cryostats all sit on a hexapod which allows easy alignment of the sample to the centre of the detectors and to the beam. This hexapod can also be used to rotate the sample so that the beam can hit the sample straight on or at an angle. Unlike PEARL and GEM that have fixed detector banks, SNAP has movable detectors. These detectors sit on an arc (shown in figure 4.8) and can be rotated to access different 2θ for example back scattering or small angle scattering. Overall SNAP has an angle coverage of $26^\circ < 2\theta < 138^\circ$ [100]. However, for diamond anvil cells the angular access is restricted and these detectors are only used in the $2\theta = 90^\circ$ geometry as shown in figure 4.8.

4.3.3 Alignment and Collimation

As the sample inside the DAC is so small the beam needs to be collimated down to the size of the sample and care must be taken with alignment of the sample to the beam. To collimate the beam to ~ 500 μm in diameter a series of steps are taken. The collimation jaws shown in figure 4.8 cut the neutron beam down to ~ 1 cm in diameter. After the jaws there is further collimation that consists of a small tube made of boron nitride followed by a collimator which is attached to the cell and membrane clamp. This final collimator goes to the back of the upstream diamond and consists of a series of steps that give it a roughly conical shape (figure 4.7). Further collimation is placed around the windows of the cell to minimise scattering from the cell body. In addition to the collimators, cadmium shielding is attached to the upstream side of the membrane press to minimise background scattering. As the sample studied here is transparent, the cell is aligned to the neutron beam via alignment to a laser which has been pre-aligned to the beam with use of the movable camera and the hexapod (figure 4.8). The sample can also be aligned by monitoring the transmission of neutrons through the sample with the downstream transmission detector and then moving the sample to a position where this is a maximum (see figure 4.8).

4.3.4 Attenuation

The attenuation caused by the upstream diamond is the most significant cause of beam loss. However, the attenuation affect of the diamonds is only found to have an effect on the intensities below 2 Å (see figure 4.9). The transmission of the diamonds is also found to decrease at higher pressures as more load is applied to them putting them under a greater strain [101]. As the separation of the contributions of the upstream and downstream diamond in the transmission is complex, a routine way of modelling this is currently under investigation [102]. As the method for correcting for the attenuation of the diamonds is an ongoing issue that is not discussed in this work, no attenuation correction has been applied and the data shown in chapter 8 are considered preliminary.

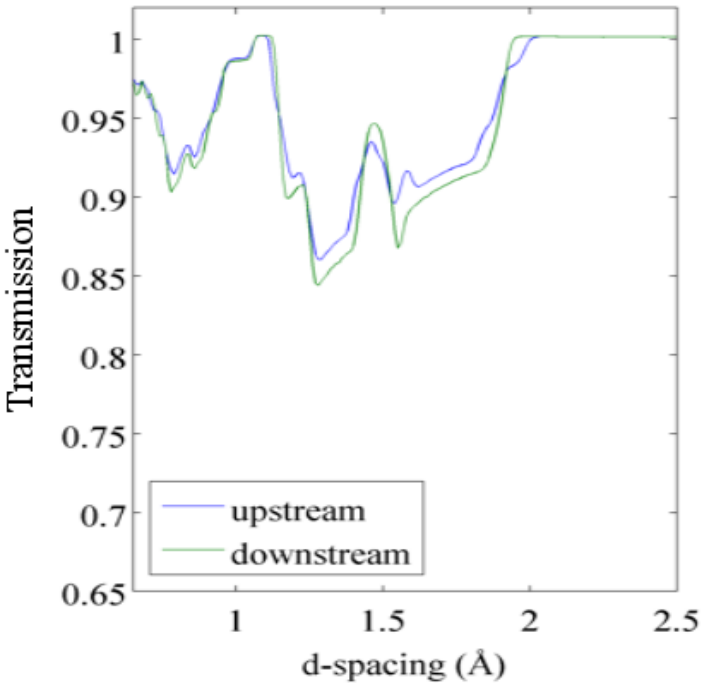

Figure 4.9 *An example of the transmission of the upstream and downstream diamonds under load showing that the attenuation will only have an effect on the intensities below 2 Å. Figure courtesy of Malcolm Guthrie.*

4.3.5 Data Preprocessing

After the data is collected it is viewed in the Mantid software where the single crystal peaks from the diamonds are masked and excluded from the data [82]. Although this has the effect of allowing small sample powder reflections at the same d-spacing as those from the diamond to be observed, this exclusion process also lowers the data statistics creating more noise in the background. In a similar fashion to the data collected on PEARL/GEM the data are then passed through the same 'focussing' procedure (section 4.1.1) to create a single diffraction pattern. An approximate background is then fitted to the data and removed before the diffraction pattern is converted into a form that allows Rietveld/Le Bail refinement in GSAS.

Chapter 5

Transitions in the Low Pressure D_2-D_2O System

Though the H_2-H_2O system has been well explored in the regimes above 1 GPa and below 0.2 GPa (see section 2.2 and references [32, 33, 34, 35, 36, 37]), there have been very few studies in the region between these pressures. The recent discovery of a new phase, C_0, at 0.5 - 0.7 GPa, that was reported to be a new clathrate structure with a H_2O network not observed in any of the known clathrates or ice phases, has prompted further studies on this system in this intermediate pressure region [34]. This chapter summarises the transitions between both metastable and stable structures in the D_2-D_2O system around 0.2 - 0.3 GPa between 130 K and 280 K. These metastable structures were observed in the stability region of the sII hydrogen hydrate clathrate and the transitions from these metastable structures occur in a sequence that is in line with Ostwald's Rule of Stages.

Three different routes were taken to study what effect temperature and pressure had on the formation of sII clathrate (shown on the phase diagram in figure 5.1). Diffraction patterns were collected with neutron diffraction *in-situ*, using the gas cell and cryostat described in section 4.1.1. All routes were started with near ambient pressure D_2O ice Ih in a D_2 atmosphere at 200 K before being compressed or cooled/compressed with D_2 gas. On route α the D_2O was taken from these initial conditions to 0.3 GPa with D_2, then warmed above the melt curve at 280 K before recooling to 200 K. Route β was similar to route α, however the ice Ih was initially cooled to 135 K near ambient pressure then compressed to

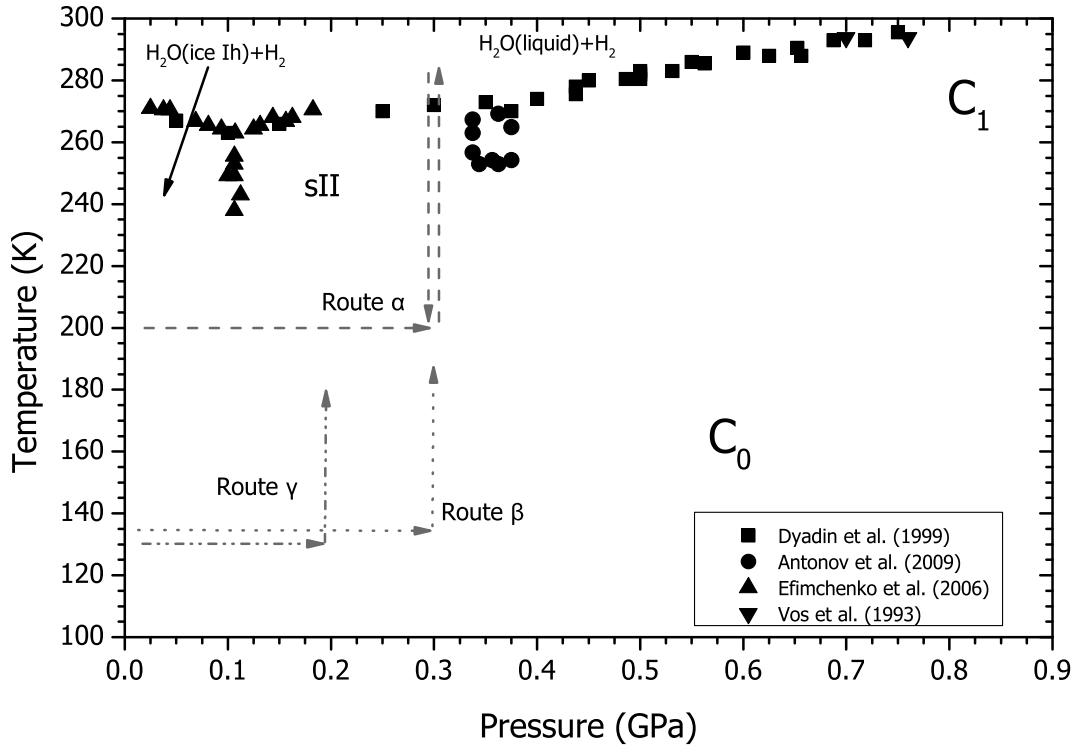

Figure 5.1 *Phase diagram of the H_2 - H_2O system showing previous experimental data on the phase boundaries obtained in references [32, 33, 34, 35, 36, 37]. The three routes taken through P-T space (α, β and γ) are marked on the diagram with dashed arrows.*

0.3 GPa with D_2 and warmed to 180 K. Route γ follows the same initial route as β but instead of compression to 0.3 GPa the sample was compressed to 0.2 GPa (γ-1) and 0.23 GPa (γ-2).

5.1 Route α

Immediately after compression to 0.3 GPa at 200 K, the ice Ih converted into the C_0 structure. The diffraction data collected at this point and in the subsequent warm-up/cool-down cycle are shown in figure 5.2. The sample was then warmed slowly in steps of 5 K and at 260 K new peaks started to appear. These reflections were indexed to the sII clathrate phase of hydrogen hydrate. As temperature was increased further the peaks from sII grew in intensity whilst the peaks arising from the C_0 structure decreased. The conversion of the sample from the C_0 structure to the sII structure was also accompanied with a large increase in the gas pressure, indicating that the C_0 structure was either denser, or richer in D_2

than sII, or a combination of both of these. It was not possible to quantify the absolute change in gas pressure due to safety reasons. As the gas cell was already operating at the maximum allowed pressure (0.3 GPa) any increase in gas pressure was immediately reduced back to 0.3 GPa. The sample was heated further and at 280 K it melted. This discrepancy in the melting temperature (∼10 K above where the sII phase in the H_2-H_2O system melts) is attributed to a slight hysteresis effect and not an isotopic effect as the sample started to refreeze into the sII structure at between 280 K and 270 K upon cooling. Further cooling resulted in the sample forming a mixture of sII and pure ice II at 250 K. The sample was further cooled to 200 K and was left at the same conditions C_0 had previously formed at (0.3 GPa and 200 K) before the warm up. However, after 10 hours there were no reflections from C_0 observed in the diffraction pattern. The non-formation of the C_0 structure at the same conditions as the previous observation suggest that the sII phase is the most stable configuration and the previous formation of C_0 at 0.3 GPa and 200 K was metastable with respect to sII. The non-formation of C_0 at these conditions is not thought to be caused by slow kinetics as C_0 formed rapidly upon the initial pressurisation from ice Ih and given the 'openness' of the cages of sII this would not have hindered the transition.

5.2 Route β

Route β was taken to investigate the impact of temperature on the formation of C_0. After the formation of ice Ih at 200 K the sample was cooled to 135 K at near ambient pressure then compressed to 0.3 GPa with D_2. At this point the diffraction pattern is still described by ice Ih (figure 5.3) despite the ice II (in pure ice) or sII (in H_2-H_2O) phases being the most stable under these conditions. The sample was heated and at 150 K it converted into a new structure, known as C_{-1} (see chapter 7 for details). The temperature was increased further where, at 180 K the sample converted into the C_0 structure.

5.3 Route γ

Route γ explores what effect pressure has on the transitions between the metastable structures observed on routes α and β, and is split into two parts

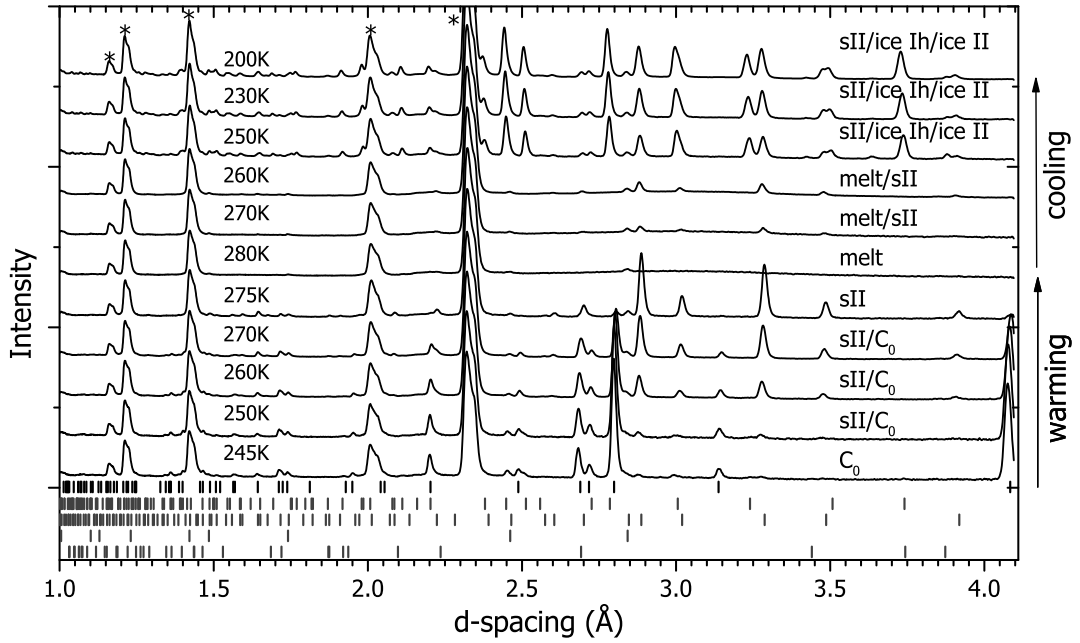

Figure 5.2 *Diffraction patterns obtained at 0.3 GPa whilst warming from 245 K to 280 K, and on cooling from 280 K to 200 K. Asterisks indicate peaks from the aluminium of the gas cell. Tick marks indicate reflections, from top to bottom, of C_0, ice II, sII clathrate, lead (gas cell seal) and ice Ih.*

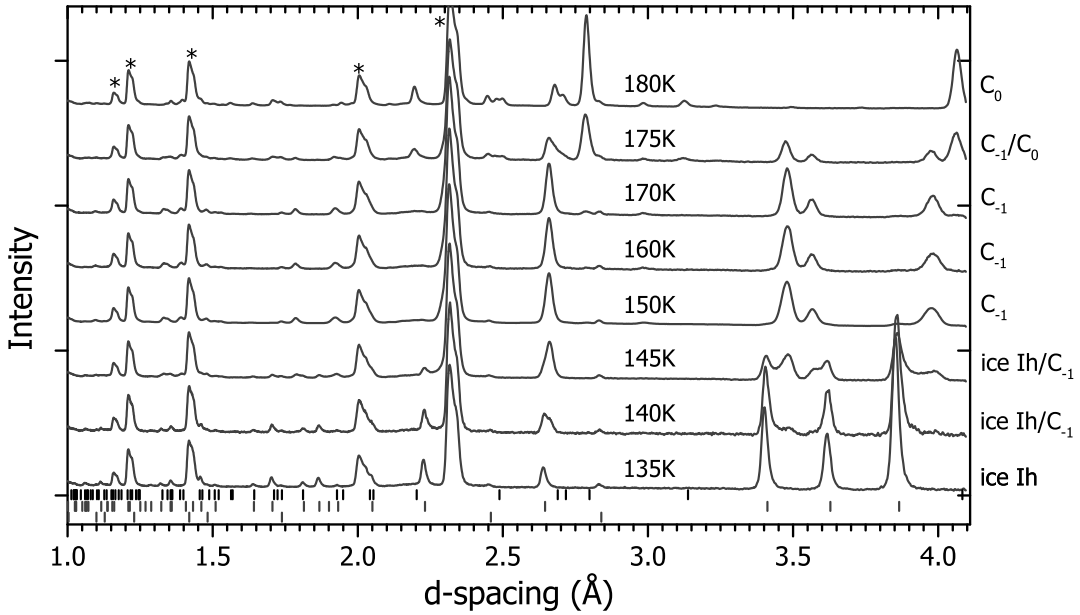

Figure 5.3 *Diffraction patterns obtained at 0.3 GPa on warming from 135 K to 180 K. Asterisks mark aluminium reflections from the gas cell. Tick marks indicate peaks that can be indexed as reflections from C_0 (top), ice Ih (middle), and lead (bottom). All other peaks are from the new structure C_{-1}.*

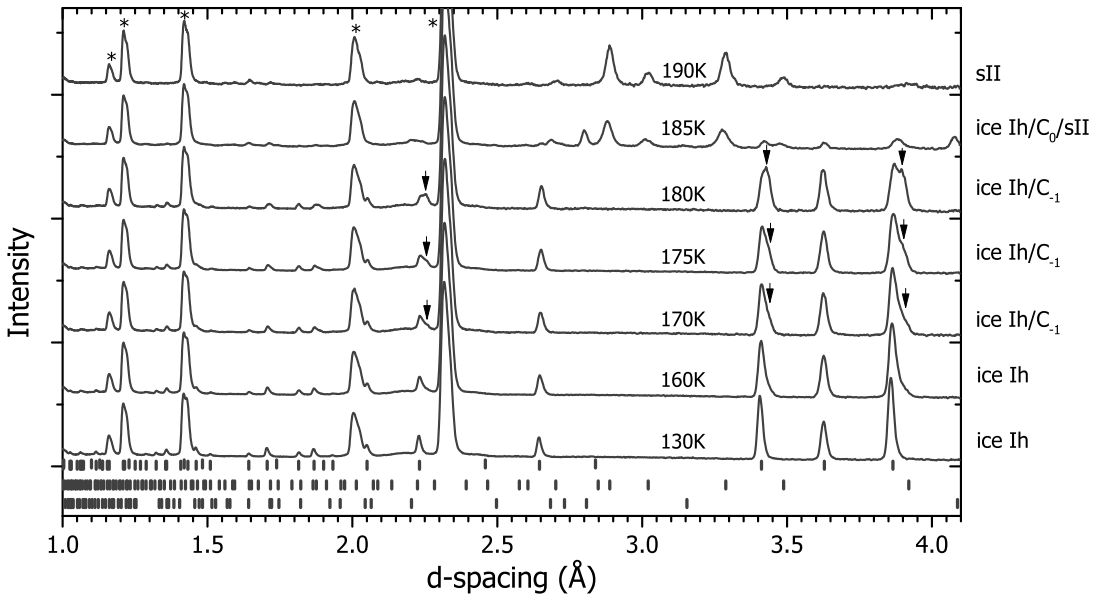

Figure 5.4 *Diffraction patterns from warming between 130 - 190 K at 0.2 GPa. Asterisks mark reflections from the aluminium gasket. Tick marks indicate peaks that can be indexed as reflections from ice Ih (top), sII (middle) and C_0 (bottom). Arrows indicate the peaks attributed to the growth of a new structure.*

γ-1 and γ-2. In a fashion similar to route β, both of these routes started as ice I at 200 K near ambient pressure before cooling to 130 K and compressed with D_2 to either 0.2 GPa (γ-1) or 0.23 GPa (γ-2). Although this change in pressure may seem relatively small, it had an effect on the transition temperature between metastable/stable phases and also allowed the behaviour of some peak shifts to be seen more clearly.

5.3.1 Route γ-1

After compression to 0.2 GPa at 130 K the diffraction pattern was still described by ice Ih (see figure 5.4), which is expected as these conditions are right on the boundary between ice I, II and IX/III [103] . As the sample was heated, splitting could be observed in some of the reflections from ice Ih, for example those at $\sim$ 3.4 Å and $\sim$ 3.85 Å in figure 5.4 at 170 - 180 K. This splitting is attributed to the appearance of a new structure that is similar in structure to ice I (structural details in chapter 7). At 185 K the sample converted into a mixture of sII and C_0, and at 190 K the diffraction pattern is described solely by sII clathrate.

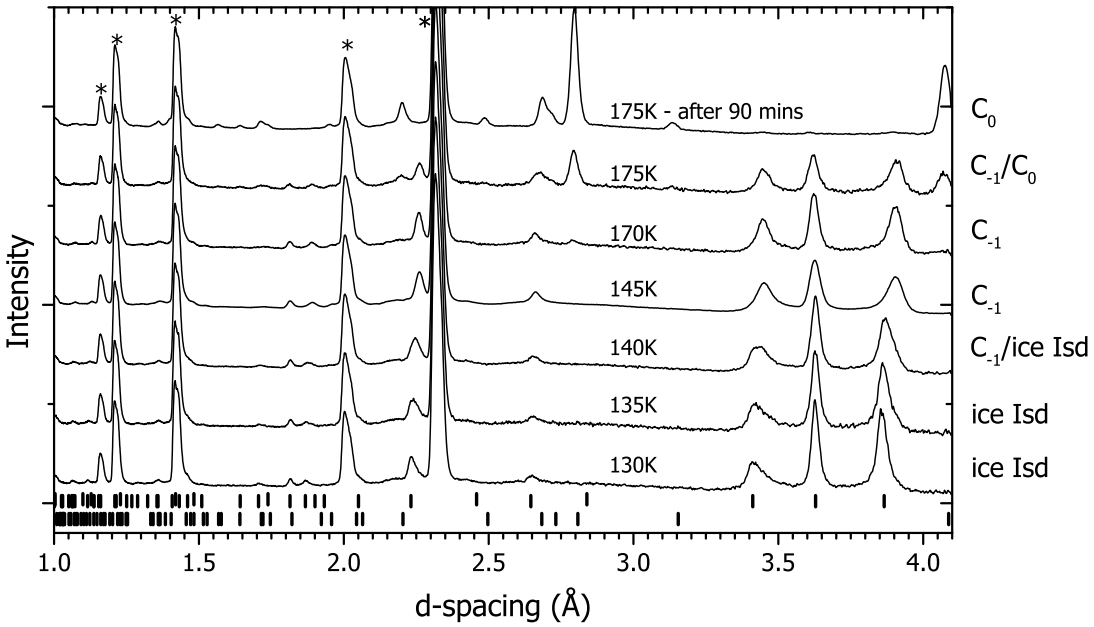

Figure 5.5 *Diffraction patterns from warming between 130 - 175 K at 0.23 GPa. Asterisks mark reflections from the aluminium gas cell. Tick marks indicate peaks that can be indexed as reflections from ice Isd (top) and C_0 (bottom).*

5.3.2 Route γ-2

Following the observation of sII clathrate in route γ-1, the sample was decompressed to near ambient pressure and warmed to convert the sample into ice Ih before repeating route γ at a slightly higher pressure. However, upon decompression of the sII clathrate the sample converted into ice Isd - a type of mixture of ices Ih and Ic that in this case can still be indexed as ice Ih in the diffraction patterns (figure 5.5). The presence of ice Isd is known to happen upon recovery from high pressure ice phases [50, 104]. A failed attempt was made to turn the cubic ice present in the sample into hexagonal ice by heating to 230 K, well past the temperature where ice Ic would normally survive to. Another way to turn the ice Isd into ice Ih would have been to melt then refreeze the water, however this would have resulted in a poor powder so it was deemed better to continue with ice Isd than to risk losing the good powder.

The sample was compressed at 130 K to 0.23 GPa with D_2 (shown in figure 5.5) and then heated. At 140 K a similar behaviour was observed with the broadening of peaks attributed to ice Ih at $\sim$ 3.4 Å and $\sim$ 4.85 Å as was observed in the sample at 0.2 GPa (figure 5.4). As temperature was increased to 145 K, the broadening that was observed at 140 K turned out to be the growth of the new

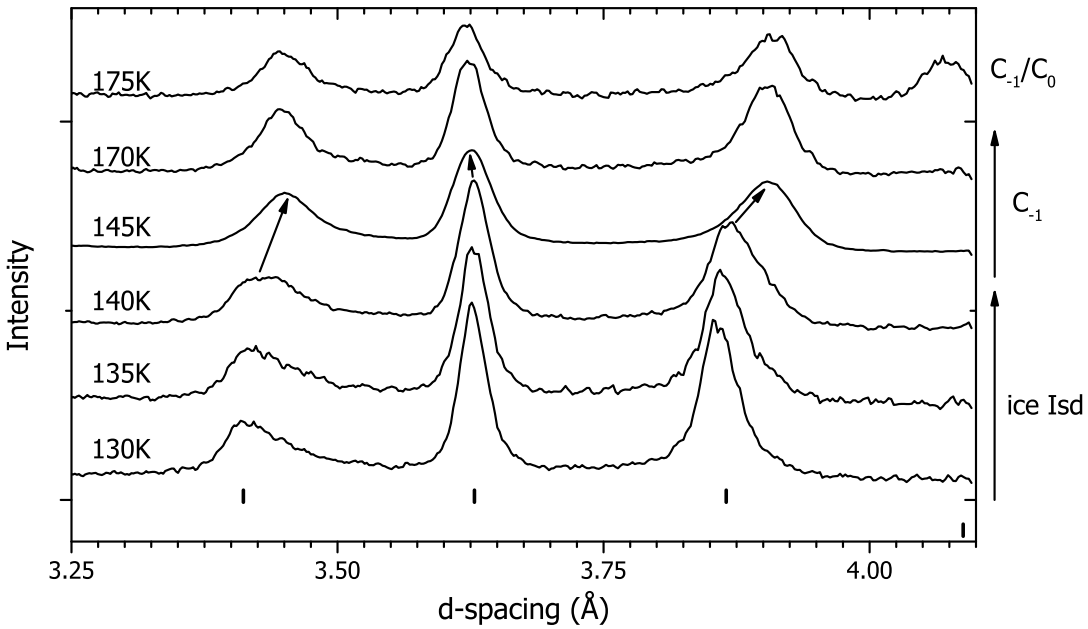

Figure 5.6 *Diffraction patterns from warming between 130 - 175 K at 0.23 GPa. Tick marks indicate peaks that can be indexed as reflections from ice Isd (top) and C_0 (bottom). Arrows show the behaviour of the ice Isd reflections as the sample transitions to C_{-1}.*

structure. These new peaks are seen more clearly in figure 5.6. At 145 K the contraction of the peak at $\sim$ 3.65 Å (figure 5.6) which suggests that this new structure is actually the lower pressure form of the C_{-1} observed at 0.3 GPa (see chapter 7). The temperature was increased further and at 175 K the C_0 phase started to grow in. At this point the gas pressure started to drop rapidly indicating either an extremely dense structure had formed or the sample was 'eating' D_2. After $\sim$ 90 minutes the gas pressure remained constant indicating the sample had fully converted to the C_0 phase (top diffraction pattern in figure 5.5).

5.4 Discussion & Summary

Figure 5.7 provides a summary of each of the phases observed on the three routes taken on the H_2-H_2O phase diagram. Though the phase boundaries of the H_2-H_2O system are relatively well known they are not for the D_2-D_2O system. At 0.3 GPa and 200 K the sample is quite near the phase boundary between sII and the suspected region where C_0 is stable [32, 34]. There is the possibility that the observation of the C_0 structure was just due to the phase boundaries being

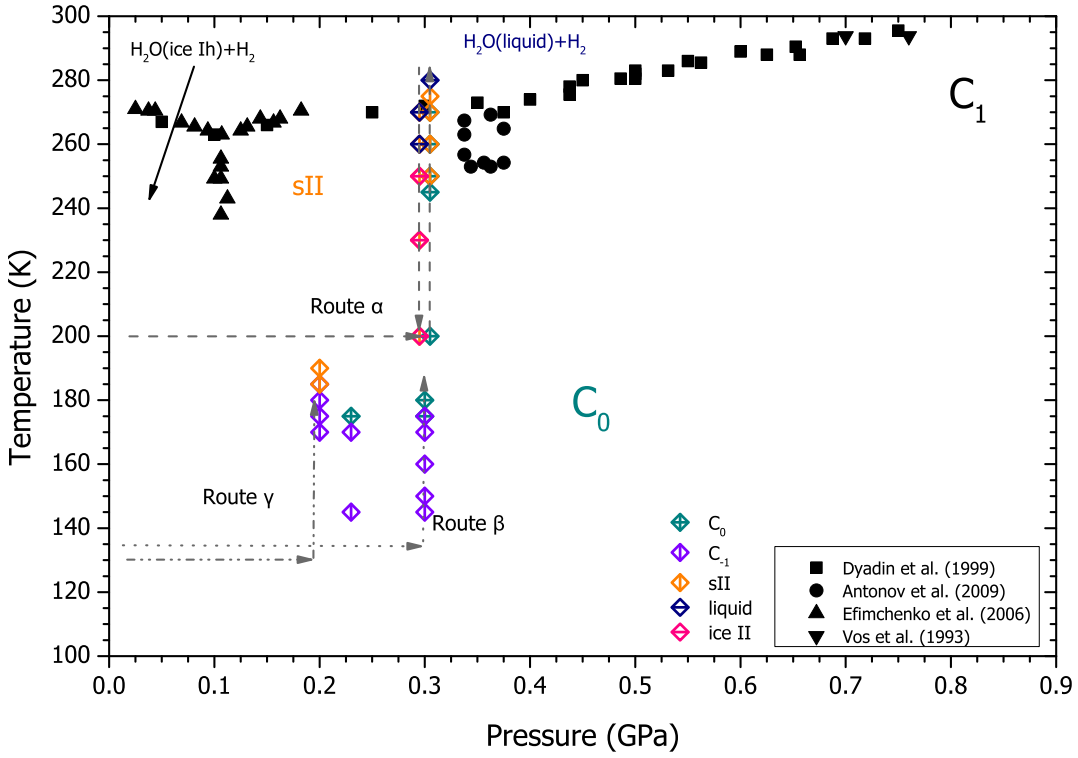

Figure 5.7 *Phase diagram of the H_2 - H_2O system showing previous experimental data on the phase boundaries obtained in references [32, 33, 34, 35, 36, 37]. The three routes taken through P-T space (α, β and γ) are marked on the diagram with dashed arrows. The phases observed on each of these routes are marked with colour symbols.*

different in the deuterated system. This possibility was ruled out by returning to same conditions via a different route (cooling from the melt in route α) and C_0 was not observed. Thus the C_0 structure is thought to be metastable at 0.3 GPa in the temperature region studied. A previous neutron diffraction study was done by Lokshin *et al.* at 0.21 GPa where they cooled from above 200 K to 40 K in which they report no observation of C_0 or any other structure such as an ice Ih based structure like C_{-1} [18]. This suggests that at 0.2 GPa the formation of both the C_0 and C_{-1} structures were also metastable with respect to sII.

If the results of the three routes explored are combined together they give a general transition sequence of ice Ih $\rightarrow$ C_{-1} $\rightarrow$ C_0 $\rightarrow$ sII at both 0.2 and 0.3 GPa on warming. At these pressures ice Ih based structures are less stable than C_0 for hydrogen hydrate [43, 44]. This means the sample goes through a series of transitions that occur in increasing stability. This cascading through metastable states from an unstable state (ice Ih in this case) to most stable (sII clathrate) is

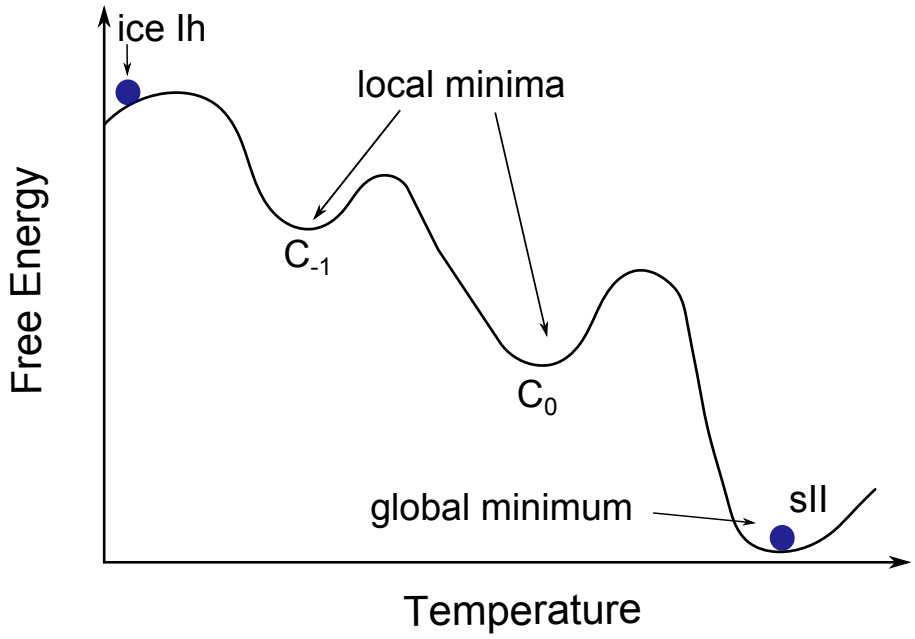

Figure 5.8 *A 1D schematic of the free energy illustrating the cascade of metastable states at 0.3 GPa from unstable ice Ih (the first blue ball) through the local minima C_{-1} and C_0 to the global minimum sII.*

known as Ostwald's Rule of Stages (also known as Law of Steps). Ostwald's Rule of Stages has long been reported to occur in colloidal crystals, proteins and only very recently in smaller molecular or atomic systems when crystallising from the melt or amorphous material [105, 106, 107]. This work also provides an example of Ostwald's Rule of Stages between crystalline structures.

When ice Ih was compressed outside its stability region at 135 K (shown as the blue ball in figure 5.8) it was no longer the lowest in free energy and thus no longer the most stable state. As the sample was warmed it transformed into a metastable state (C_{-1}) that was lower in free energy than ice Ih at 0.3 GPa but higher than C_0. As the sample was heated further it acquired enough energy to overcome the energy barrier to fall into the next local minimum in the free energy landscape, C_0, and upon further heating the sample overcame the energy barrier to form sII clathrate which would be the global minimum of the free energy landscape at 0.3 GPa (the second blue ball in figure 5.8).

The D_2-D_2O system was explored between 0.2 - 0.3 GPa at 130 - 280 K and two

metastable structures were observed when transitioning from ice Ih to the sII clathrate structure. The general transition sequence observed at 0.2 and 0.3 GPa was from ice Ih $\rightarrow C_{-1} \rightarrow C_0 \rightarrow$ sII and this is thought to follow Ostwald's Rule of Stages.

Chapter 6

The Crystal Structure of C_0

Although C_0 has been previously observed by others in the hydrogen hydrate system above 0.5 GPa, there have been several crystal structures and H_2:H_2O stoichiometries proposed to fit this structure (see 2.2.2). In this chapter these C_0 structural models are fitted to the neutron diffraction data collected, however none of these were successful in fitting the data, and a space group that provides a better fit to the data is proposed. The possibility of deuterium-ordering within the host framework is also examined. An approximate value for the guest deuterium content and how this changes slightly within the small pressure and temperature regime studied are given. Two attempts of recovering the C_0 structure to ambient pressure and how the structure decomposes into ice Isd are also presented.

6.1 Crystal Structure of C_0

In chapter 5, a good method for synthesising the C_0 phase at low pressures was found by compressing either ice Ih or Isd to above 0.2 GPa at low temperatures ($\sim$ 130 K) and then warming to around 180 K (route γ in chapter 5). A sample of C_0 was made via this route and after the sample converted from an ice I - like structure into the C_0 structure, the D_2 gas pressure was kept constant to ensure full conversion to the C_0 phase. This was complete within sixty minutes when no reflections from contaminant ice phases could be observed in the diffraction pattern. After full conversion at 0.23 GPa and 175 K the gas pressure was increased further to 0.26 GPa, and then to 0.3 GPa where a good quality

diffraction was collected for several hours to improve statistics.

Background Features in the Diffraction Pattern

Whilst transmission data were collected for the attenuation correction procedure outlined in section 4.1.2, a diffraction pattern of the empty aluminium gas cell and cryostat experimental set up were also collected, and in this a series of features were identified. The two main features identified in the background were large bumps between 2 - 3 Å and diffraction from the aluminium of the gas cell with a non-conventional profile shape. The first of these was easily dealt with by fitting a background function during the refinement process that contained a large number of terms (a sum of cosines with 10 or 12 terms - GSAS function 2) [69, 76]. As the aluminium peaks shifted slightly in pressure and temperature a procedure to deal with this in the refinement of the structures was developed. Although aluminium has a well known cubic structure under these conditions, the peaks arising from the gas cell could not be fitted by this structure due to the highly textured nature of the Al within the gas cell and also the gas cell walls not being located in the centre of the transverse detector bank. Originally the data ranges of, and around, these peaks were excluded before Rietveld refinement of the sample peaks however, this caused difficulties in accurately fitting the sample peaks close to the Al peaks. Le Bail fitting two cubic unit cells with slightly different lattice parameters was found to be a better approach as this allowed sample peaks located in close proximity to the aluminium peaks to be fitted and the refinement was found to be overall more stable treating the Al peaks this way.

6.1.1 Initial Refinements

The initial C_0 crystal structure proposed had an unconventional crystal structure described by the trigonal space group $P3_121$ (more details can be found in section 2.2.2). This structure had disordered hydrogen bonds between the H_2O molecules and a third occupied H_2O molecules located alongside 'guest' positions in a spiral located in the centre of a cavity formed by the H_2O molecules [34, 40]. The data collected here at 0.3 GPa and 175 K were used in a Rietveld refinement of this proposed structural model and found to give a reasonable fit with the peak positions, however there were some obvious discrepancies in the intensities between the calculated and observed data such as the peak at ~ 4.07 Å(see figure

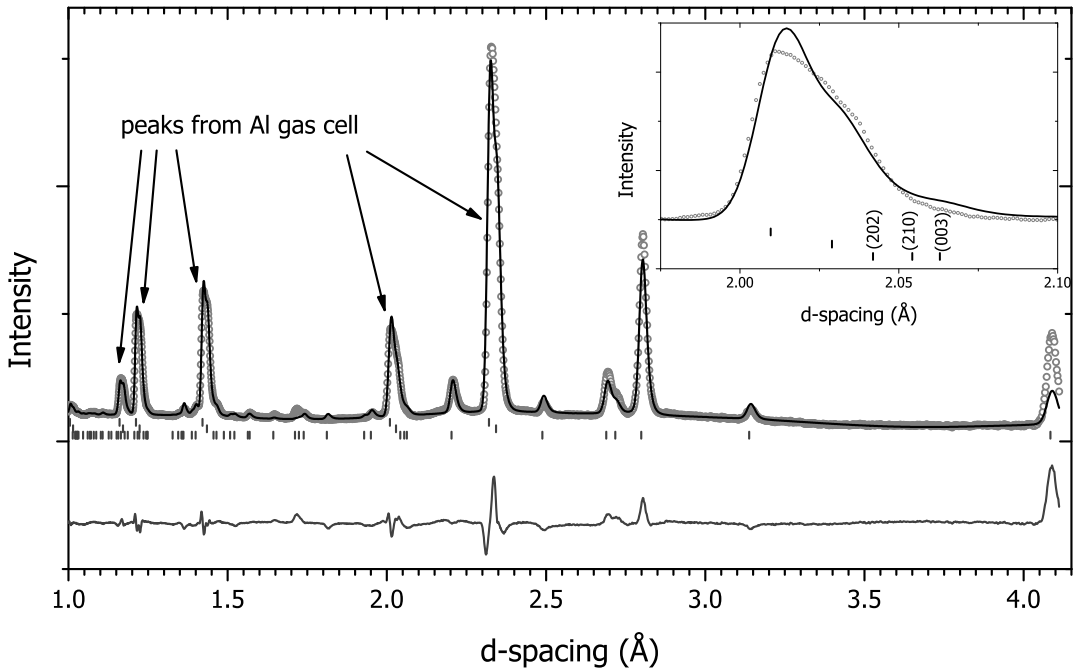

Figure 6.1 *The refinement of the C_0 model proposed by Efimchenko et al. to the diffraction data collected at 0.3 GPa and 175 K. Circles show observed data, the dark line shows the fit of the model, and the bottom curve the difference between observed and calculated diffraction patterns. Tick marks indicate the peaks arising from diffraction of the Al gas cell (top and middle) and from the sample (bottom).*

6.1). Further attempts were made to refine the atomic positions and thermal parameters of the model against the data but these were extremely unstable and unsuccessful.

The (003) Peak and Space Group Determination

In addition to some of the intensities of the model not fitting with the data the (003) peak which was used as the basis for the determination of a trigonal unit cell and space group $P3_221$, was not obviously observable in the data collected here (see inset in 6.1). This combined with the unstable refinement of the model proposed by Efimchenko *et al.* opened up the possibility that the unit cell or space group originally determined for the C_0 phase could be incorrect [34]. Following this the unit cell was determined from this diffraction data by determining the *d*-spacing of individual reflections and putting them through an auto-indexing software (DICVOL in this case) which returned a number of candidate unit cells with various lattice parameters, and of these only one hexagonal cell had

sensible lattice parameters[1] [108]. By considering the reflection conditions of hexagonal/trigonal unit cells and the non-obvious presence of the (003) peak, the hexagonal space groups with reflection condition $l = 6n$ were considered as candidate space groups in addition to the those proposed previously with the highest possible symmetry being $P6_122/P6_522$ [32, 34, 43, 109]. These two space groups are equivalent and the only difference between them is the chirality of the screw axes. This chirality can not be determined from powder diffraction data, so where the space group is noted as $P6_122$ in the following discussion the space group could equally be described by $P6_522$.

Guest D_2 Molecules

The Rietveld refinement of the original structural model proposed by Efimchenko *et al.*, and the models discussed from now on, were made by treating the guest deuterium as large, initially spheres of scattering intensity in a similar way to a previous neutron diffraction study at ~ 0.2 GPa on sII clathrate in the D_2 - D_2O system [18]. This study found that the guest molecules located in the cages of the sII structure were not at fixed positions above 50 K and instead the D_2 molecules were randomly distributed in a sphere in the cavity. This suggested that the D_2 molecules in the sII clathrate at relatively high temperatures are fairly mobile and given the similarity in conditions thought to be the case in the C_0 phase. The mobility of the guest D_2 molecules within the sample are difficult to model in an accurate way when fitting the diffraction data and caused problems in refining the overall structural model. A simple fix for this was to treat the guests as large spheres of scattering density by giving them initially large isotropic thermal parameters and then allowing the shape of these spheres to be refined. Although this did prove to make the refinements more stable it was unable to fully capture the mobility of the guest D_2 molecules and as such some deviations from the 'ideal' hydrogen - bonded D_2O morphology were observed in the refined models[2].

[1] The d-spacing of individual reflections were determined by Le Bail fitting each peak with a cubic phase in GSAS as this is able to deal with the profile shape that results from ToF neutron data. The lattice parameter of that cubic phase is then simply d-spacing of the reflection. The uncertainty in the d-spacing was then set as the resolution of the PEARL instrument $\Delta d/d$ 0.65% . A similar procedure is carried out in reference [20].

[2] The ideal hydrogen-bond morphology has O-H bonds of around 1 Å and a O-H..O bond of around 2.8 Å. In addition to bond length conditions there is also a restriction that the O-H..O bond angle is ideally around 109°.

Model	R_{wp} (before)	R_{wp} (after)	No. of parameters refined	O-D bond length range (Å) min/max	O-D...O bond length range (Å) min/max	D-O-D angle range (degrees) min/max
Efimchenko *et al.*	6.74	diverged	40	——	——	——
Smirnov *et al.*	10.04	4.08	36	0.69(4) / 1.26(3)	2.6111(6) / 3.2365(6)	78.0(4) / 176.0(7)
Qian *et al.*	6.40	diverged	38	——	——	——
Qian *et al.* (disordered)	11.22	4.80	50	0.75(6) / 1.60(9)	1.9914(1) / 4.2000(2)	64(4) / 156(8)
Strobel *et al.* (tetragonal)	11.41	diverged	10	——	——	——
Strobel *et al.* (α-quartz)	11.36	6.41	21	1.7178(2) / 2.8522(4)	4.2496(3) / 5.5530(8)	71.3(1) / 77.3(1)
Amos	5.86	4.37	24	0.958(8) / 0.977(9)	2.7558(3) / 2.7677(1)	105.8(8) / 119.9(13)
			'Ideal' values:	$\sim$ 1Å	$\sim$ 2.8Å	$\sim 109^\circ$

Table 6.1 *The R_{wp} of the structural models detailed in the text before (with only lattice parameters and peak profile widths refined) and after full Rietveld refinement (of atomic coordinates and thermal parameters). Following this, are the total number of parameters refined or, in the case of divergence, the number of parameters refined just before divergence occurred for each model. The resultant O-D and O-D...O bond lengths, and D-O-D angle ranges are also included for the converged Rietveld refinements.*

6.1.2 Refinement of Proposed Models

Before this work there had been several proposed structural models in addition to the one discussed above that was reported by Efimchenko *et al.* which are fully outlined in more detail in section 2.2.2 and only described briefly here. A modified version of the Efimchenko *et al.* structure proposed by Smirnov *et al.*, is almost the same but with no third occupied H_2O positions in the spiral. A further model similar to this structure was found in a structure search by Qian *et al.* however this model had ordered hydrogen bonds. As well as fitting this model with ordered hydrogen bonds, a further model with disordered hydrogen bonds was also fitted as structure searches only return fully ordered models. In addition to these spiral guest models, two further structures were proposed by Strobel *et al.* the first of these was the tetragonal clathrate structure found in argon and nitrogen clathrates, and also a structure similar to α-quartz. Concurrent with this work a similar structure was found to exist in the CO_2 hydrate system that reported a higher symmetry space group ($P6_122$) and partially occupied CO_2 guest sites which form a spiral in the centre of the channel in a similar way to the structures described above [20].

Attempts were made to Rietveld refine these models to the data, however the refinements of three of the seven models were extremely unstable despite multiple attempts and they diverged every time. The other four models that did not diverge with final R_{wp} values of 4.08%, 4.37%, 4.80%, 6.41% were, respectively, the modified $P3_121$ structure proposed by Smirnov *et al.*, the $P6_122$ structure found by Amos, a hydrogen-bond disordered version of the $P3_2$ structure originally proposed by Qian *et al.*, and the α-quartz based model proposed by Strobel *et al.*. Though the Smirnov *et al.* model gave a smaller R_{wp} value, this model was ruled out due the refined O - D...O bond lengths of 3.2 Å, which is almost 14% more than the 'ideal' O - D...O length of $\sim$ 2.8 Å. In addition to this much larger than anticipated bond length, the D - O - D bond angles are much lower than the 'ideal' tetrahedral angle expected (78° or 176° compared to the 'ideal' $\sim$ 109°). The hydrogen-bond disordered $P3_2$ model and the α-quartz model were also disregarded due to the resultant unphysical bond lengths. For the latter of these, the α-quartz model the O - D...O bonds were extremely large as were the resultant O - D bond lengths (see table 6.1 for details on the range of values). The disordered $P3_2$ model gave smaller O - D...O bond lengths that were still not physical, and the length of the O - D bonds varied between 0.75 and 1.6 Å (see table 6.1 for details on the range of values) . In addition to the long bond lengths

in this model the D atom describing the guest molecules was observed to have an occupancy of 6.8 and a large anisotropic thermal motion that resulted in a spiral in the cage centre. This spiral shape and large anisotropic thermal motion was also seen in the resultant $P6_122$ model. However, the $P6_122$ model resulted in more physical bond lengths (summarised in table 6.2) and a smaller occupancy of the guest deuterium sites which could be due to the presence of more guest D sites in this model.

6.1.3 Hydrogen Ordering

The models tested up to this point were predominantly with disordered hydrogen (deuterium) bonds (see section 2.1.2), the only exception being the model proposed by Qian *et al.*. In the space group $P6_122$ the structure cannot be deuterium ordered so the symmetry has to be lowered to at least $P6_1$. To test the possibility of deuterium ordering within the host structure two procedures were carried out. The first of these involved refining the 12 unique models of ordering the hydrogen bonds within the host network. Despite maximum damping, the refinements of these 12 models to the data either diverged, or the resultant structures were unphysical with the deuterium atoms not occupying sites between neighbouring oxygen atoms but within the channel (where the guest D_2 are located). The second procedure was to test the possibility of partial ordering within the structure. This involved dropping the symmetry to the lower symmetry space group $P6_1$ and the occupancy of the deuterium atoms initially all set to be 0.5 (disordered) before being refined against the data. The refinement of the occupancy of the deuterium atoms resulted in no significant deviations from 0.5 (a maximum of 0.6% change in occupancy) and no major improvement to the fit. Only one atom had any significant deviation from 0.5 to 0.55, however upon inspection of the resultant unit cell it was seen that this atom had moved slightly toward the centre of the channel and the D_2 guest sites. This slight deviation was then ruled out as not real and was most likely caused by the difficulties in modelling the mobile D_2 guests.

6.1.4 Final Refinement and Structure

The C_0 phase was found to be best described by the hexagonal space group $P6_122$ with lattice parameters $a = 6.27632$ Å and $c = 6.18750$ Å at 0.3 GPa and 175

K. The final Rietveld refinement and the fractional atomic coordinates for C_0 are shown in figure 6.2 and table 6.2 respectively. As can be seen in figure 6.2 this model provides an improved fit to the data than that of the model proposed by Efimchenko *et al.*. Specific regions where this improved fit can be seen is in the peak at $\sim$ 4.07 Å , the group of reflections between $\sim$ 2.6 Å and 2.85 Å , and in the group of reflections between $\sim$ 1.6 Å and 1.85 Å . It comprises a similar water network to that reported by Efimchenko *et al.* with two spirals of D_2O molecules forming a channel between them (see figures 6.3 and 6.4), and the hydrogen bonds of the host D_2O framework are best described by disordered $O - D...O$ bonds. The guest molecules were found to be highly mobile within the structure and were spread out roughly in a spiral at the centre of the cavity. This spiral is thought to be due to the space group and the highly mobile guest D_2 are most likely not at fixed positions within the structure under the conditions studied (0.3 GPa and 175 K). As the guest D_2 are not at fixed positions the structure can be described purely by the symmetry of the D_2O host network $P6_122$. It is possible that if the sample were cooled to low temperatures the guest D_2 molecules would be in fixed positions and would result in a different unit cell as this behaviour is observed in the CO_2 hydrate HP phase with the same structure [20]. In the temperature range studied down to 80 K no evidence of fixed D_2 positions were observed.

Though the guest D_2 molecules are highly mobile a rough estimate of the deuterium content was determined by refining the occupancy of the D_{guest} sites. At 0.3 GPa and 175 K the occupancy of the guest sites was refined to be 0.82(2) giving a molecular D_2 content of 29(1)%. At a lower pressure (0.23 GPa) the occupancy of the guest site was found to be slightly less at 0.79(2) which would give a D_2 content of 28(1)%, meaning that as pressure was increased the D_2 content was also found to increase slightly. However, given the uncertainty in each of these measurements it is possible the deuterium content of the sample remained constant. In addition, any attempt to model the guest deuterium molecules as molecules with 2 atoms with smaller thermal parameters resulted in significant distortion of the host deuterium atoms. This is discussed further below. For this reason the D_2 content determined above is only an estimate. If pressure was increased further to $\sim$ 0.7 GPa there is the possibility of the D_2:D_2O content increasing even further to be closer to 1:2 (33.3% D_2) which has been proposed by others [32, 43].

As can be seen in table 6.2 the bond angles of the host D_2O structure differ from that of the 'ideal' tetrahedral angle ($\sim 109°$) with a range of angles between

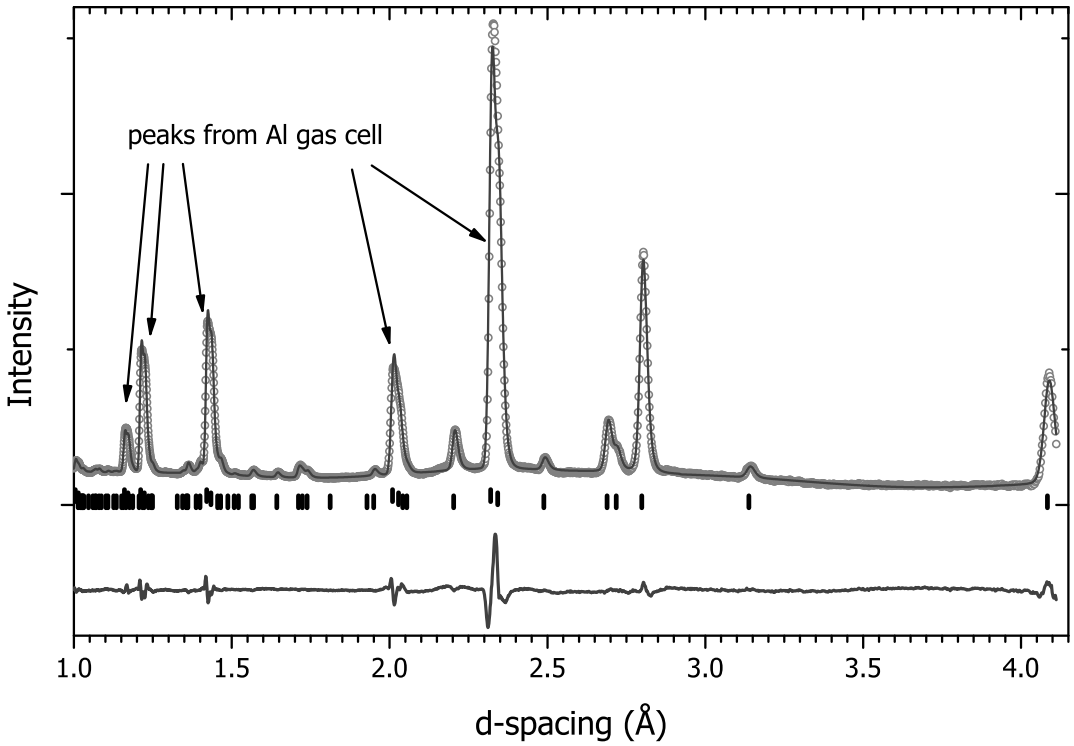

Figure 6.2 *Fit of the refined model of C_0 to neutron diffraction data collected at 0.3 GPa and 175 K. Open circles show the observed data, the black line the fit of the model refined to the data, and the bottom curve shows the difference between observed data and the refined model diffraction pattern. Tick marks indicate the position of reflections from the C_0 structure (bottom) and Al (middle and top).*

C_0 structure at $P = 0.3$ GPa, $T = 175$ K
Space group: $P6_122$
$a = 6.2763(5)$Å, $c = 6.188(1)$Å, $V = 211.08(3)$ Å^3
U_{iso} (host) = 1.4(1) x 10^{-2} Å^2

Atom	Site	x	y	z	F
O_1	6b	0.7637(6)	0.527(11)	0.25	1.0
D_1	12c	0.3771(12)	0.0707(17)	0.5317(17)	0.5
D_2	12c	0.5626(17)	0.3345(16)	0.4578(17)	0.5
D_{guest}	6b	0.1067(15)	0.213(3)	0.25	0.82(2)

Bond	Length (Å)	Bond	Angle (degrees)
$O_1 - D_1$	0.958(8)	$D_1 - O_1 - D_1$	114.4(11)
$O_1 - D_2$	0.977(9)	$D_1 - O_1 - D_2$	105.8(8)
O_1... O_1	2.7558(3)	$D_2 - O_1 - D_2$	119.9(13)
O_1... O_1	2.7677(1)		

Table 6.2 *Lattice parameters/volume, thermal parameter of the D_2O host, atomic coordinates and bond lengths/bond angles of the D_2O network of the C_0 phase at 0.3 GPa and 175 K. Atom subscripts are used as descriptors and do not refer to molecules in the case of D_2. As the guest deuterium molecules were modelled in the refinements by one atom with a large variable anisotropic thermal parameters and site occupancy, the D_{guest} described here shows the occupancy of that site and so the molecular deuterium occupancy of the guest site is then half of that shown.*

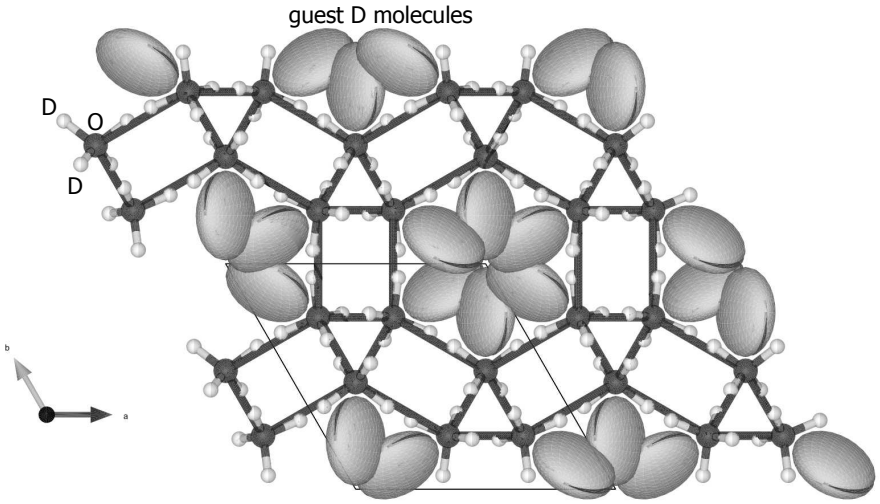

Figure 6.3 *The refined C_0 crystal structure down the c-axis.*

105.8° and 119.9°. This is thought to be due to the guest molecules being highly mobile which results in a difficulty pinpointing the exact location of the host deuteriums. As the guest D_2 molecules are modelled in the refinement with large anisotropic thermal parameters to capture this mobility it is most likely that this is unable to fully capture their distribution within the channel and results in the host deuterium atoms being moved to slightly different positions to account for this. In order to fully pinpoint the exact positions of the host structure, two attempts were made to 'empty' the structure of D_2 so that data could be collected on the pure D_2O host framework of the C_0 phase.

6.2 Sample Recovery

Following the formation of the C_0 phase, two attempts were made to recover the structure to ambient pressure and attempt to 'empty' the D_2 guests out of the crystal, which would result in a sample of the host D_2O framework. This would allow diffraction data to be collected on the host that could be used to determine the exact positions of the O/D atoms without any 'contamination' from the mobile guest molecules (section 6.1.4). A better procedure was published around the time of this work on forming ice XVI by 'emptying' neon sII clathrate by recovering the structure to ambient pressure at 80 K, warming slightly and waiting for the neon guest atoms to diffuse out of the structure [24].

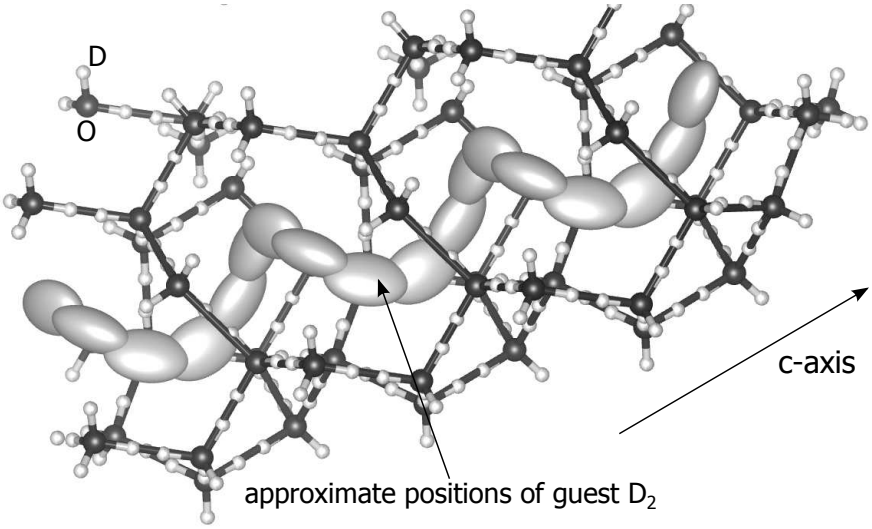

Figure 6.4 *The refined C_0 crystal structure along the c-axis. The spiral of ellipsoids in the centre of the cavity represent approximate positions for the guest D_2 molecules and the spiral shape is most likely an effect of the space group (discussed further in the text).*

6.2.1 Recovery Attempt 1

The first attempt at recovering the sample was made following the formation of C_0 at 175 K and 0.3 GPa. The sample was then cooled to 80 K and throughout this the lattice parameters were observed to contract as expected and no significant differences in intensities of the diffracted peaks were observed. Upon trying to recover the sample to ambient pressure at 80 K, no significant differences were observed in the diffracted intensities and the lattice parameters remained constant. This was noted as odd and is thought to be attributed to the sample not reacting to the release of gas pressure and the sample remaining at pressure.

At this point the sample was then slowly warmed from 80 K to 260 K at ambient gas pressure and was observed to transform from C_0 into ice Isd at 175 K. Just before this happened changes were observed in the diffracted intensities and shifts in the positions of the peaks at 170 K. As seen in the top diffraction pattern in figure 6.5, the peaks originally at $\sim$ 2.80 Å and 4.08 Å switch in relative intensity and shift to higher d-spacing. This indicated there could be a change in the C_0 structure right before decomposition.

Upon Rietveld refining the diffraction patterns collected between 80 K and 170 K the lattice parameters/volume were seen to expand during warm up as expected until at 170 K the *c*-axis was observed to drastically decrease in size,

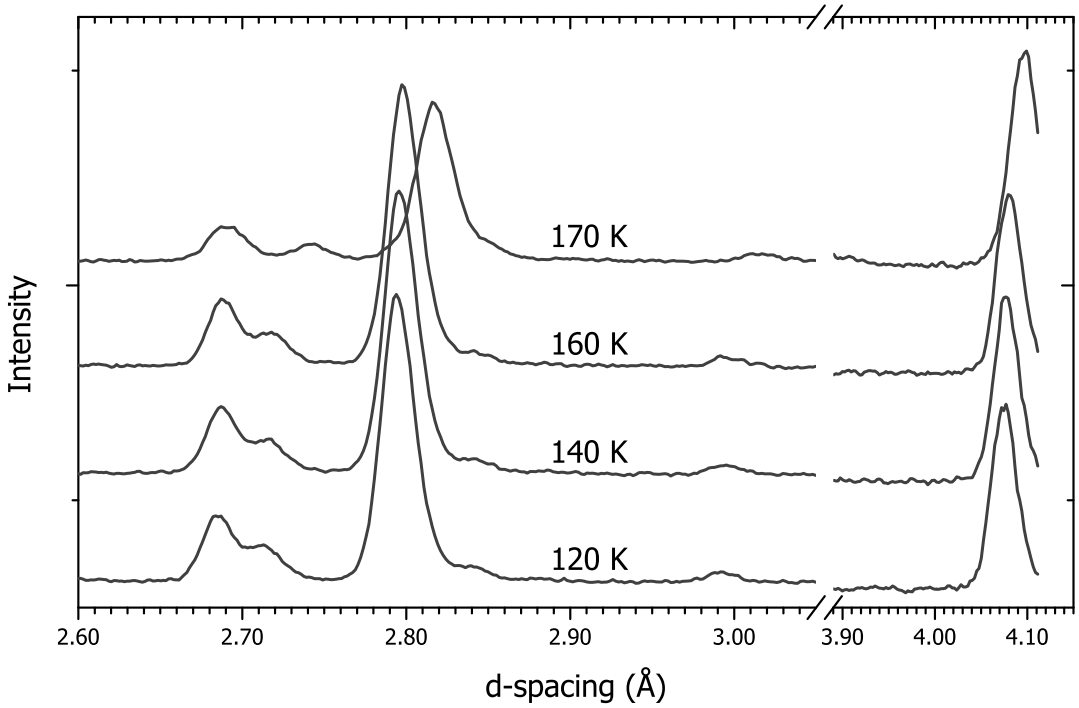

Figure 6.5 *Neutron diffraction patterns of the recovered C_0 phase during heating from 120 K to 170 K at ambient gas pressure. All peaks are reflections from the C_0 structure with the exception of the one at $\sim$ 2.84 Å which is attributed to the lead seal of the gas cell.*

whilst the *a*-axis and the volume were observed to expand. This behaviour was unexpected and could be indicative of 'emptying' the structure of D_2, however as this diffraction data was collected on a polycrystalline sample the diffracted intensities were unreliable and a second recovery attempt was made on a better powder.

6.2.2 Recovery Attempt 2

A second 'emptying' attempt was made on a sample that was initially made from a good powder at 185 K and 0.3 GPa. Unlike the first recovery attempt this sample was not taken across the melt line which would ensure the sample remained as a good powder. This sample was cooled from 185 K to 110 K and no obvious changes in the intensities of the diffraction pattern were observed. However, on refining the model to the diffraction data collected the occupancy of the guest deuterium sites was found to increase from 0.82(2) to 1.05(2) corresponding to an increase in deuterium content from 29% to 34 % D_2.

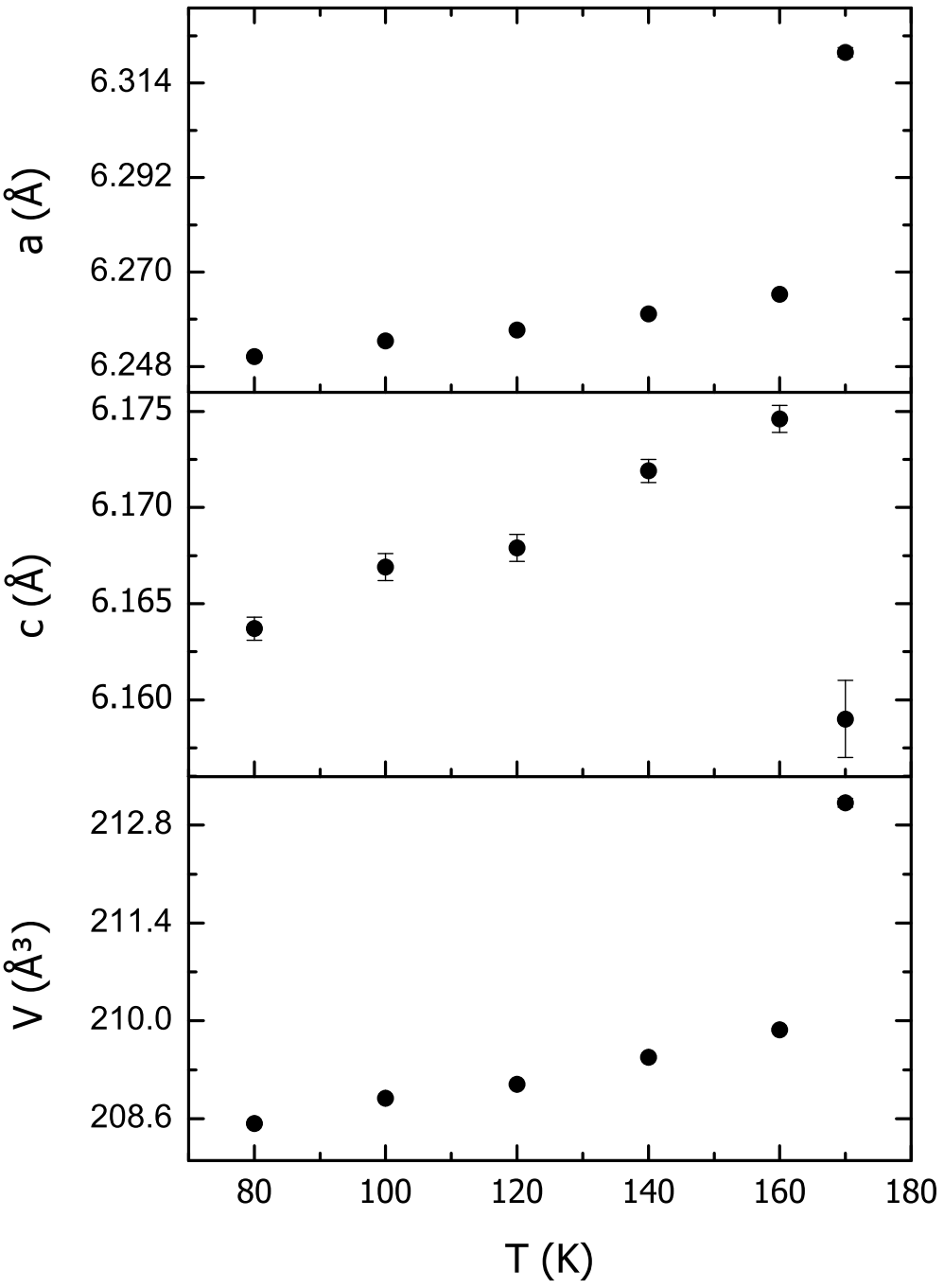

Figure 6.6 *Lattice parameters (a and c) and volume (V) of the C_0 phase during a warm up from 80 K to 170 K after recovery to ambient gas pressure. Error bars for the a axis and volume are the same size as the data points and are therefore excluded.*

At 110 K the sample was recovered to ambient pressure, by first stepping to 0.2 GPa, and then to 0.01 GPa (as close to ambient as the compressor would allow). During this the D_2 content was found to decrease to 26(2)%, and also the lattice parameters/volume were observed to increase slightly as expected with decreasing pressure. This behaviour was not observed during the first recovery attempt and is thought to be a temperature effect as the ice is not as 'locked' in as it was on the previous recovery at 80 K.

Upon warming the sample from 110 K to 160 K, the lattice parameters were found to contract/expand (figure 6.7). The *a*-axis was found to expand slightly with warming, as expected, however the *c*-axis contracted on warming. This is similar behaviour to that observed at the decomposition point during the first recovery. The intensities of the two main peaks were observed to change during this period too, which was attributed to D_2 slowly leaking out of the structure. Examples of the Rietveld refinements of the C_0 structure to the data collected at 110 K and 140 K are shown in figure 6.8. An estimate of the D_2 content came from refining the fractional occupancy of the guest site and it was seen that as the sample was warmed the D_2 content decreased to $\sim 0.34(2)$ D/site, giving a D_2 content of around 15(1)% which corresponds to approximately one D_2 molecule per unit cell (figure 6.9). In figure 6.9 the data point at 140 K can be seen not to obey the trend in decreasing D_2 content, this is most likely due to this point being determined from diffraction data with bad statistics resulting in unreliable intensities due to an intermittent neutron beam. This is also the reason why no data was collected at 150 K.

At 160 K the sample was observed to remain with 15(1)% D_2 for several hours. As temperature was increased to 170 K, all diffraction peaks from the sample started to decrease in intensity and peaks attributed to ice Isd were observed to grow (figure 6.10). During this the occupancy of the D_2 guest sites was found to remain fairly constant at 0.34(1) even during conversion to ice Ih/ice Ic. This may imply that the C_0 structure has to have a minimum of one guest molecule in its 'cage' to be stable. As can be seen in figures 6.7 and 6.10 there is a gradual change of the lattice parameters/diffracted intensities as the sample decomposes into ice Isd and not the dramatic change as observed in the first recovery attempt. This suggests that the dramatic change was due to that sample being polycrystalline in nature and decomposing rapidly, whereas the true behaviour is a more gradual decomposition with the D_2 slowly leaving the structure until there is approximately one D_2 molecule per unit cell and after this

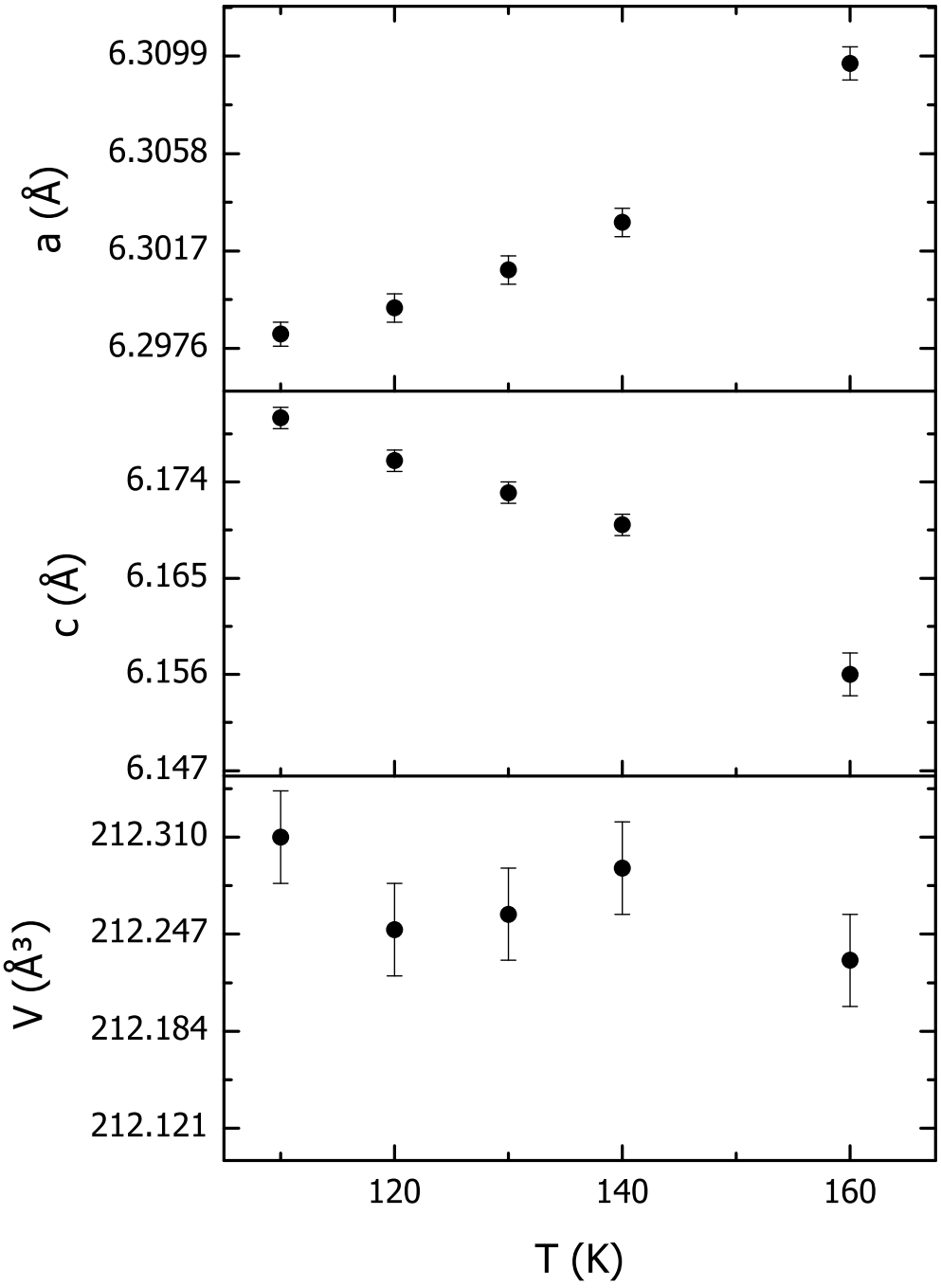

Figure 6.7 *Lattice parameters (a and c) and volume (V) of the C_0 phase during a warm up from 110 K to 160 K after recovery to ambient pressure.*

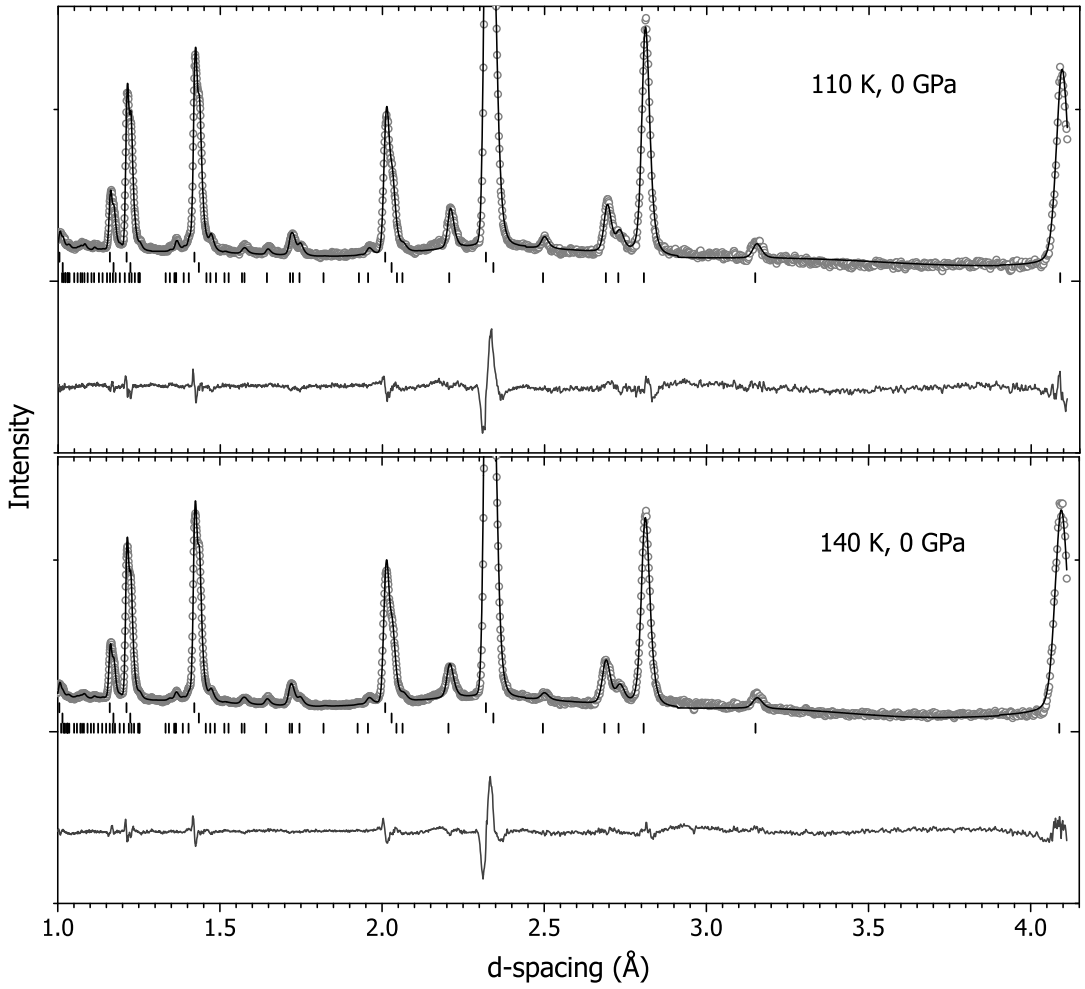

Figure 6.8 *Rietveld refinements of the C_0 structure to the data collected at ambient pressure at 110 K (after recovery) and 140 K (before observation of ice Isd). In each panel grey circles indicate observed data, the black curve shows the calculated diffraction pattern from the refined C_0 model and the lower curve the difference between the observed and calculated diffraction patterns. Tick marks indicate the calculated positions of reflections from C_0 (bottom) and Al (middle and top).*

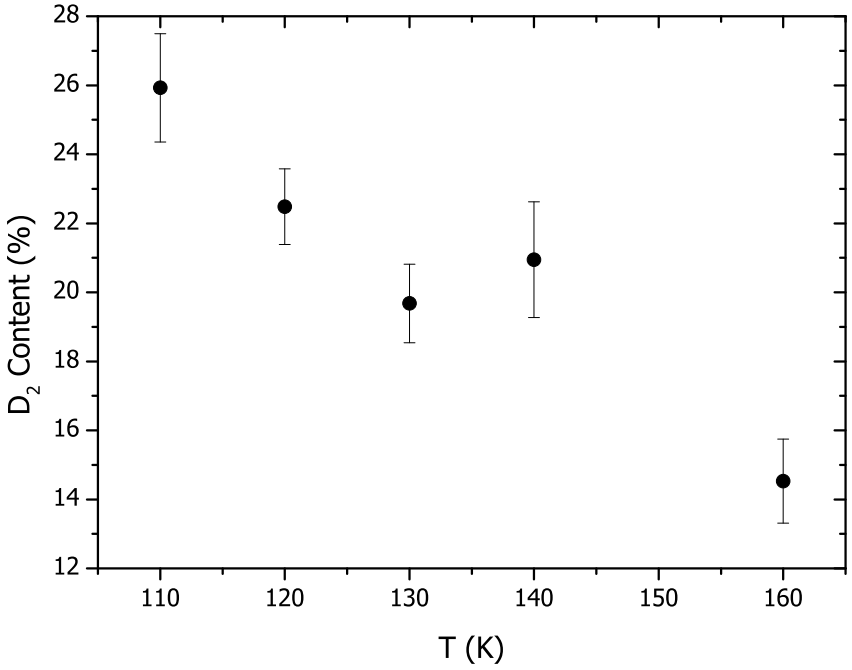

Figure 6.9 *Estimated D_2 content of the C_0 phase during a warm up from 110 K to 160 K after recovery to ambient pressure. The data point at 140 K was determined from poor quality diffraction data and may be unreliable.*

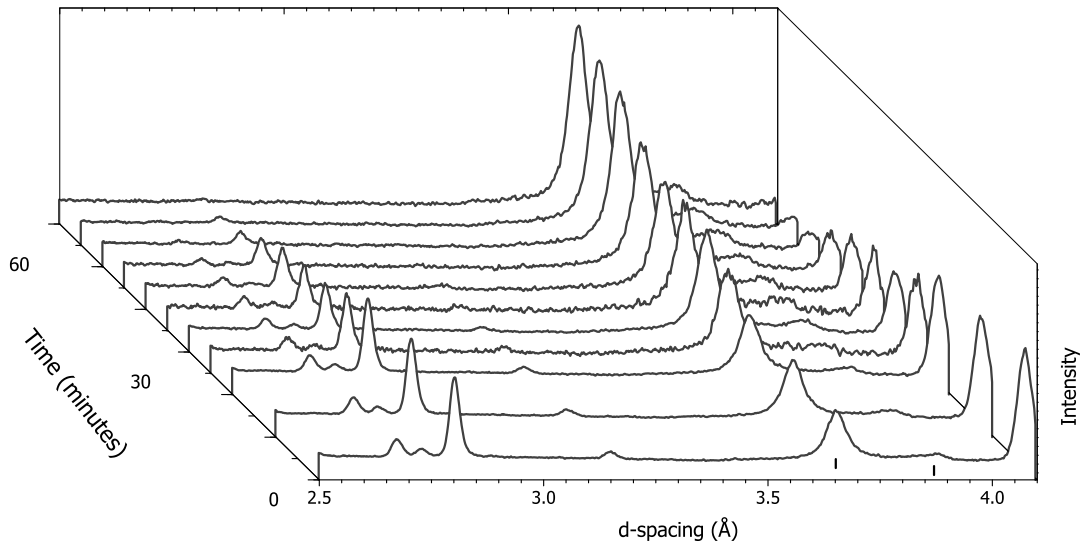

Figure 6.10 *Neutron diffraction patterns taken of the C_0 phase during decomposition to ice Ic and D_2 gas at ambient pressure and 170 K. Tick marks indicate the calculated positions of reflections from ice Ih (bottom) and ice Ic (top). All other peaks are from C_0.*

point the sample starts to decompose into ice.

6.3 Summary

Though the crystal structure of the C_0 phase was proposed prior to this work it was unable to fit the data collected here and a new structure that better fits the data was determined. This structure has a higher symmetry - $P6_122$ compared to the originally proposed $P3_121$ - based on the possible absence of the (003) peak in the data collected at 0.3 GPa and 175 K. This symmetry is only the symmetry that describes the host D_2O network. As the D_2 molecules are believed to be highly mobile under these conditions with no fixed positions based on observations from another diffraction study at similar conditions, the structure as a whole could be described purely by the symmetry of the host framework with large thermal parameters capturing the mobility of the D_2 guests [18]. The host D_2O molecules form a disordered deuterium(hydrogen)-bonded framework with open cavities in a channel-like structure. At the centre of this channel the highly mobile D_2 guests form a spiral (helix) and at the maximum pressure studied here (0.3 GPa) the D_2 content was estimated to be 29(1)% which corresponds to a D_2:D_2O ratio just under 1:2 with this increasing at lower temperatures ($\sim$ 100 K). The spiral shape of the guest D_2 molecules is thought to be an artefact of the space group.

The open channels within this structure are similar to those found in the filled ice structures present in the clathrate hydrates at high pressures (FIS-Ih) or those with small guest species such He or H_2 (FIS-II) (section 2.1). However, unlike the filled ices, the host framework present in C_0 is not based on any of the known ice phases which makes the C_0 host a new stable water network. The C_0 phase is also unlike the filled ices as the shape of the guest channel is more similar to the typical cages observed in the traditional clathrate structures sI and sII, which would make the C_0 structure a cross between a filled ice and a clathrate. The C_0 phase is also more like the traditional clathrates sI/sII as it was recently found to occur in the CO_2 hydrate system [20]. As it occurs in two hydrate systems with guest species of very different sizes this structure is now dubbed with the name 's-Sp' for spiral structure to keep it in line with other clathrates such as sH for hexagonal structure.

Two attempts were made to study the pure host structure by emptying the D_2 out of the structure. Both of these attempts failed to catch the structure before it fully decomposed into ice Ic/Ih. However, in the diffraction data collected up to decomposition it was observed that at least one D_2 molecule/unit cell had to be present for the structure to be stable; any less would result in the C_0 phase decomposing into ice Isd. Although this work was unable to empty the structure it may still be possible to do it by recovering at 80 K and warming to around 100 K and waiting for the D_2 to diffuse out, similarly to that done by Falenty *et al.* [24].

Chapter 7

The Crystal Structure of C_{-1}

In chapter 5 a new phase was observed when ice Ih was compressed above 0.2 GPa at low temperatures and then warmed. This phase was called C_{-1} as it occurs at lower pressures/temperatures than C_0. In this chapter a contaminant-free diffraction pattern of C_{-1} is compared to the contaminated diffraction pattern collected in chapter 5. Initial refinements of various proposed structural models to the clean data are compared (section 7.4) and then possible unit cells and space groups are determined. Following this diffraction data collected on recovery of the structure to ambient pressure are shown. The C_{-1} formation process is also observed in data collected around similar conditions on the He-D_2O system. The same structural models refined to the C_{-1} data are also refined to the data collected on the helium hydrate system. Following this a possible structure is proposed for C_{-1} and comparisons of the He and D_2 hydrate data given.

7.1 Initial Observations

A sample of polycrystalline ice Ih was cooled to 135 K in an Al gas cell and then compressed to 0.3 GPa with D_2 gas. Further details on experimental setup and data pre-processing can be found in section 4.1. As shown in figure 7.1 after compression to 0.3 GPa the sample peaks can be seen to shift to lower d-spacing as expected. At this point the sample can be described by pure ice Ih. Slight deviations from expected intensity are observed due to the liquid D_2O being frozen *in-situ* which created a polycrystalline sample. The sample was then warmed to

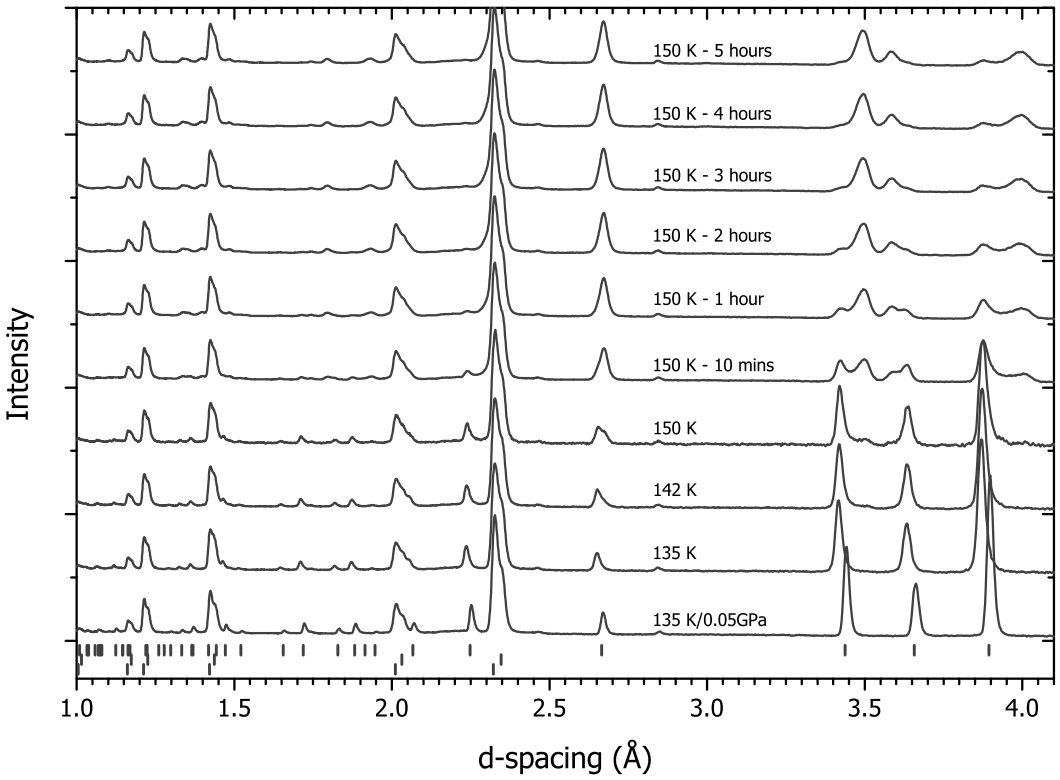

Figure 7.1 *Diffraction patterns collected of a sample of polycrystalline D_2O ice Ih on compression to 0.3 GPa with D_2 gas and subsequent heating from 135 K to 150 K. The diffraction patterns collected at 150 K show the time dependence of the transition from ice Ih to the new phase C_{-1}. Tick marks indicate the position of reflections from ice Ih and all other reflections are from the new phase, with the exception of reflection at 2.8 Å which is from the lead seal of the gas cell.*

150 K and during this the ice Ih reflections shifted to slightly higher d-spacing. This indicated an expansion of the unit cell on heating as expected. At 150 K a small peak could be seen to the right of the (101) and (102) reflections at 3.50 Å and 2.67 Å, respectively. After ten minutes these new peaks had increased in intensity. This was also accompanied with a decrease in intensity of all ice Ih peaks and the growth of two new peaks at 3.59 Å and 4.00 Å. With these changes the D_2 gas pressure decreased dramatically. This indicates either a transition to an extremely dense phase or the inclusion of gas into the ice. Over a period of five hours these new peaks grew in intensity whilst those from ice Ih decreased. After five hours no further changes occurred even when the sample was left for a further five hours.

The resultant diffraction pattern was analysed with Rietveld refinement of various clathrate and ice models. However, no single phase of either clathrate or pure ice

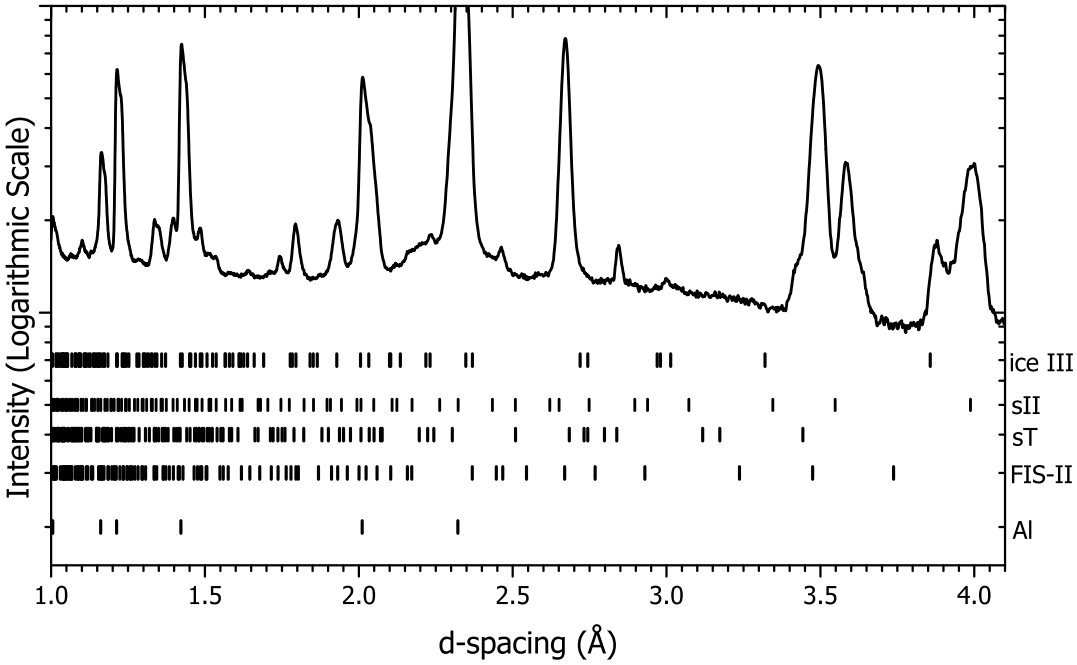

Figure 7.2 *A diffraction pattern collected of the sample after 10 hours shows that the observed reflections can be explained by the presence of a combination of clathrate (sII, sT), filled ice (FIS-II) and pure ice (ice III) structures. Though these structures could describe the positions of reflections they were unable to reproduce the intensities of the reflections.*

could describe all of the peaks observed from the sample. Instead, the reflections could be described by several combinations of ice, clathrates and lead (from the Bridgman seal) as can be seen in figure 7.2. Though these structures could describe the positions of reflections they were unable to reproduce the intensities of the reflections. This was thought to be either due to the polycrystalline nature of the sample or that the new phase C_{-1} diffraction pattern was contaminated with unconverted pure ice, or some combination of both of these. Though effort was made to ensure that the D_2 gas pressure, and hence sample pressure, remained constant throughout the transition, any decrease in pressure caused by either the uptake of D_2 by the sample or conversion to a dense phase could halt the transition. The contamination of unconverted ice could also come from larger pieces of ice that have been converted to C_{-1} on the outside and the centre is still pure ice. The latter of these contamination sources is very common in the formation of clathrates with larger guest species such as methane. This is thought to be less likely under the conditions here as deuterium/hydrogen is known to be extremely diffusive, and can penetrate through more closed structures such as diamonds and metals [110].

7.2 A Contaminant-free Sample

A phase-pure contaminant-free sample was synthesised following the same initial route as that of the one described above. The initial starting material was a powder of ice Ih which was made by freezing D_2O in a liquid nitrogen cooled bowl before being ground to a fine powder. This good powder of ice Ih was compressed to form other structures in the D_2-D_2O system (such as C_0) before recovery to ambient pressure for the subsequent experiment. As can be seen in figure 7.3 the diffraction pattern taken of the ice before compression (and formation of C_{-1}) showed that it was mainly composed of ice Ih with some ice Ic due to the ice being recovered from high pressure phases [50, 104]. The poor fit to the observed data, especially between 3.4 and 3.9 Å, is thought to be due to the presence of ice Isd (a type of 'mixture' of ice Ih and Ic) [50]. The presence of ice Isd is usually characterised by a region of 'raised intensity between 3.43 and 3.86Å' [50]. As can be seen in the inset of figure 7.3 between a comparison of the data collected here and a sample of ice Ih in the same sample environment there is a raising of the background intensity between $\sim$ 3.4 and 3.9 Å. The small offset in the background outside of this region is caused by the presence of a D_2 atmosphere

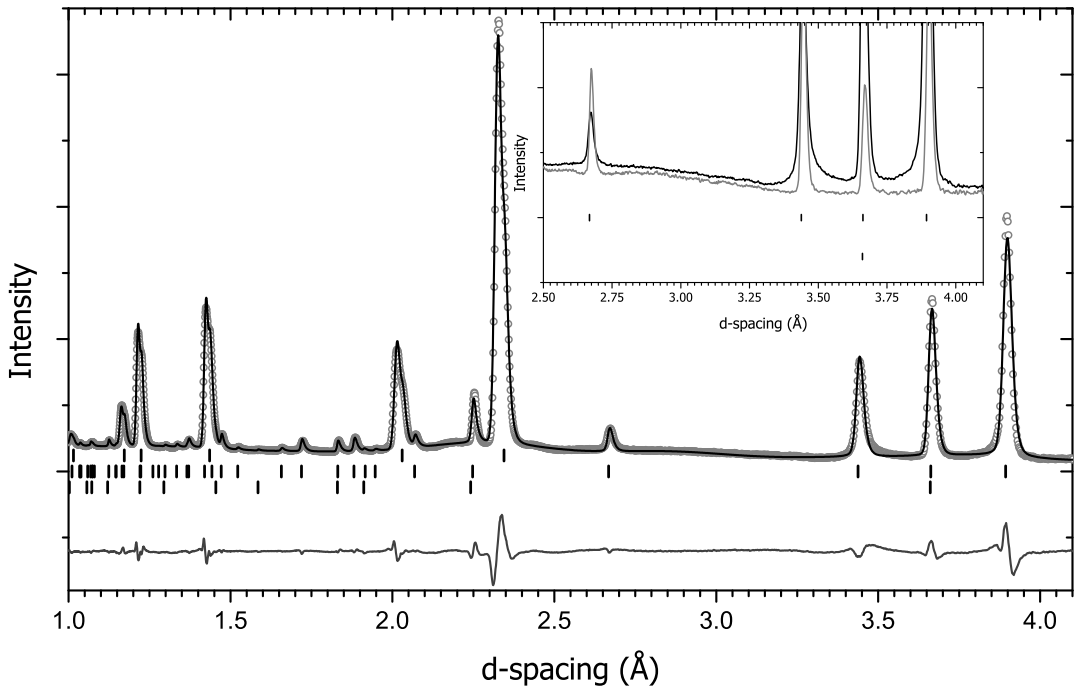

Figure 7.3 *Rietveld refinement of ice Ih and Ic to the powder D_2O starting material for the synthesis of C_{-1}. The black curve shows the refinement of the ice Ih and Ic model to the observed data (grey circles) and the bottom curve shows the difference between observed and calculated data. Tick marks indicate the position of reflections from Al (top), ice Ih (middle) ice Ic (bottom). Discrepancies between the fitted model and observed data, especially in the reflections between 3.4Å and 4 Å, are believed to be due to the presence of ice Isd. Inset shows a comparison between the starter material (black line) and a sample of ice Ih (with preferred orientation in the [101] direction) which indicates a larger increase in the background between 3.4 Å and 3.9 Å.*

in the data collected here. However, as can be seen in the figure this offset is constant and does not fully account for the raised background intensity in the region between 3.4 and 3.9 Å. Thus the starter material used to prepare a clean sample of the C_{-1} phase is thought to be ice Isd.

After compression to 0.28 GPa at 120 K the reflections from ice Ih were observed to shift to lower d-spacing as expected (figure 7.4). As the sample was warmed the D_2 gas pressure was held constant and not allowed to decrease below 0.275 GPa to ensure full conversion of the ice. At 130 K the reflections from ice Ih started to decrease in intensity. This was accompanied by the appearance of two new peaks to the right of the (101) and (102) reflections at 3.51 Å and 2.67 Å, respectively. A similar behaviour was observed at the onset of transition in

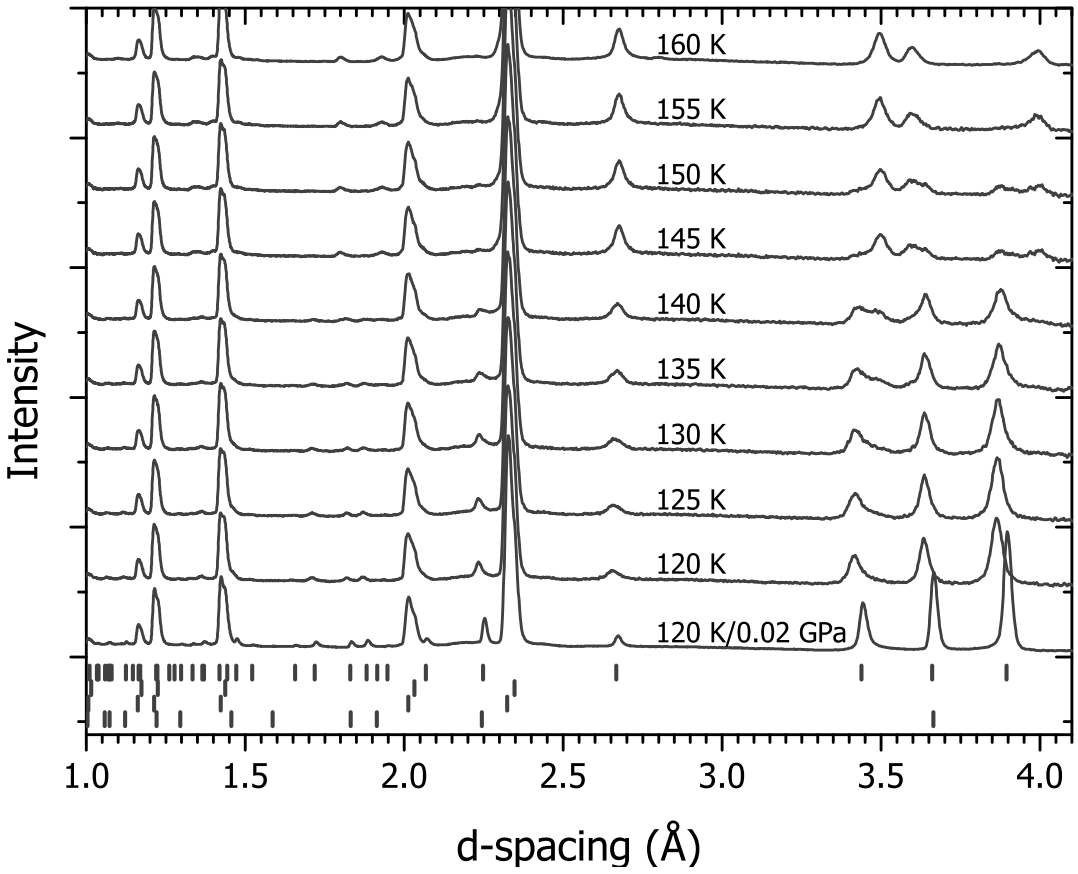

Figure 7.4 *Diffraction patterns collected of a sample of D_2O ice Isd on compression to 0.28 GPa with D_2 gas and subsequent heating from 120 K to 160 K. At 140 K the clear transition from ice Isd to C_{-1} is observed. Tick marks indicate the position of reflections from ice Ih (top), both unit cells used to fit the Al from the gas cell (middle), ice Ic (bottom) and all other reflections are from the new C_{-1} phase.*

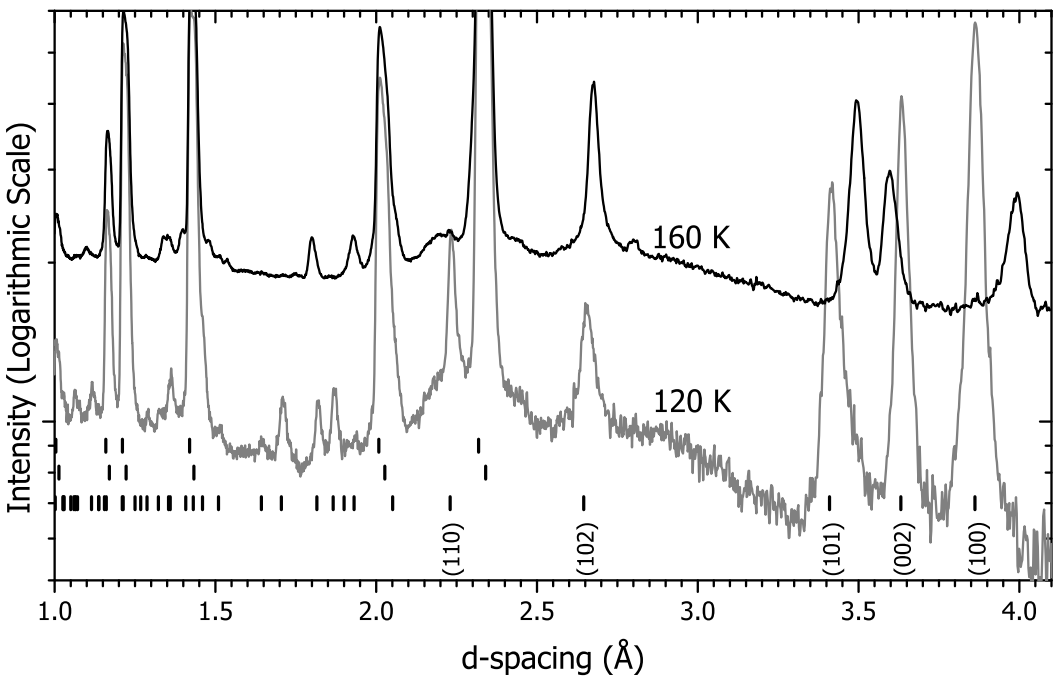

Figure 7.5 *Comparison of the diffraction patterns collected of a sample of D_2O ice Isd compressed to 0.28 GPa with D_2 gas (120 K) and its transition to the C_{-1} structure (160 K). Tick marks indicate the position of reflections both unit cells used to fit the Al from the gas cell (top and middle) and ice Isd (bottom). Five of the ice Isd reflections with the highest d-spacings are labelled and their behaviour on transformation to C_{-1} are discussed in the text.*

the contaminated sample discussed above. As the sample is warmed further these two peaks grow in intensity whilst the (101) and (102) peaks decrease in intensity (figure 7.4). Until 140 K it is only these two peaks that appeared to be changing. Above 140 K the (002) peak is observed to move to lower d-spacing (opposite to the direction of the other peaks) and decrease in intensity as seen in figure 7.5. Above 140 K there was also a decrease in intensity of the (100) peak (at $\sim$ 3.9 Å) and the appearance of a new peak at 4.00 Å. As the sample was warmed further the peaks from pure ice Ih decreased in intensity whilst those from the new phase increased. By 160 K the sample had completely converted and a comparison of the diffraction patterns collected at 120 K and 160 K is shown in figure 7.5. At 160 K a small peak at 2.78 Å could be observed. This small peak was attributed to the main reflection of C_0 and on further heating the sample converted into C_0.

As can be seen by comparison of the data in figures 7.6 and 7.2, the clean diffraction pattern has almost no contamination from any ice or clathrate phases. The only contaminant observed is the main C_0 peak at 2.8 Å and the second most intense C_0 reflection at 4.05 Å. The similarity of the diffraction patterns

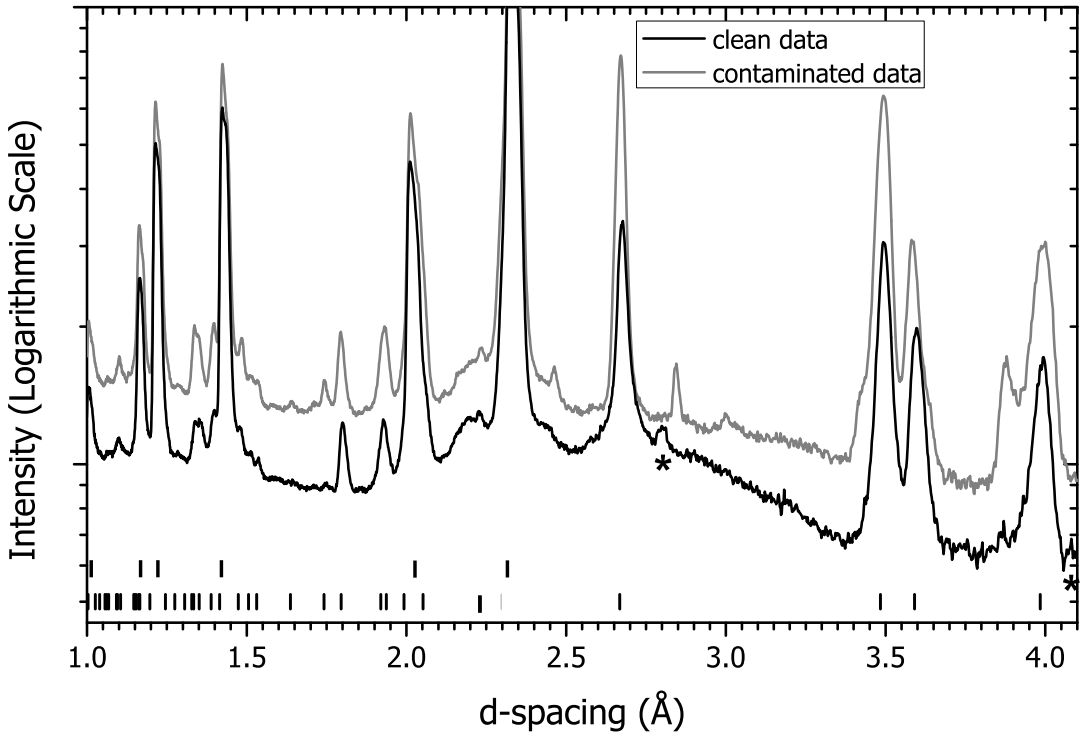

Figure 7.6 *Comparison of the contaminated and uncontaminated diffraction patterns. Tick marks indicate reflections from C_{-1} (bottom) and the Al of the gas cell (top). Asterisks mark peaks attributed to the growth of C_0.*

shows that this phase can be reproduced following the same route and was not a purely random formation. The only differences in the diffraction patterns, with the exception of the contaminant peaks, is the reduction in intensity due to a smaller sample size and difference in the ratio of intensities at $\sim$ 2.7 Å and 3.45 Å. This change in the ratio of intensities is thought to be due to the textured nature of the powder in contaminated data. The contaminated data was collected on a sample formed from freezing liquid D_2O inside the gas cell, whereas the clean data is formed powdered D_2O ice that was loaded into the gas cell. Despite the clean diffraction pattern, the reflections and intensities observed could still not be fully described by any known clathrate or pure ice phase.

7.3 The C_{-1} Structure at Low Pressures

In chapter 5, similar behaviour to that described above was seen at lower pressure (0.2 GPa). On compression of ice Ih to 0.2 GPa, the reflections of ice Ih were observed to move to lower d-spacing as expected. As the ice Ih was heated to 190 K, splitting of the (100) and the (101) peaks was observed clearly from 170 K (indicated by arrows in figure 7.7). Given the similarity in growth behaviour, this is thought to indicate the partial formation of C_{-1} that could not be fully completed due to the low pressure.

7.4 Comparison of Structural Models

A number of ice Ih based structural models were Rietveld refined to the data collected at high pressures. To ensure comparison between the models were consistent the same background was used, the thermal parameters of the host D_2O network were set to the same initial value and the occupancy of the guest D sites adjusted so that the overall D_2:D_2O ratio was 1:2. This ratio was chosen as an ice-Ih based model (ice Ih-C_0) was reported to be stable in the hydrogen hydrate system with this ratio [43]. Other models refined against the data were pure ice Ih, ice Ih with guest D in the hexagonal channels and two ordered ice Ih networks ($Cmc2_1$ and $Pna2_1$) [111]. A selection of the initial refinements of these models to the data (with only lattice parameters and profile shapes being refined) are shown in figure 7.8 (left).

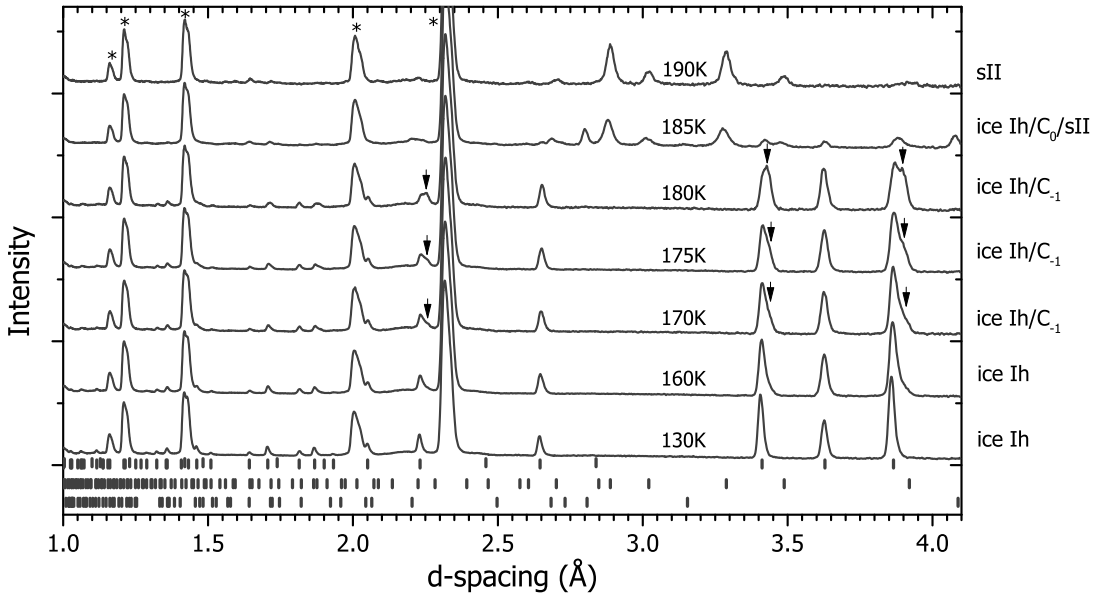

Figure 7.7 *Diffraction patterns collected of a sample of D_2-D_2O on compression to 0.2 GPa and subsequent heating from 130 K to 190 K. Tick marks indicate the position of reflections of ice Ih (top), sII clathrate (middle) and C_0 (bottom). Asterisks indicate the reflections from the Al gas cell. At 170 K the onset of splitting can be seen in some peaks of ice Ih (indicated by the arrows).*

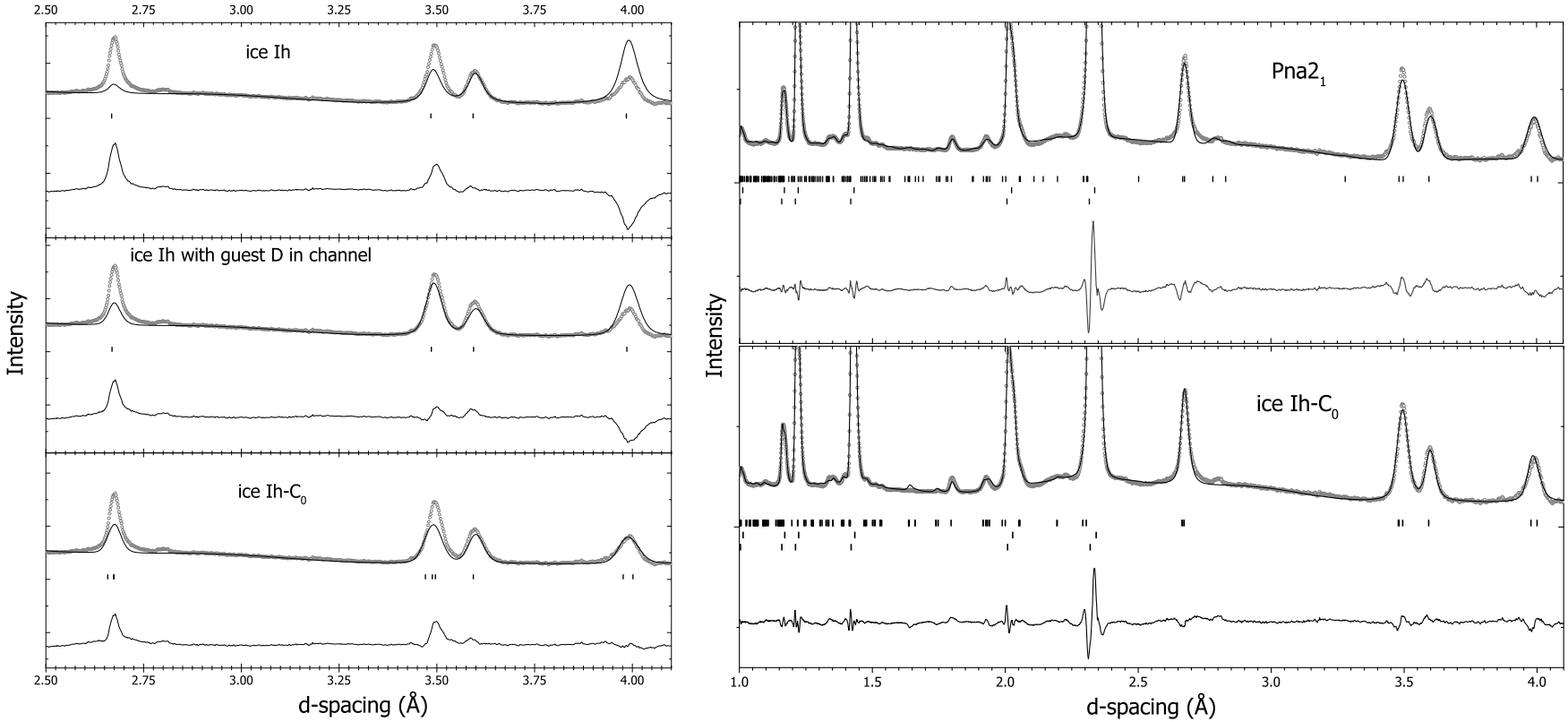

Figure 7.8 *(Left) Partial Rietveld refinement (lattice parameters and profile shapes only) of various models for C_{-1} to the data collected at 0.3 GPa and 160 K for the four peaks observed with strongest intensity. The top panel shows the fit of ice Ih to the data, middle panel shows the fit of ice Ih with a guest deuterium located in the channels, and the lower panel shows the fit of the 'ice Ih-C_0' structure proposed by Qian et al. [43]. (Right) Full Rietveld refinement of the $Pna2_1$ and ice Ih-C_0 models to the same data. In all panels open grey circles show observed data, the dark line shows the fit of the model, and the bottom curve the difference between observed and calculated diffraction patterns. Tick marks indicate the reflection positions of the model being refined and in the panels on the right the middle and bottom tick marks indicate positions of Al reflections.*

Model	R_{wp} (before refinement)	R_{wp} (after refinement)	No. of parameters refined
ice Ih	7.73	diverged	16
ice Ih with guest	6.48	diverged	9
Qian *et al.* (ice Ih-C_0)	6.25	4.23	33
ice XI ($Cmc2_1$)	6.91	diverged	14
$Pna2_1$	7.51	4.22	39

Table 7.1 *The R_{wp} of the structural models detailed in the text before (with only lattice parameters and profile shapes refined) and after full Rietveld refinement (of atomic coordinates and thermal parameters). The last column gives the number of parameters refined or, in the case of divergence, the number of parameters refined prior to divergence.*

A summary of the R_{wp} for each model is shown in table 7.1. Of these only two models could be fully refined to fit the data; ice Ih-C_0 and $Pna2_1$ ordered ice. The final fits of these models to the data are shown in figure 7.8 (right). Though both of the refinements of these models to the data converged, the fits are still quite poor (figure 7.8) and the resultant structures have host D_2O networks that are far from the 'ideal' geometry of ice networks. For example the O-D bond lengths range between 0.75 Å and 1.9 Å, and O-D...O bond lengths are much larger than the ideal 2.8 Å at 3.1 Å. One of the reasons for the difficulty in fitting this data may be caused by the starting material. If the C_{-1} structure is based on ice I and the starting material is ice Isd which is a mix of ice Ih and Ic, then the resultant C_{-1} structure could also have similar stacking disorder features. As the ice Ic and ice Ih reflections that contribute to the ice Isd diffraction pattern always overlap the starter material data would have to be further analysed to determine how cubic or hexagonal the sample is, and then determine if the compression with D_2 gas would have an impact on this cubic/hexagonal composition. In addition there may be a further complication in that the hexagonal and cubic constituents of the sample may uptake different quantities of guest deuterium.

7.5 Indexing of the C_{-1} Structure

As none of the Rietveld refinements for the models above yielded positive results, candidate unit cells were determined from the data. This was done using the same process as for C_0 in section 6.1.1. The unit cell was determined from the

Crystal System	Lattice Parameters & Volume	R_{wp}
Hexagonal	$a = 9.22(2)$ Å $c = 7.16(2)$ Å $V = 526.91$ Å^3	3.20
Orthorhombic	$a = 7.16(1)$ Å $b = 4.539(9)$ Å $c = 3.994(5)$ Å $V = 129.76$ Å^3	3.52

Table 7.2 *Candidate unit cells for the C_{-1} structure in the D_2-D_2O system. First column is the crystal system, second column gives the lattice parameters and volume, and the last column gives the R_{wp} of the Le Bail extraction fits in figure 7.9.*

diffraction data collected at 0.3 GPa and 160 K by determining the d-spacing of individual reflections[1] and putting them through an auto-indexing software (DICVOL in this case) which returned a number of candidate unit cells with various lattice parameters [108]. The uncertainties in the d-spacings were set as the resolution of the PEARL instrument which is $\Delta d/d = 0.65\%$ [85]. Two of the candidate unit cells are shown in table 7.2. In addition to the unit cells described in table 7.2 over 50 monoclinic and triclinic unit cells were also determined by the auto-indexing software as possible candidates. As an extremely large number of the monoclinic and triclinic unit cells were identified the focus of the discussion of candidate cells will be only on the hexagonal and orthorhombic unit cells.

The Le Bail extraction fits of the hexagonal and orthorhombic unit cells are shown in figure 7.9. As can be seen from the R_{wp} values (figure 7.9 and table 7.2) the hexagonal unit cell gives a marginally better fit to the data. However, this improvement in fit by the hexagonal unit cell could be due to the increased number of possible reflections that result from a larger sized unit cell. These excess reflections could improve the fit by better describing small variations in the background than the fitted background function does. It should also be noted here that the hexagonal unit cell also has an a-axis that is twice the size of the ice Ih unit cell refined to the data in the previous section (section 7.4). A Le Bail extraction fit of this smaller unit cell was also done to determine if this smaller hexagonal unit cell gave a better fit to the data than the larger one identified by

[1]The d-spacing of individual reflections were determined by Le Bail fitting each peak with with a cubic phase in GSAS as this is able to deal with the profile shape that results from time–of–flight (ToF) neutron data. The lattice parameter of that cubic phase is then simply the d-spacing of the reflection. A similar procedure is carried out in reference [20].

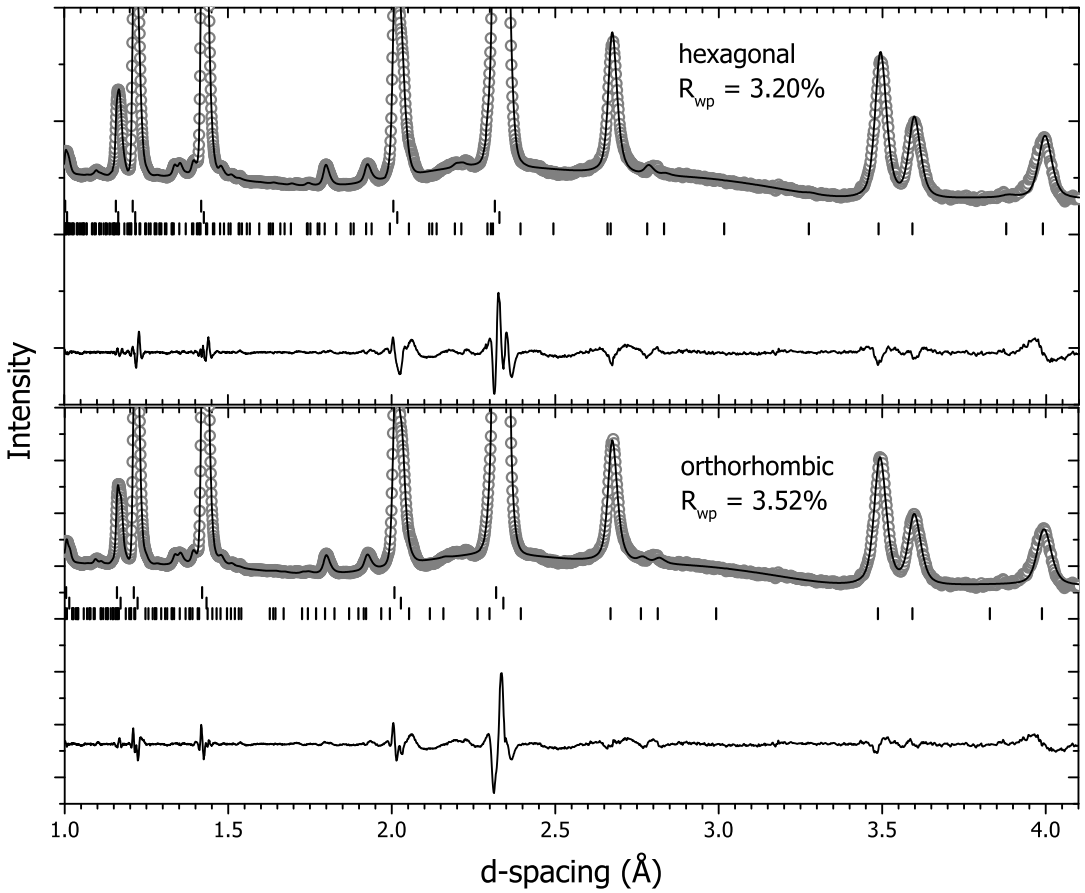

Figure 7.9 *Le Bail extraction fits of the candidate unit cells to the data. Grey circles indicate observed data, the black curve shows the fit of the model, and the lower curve the difference between the calculated and observed diffraction patterns. Tick marks indicate the calculated positions of reflections from the candidate unit cells (bottom) and Al from the gas cell (middle and top).*

the auto-indexing software. This returned a R_{wp} of 3.79% which is more than the R_{wp} calculated for both of the unit cells determined by the auto-indexer. Again a possible explanation of this could be due to the increase in the number of reflections for the larger unit cell better fitting small features in the background.

As none of the unit cells described above gave a substantially better fit to the data over the others, candidate space groups were identified from comparison of the (hkl) of the observed reflections and the reflection conditions listed in reference [109]. As a number of reflections that could have been used to further reduce the number of candidate space groups were obscured by the aluminium diffraction peaks the following list is considered preliminary. The identified space groups were:

- **Orthorhombic:** $P222$, $Pmm2$, $Pmmm$, $P2_122$, $P2_12_12$, $P2_1mn$, $Pmmn$, $Pb2n$, $Pbmn$, $Pbm2$, $Pb2_1m$, $Pbmm$
- **Hexagonal:** All those with $l \neq 3n$ for $(000l)$ reflections
- **Half-hexagonal:** All those with $l \neq 3n$ for both the $(000l)$ and $(hh2\bar{h}l)$ reflections

In addition to the space group determination described above attempts were made to determine how many D_2O molecules and guest D_2 could fit into the unit cells identified. However, as the D_2:D_2O composition was variable throughout C_{-1} formation and the likelihood of this structure being metastable under the conditions studied further studies on the 'host' structure and/or fixed compositions are needed.

7.6 Recovery of C_{-1}

In a similar procedure to that for C_0, the synthesis of a sample of 'empty' C_{-1} was also attempted (section 6.2). This was done to confirm whether the host D_2O framework is based on ice Ih or not. The sample of C_{-1} synthesised at 0.3 GPa was cooled to 85 K and then recovered to ambient pressure (figure 7.10). On recovery from 0.3 GPa to ambient pressure the sample reflections were observed to move to higher d-spacing as expected. Upon heating from 85 K the sample immediately started to transform back to an ice Ic/Ih mixture. By 120 K the sample had fully transformed from C_{-1}. A comparison of the diffraction patterns collected on the recovered D_2O ice and the 'starter' ice (see section 7.2) can be seen in figure 7.11. This showed that the diffraction patterns collected on the starter and recovered ice were extremely similar, and the only differences observed were the presence of a larger background in the starter material as a result of the presence of D_2 atmosphere, and an increase in the peak width in the recovered ice as a result of the higher temperature. In general ice I recovered from high pressure clathrate or ice structures usually contains a larger cubic component than the starting ice and the recoverability of the same starter ice here is noted as being odd [50, 104]. This 'recoverability' of the initial ice Ic/ice Ih mixture may be evidence that the host D_2O network in C_{-1} is not that different from pure ice Ih/Ic and the inclusion of molecular deuterium into the structure results in a reversible distortion to the host D_2O network.

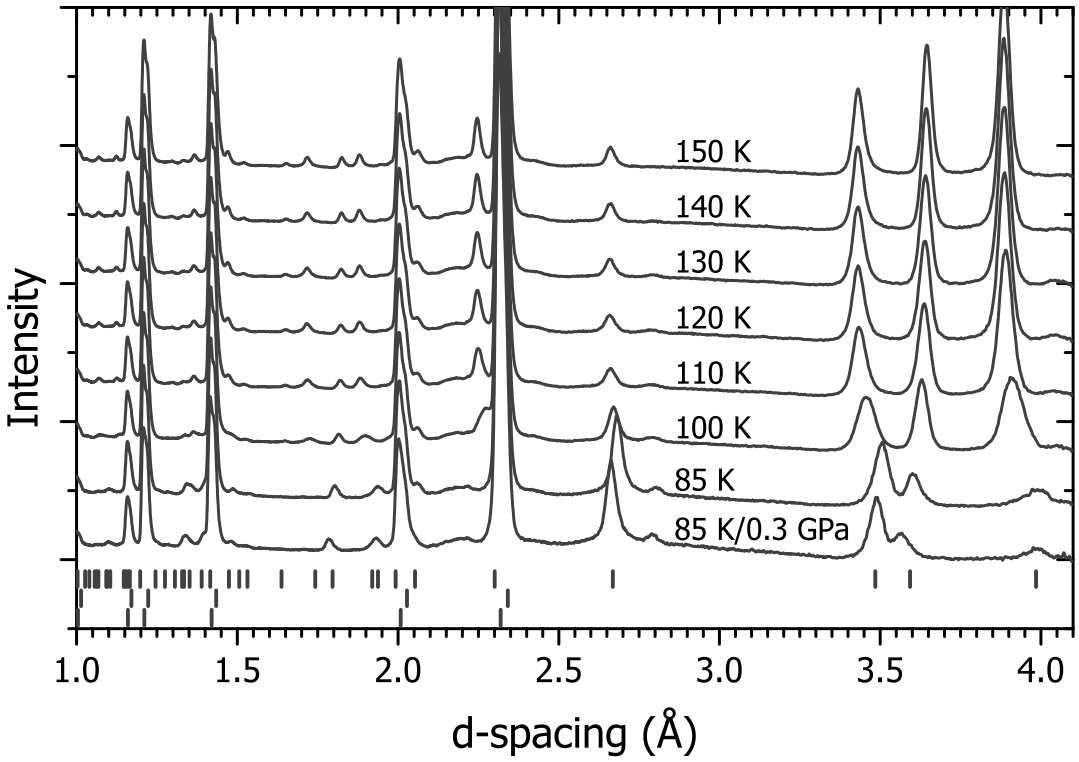

Figure 7.10 *Diffraction patterns collected of a sample of D_2-D_2O C_{-1} on recovery to ambient pressure and subsequent warm up. The bottom diffraction pattern is the sample at 85 K at 0.3 GPa before recovery to ambient pressure. All other data was collected at ambient pressure. Tick marks indicate the positions of reflections from C_{-1} (top) and Al (middle and bottom).*

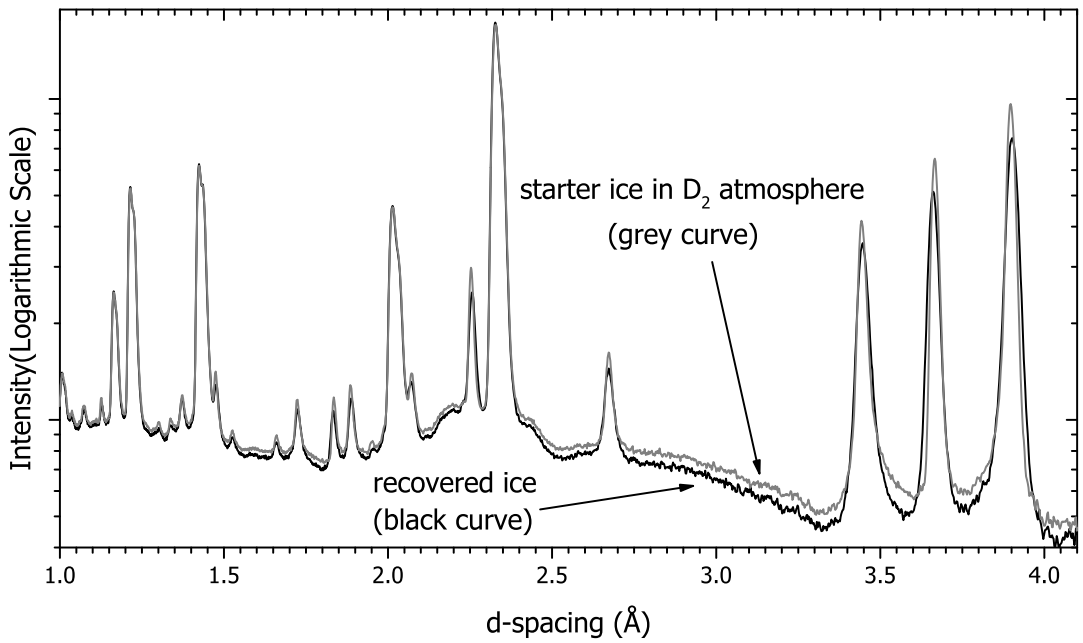

Figure 7.11 *Comparison of the diffraction patterns collected on the recovered ice (at 160 K) and the starter ice (at 120 K). The difference in background intensity is from the presence of a D_2 atmosphere in the starter material.*

7.7 The He–D_2O System

The crystal structures formed in the helium and hydrogen hydrate systems are thought to be the same as both systems form FIS-II (chapter 2). The same filled ice structures based on the Ih network that were proposed to form in the hydrogen hydrate system at low pressure are also proposed to form in helium hydrate [43, 44]. To test whether the behaviour observed above on the transition to C_{-1} from ice Ih also occurs in the helium hydrate system, similar cool and compress routes were taken to study the formation. Powdered D_2O ice was loaded into a TiZr gas cell and set up as described in section 4.1. Data were collected on the GEM instrument and processed using the Mantid software as described in section 4.1.1.

7.7.1 Attenuation

The gas cell used for this sample is made from the null scattering alloy TiZr. Though the material does not have the Bragg scattering that was present for the Al gas cell, there is still some attenuation of the beam. This attenuation is a linear

function dependent on wavelength [72]. The attenuation correction for the data collected on He-D_2O is applied in the Rietveld refinement. This is done within the GSAS software suite and adds an additional parameter to be refined whilst the model is being refined [76]. The effect essentially raises or lowers intensities as a linear function of wavelength.

7.7.2 At 0.2 GPa

Upon compression with He gas to 0.2 GPa at 110 K, all reflections shifted to lower d-spacing and the diffraction pattern could still be described purely as ice Ih (bottom diffraction pattern in figure 7.12). The sample continued to cool to 100 K and during this a number of sample peaks, for example the one at 2.25 Å , split (figure 7.12). The reflections that split were indexed as (200), (201) and (110). All reflections that indexed as $(00l)$ showed no significant deviation from their original d-spacing. This is similar to the behaviour observed upon transformation to C_{-1} described above for D_2. In D_2 this behaviour was originally thought to need warmer temperatures (above 130 K) to transform. Here the behaviour seems to be independent of temperature and occur as a function of time as the peaks continue to change even as the sample cools. At 100 K the sample started to warm to 120 K. On this warm up the intensity of the split reflections changed. The contribution to the split reflection that was lower in d-spacing decreased in intensity, whereas the one at slightly higher d-spacing increased. This change in intensity continued and at 120 K only the 'higher d-spacing' reflection could be seen for all peaks that had split. At 120 K a leak in the gas cell was discovered and the sample had to be recovered to ambient pressure to be resealed.

After the leak had been fixed the same process as above was repeated a second time. However, after compression to 0.2 GPa and heating from 105 K the same behaviour was not observed (figure 7.13). The data collected could be well fitted with pure ice Ih (see figure 7.14). From 130 K onwards although the diffraction pattern can be indexed by the Miller indices of ice Ih the intensities of the observed diffraction pattern could not be fully described by ice Ih. The refinement of the ice Ih model to the data were unsuccessful (would not converge) and also did not fully describe the intensities of the observed reflections (see figure 7.14). From 130 K it should also be noted that the same reflections that split during the first warm up became broader. This is thought to be unresolved splitting. As this splitting is unresolved the diffraction peaks can still be described by a single reflection.

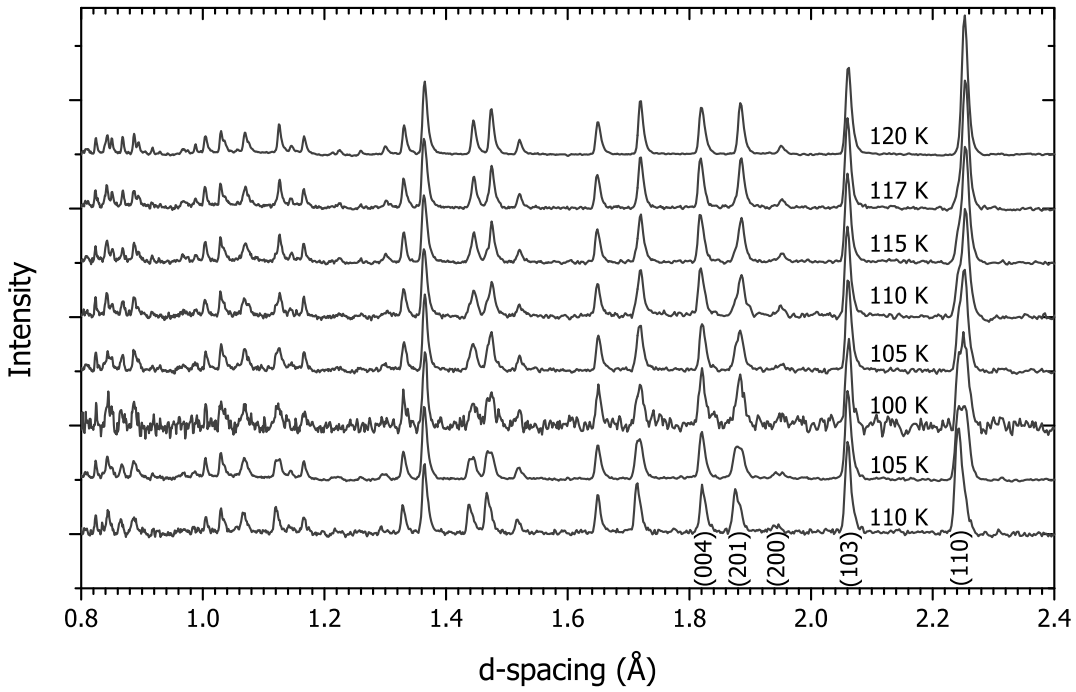

Figure 7.12 *Diffraction patterns collected of a sample of He-D_2O on compression to 0.2 GPa and subsequent heating from 100 K to 120 K. In the diffraction pattern 2nd from the bottom clear splitting is observed in the peaks at 2.25 Å and 1.88Å. These split reflections then redistribute into one as the sample is warmed. The indexing of 5 of the 6 highest d-spacing peaks are shown. The (112) reflection label is omitted here for clarity. It is extremely weak and located between the (201) and (200).*

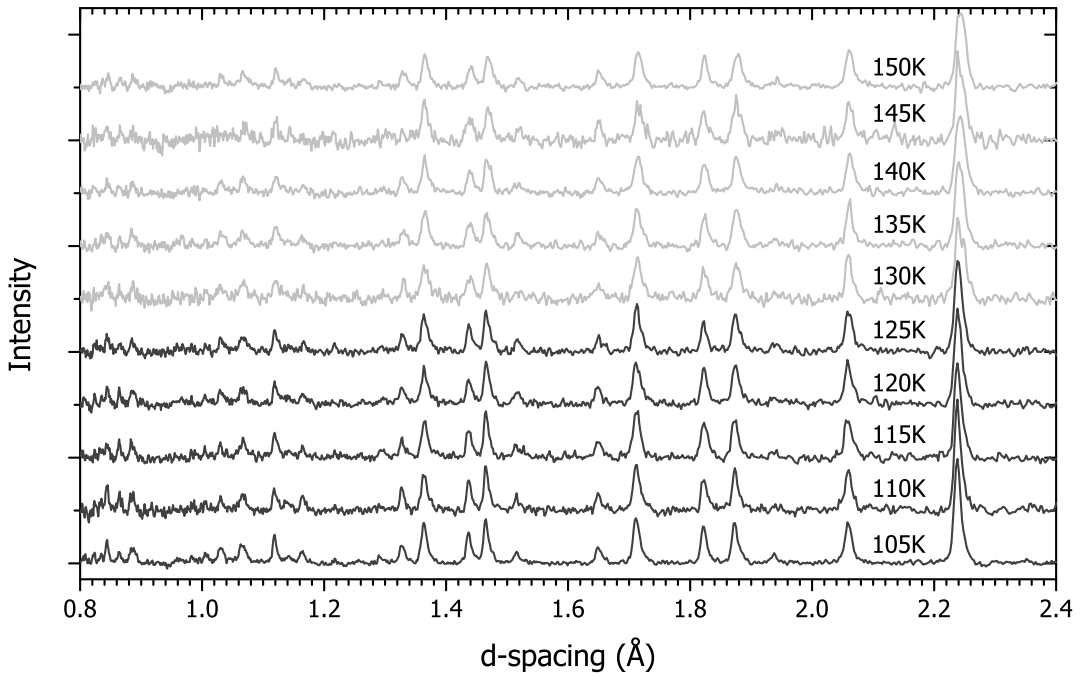

Figure 7.13 *Diffraction patterns collected of a sample of He-D_2O on compression to 0.2 GPa and subsequent heating from 105 K to 150 K. All reflections can be indexed to ice Ih, however, from 130 K the intensities of the observed reflections can no longer be described purely as ice Ih.*

As seen in figure 7.15 the lattice parameters and volume (determined from Le Bail refinement of the ice Ih unit cell to the data) increases with temperature as expected. However, in both the volume and a lattice parameter there may be anomalies in the curves around 130 K. The uncertainties in these quantities also become larger at 130 K but this could be due to low quality data. The difference between the behaviour observed during these two data collections is probably due to the leak as pressure of the sample may have been higher or lower than what the pump was reading. Another attempt to repeat the results of the first time were done at a higher pressure.

7.7.3 At 0.4 GPa

Upon compression to 0.4 GPa at 100 K the reflections from ice Ih shifted to lower d-spacing as expected as seen in figure 7.16. This was also accompanied by the appearance of new peaks at higher d-spacing next to some reflections such as the (200), (201) and (110). These are the same reflections that were observed to split at lower pressure. As the (200), (201) and (110) reflections decreased

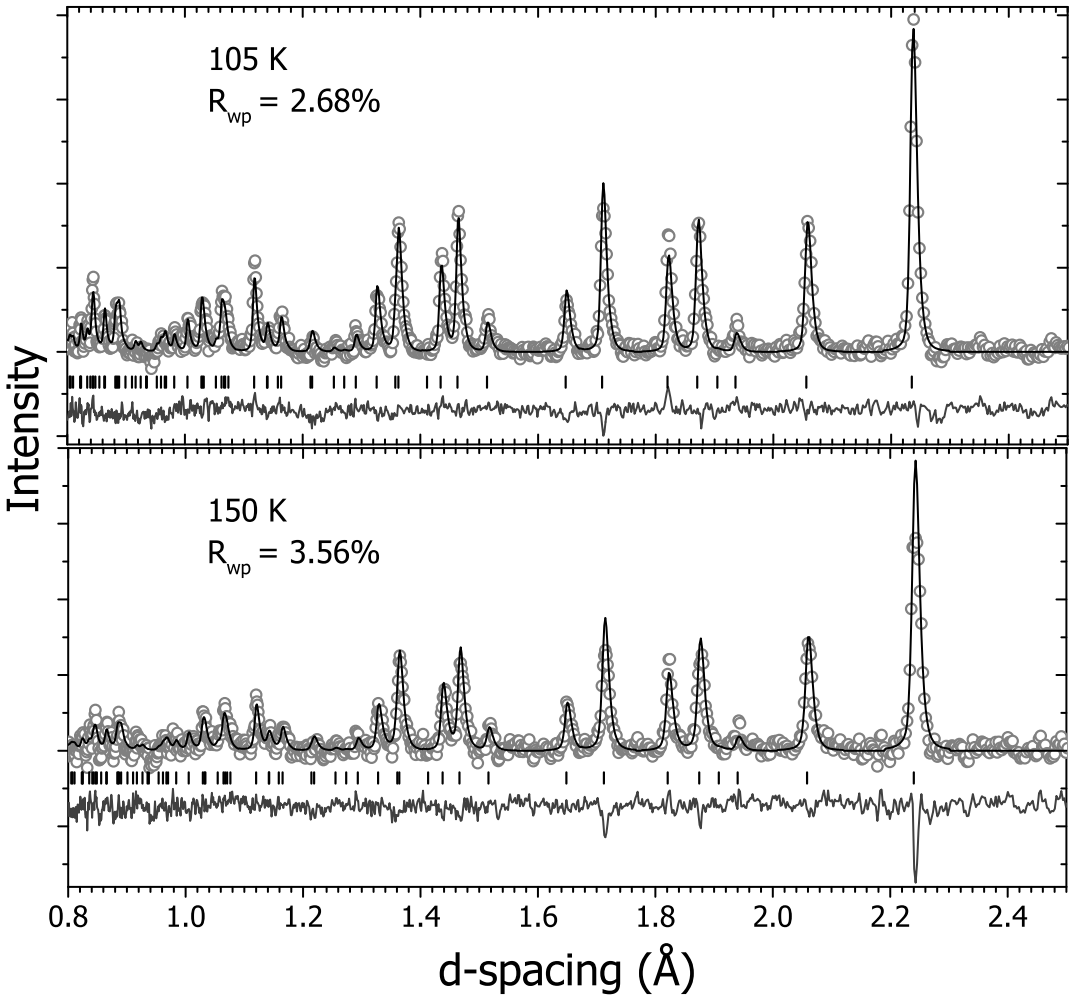

Figure 7.14 *Rietveld refinements of ice Ih to the data collected at 105 K and 150 K at 0.2 GPa. Grey circles are observed data, the black curve shows the fit of the refined ice Ih model to the data collected and the lower curve shows the difference between the observed and calculated diffraction patterns. Tick marks indicate the calculated positions of ice Ih reflections.*

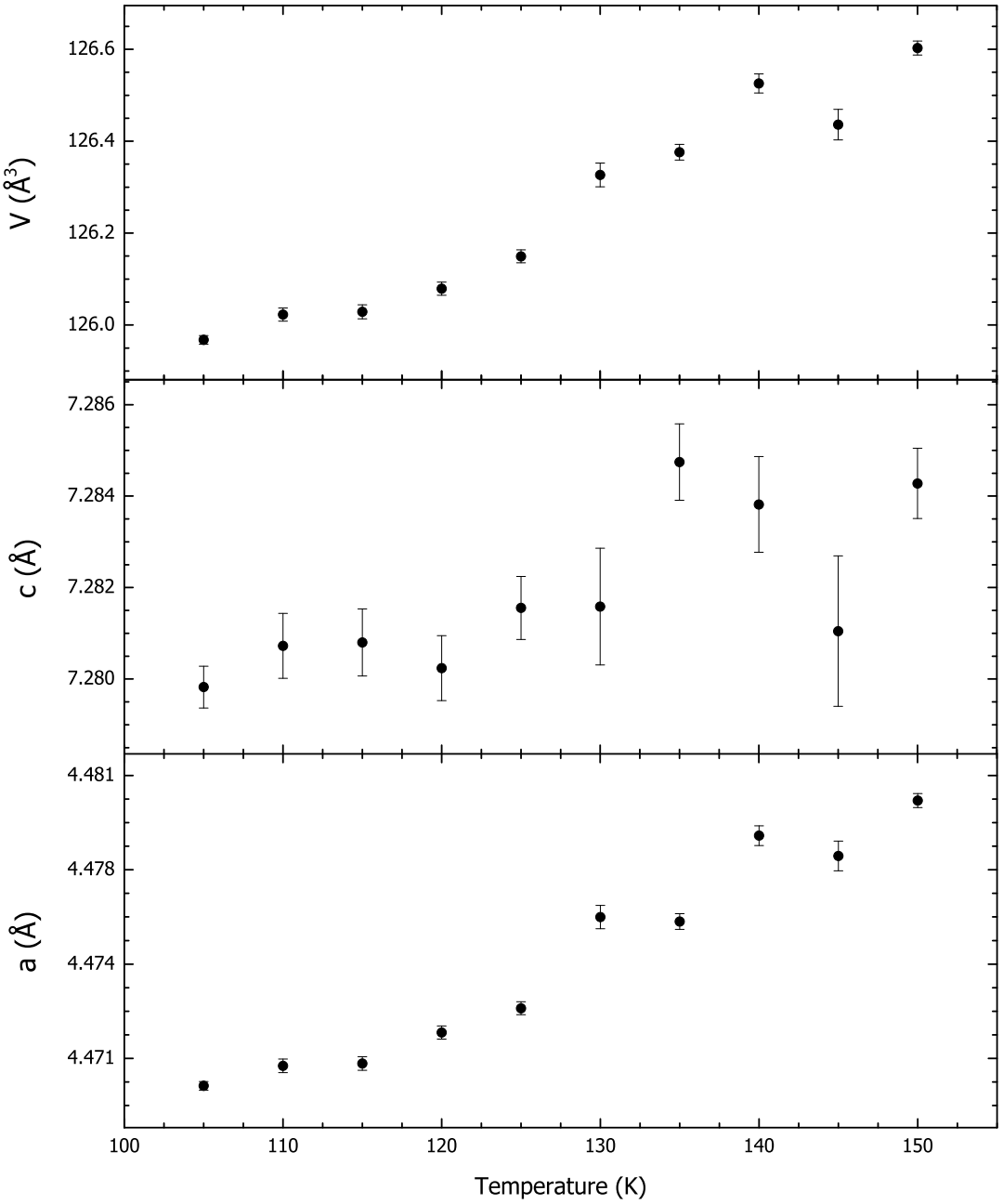

Figure 7.15 *Variation of the lattice parameters and volume of ice Ih fitted to data collected on the He-D_2O system during heating at 0.2 GPa between 105 K and 150 K.*

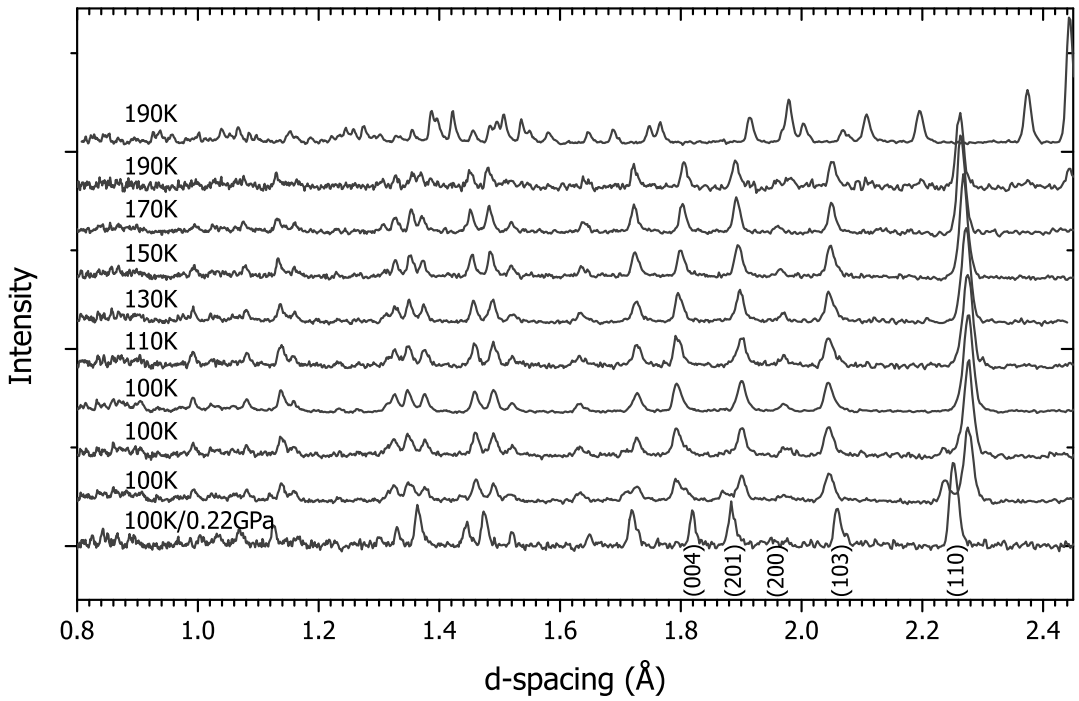

Figure 7.16 *Diffraction patterns collected of a sample of He-D_2O on compression to 0.4 GPa and subsequent heating from 100 K to 190 K. The bottom diffraction pattern was collected at 0.22 GPa before compression to 0.4 GPa. All other patterns were collected at 0.4 GPa. The indexing of 5 of the 6 highest d-spacing peaks for ice Ih are given. The (112) reflection label is omitted here for clarity. It is extremely weak and located between the (201) and (200)*

in intensity, those that appeared next to them at higher d-spacing increased. A similar behaviour was seen in the C_{-1} formation in D_2-D_2O. The sample was kept at 100 K until the sample had fully transformed before warming to 190 K. Throughout warming to 190 K no significant changes were observed in intensity. At 190 K the sample converted to the known FIS-II phase of helium hydrate.

As seen in figure 7.17 the lattice parameters (determined from Le Bail refinement of the ice Ih unit cell to the data) displayed some unconventional behaviour during heating. The *a* axis and the volume were observed to contract whereas the *c*-axis was observed to expand. This is similar to the anisotropic lattice parameter behaviour observed in C_0 where in warming the sample up there was contraction along the channel axis during decomposition (see figure 6.7).The anomalies observed at 150/160 K may be a change in the structure or could be attributed to low quality data.

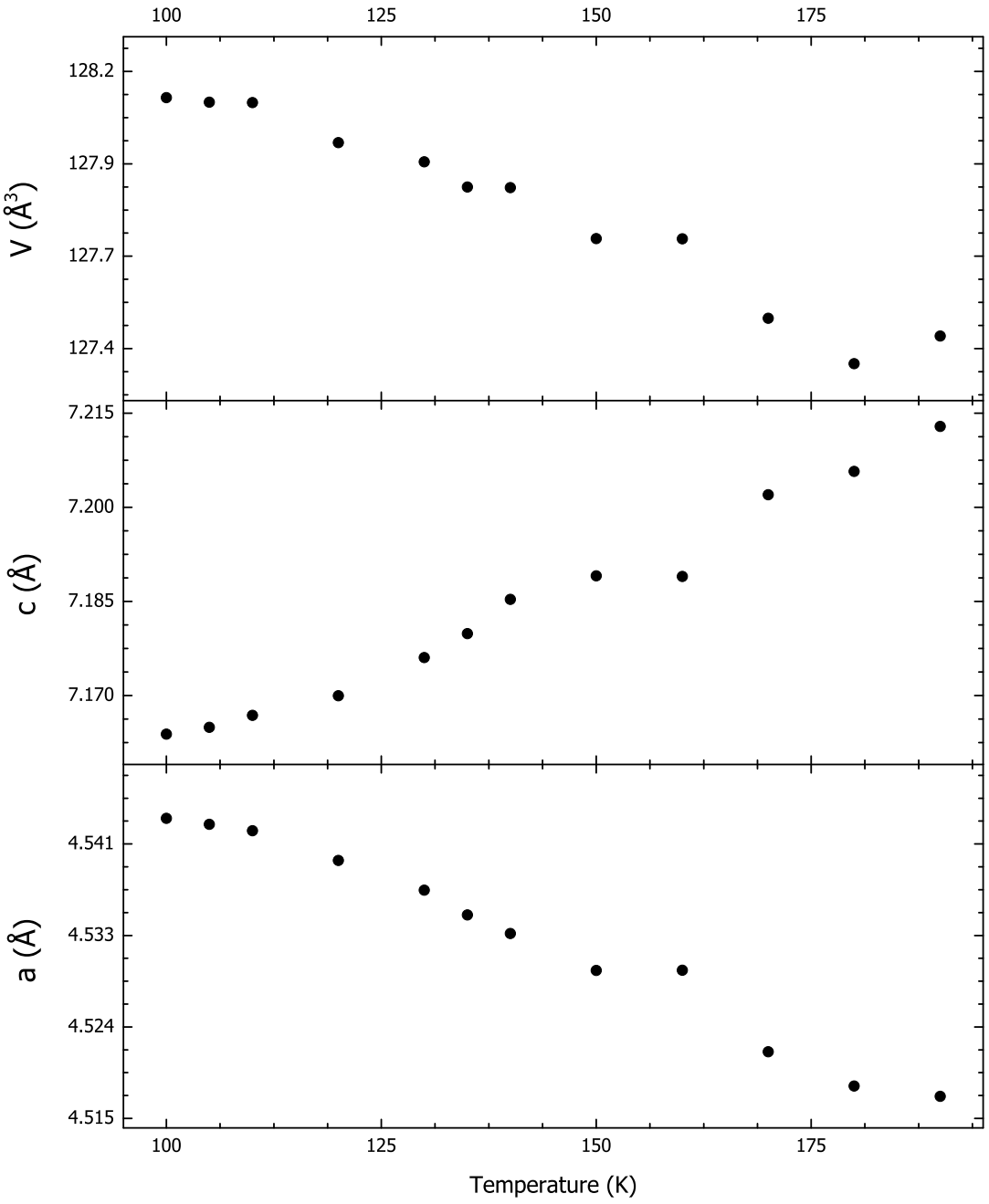

Figure 7.17 *Variation of the lattice parameters and volume of ice Ih fitted to data collected on the He-D_2O system during heating at 0.4 GPa between 100 K and 190 K. Error bars are excluded here as they are the size of the data points.*

Model	R_{wp} (before refinement)	R_{wp} (after refinement)	No. of parameters refined
ice Ih	4.54	3.40	11
ice Ih with guest	3.85	1.99	14
Qian *et al.* (ice Ih-C_0)	5.09	2.89	30
ice XI ($Cmc2_1$)	6.45	2.91	22
$Pna2_1$	7.69	3.11	30

Table 7.3 *The R_{wp} of the structural models detailed in the text before (with only lattice parameters, attenuation parameter and profile shapes refined) and after full Rietveld refinement (of atomic coordinates and thermal parameters). The last column gives the total number of parameters refined.*

7.7.4 Structure Refinement

Following the conversion of ice Ih to the C_{-1} phase at 100 K and 0.4 GPa high quality data were collected. Several models that have been proposed for both the hydrogen hydrate and helium hydrate systems were then refined against the data. These were pure ice Ih, ice Ih with a guest located in the centre of the hexagonal channels, the ice Ih-C_0 monoclinic structure proposed by Qian *et al.*, and two ordered ice Ih networks that were candidates for ice XI ($Cmc2_1$ and $Pna2_1$). To ensure that the comparison between the models is consistent, all were fitted with the same background. All He guests started with the same site occupancy and thermal parameter of 1 and 30x10^{-2} Å^2, respectively. This value was chosen for the thermal parameter as at 0.4 GPa the He atom was determined to have that value in the channels of FIS-II [112].

As can be seen in table 7.3 the atomic and thermal parameters of all models could be fully Rietveld refined to the data. Despite being able to be fully refined to the data, only two models resulted in non-negative thermal parameters and good values for both O-D and O-D...O bond lengths. These were the ice Ih models with and without guest. Of these the ice Ih model with a guest in the channel provided a better fit to the data. The Rietveld refinement of this structure to the data is shown in figure 7.18 and details of the resultant structure given in table 7.4. This structure also gave an improved fit to the data collected at low pressures, for example at 150 K and 0.2 GPa (figure 7.14), than pure ice Ih with an R_{wp} of 3.27 % compared to 3.56% for pure ice Ih.

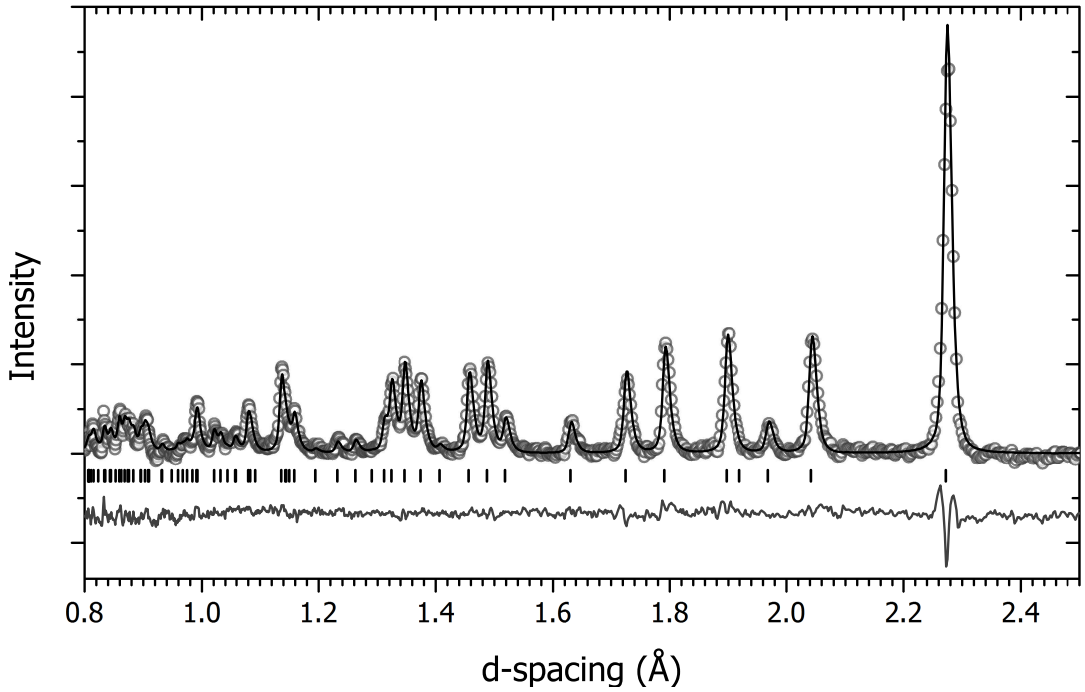

Figure 7.18 *Rietveld refinement of ice Ih with guest He model to data collected at 0.4 GPa and 100 K. Grey circles indicate observed data, the black line is the calculated pattern, and the bottom curve shows the difference between the observed and calculated diffraction patterns. Tick marks indicate the calculated positions of reflections.*

Proposed C_{-1} structure at P = 0.4 GPa, T = 100 K
Space group : $P6_3/mmc$
a = 4.5442(1) Å, c = 7.1637(4) Å, V = 128.108(9) Å^3
U_{iso} (O) = 2.23 x 10^{-2} Å^2
U_{iso} (D) = 3.72 x 10^{-2} Å^2
U_{iso} (He) = 6.10 x 10^{-2} Å^2

Atom	Site	x	y	z	F
O_1	4f	0.3333	0.6667	0.0579(4)	1.0
D_1	4f	0.3333	0.6667	0.1983(5)	0.5
D_2	12k	0.4537(3)	0.9074(7)	0.0149(4)	0.5
He	4e	0	0	0.24(1)	0.40(3)

Bond	Length (Å)	Bond	Angle (degrees)
$O_1 - D_1$	1.0058(1)	$D_1 - O_1 - D_2$	108.013
$O_1 - D_2$	0.9961(1)	$D_2 - O_1 - D_2$	110.890
O_1... O_1	2.7521(2)		

Table 7.4 *Table giving the lattice parameters/volume, thermal parameters of the D_2O host and He guest, atomic coordinates and bond lengths/bond angles of the D_2O network of a candidate structure for C_{-1} at 0.4 GPa and 100 K.*

7.7.5 Occupancy

The model determined above (table 7.4) was refined against the data collected on warming between 100 K and 190 K. The refined He guest site occupancy and isotropic thermal parameter (U_{iso}) are shown with varying temperature in figure 7.19. The large variations observed in U_{iso} are most likely due to poor data quality collected through the warm up. Though there are some variations in site occupancy there is a general downwards trend. This suggests that as the sample was warmed up there was a decrease in He content. This behaviour has been seen before in various other clathrate structures such as those in hydrogen hydrate [18, 34].

7.8 Summary

Although the structure of the C_{-1} phase in the D_2-D_2O was not fully determined, a candidate structure has been proposed based on the similar behaviour observed in the He-D_2O system. A proposed structure for the C_{-1} phase in helium hydrate is given in section 7.7.4. This structure has an ice Ih host D_2O network with guest He atoms located in the hexagonal channels. This would make the structure found here the true FIS-Ih rather than the FIS-Ih structure found to form in gas hydrate systems with 'large' guest species such as methane (see section 2.1. However, it is unclear whether this filled ice Ih structure as described for helium hydrate is the same as the structure formed in D_2-D_2O.

The contamination of the C_{-1} phase in the D_2 hydrate is a problem. As seen in section 7.1 unless the gas pressure is kept constant, there is the possibility of contamination from pure ice or clathrate phases. The starting material may also have an effect on the formation of the C_{-1} phase. In section 7.2, a starting sample thought to be ice Isd was compressed to 0.3 GPa to form C_{-1}. This same sample was then recovered to ambient pressure where it transformed back into ice Isd with an identical diffraction pattern to the starting material. Recovery from high pressure ice and clathrate phases usually results in an increase in the cubic composition of the ice I formed. As the recovered material and starter material have identical diffraction patterns it is thought that the starting ratio of ice Ic/Ih was recovered. This suggests that the C_{-1} phase may be related to an ice I network. If this is the case then there could be ice Ic or filled ice Ic

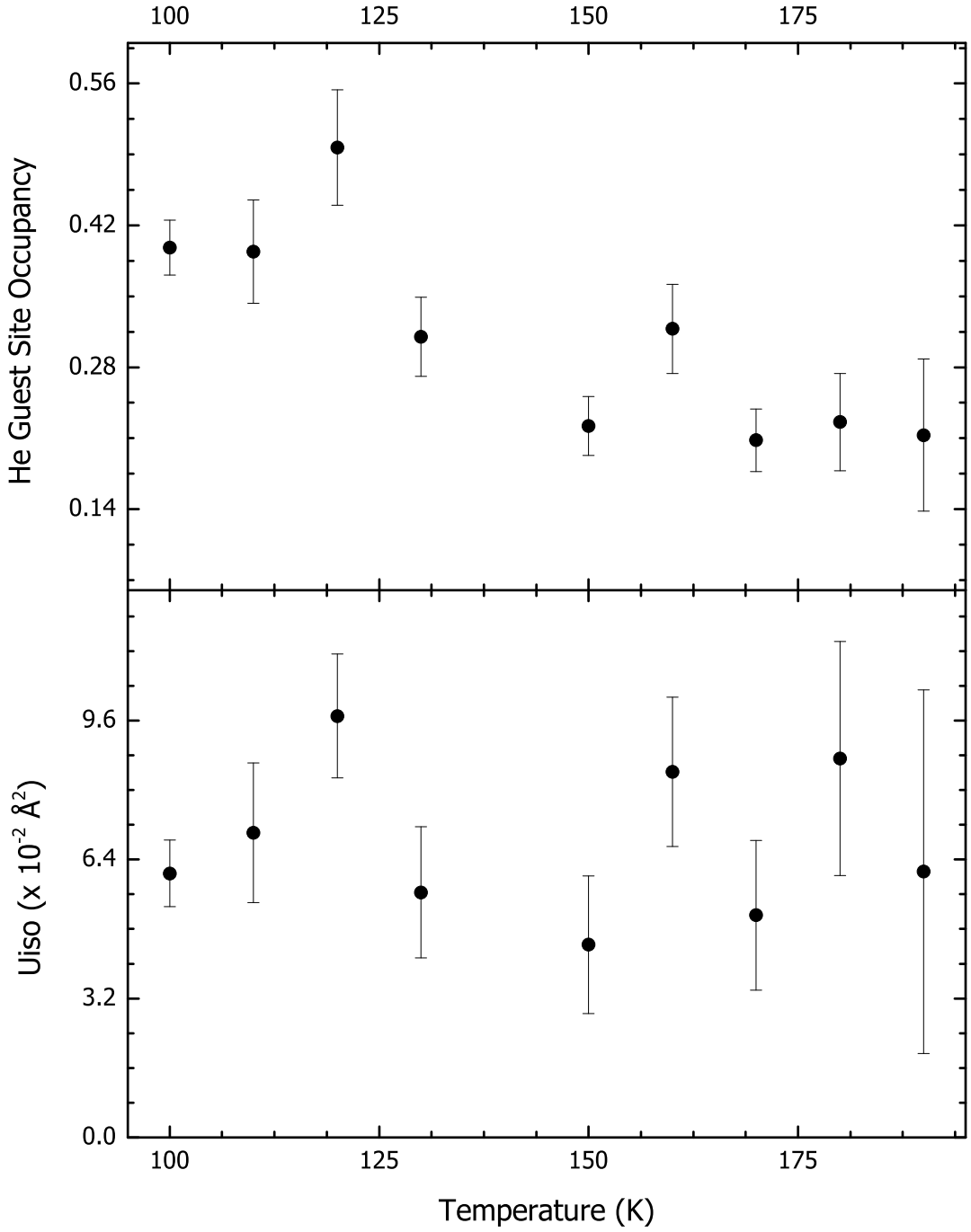

Figure 7.19 *Variation of the He guest site occupancy and thermal parameter (U_{iso}) with increasing temperature at 0.4 GPa.*

contaminating the C_{-1} diffraction pattern at 0.3 GPa. This work presented here does not look at the modelling of the ice Isd starting material and the possibility of an ice Isd clathrate as it is difficult to determine if the deuterium uptake of the cubic and hexagonal portions of the ice Isd are similar. Further modelling and experimental data would be needed to determine this. To confirm if the structure formed in the He hydrate is the same as that formed in D_2 a clean sample made from a pure ice Ih starting material is needed.

The formation and decomposition behaviours in both hydrate systems were also studied. In the He-D_2O system a similar formation process was observed to that in D_2-D_2O. At 0.4 GPa (He-D_2O) and 0.3 GPa (D_2-D_2O) at the onset of transition, reflections that are not purely attributed to the c-axis ($(00l)$ reflections) are observed to move to higher d-spacing. The reflections that are described by $(00l)$ shift to lower d-spacing. If the process is as described here, the low pressure splitting observed in the D_2-D_2O system could be mixed C_{-1}/ice Ih and there is not enough pressure to fully convert to the C_{-1} structure.

The C_{-1} structure once formed in the He-D_2O system displayed unexpected behaviour on warming at 0.4 GPa with the contraction of the a-axis and volume whilst the c axis expanded. This may be to do with the guest occupancy. As ice Ih converts to C_{-1} the a/b axes expand to accommodate the guest helium atoms whilst the c-axis contracts slightly. This can be observed in the behaviour of the reflections on formation with the purely $(00l)$ reflections shifting to lower d-spacings and those not purely attributed to the c-axis shifting to higher d-spacing. After the sample was warmed from this initial formation a general decrease in occupancy He guest atom with temperature is observed. During this warm up the the c-axis is observed to expand and the a-axis contracts. This suggests that as He leaves the structure, the lattice parameters tend to contract/expand back to the same parameters pure ice Ih would have at that pressure.

Chapter 8

Other High Pressure Studies

Although the gas cell used to carry out the studies on the low pressure D_2-D_2O system in the previous chapters has many benefits such as good sample to background ratio and easy control of the pressure, it is limited to a maximum pressure of 0.3 GPa. This is insufficient to access the C_1 and C_2 structures. To extend the previous work to pressures beyond 0.3 GPa, two other high pressure devices were used, the Paris-Edinburgh press and diamond anvil cell (both described in full in sections 4.2 and 4.3.2 respectively).

The first of these, the Paris-Edinburgh (PE) press is a long established tool for high pressure neutron diffraction, however only recently was a hydrogen-compatible gas-loading apparatus developed by Klotz *et al.* [87]. Prior to the work presented here a series of successful tests were carried out in which D_2 was successfully loaded into a PE press [87]. The work presented in this chapter aimed to develop the loading procedure for this apparatus by loading a mixed sample where one constituent was a solid rather than liquid D_2O. This 'less risky' sample was deuterated urea and D_2 gas as it has been proposed to form inclusion compounds and may have been of interest as a possible hydrogen storage material [8]. However, the results presented in this chapter indicate that D_2 does not form inclusion compounds with urea under the pressure/temperatures studied. This work has been published in reference [113]. A further test of the loading procedure was made with neon and D_2O as the filled ice II structure observed in the H_2 hydrate system (C_1) was also predicted to occur in this system, and at the time of the work it was unknown whether FIS-II formed in the Ne-D_2O system. The loadings of these samples were unsuccessful and are discussed in part 8.1.4.

The latter half of the chapter is focused on neutron diffraction experiments in diamond anvil cells and looks at a preliminary result of the D_2-D_2O system up to $\sim$ 28 GPa at room temperature.

8.1 Urea - Deuterium Mixtures

Below 0.3 GPa, an aluminium gas cell was used on the PEARL instrument at the ISIS neutron source as described in 4.1. Powdered deuterated urea was placed in the gas cell and then pressurised using D_2 gas. Diffraction data were collected in the 90° scattering geometry at room temperature at a series of gas pressures up to 0.3 GPa. For the higher pressure neutron diffraction experiments above 0.3 GPa, a PE press was used to generate pressure on a mixture of deuterium and urea. The loading procedure for this can be found in detail in section 4.2. After the PE press was loaded with a mixture of D_2 and urea it was mounted on the PEARL instrument at the ISIS neutron source and diffraction patterns were obtained in the 90° scattering geometry with increasing applied hydraulic load to increase the sample pressure. Each diffraction pattern was collected over approximately 3-4 hours. For both pressure regimes, data were reduced using the Mantid software suite and the resulting diffraction patterns were analysed by Rietveld profile refinement using the GSAS software suite (see chapter 4 for more details). The data were analysed by Rietveld refinement, however the relatively small proportion of urea in the sample volume that was necessary for the deuterium loading procedure resulted in a low sample signal-to-background ratio which prevented full refinement of the atomic fractional coordinates.

8.1.1 At Low Pressures

The bottom diffraction pattern in figure 8.1 shows a neutron diffraction pattern of the as-loaded deuterated urea sample at 293 K in the aluminium gas cell. The diffraction peaks can be assigned to the known tetragonal phase I of urea and the aluminium of the gas cell. To check whether there was any filling of hydrogen into the voids of the known urea structures, the lattice parameters of the unit cell were followed as a function of pressure and if there was some inclusion of the D_2 into the structure this would be expected to be manifested in anomalies in the lattice parameters and changes in the relative intensities of the reflections.

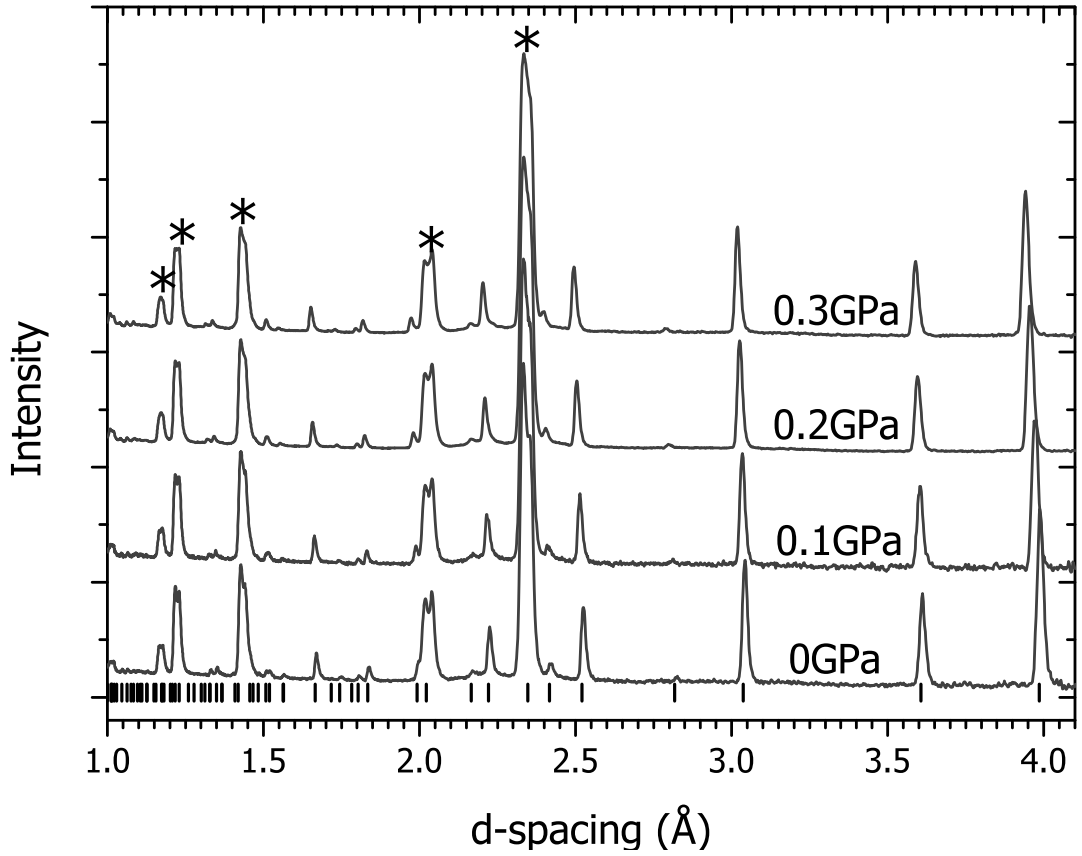

Figure 8.1 *The neutron diffraction patterns from urea compressed with D_2 gas between 0 and 0.3 GPa. Asterisks mark contaminant reflections from the gas cell and the ticks mark reflections from the tetragonal phase I of urea.*

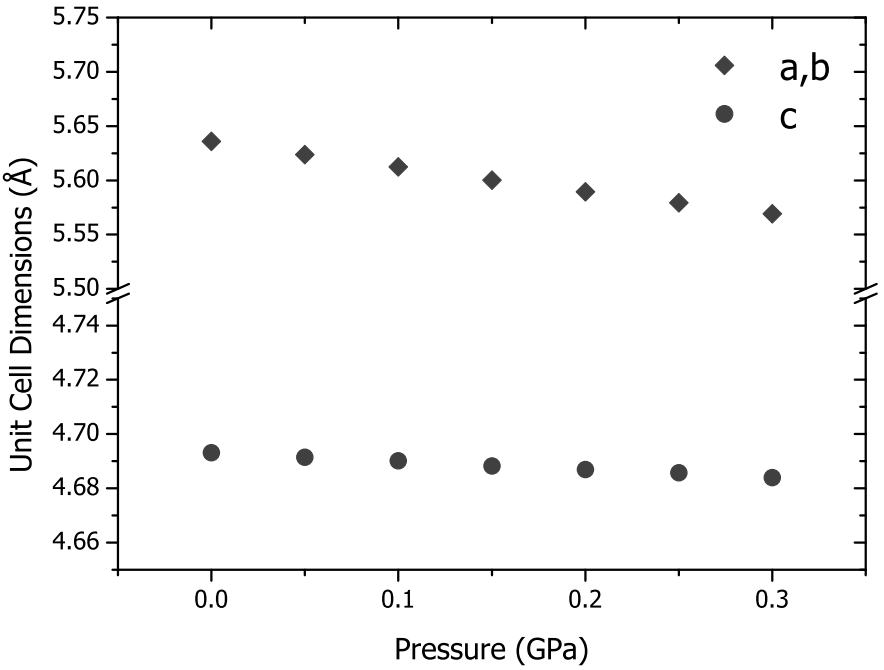

Figure 8.2 *The pressure dependence of the lattice parameters obtained from Rietveld refinement of phase I of urea to the diffraction patterns shown in 8.1.*

Upon pressurisation of the sample with D_2 gas, the reflections move to lower d-spacing as expected with increasing pressure as shown in figure 8.1. The refined lattice parameters as determined by Rietveld analysis of the patterns shown in figure 8.1 are shown in figure 8.2. No anomalies are observed in the unit cell parameters upon compression suggesting that no deuterium has entered the phase I structure and that normal compression behaviour of the sample is being observed. Based on the gas cell data the bulk modulus of the sample in the range 0 - 0.3 GPa was determined to be 10.4(2) GPa (with V_0 = 149.08(2) Å^3 and K' = 9(2)) using a Murnaghan equation of state [114]. At pressures up to 0.3 GPa, the diffraction patterns are all well fitted by the known structure of tetragonal phase I of urea, and there is no obvious transition to a new inclusion phase (see diffraction patterns in figure 8.1).

8.1.2 At High Pressures

At pressures above 0.3 GPa, the Paris-Edinburgh press was used to compress a mixture of deuterium and deuterated urea. A neutron diffraction pattern of

the as-loaded sample (with no load applied on the PE press) is shown in figure 8.3. Rietveld refinements (figure 8.3) of these data showed that all peaks can be explained by orthorhombic urea phase-III, or the gasket and anvil material surrounding the sample and that the sample pressure (all pressures above 0.3 GPa were determined by comparison of the unit cell volumes obtained from Rietveld refinements of the urea phase with those found by a previous study by Olejniczak et al. [66]) was 0.8 GPa. This high pressure of the as-loaded sample is a result of the load applied to the clamp that is required to seal the D_2 gas into the sample chamber combined with the 0.2 GPa pressure at which the gas was loaded. The pressure of 0.8 GPa is quite high given the relatively small applied load of 12 tonnes. This provides a clear indication that a full charge of deuterium had been sealed. The amount of urea loaded into the sample chamber filled less than half of the available volume and so had no gas been loaded when the clamp was sealed the pressure would have been close to ambient. Furthermore, as the load was increased the pressure rose at a rate that indicated the sample chamber was filled with D_2+urea rather than just pure urea. And, in phase III there is no evidence of peak broadening indicating that the sample is under near-hydrostatic conditions. Experience suggests that urea peaks broaden considerably without a hydrostatic medium such as deuterium [65, 67]. These observations are important because they confirm indirectly the presence of deuterium which is a fluid at these pressures and temperatures and so cannot be observed directly in the diffraction signal. The pressure dependence of the axial ratios (c/a, b/a, b/c) are shown in figure 8.5. At an applied load of 35 tonnes (figure 8.4), corresponding to a sample pressure of approximately 2.75 GPa, a clear change in the diffraction pattern was observed. The diffraction peaks from the sample can be indexed as the orthorhombic phase IV of urea and this can be seen from the change in the axial ratios in figure 8.5. Up to the maximum pressure of 3.7 GPa, no evidence was found of any peaks which could not be explained by either a known phase of urea or the gasket (beryllium copper) or anvil (tungsten carbide with nickel binder) materials.

The ratios of the refined lattice parameters (c/a, b/a, b/c) are shown as a function of pressure alongside data from a previous x-ray diffraction study on pure urea by Olejniczak et al. in figure 8.5 [66]. Although the unit cell volume is used to determine the pressure here, it is extremely unlikely that formation of an inclusion compound would give a unit cell whose shape and size were identical to those of pure urea. Hence, the fact that the unit cell shapes (the c/a, b/a, b/c ratios) shown in Figure 8.5 are the same as those of pure urea for a given pressure (or

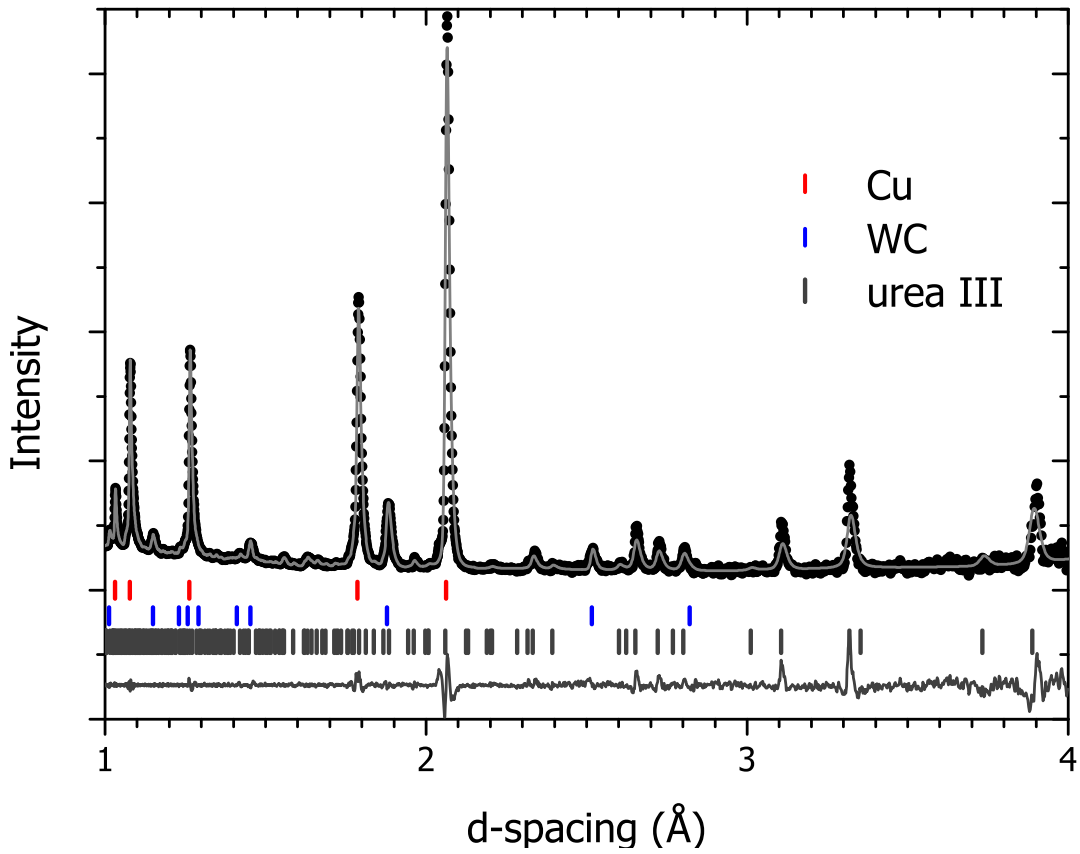

Figure 8.3 *Rietveld refinement of the urea phase III structure to the profile of the as-loaded urea and D_2 sample.*

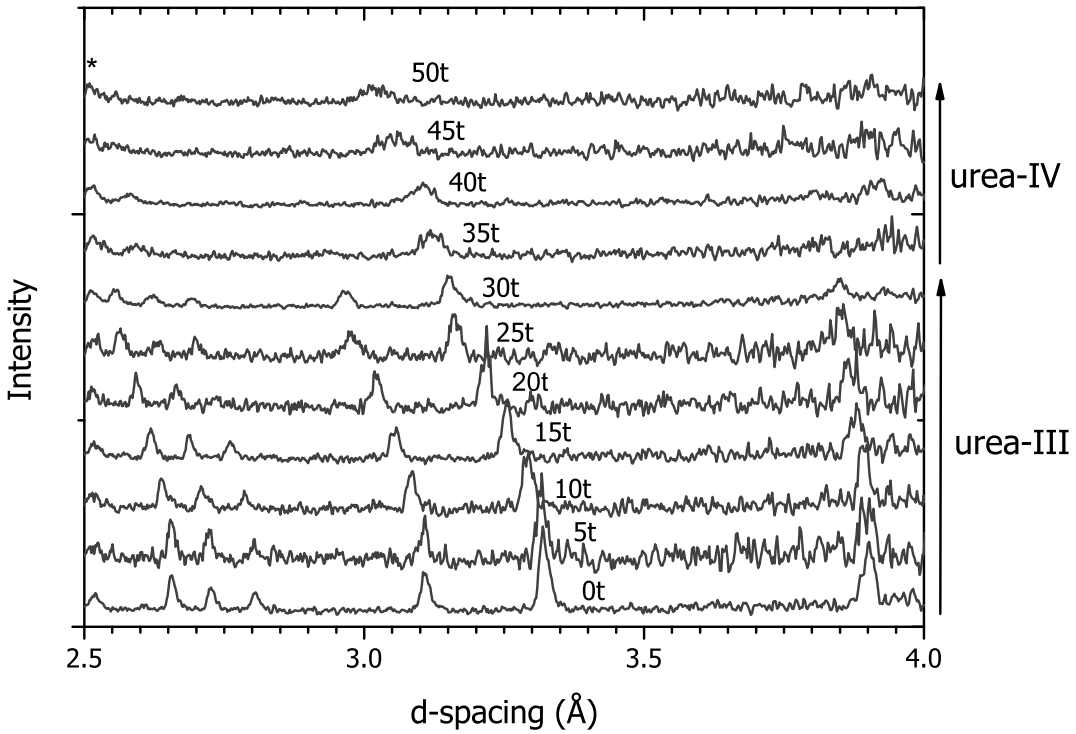

Figure 8.4 *Diffraction patterns of urea and D_2 compressed with increasing load applied to the Paris-Edinburgh press showing the transition from phase III to phase IV of urea. Data below 2.5 Å are not shown here as sample peaks could not be seen upon load being applied to the sample due to the low sample-to-background signal and low quality data.*

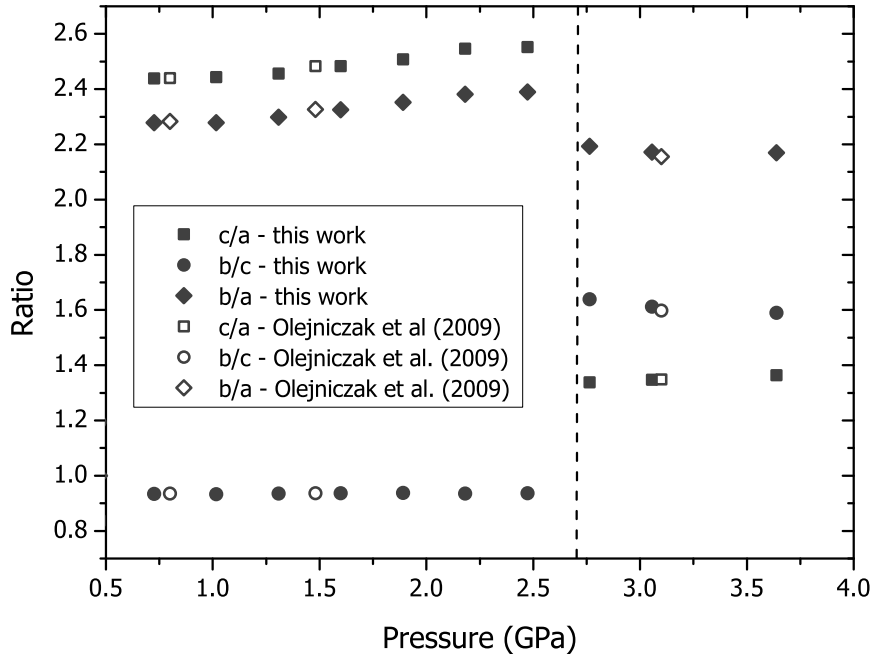

Figure 8.5 *The ratios of the unit cell parameters obtained from Rietveld refinements of the diffraction data shown in figure 8.4. Squares, circles and diamonds show the c/a, b/c and b/a ratios respectively, and the filled symbols show the data from this study while the open symbols represent data measured by Olejniczak et al. [66]. The dotted line at approximately 2.75 GPa marks the phase boundary between the orthorhombic phase III ($P2_12_12_1$) and the orthorhombic phase IV ($P2_12_12$) of urea. Estimated uncertainties were smaller than symbol sizes and so have not been included. Pressures were determined from the measure unit cell volumes using the EoS data from Olejniczak et al. [66].*

unit cell volume) indicates that there is no measurable hydrogen uptake in the pressure range studied [66].

8.1.3 Discussion

Thus, the behaviour of the urea sample conforms to that reported for pure urea [65, 66, 67]. No evidence is seen of any new phases in the diffraction signal and all transitions occur at the expected unit cell volumes, and hence pressures, as the transition pressures found for pure urea [65, 66, 67]. Furthermore, the axial ratios of the various unit cells are again within error of those observed in pure urea for the same unit cell volume (or pressure) [66]. The absence of any new unexplained phase, or anomalies in the transition pressures and unit cell dimensions of the high pressure phases, indicates that there is no incorporation of deuterium into the urea lattice and that urea-hydrogen clathrates do not form under the pressures studied at room temperature. It might appear that formation of inclusion compounds under these conditions is kinetically inhibited because hydrogen is unable to enter the bulk material. However, hydrogen is known to be extremely diffusive at high pressure and is found to penetrate metals and even diamond [110]. Given the 'openness' of the crystal structures formed by urea there should be no problem for hydrogen to diffuse into the bulk material. This is why the absence of inclusion compound formation observed here represents the true thermodynamic behaviour.

8.1.4 The Neon-Water System and Possible Further Work

A test was done using the gas loader on another mixed system this time with a liquid and a gas. There is a risk that during the process the liquid D_2O would evaporate. To test whether much of the D_2O would evaporate Ne gas was chosen rather than D_2 as this gas requires a more simple loading process and no helium check has to be done. The Ne-D_2O system was also chosen as, at the time, no neon hydrates had ever been observed in the system despite some evidence that there might be one at low pressures with the speculation that this is the same FIS-II structure found in the helium hydrate and in hydrogen hydrate [44]. It is now known that the Ne-D_2O system has an FIS-II phase at 0.48 GPa and below 260 K [23]. Two samples were prepared the same way but both samples were initially in different states. The first sample (cell 1) was already frozen into ice

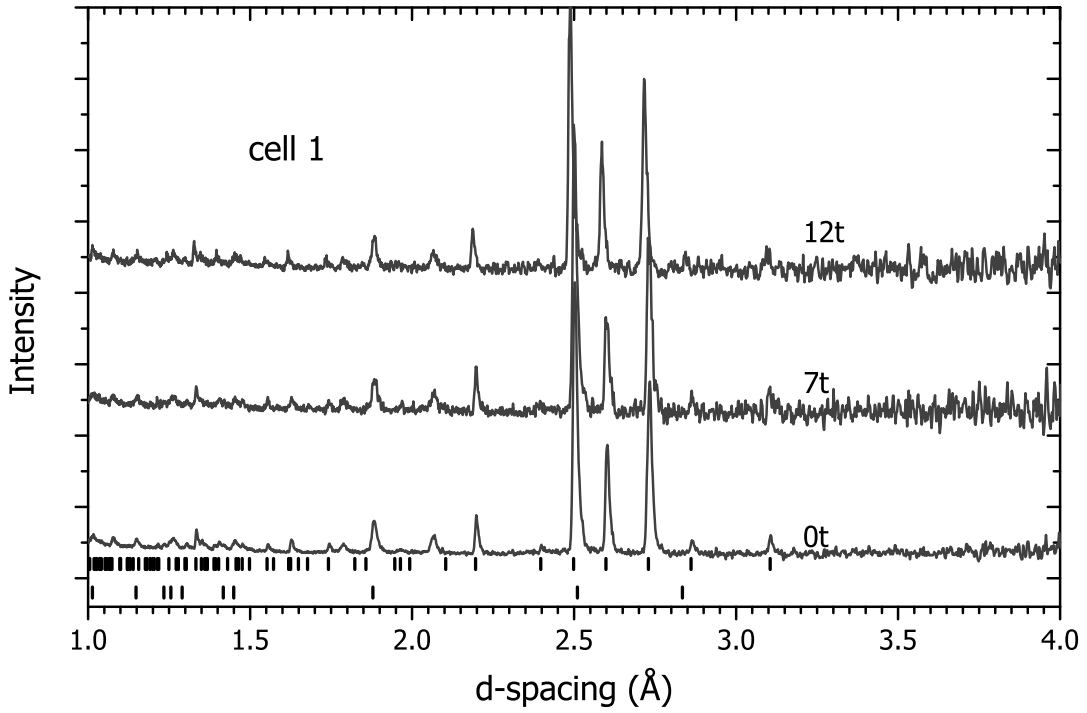

Figure 8.6 *Neutron diffraction patterns of the first sample of Ne and D_2O in a gas loaded Paris-Edinburgh press at various hydraulic loads (0 - 12 tonnes). Tick marks indicate the position of reflections from the ice VI (top) and tungsten carbide of the anvils (bottom) and can describe all peaks with the exception of those at $\sim$ 2.06 Å and 1.78 Å which are from the nickel binding material of the anvils.*

VI whereas the other sample (cell 2) was still in a liquid state.

Sample 1

As seen from the diffraction patterns in figure 8.6 the sample after loading was determined to be polycrystalline ice VI from the diffraction patterns not being consistent across all detectors (bottom pattern). The pressure of the sample was determined to be ~ 0.8 GPa from the equation of state of ice VI [115]. The sample was originally loaded in a neon atmosphere at 0.2 GPa and this extremely high pressure of the sealed sample is thought to be attributed to a full sample volume most likely due to the overfilling of the gasket with water which was done to make up for any water lost from the sample via evaporation during the loading procedure.

As the load on the press was increased to 7 tonnes, and then to 12 tonnes, the sample pressure was found to increase slightly to 0.83 GPa and 1.15 GPa

respectively. During this the sample was observed to remain as ice VI and no other peaks which could indicate a high pressure hydrate phase could be observed. Although there was no observation of a neon hydrate phase there is the possibility that no neon was loaded as the gasket cups were filled with D_2O.

Sample 2

The second sample was loaded following the same procedure as that done for sample 1, however the diffraction pattern collected at a load of 2.5 tonnes showed the sample to still be liquid D_2O (bottom pattern in figure 8.7). As the load on the sample was increased the sample was found to be a mixture of textured ice VI and ice VII powders at 30 tonnes and the pressure was determined from equation of state to be 2.02 GPa (ice VI) and 2.39 GPa (ice VII), with the most probable sample pressure being somewhere in between them at the boundary line [115, 116]. As load was increased the sample then converted to a decent powder of ice VII, and the pressure in the sample was determined from the equation of state to be 2.44 GPa. There were no significant deviations observed in the intensities from those of pure ice VII suggesting that no uptake of neon had occurred if there had been any Ne gas loaded into the sample.

Further Work

From the data collected on both samples no deviations from the behaviour of pure ice were observed on compression at room temperature. This suggests that either neon does not form a clathrate hydrate at room temperature or that no neon was originally loaded into the samples. During the gas loading procedure of the Ne - D_2O some evaporation of the liquid D_2O was initially expected to occur. However, as seen in the diffraction data for both samples, the sample volume is most likely entirely D_2O which would result in no neon being loaded. This suggests that the overfilling of the gasket cups to make up for any D_2O lost in the couple of hours it takes to gas load is not needed. Further tests should be done on a gas that is known to form a clathrate at room temperature should be tested to check the loading procedure before D_2 is used. During the loading procedure for D_2, a helium pressure test has to be completed prior to D_2 being put into the gas loading apparatus and there is a risk that the sample could be affected

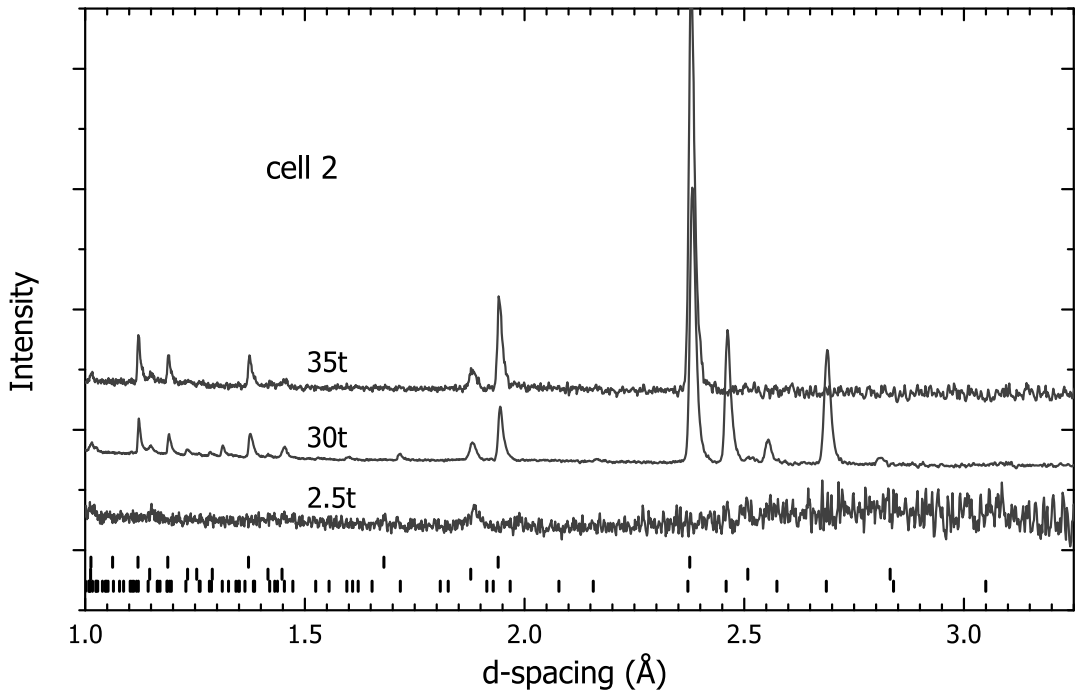

Figure 8.7 *Neutron diffraction patterns of the second sample of Ne and D_2O at various hydraulic loads as it transitions from liquid D_2O to an ice VI/ice VII mixture and then to pure ice VII. Tick marks indicate the positions of the reflections from ice VI (bottom), tungsten carbide from the anvils (middle) and ice VII (top).*

by this[1]. However, as He forms a hydrate around these pressures it is thought this would happen during the pressure test and upon removing pressure prior to loading with D_2 the hydrate would dissociate and leave liquid D_2O behind. The hope is that this would occur with minimal loss of D_2O.

Despite both samples being loaded with the same method both samples were at different pressures initially. This may be due to an increased evaporation of the D_2O which could be caused by slight changes out with control occurring within the loading environment prior to the sample clamp being sealed in the pressure chamber. This could become an issue as exact ratios of D_2:D_2O are needed and any leftover D_2O or D_2 would result in contaminant phases being present which would reduce the diffraction signal of the sample of interest further.

8.2 The D_2 – D_2O System at High Pressures

Although the procedure for loading gases such as deuterium into PE presses is still under development it is more routine for diamond anvil cells especially when one component is a liquid. In addition to an easier and routine loading procedure, diamond anvil cells also offer greater control over the ratio of constituents, for example the ratio of D_2:D_2O. A sample of D_2–D_2O was prepared using the method outlined in 4.3.1 with an approximate molar D_2:D_2O ratio of 1:1. After successfully loading the D_2 into the cell at 0.2 GPa, the sample pressure was increased to 3.6 GPa as determined by ruby fluorescence. Neutron diffraction data were then collected on SNAP at the SNS and all the setup/preprocessing procedure is described in section 4.3.2. The sample was then compressed by applying load with the membrane attached to the cell and the pressure determined for each load which can be seen in figure 8.9. As the sample was compressed by increasing the pressure in the membrane from 0 to 60 bar, the extraction of D_2 from the C_2 phase was observed to occur above 18 GPa (membrane pressure of 40 bar) and is discussed below (8.2.2) after a discussion on how the sample pressure was determined at the maximum membrane pressure.

[1]The helium pressure test is done prior to taking the gas loading apparatus up to 0.2 GPa with hydrogen/deuterium. This is when the clamp is placed in the pressure chamber and the gas loading apparatus taken to 0.2 GPa with helium gas and left for one hour to ensure that all seals have been made correctly before hydrogen/deuterium are loaded. During the helium pressure test and subsequent hydrogen/deuterium loading the sample remains sealed within the pressure chamber.

8.2.1 Sample Pressure Determination

The pressure of the sample in diffraction patterns collected up to 18 GPa were determined by ruby fluorescence, however for the last diffraction pattern collected (corresponding to a membrane pressure of 60 bar) no signal from the ruby could be observed. The ruby signal could be seen up to membrane pressures of 55 bar which corresponded to a pressure of $\sim$ 25.5 GPa. Attempts were made to determine the pressure of the sample at membrane pressure of 60 bar with the equation of state (EoS) of ice VII, D_2 and C_2 (see figure 8.8). However, these were ruled out as possibilities due to the resultant pressures not being consistent for each pressure studied. For example, at 18 GPa the pressure determined by the EoS of D_2 was in close agreement with the pressure given by ruby fluorescence (figure 8.8), however as membrane pressure was increased to 60 bar the EoS gave a sample pressure of 24.5 GPa. This pressure is below the pressure determined from ruby fluorescence at a membrane pressure of 55 bar (25.5 GPa) so the EoS of D_2 was determined not to be reliable for pressure determination. This may be due to the D_2 that is present in the sample above 18 GPa most likely consisting of multiple large single crystals in random orientations which could result in the compression data being compromised. A similar issue is also expected for sample pressures determined from ice VII. In addition the hydrostaticity of the environments in which the D_2 and ice VII are located are unknown. The sample pressures given by the EoS for C_2 (filled circles in 8.8) are in good agreement with the ruby fluorescence pressures between 3.6 and 6.8 GPa, however at 18 GPa there is a massive divergence between the C_2 EoS pressure and the ruby pressure ($\sim$ 8.5 GPa). In the diffraction patterns collected at 18 GPa there is also the sudden appearance of D_2 present in the diffraction patterns which suggests a possible structural change which would make the EoS for C_2 unreliable at these higher pressures (this is discussed further in 8.2.2).

Another usually less reliable method for determining the sample pressure is from the 'pressure-load' curve which is a plot of the pressure in the membrane versus the resultant sample pressure (figure 8.9). This is unreliable as it relies on the quality of the loading and does not follow a linear trend below membrane pressures of around 20 bar. From around 20 bar onwards the pressure-load curve follows a roughly linear trend unless the sample/gasket starts to 'blow out'. In figure 8.9 the membrane pressure-sample pressure curve is plotted for this sample and two pure ice VII samples. As can be seen in figure 8.9, from around 20 bar in membrane pressure the curve follows a linear trend for all three samples. For the

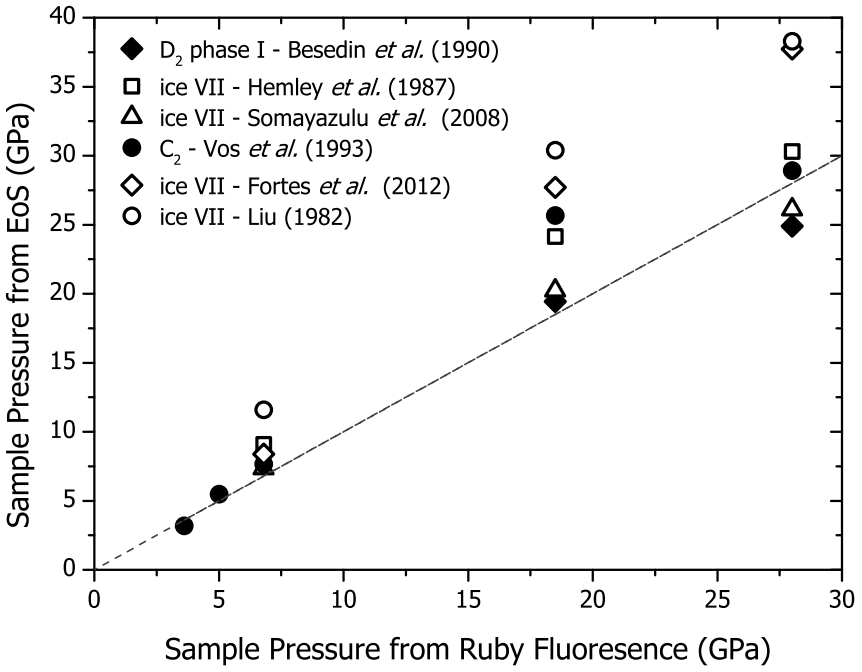

Figure 8.8 *Sample pressures as determined from various equation of states (EoS) for the pressure points studied for ice VII, D_2 phase I and the C_2 phase. The vertical axis shows the pressure determined from the various EoS, and the horizontal axis is the pressure as determined from ruby fluorescence (with the exception of the pressure at 28 GPa which was determined from extrapolation of the membrane pressure – sample pressure curve - figure 8.9). Filled diamonds and circles represent sample pressures calculated from the EoS for phase I D_2 and C_2 hydrogen hydrate [37, 91]. Open symbols (squares, triangles, diamonds and circles) indicate the pressures calculated from several EoS for ice VII, respectively, found in references [116, 117, 118, 119].*

pure ice VII samples there was no optical access to the cells so sample pressures were determined from the EoS for ice VII only. These sample pressures (pure ice VII) are thought to be more reliable than those determined for the ice VII present in this sample as they were determined from samples that consisted of good powders (not consisting of large single crystals) which would give reliable compression data [116]. The ice VII pressures are found to be in agreement with those from ruby fluorescence. The data from ice VII (run A) seems to show a slight deviation from the linear trend at high pressures and this is thought to be due to the quality of the loading as the gasket was originally thinner than desired. The pressure of this sample was then extrapolated from the linear trend shown in figure 8.9 at the top load of 60 bar was determined to be $\sim$ 28 GPa.

8.2.2 Extraction of D_2 from C_2

At 3.6 GPa the sample was observed to be a mixture of the C_1 and C_2 phases of hydrogen hydrate (bottom diffraction pattern in 8.10). The Le Bail refinement of the unit cells for C_1 and C_2 to this data are shown in figure 8.11. Le Bail refinement was chosen over Rietveld as the intensities of the sample below 2 Å are unreliable as they are greatly affected by the attenuation of the upstream diamond, with this effect becoming greater as more load is applied to the cell. At this time the issue of routinely correcting for attenuation of the diamond is still in development [102]. Given that the majority of sample peaks are below 2 Å, this work here is considered preliminary and only peak positions are considered.

As the sample was compressed to 5 GPa, only one diffraction peak attributed to the C_2 structure could be observed. At this point it was thought that the sample had fully converted to C_2 and was phase pure as no obvious contaminant ice or deuterium peaks are present in the diffraction pattern. However, as the data collected at this pressure was of poorer quality there is the possibility that a peak from ice VII could be 'hidden' in the noise at a slightly higher d-spacing than the peak from C_2 at $\sim$ 2.2 Å

At 6.8 GPa the appearance of a peak from ice VII is attributed to possible 'dehydration' and the sample of C_2 becoming more rich in deuterium which is expected at high pressures as more D_2 is forced into the structure. However, without better quality data at lower pressures and refinable intensities there is the possibility that the sample originally had an abundance of D_2O and is richer in water than the intended molar ratio of 1:1. As the sample was compressed

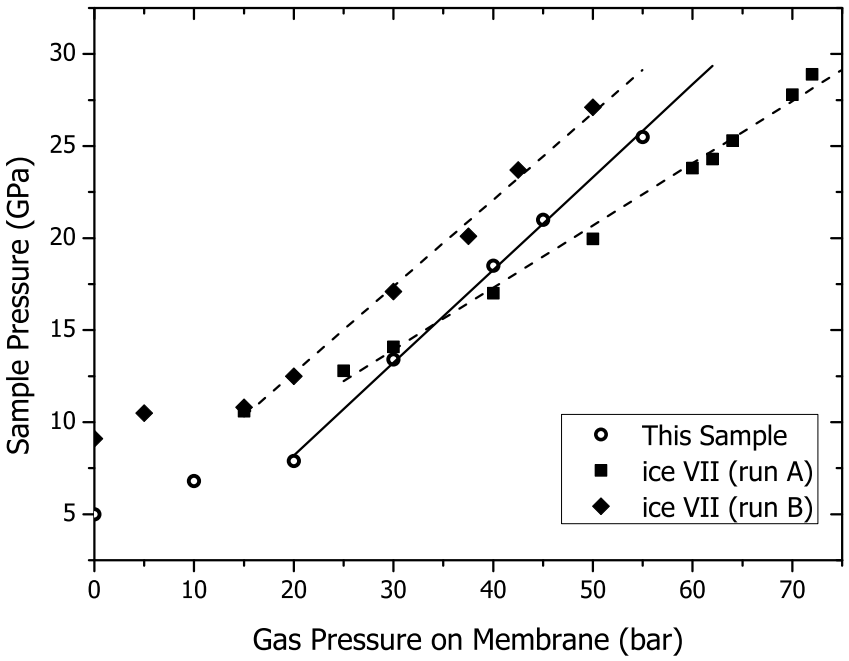

Figure 8.9 *The pressure of the sample as determined from ruby fluorescence/equation of state for ice VII for various membrane gas pressures applied to the same design of cell with approximately the same diamond culet size. Filled symbols indicate the membrane pressure − sample pressure curves for two samples of ice VII determined from the EoS of ice VII [116]. Open symbols indicate the membrane pressure − sample pressure curves for this sample of D_2−D_2O with the pressures determined by ruby fluorescence. Between 15-25 bar the curves start to follow an approximate straight line unless the gasket starts to 'blow out'. Lines of best fit are shown for each of the data sets (dashed lines for each of the ice VII runs and a solid line for this D_2−D_2O sample). Extrapolation of the straight line segment of the membrane pressure − sample pressure curve for the data collected on this sample show that at 60 bar the sample pressure should be ∼ 28 GPa.*

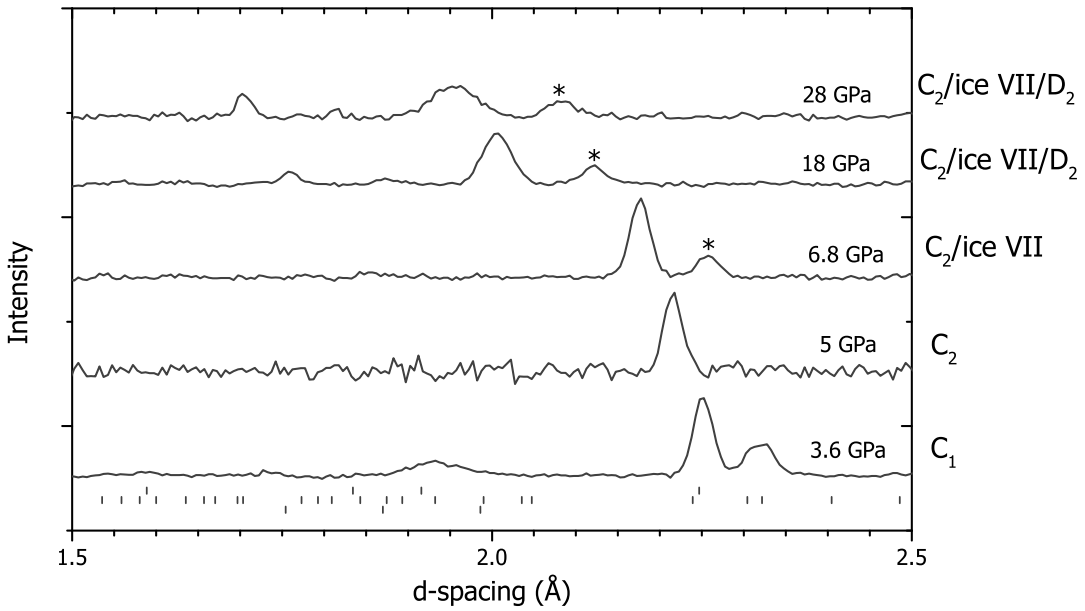

Figure 8.10 *Neutron diffraction patterns of the D_2–D_2O system with increasing pressure. Tick marks indicate the positions of reflections from the C_2 and C_1 phases of D_2–D_2O (top and middle respectively) and phase I of D_2 at 18 GPa (bottom). Asterisks mark the position of the reflection from ice VII. Data excluded below 1.5 Å as no more sample peaks could be observed.*

further to 18 GPa reflections attributed to phase I of D_2 were observed. This combined with the continued presence of ice VII was originally unexpected as it suggested that the sample had dissociated and it was unclear whether this was usual behaviour for the sample. However, the extraction of D_2 from the C_2 structure has been observed previously in a Raman spectroscopy study by Machida *et al.* who reported the presence of a vibron of attributed to pure H_2 that was observed in compression of C_2 hydrate above 20 GPa [47]. This giving up of D_2 is proposed as mechanism to stabilise the C_2 structure as the rotation mode of the H_2 molecules becomes increasingly damped as pressure was increased to 20 GPa as the H_2 molecules become more confined and their motion becomes damped. After some of the H_2 was extracted the rotational modes of the H_2 remaining within the structure, and thus the rotational motion, recovered [47].

8.2.3 Deviation from Cubic Symmetry

In addition to the observation of phase I D_2 above 18 GPa, the main reflection from C_2 at 2 Å becomes increasingly broader at the same pressures. This could be an effect of non-hydrostatic stress on the sample, however the reflections from

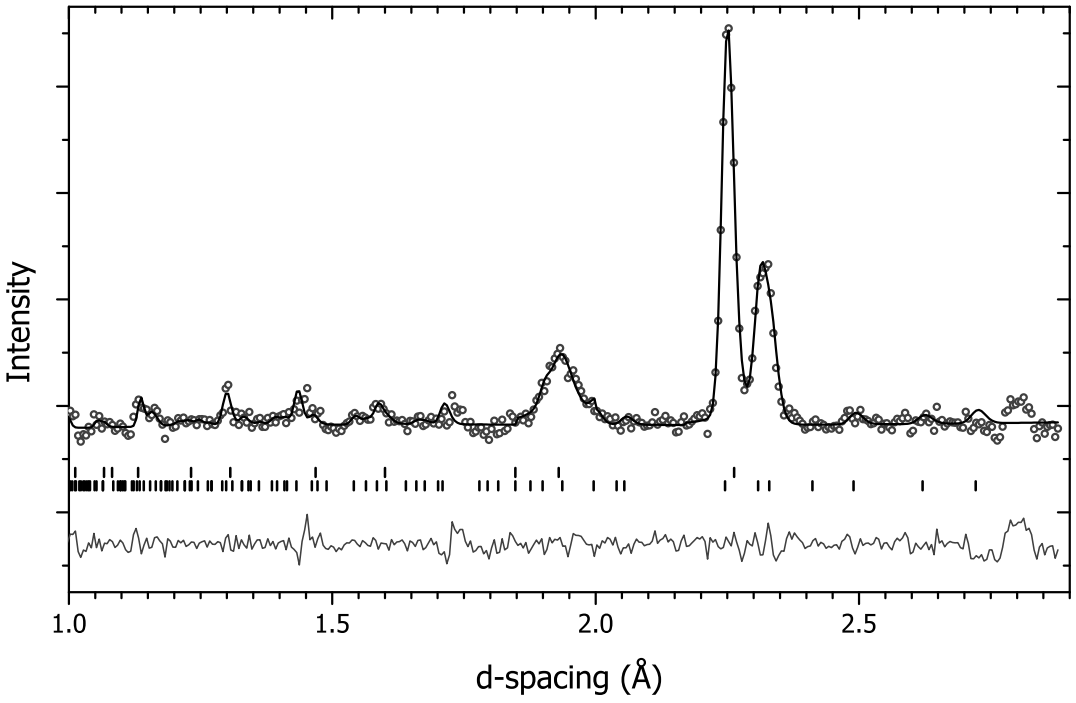

Figure 8.11 *Le Bail refinement of the C_1 and C_2 unit cells to data collected on the D_2–D_2O system at 3.6 GPa. Circles indicate observed data and the black curve shows the calculated diffraction pattern of the Le Bail refinement of the C_1 and C_2 unit cells. The curve at the bottom shows the difference between observed and calculated diffraction patterns. Tick marks indicate the positions of reflections from the C_2 and C_1 phases of D_2–D_2O (bottom and top respectively).*

ice VII and D_2 phase I do not show similar behaviour (see top two diffraction patterns in figure 8.10). In a previous x-ray diffraction study it was reported that above 20 GPa hydrogen hydrate distorts slightly from a cubic unit cell to a tetragonal one [46]. To test this possible deviation from cubic, Le Bail refinements of tetragonal unit cells were fitted to the data at both 18 and 28 GPa. At 28 GPa the tetragonal cell did not result in a better fit to the data as the refinement was unstable probably due to the poor diffraction statistics and increased overlapping of the C_2 and D_2 peaks. At 18 GPa the tetragonal unit cell gave a slightly improved fit of the data with a R_{wp} of 13.6% for the tetragonal unit cell compared with a R_{wp} of 16.5% for cubic. However, this small difference did not result in any obvious improvement to the fit of the model to the data and is thought that this improvement may just be due to the tetragonal cell being better at describing the broad sample peaks than the cubic unit cell. From the pressures determined from the C_2 EoS shown in figure 8.8 it can be seen that the EoS pressures below 6.8 GPa are in relatively good agreement with those determined from ruby fluorescence and at 18 GPa the pressure determined from the EoS is much higher than expected. This deviation could also be indicative of a structural transition as the C_2 EoS parameters do not give the correct relationship between the pressure-volume data.

8.2.4 Discussion

The lack of peaks in the diffraction data (figure 8.10) is due to the single crystal masking procedure carried out in data preprocessing. Whilst this preprocessing removes the reflections from the single crystal diamond anvils allowing smaller powder sample peaks to be observed at that d-spacing, it also lowers the data quality and weak sample reflections can no longer be observed in the background noise. A better method for dealing with the diffraction from the anvils is currently under development [102]. The decrease in the D_2 content of the sample at 18 GPa combined with the possible lack of cubic symmetry give way to the possibility that there might be a structural change in the D_2–D_2O system above these pressures. However, as this is a preliminary study and the intensities are not refinable in their current state it is unclear whether this possible structural transition is just a slight shift in position of the guest D_2, if the host D_2O network is also rearranged or some combination of both. If this structural transition was a significant structural arrangement of both the D_2 and D_2O molecules this could impact the compressibility and the pressure at which the O–D...O bond becomes

symmetric in the D_2–D_2O system could be much higher than expected $\sim$ 60 GPa.

8.3 Summary

The data collected on urea-deuterium mixtures at both low pressures with use of a gas cell, and at high pressure with use of a gas loaded PE press show that urea does not form an inclusion compound with deuterium at room temperature in the pressure region studied (between 0 and $\sim$ 3.7 GPa) . However, it did show that a PE press could be successfully loaded with a mixed sample of a solid and D_2 gas in the loader developed by Klotz *et al.*, and then compressed. Two attempts were made to load a mixed gas-water system – the Ne–D_2O system. These sample loadings were either unsuccessful or showed that neon did not form a clathrate at the pressures studied at room temperature as only ice VI and/or VII were observed in both samples. Despite the lack of success with the Ne –D_2O sample loadings, they did show that the excessive overfilling of the gasket to make up for any D_2O evaporated or spilled out of the gasket during the loading procedure is not required.

In addition to this work with gas loaded PE presses a preliminary study on a diamond anvil cell loaded with a mixture of D_2 and D_2O was done between 3.6 and 28 GPa. At low pressures the sample behaved as expected but at 18 GPa there was a decrease in the D_2 content of C_2 as pure phase I of deuterium was observed at these pressures. Above 18 GPa the main peak from C_2 broadened considerably and this is thought to be due to the lowering of the unit cell symmetry from cubic to tetragonal as this provides a better fit to the data. This distortion of the unit cell from cubic symmetry combined with the extraction of D_2 suggest that there is a possible change in the crystal structure of C_2 above 18 GPa. In addition to the broadening of the main diffraction peak of C_2, the pressures determined from the equation of state for C_2 hydrogen hydrate stop being in agreement with those determined from ruby fluorescence and the sample pressure- membrane pressure curve, above 18 GPa which further suggests a change in the structure. Similar behaviour has been observed in the hydrogenous analogue at 20 GPa by Machida *et al.*. However, given the lack of attenuation correction for the data collected here means that the intensities are not refinable and a full structural refinement could not be done to determine how much deuterium was extracted and what changes occur in the structure.

Chapter 9

Conclusion

In chapter 5 the phase diagram of the deuterated analogue of the H_2-H_2O system is explored at low pressure. This identified several transitions between metastable and stable phases. The series of transitions through metastable phases to stable phase observed was ice Ih $\rightarrow$ C_{-1} $\rightarrow$ C_0 $\rightarrow$ sII at both 0.2 and 0.3 GPa. At these pressures ice Ih-like networks have been calculated to be less stable than the C_0 structure for hydrogen hydrate [43, 44]. This means the sample went through a series of transitions that occur with increasing stability. The general transition sequence observed from ice Ih $\rightarrow$ sII is thought to follow Ostwald's Rule of Stages. If the C_{-1} structure is indeed based on ice Ih then this transition sequence through metastable structures provides an example of Ostwald's Rule of Stages occurring between crystalline structures.

Though the crystal structure of the C_0 phase was proposed prior to this work it was unable to fit the data collected in this work and a new structure that better fit the data was determined in chapter 6. This structure had a higher symmetry - $P6_122$ when compared to the originally proposed $P3_121$. This symmetry is also the symmetry that describes the host D_2O network and as the D_2 molecules are highly mobile with no fixed positions, the whole structure could be described purely by the symmetry of the host framework. At the maximum pressure studied here (0.3 GPa) the D_2 content was estimated to be 29(1)% which corresponds to a D_2:D_2O ratio just under 1:2 with this increasing to a greater than 1:2 ratio at lower temperatures ($\sim$ 100 K). Two attempts were made to study the pure host structure by emptying the D_2 out of the structure, however both attempts failed to catch the structure before it fully decomposed into ice Ic/Ih. The diffraction data

collected during these recovery attempts found that at least one D_2 molecule/unit cell had to be present for the phase to be stable; any less would result in the C_0 phase decomposing into ice Ic.

The open channels within C_0 are similar to those found in the filled ice structures present in the clathrate hydrates at high pressures ('FIS-Ih') or those with small guest species such He or H_2 (FIS-II). However, unlike the filled ices, the host framework present in C_0 is not based on any of the known ice phases. This makes the C_0 host a new stable water network. The C_0 phase is also unlike the filled ices in that the shape of the guest channel is more similar to the typical cages observed in the traditional clathrate structures sI and sII. This suggests that the C_0 structure is a cross between a filled ice and a clathrate. One of the other reasons the C_0 phase is more like the traditional clathrates sI/sII is that the same structure was recently found to occur in the CO_2 hydrate system [20]. As it occurs in two hydrate systems with guest species of very different sizes this structure is now dubbed with the name 's-Sp' for spiral structure to keep it in line with other clathrates such as sH for hexagonal structure.

Though the structure of the C_{-1} phase in the D_2-D_2O was not fully determined in chapter 7, a candidate structure has been proposed based on the similar behaviour observed in the He-D_2O system. The contamination of the C_{-1} phase is a problem. This contamination is not only if the gas pressure is not kept constant but is also from the starting material. If the starting material is not purely ice Ih then there could be contamination of the C_{-1} diffraction pattern by ice Isd or some partially filled ice Ic (C_2 clathrate). It is unclear if this filled ice Ih structure as described for helium hydrate is the same as the structure formed in D_2-D_2O. A selection of candidate unit cells and space groups were also determined for the C_{-1} structure in the D_2-D_2O system. A clean sample made from a pure ice Ih starting material is needed to confirm this.

In chapter 8 several further high pressure studies were done on the urea-deuterium and D_2-D_2O systems. The data collected on urea-deuterium mixtures show that urea does not form an inclusion compound with deuterium at room temperature under the pressure region studied (between 0 and $\sim$ 3.7 GPa). Two attempts were made to load a mixed water-gas system – the Ne–D_2O system. These sample loadings were either unsuccessful or showed that neon did not form a clathrate at the pressures studied at room temperature as only ice VI and/or VII were observed in both samples. Despite the lack of success with the Ne–D_2O sample loadings, they did show that the excessive overfilling of the gasket to make up for

any D_2O evaporated or spilled out of the gasket during the loading procedure is not needed. A preliminary study on a diamond anvil cell loaded with a mixture of D_2 and D_2O was done between 3.6 and 28 GPa. At low pressures the sample behaved as expected but at 18 GPa there was a decrease in the D_2 content of C_2 as pure phase I of deuterium was observed at these pressures. Above 18 GPa there was a possible distortion of the cubic unit cell and a decrease in the D_2 content. Similar behaviour has been observed in the hydrogenous analogue at 20 GPa by Machida *et al.*. However, an attenuation correction is needed to determine how much the deuterium content decreases by and what structural changes occurred.

The work presented within this thesis has contributed to the knowledge known about hydrogen inclusion compounds at high pressure. Though the crystal structure for C_0 has now been fully determined, the structure of the new phase, C_{-1}, has not been fully determined in this work. This is due to contamination by ice and a clean diffraction pattern synthesised from a pure ice Ih should determine whether this structure is the same as the filled ice Ih structure which was determined for helium hydrate under similar conditions. In addition to this work at low pressures, further high pressure studies were conducted on not only the D_2-D_2O system but also the deuterium-urea and Ne-D_2O systems. Although the urea-deuterium system did not form any inclusion compounds in the pressure region studied and the Ne-D_2O sample loading failed, they do provide the groundwork for future successful sample loadings of D_2-D_2O that could be used to study the crystal structure of C_1 clathrate. Unfortunately the data collected in a large-volume diamond anvil cell could not be fully Rietveld refined. However, with better methods to determine the attenuation correction caused by the single crystal diamond anvils, the study of the deuterated analogue of the hydrogen hydrate system to relatively high pressures with neutron diffraction could be further studied to explore not only the crystal structures formed with the D_2-D_2O system but could also study how the O-D bond length within these structures varies with pressure.

Bibliography

[1] J. V. der Waals and J.C.Platteeuw, "Clathrate Solutions," *Advances in Chemical Physics*, vol. 2, 1–57, 1959.

[2] J. S. Loveday and R. J. Nelmes, "High-pressure gas hydrates," *Physical Chemistry Chemical Physics*, vol. 10, no. 7, 937–950, 2008.

[3] E. G. Hammerschmidt, "Formation of Gas Hydrates in Natural Gas Transmission Lines," *Industrial & Engineering Chemistry*, vol. 26, no. 8, 851–855, 1934.

[4] E. D. Sloan and C. A. Koh, *Clathrate Hydrates of Natural Gases*. CRC Press, 2007. 3rd edition.

[5] R. Boswell and T. S. Collett, *Current perspectives on gas hydrate resources*. 2011.

[6] D. Cyranoski, "Japanese test coaxes fire from ice," *Nature*, vol. 469, no. 409, 2013.

[7] P. Linga, R. Kumar, and P. Englezos, "The clathrate hydrate process for post and pre-combustion capture of carbon dioxide," *Journal of Hazardous Materials*, vol. 149, no. 3, 625–629, 2007.

[8] T. A. Strobel, K. C. Hester, C. A. Koh, A. K. Sum, and E. D. Sloan, Jr., "Properties of the clathrates of hydrogen and developments in their applicability for hydrogen storage," *Chemical Physics Letters*, vol. 478, no. 4-6, 97–109, 2009.

[9] D. M. D'Alessandro, B. Smit, and J. R. Long, "Carbon Dioxide Capture: Prospects for New Materials," *Angewandte Chemie*, vol. 49, no. 35, 6058–6082, 2010.

[10] Y. Song, "New perspectives on potential hydrogen storage materials using high pressure," *Physical Chemistry Chemical Physics*, vol. 15, no. 35, 14524–14547, 2013.

[11] W. F. Kuhs, A. Klapproth, and B. Chazallon, "Chemical physics of air clathrate hydrates," *Physics of Ice Core Records*, 373–392, 2000.

[12] S. L. Miller, "Occurrence of gas hydrates in solar system," *Science*, vol. 134, no. 348, 1431, 1961.

[13] J. S. Loveday, R. J. Nelmes, M. Guthrie, S. A. Belmonte, D. R. Allan, D. D. Klug, J. S. Tse, and Y. P. Handa, "Stable methane hydrate above 2 GPa and the source of Titan's atmospheric methane," *Nature*, vol. 410, 661–663, 2001.

[14] M. Guthrie, *Developments in single-crystal neutron diffraction at high pressure*. PhD thesis, The University of Edinburgh, 2002.

[15] H. Davy, "On a combination of oxymuriatic gas and oxygene gas," *Philosophical Transactions of the Royal Society of London*, vol. 101, 155–162, 1811.

[16] H. Shimizu, S. Hori, T. Kume, and S. Sasaki, "Optical microscopy and Raman scattering of a single crystalline argon hydrate at high pressures," *Chemical Physics Letters*, vol. 368, 132–138, 2003.

[17] W. F. Kuhs, B. Chazallon, P. G. Radaelli, and F. Pauer, "Cage occupancy and compressibility of deuterated N2-clathrate hydrate by neutron diffraction," *Jounral of Inclusion Phenomena*, vol. 29, 65–77, 1997.

[18] K. A. Lokshin, Y. S. Zhao, D. W. He, W. L. Mao, H. K. Mao, R. J. Hemley, M. V. Lobanov, and M. Greenblatt, "Structure and dynamics of hydrogen molecules in the novel clathrate hydrate by high pressure neutron diffraction," *Physical Review Letters*, vol. 93, no. 12, 125503, 2004.

[19] H. Hirai, K. Komatsu, M. Honda, T. Kawamura, Y. Yamamoto, and T. Yagi, "Phase changes of CO2 hydrate under high pressure and low temperature," *Journal of Chemical Physics*, vol. 133, no. 12, 124511, 2010.

[20] D. Amos, *High Pressure Hydrates of CO_2 & Materials for Carbon Storage*. PhD thesis, The University of Edinburgh, 2015.

[21] C. A. Tulk, S. Machida, D. D. Klug, H. Lu, M. Guthrie, and J. Molaison, "The structure of CO_2 hydrate between 0.7 and 1.0 GPa," *Journal of Chemical Physics*, vol. 141, no. 17, 174503, 2014.

[22] A. Y. Manakov, V. I. Voronin, A. V. Kurnosov, A. E. Teplykh, V. Y. Komarov, and Y. A. Dyadin, "Structural investigations of argon hydrates at pressures up to 10 kbar," *Journal of Inclusion Phenomena and Macrocyclic Chemistry*, vol. 48, no. 1-2, 11–18, 2004. 9th International Seminar on Inclusion Compounds (ISIC-9), Novosibirsk, Russia, Jun 23-27, 2003.

[23] X. Yu, J. Zhu, S. Du, H. Xu, S. C. Vogel, J. Han, T. C. Germann, J. Zhang, C. Jin, J. S. Francisco, and Y. Zhao, "Crystal structure and encapsulation dynamics of ice II-structured neon hydrate," *Proceedings of the National Academy of Sciences of the United States of America*, vol. 111, no. 29, 10456–10461, 2014.

[24] A. Falenty, T. C. Hansen, and W. F. Kuhs, "Formation and properties of ice XVI obtained by emptying a type sII clathrate hydrate," *Nature*, vol. 516, 231–233, 2014.

[25] J. D. Bernal and R. H. Fowler, "A theory of water and ionic solution, with particular reference to hydrogen and hydroxyl ions," *Journal of Chemical Physics*, vol. 1, no. 8, 515–548, 1933.

[26] R. Howe and R. W. Whitworth, "A determination of the crystal structure of ice XI," *Journal of Chemical Physics*, vol. 90, no. 8, 4450–4453, 1989.

[27] S. M. Jackson, V. M. Nield, R. W. Whitworth, M. Oguro, and C. C. Wilson, "Single-crystal neutron diffraction studies of the structure of ice XI," *Journal of Physical Chemistry B*, vol. 101, no. 32, 6142–6145, 1997. Symposium on Physics and Chemistry of Ice 1996, Hanover, NH, AUG 27-31, 1996.

[28] C. Lobban, J. L. Finney, and W. F. Kuhs, "The structure and ordering of ices III and V," *Journal of Chemical Physics*, vol. 112, no. 16, 7169–7180, 2000.

[29] S. J. La-Placa, W. C. Hamilton, B. Kamb, and A. Prakash, "Nearly proton-ordered structure for ice IX," *Journal of Chemical Physics*, vol. 58, no. 2, 567–580, 1973.

[30] D. Londono, W. F. Kuhs, and J. L. Finney, "Enclathration of helium in ice-II - the 1st helium hydrate," *Nature*, vol. 332, no. 6160, 141–142, 1988.

[31] R. J. Nelmes, J. S. Loveday, W. G. Marshall, G. Hamel, J. Besson, and S. Klotz, "Multisite disordered structure of ice VII to 20 GPa," *Physical Review Letters*, vol. 81, no. 13, 2719–2722, 1998.

[32] T. A. Strobel, M. Somayazulu, and R. J. Hemley, "Phase Behavior of H_2 + H_2O at High Pressures and Low Temperatures," *Journal of Physical Chemistry C*, vol. 115, no. 11, 4898–4903, 2011.

[33] Y. A. Dyadin, E. Y. Aladko, A. Y. Manakov, F. V. Zhurko, T. V. Mikina, V. Y. Komarov, and E. V. Grachev, "Clathrate formation in water-noble gas (hydrogen) systems at high pressures," *Journal of Structural Chemistry*, vol. 40, no. 5, 790–795, 1999.

[34] V. S. Efimchenko, M. A. Kuzovnikov, V. K. Fedotov, M. K. Sakharov, S. V. Simonov, and M. Tkacz, "New phase in the water-hydrogen system," *Journal of Alloys and Compounds*, vol. 509, no. 2, S860–S863, 2011. 12th International Symposium on Metal-Hydrogen Systems, Fundamentals and Applications (MH2010), Moscow, Russia, Jul 19-23, 2010.

[35] V. E. Antonov, V. S. Efimchenko, and M. Tkacz, "Phase Transitions in the Water-Hydrogen System at Pressures up to 4.7 kbar," *Journal of Physical Chemistry B*, vol. 113, no. 3, 779–785, 2009.

[36] V. S. Efimchenko, V. E. Antonov, O. I. Barkalov, A. I. Beskrovnyy, V. K. Fedotov, and S. N. Klyamkin, "Phase transitions and equilibrium hydrogen content of phases in the water-hydrogen system at pressures to 1.8 kbar," *High Pressure Research*, vol. 26, no. 4, 439–443, 2006. 44th Annual Meeting of the European-High-Pressure-Research-Group Meeting (EHPRG 44), Prague, Czech Republic, Sep 04-08, 2006.

[37] W. L. Vos, L. W. Finger, R. J. Hemley, and H. K. Mao, "Novel H_2-H_2O clathrates at high-pressures," *Physical Review Letters*, vol. 71, no. 19, 3150–3153, 1993.

[38] W. L. Mao, H. K. Mao, A. F. Goncharov, V. V. Struzhkin, Q. Z. Guo, J. Z. Hu, J. F. Shu, R. J. Hemley, M. Somayazulu, and Y. S. Zhao, "Hydrogen clusters in clathrate hydrate," *Science*, vol. 297, no. 5590, 2247–2249, 2002.

[39] Y. A. Dyadin, E. G. Larionov, A. Y. Manakov, F. V. Zhurko, E. Y. Aladko, T. V. Mikina, and V. Y. Komarov, "Clathrate hydrates of hydrogen and neon," *Mendeleev Communications*, no. 5, 209–210, 1999.

[40] M. Kuzovnikov, *STRUKTURA, TERMODINAMICHESKAYA USTOYCHIVOST' I KOLEBATEL'NYYe SPEKTRY GIDRIDOV VYSOKOGO DAVLENIYA*. PhD thesis, Institute of Solid State Physics, Chernogolovka, Russia, 2013.

[41] G. S. Smirnov and V. V. Stegailov, "Toward Determination of the New Hydrogen Hydrate Clathrate Structures," *Journal of Physical Chemistry Letters*, vol. 4, no. 21, 3560–3564, 2013.

[42] H. Mao, "A new role for diamond-anvil cells in extreme-conditions neutron science." Plenary at the International Conference on Neutron Scattering, Edinburgh International Conference Centre, Edinburgh, 8th - 12th July 2013 .

[43] G.-R. Qian, A. O. Lyakhov, Q. Zhu, A. R. Oganov, and X. Dong, "Novel Hydrogen Hydrate Structures under Pressure," *Scientific Reports*, vol. 4, 5606, 2014.

[44] P. Teeratchanan and A. Hermann, "Computational phase diagrams of noble gas hydrates under pressure," *Journal of Chemical Physics*, vol. 143, no. 15, 154507, 2015.

[45] W. L. Vos, L. W. Finger, R. J. Hemley, and H. K. Mao, "Pressure dependence of hydrogen bonding in a novel H_2O-H_2 clathrate," *Chemical Physics Letters*, vol. 257, no. 5-6, 524–530, 1996.

[46] S.-i. Machida, H. Hirai, T. Kawamura, Y. Yamamoto, and T. Yagi, "Structural changes of filled ice Ic structure for hydrogen hydrate under high pressure," *Journal of Chemical Physics*, vol. 129, no. 22, 224505, 2008.

[47] S.-i. Machida, H. Hirai, T. Kawamura, Y. Yamamoto, and T. Yagi, "Raman spectra for hydrogen hydrate under high pressure: Intermolecular interactions in filled ice Ic structure," *Journal of Physics and Chemistry of Solids*, vol. 71, no. 9, 1324–1328, 2010.

[48] H. Hirai, S. Kagawa, T. Tanaka, T. Matsuoka, T. Yagi, Y. Ohishi, S. Nakano, Y. Yamamoto, and T. Irifune, "Structural changes of filled ice Ic hydrogen hydrate under low temperatures and high pressures from 5 to 50 GPa," *Journal of Chemical Physics*, vol. 137, no. 7, 074505, 2012.

[49] R. Kumar, D. D. Klug, C. I. Ratcliffe, C. A. Tulk, and J. A. Ripmeester, "Low-Pressure Synthesis and Characterization of Hydrogen-Filled Ice Ic," *Angewandte Chemie-International Edition*, vol. 52, no. 5, 1531–1534, 2013.

[50] T. L. Malkin, B. J. Murray, C. G. Salzmann, V. Molinero, S. J. Pickering, and T. F. Whale, "Stacking disorder in ice I," *Physical Chemistry Chemical Physics*, vol. 17, 60–76, 2015.

[51] L. Schlapbach, "Hydrogen-Fuelled Vehicles," *Nature*, vol. 460, no. 7257, 809–811, 2009.

[52] V. Diatschenko, C. W. Chu, D. H. Liebenberg, D. A. Young, M. Ross, and R. L. Mills, "Melting Curves of Molecular Hydrogen and Molecular Deuterium Under High Pressures Between 20 and 373 K," *Physical Review B*, vol. 32, 381–389, 1985.

[53] K. L. Lim, H. Kazemian, Z. Yaakob, and W. R. W. Daud, "Solid-state Materials and Methods for Hydrogen Storage: A Critical Review," *Chemical Engineering & Technology*, vol. 33, no. 2, 213–226, 2010.

[54] T. Strobel, Y. Kim, G. Andrews, J. Ferrell, C. Koh, A. Herring, and E. Sloan, "Chemical-clathrate Hybrid Hydrogen Storage: Storage in Both Guest and Host," *Journal of the American Chemical Society*, vol. 130, no. 45, 14975–7, 2008.

[55] D. E. Palin and H. M. Powell, "Hydrogen bond linking of quinol molecules," *Nature*, vol. 156, no. 3959, 334–335, 1945.

[56] D. E. Palin and H. M. Powell, "The structure of molecular compounds 6. The beta-type clathrate compounds of quinol," *Journal of the Chemical Society*, 815–821, 1948.

[57] D. E. Palin and H. M. Powell, " The structure of molecular compounds 3. Crystal structure of addition complexes of quinol with certain volatile compounds," *Journal of the Chemical Society*, 208–221, 1947.

[58] T. Mak, J. Tse, C. Tse, K. Lee, and Y. Chong, "Crystal-structrue of a Clathrate Inclusion Compound of Hydroquinone and Hydrogen-sulfide," *Journal of the Chemical Society - Perkin Transactions 2*, no. 10, 1169–1172, 1976.

[59] J.-W. Park, S. An, Y. Seo, B.-S. Kim, and J.-H. Yoon, "Temperature-Dependent Release of Guest Molecules and Structural Transformation of Hydroquinone Clathrates," *Journal of Physical Chemistry C*, vol. 117, no. 15, 7623–7627, 2013.

[60] J.-H. Yoon, Y.-J. Lee, J. Park, T. Kawamura, Y. Yamamoto, T. Komai, S. Takeya, S. S. Han, J.-W. Lee, and Y. Lee, "Hydrogen Molecules Trapped in Interstitial Host Channels of alpha-Hydroquinone," *Chemphyschem*, vol. 10, no. 2, 352–355, 2009.

[61] V. F. Rozsa and T. A. Strobel, "Triple Guest Occupancy and Negative Compressibility in Hydrogen-Loaded β-Hydroquinone Clathrate," *Journal of Physical Chemistry Letters*, vol. 5, no. 11, 1880–1884, 2014.

[62] K. W. Han, Y.-J. Lee, J. S. Jang, T.-I. Jeon, J. Park, T. Kawamura, Y. Yamamoto, T. Sugahara, T. Vogt, J.-W. Lee, Y. Lee, and J.-H. Yoon, "Fast and reversible hydrogen storage in channel cages of hydroquinone clathrate," *Chemical Physics Letters*, vol. 546, 120–124, 2012.

[63] W. Schlenk, "Die harnstoff-addition der aliphatischen verbindungen," *Annalen der Chemie-Justus Liebig*, vol. 565, no. 3, 204–240, 1949.

[64] A. E. Smith, "The crystal structure of the urea-hydrocarbon complexes," *Acta Crystallographica*, vol. 5, no. 2, 224, 1952.

[65] W. Marshall and D. Francis, "Attainment of near-hydrostatic compression conditions using the Paris-Edinburgh cell," *Journal of Applied Crystallography*, vol. 35, no. 1, 122–125, 2002.

[66] A. Olejniczak, K. Ostrowska, and A. Katrusiak, "H-Bond Breaking in High-Pressure Urea," *Journal of Physical Chemistry C*, vol. 113, no. 35, 15761–15767, 2009.

[67] H. P. Weber, W. G. Marshall, and V. Dmitriev, "High-pressure polymorphism in deuterated urea," *Acta Crystallographica Section A (Supplement)*, vol. 58, no. s1, c174, 2002.

[68] D. S. Sivia, *Elementary Scattering Theory for X-ray and Neutron Users*. Oxford University Press, 1st ed., 2011.

[69] E. H. Kisi and C. J. Howard, *Applications of Neutron Powder Diffraction*. Oxford University Press, 1st ed., 2008. Published as part of the Oxford Series on Neutron Scattering in Condensed Matter (Book 15).

[70] C. Giacovazzo, H. L. Monaco, G. Artioli, D. Viterbo, G. Ferraris, G. Gilli, G. Zanotti, and M. Catti, *Fundamentals of Crystallography*. Oxford University Press, 2nd ed., 2002. First published in 1992.

[71] R. Pynn, "Neutron scattering - a primer," *Los Alamos Science*, vol. 19, 1990.

[72] S. Klotz, *Techniques in High Pressure Neutron Scattering*. CRC Press, 2012.

[73] V. F. Sears, "Neutron scattering lengths and cross sections," *Neutron News*, vol. 3, no. 3, 26–37, 1992.

[74] "Neutron scattering lengths and cross sections." `https://www.ncnr.nist.gov/resources/n-lengths/`. Accessed: 15-05-2016.

[75] H. M. Rietveld, "A profile refinement method for nuclear and magnetic structures," *Journal of Applied Crystallography*, vol. 2, no. 2, 65–71, 1969.

[76] A. C. Larson and R. B. Von Dreele, "GSAS general structure analysis system," *Los Alamos National Laboratory Report LAUR 86*, 1994.

[77] A. Le Bail, H. Duroy, and J. L. Fourquet, "Ab Initio Structure Determination of LiSbWO6 by X ray Powder Diffraction," *Materials Research Bulletin*, vol. 23, no. 3, 447–452, 1988.

[78] G. Oszlányi and A. Süto, "Ab initio structure solution by charge flipping," *Acta Crystallographica A*, vol. 60, no. 2, 134–141, 2004.

[79] "How the Spallation Neutron Source Works." `http://neutrons2.ornl.gov/facilities/SNS/works.shtml`. Accessed: 30-06-2016.

[80] R. Boehler, M. Guthrie, J. J. Molaison, A. M. dos Santos, S. Sinogeikin, S. Machida, N. Pradhan, and C. A. Tulk, "Large-volume diamond cells for neutron diffraction above 90GPa," *High Pressure Research*, vol. 33, no. 3, SI, 546–554, 2013.

[81] M. I. Eremets, *High Pressure Experimental Methods*. Oxford Science Publications, 1997.

[82] O. Arnold, J. C. Bilheux, J. M. Borreguero, A. Buts, S. I. Campbell, L. Chapon, M. Doucet, N. Draper, R. F. Leal, M. A. Gigg, V. E. Lynch, A. Markyardsen, D. J. Mikkelson, R. L. Mikkelson, R. Miller, K. Palmen, P. Parker, G. Passos, T. G. Perring, P. F. Peterson, S. Ren, M. A. Reuter, A. T. Savici, J. W. Taylor, R. J. Taylor, R. Tolchenoy, W. Zhou, and J. Zikoysky, "Mantid-Data analysis and visualization package for neutron scattering and mu-SR experiments," *Nuclear Instruments & Methods in Physics Research Section A-Accelerators Spectrometers Detectors and Associated Equipment*, vol. 764, 156–166, 2014.

[83] W. G. Williams, R. M. Ibberson, P. Day, and J. E. Enderby, "GEM - General Materials Diffractometer at ISIS," *Physica B-Condensed Matter*, vol. 241, 234–236, 1997. International Conference on Neutron Scattering, Toronto, Canada, Aug 17-21, 1997.

[84] "ISIS - GEM Instrument Overview." `http://www.isis.stfc.ac.uk/instruments/gem/gem2467.html`. Accessed: 15-05-2016.

[85] "ISIS - PEARL Technical Information." http://www.isis.stfc.ac.uk/instruments/pearl/technical/pearl-technical-information7262.html. Accessed: 15-05-2016.

[86] J. M. Besson, R. J. Nelmes, G. Hamel, J. S. Loveday, G. Weill, and S. Hull, "Neutron powder diffraction above 10 GPa," *Physica B*, vol. 180, no. B, 907–910, 1992. International Conference on Neutron Scattering (ICNS 91), Oxford, England, Aug 27-30, 1991.

[87] S. Klotz, J. Philippe, C. L. Bull, J. S. Loveday, and R. J. Nelmes, "A 3 kbar hydrogen-compatible gas loader for Paris-Edinburgh presses," *High Pressure Research*, vol. 33, no. 1, 214–220, 2013.

[88] S. Klotz, T. Strässle, A. L. Cornelius, and T. Hansen, "Magnetic Ordering in Solid Oxygen up to Room Temperature," *Physical Review Letters*, vol. 104, no. 11, 115501, 2010.

[89] S. Klotz, G. Hamel, and J. Frelat, "A new type of compact large-capacity press for neutron and X-ray scattering," *High Pressure Research*, vol. 24, no. 1, 219–223, 2004. Meeting on Matter Under Extreme Conditions, Paris, France, May 16, 2003.

[90] M. I. McMahon, "High-Pressure Crystallography," in *Advanced X-Ray Crystallography* (Rissanen, K, ed.), vol. 315 of *Topics in Current Chemistry*, 69–109, 2012.

[91] S. P. Besedin, I. N. Makarenko, S. M. Stishov, V. P. Glazkov, I. N. Goncharenko, A. V. Irodova, V. A. Somenkov, and S. S. Shil'stein, "Equation of state of molecular deuterium at pressures up to 31 GPa," *High Pressure Research*, vol. 4, 447–449, 1990.

[92] S. P. Besedin, I. N. Makarenko, S. M. Stishov, V. P. Glazkov, I. N. Goncharenko, and V. A. Somenkov, "Diamond anvil cells for neutron diffraction," *High Pressure Research*, vol. 14, no. 1-3, 193–197, 1995. International Seminar on Neutron Scattering at High Pressure, Dubna, Russia, Oct 05-07, 1994.

[93] I. N. Goncharenko, I. Mirebeau, and A. Ochiai, "Magnetic neutron diffraction under pressures up to 43 GPa. Study of the EuX and GdX compounds," *Hyperfine Interactions*, vol. 128, no. 1-3, 225–244, 2000. International Symposium on Physics of Solids Under High Pressure Using Nuclear Probes, Cologne, Germany, Sep 05-08, 1999.

[94] M. Guthrie, R. Boehler, C. A. Tulk, J. J. Molaison, A. M. dos Santos, K. Li, and R. J. Hemley, "Neutron diffraction observations of interstitial protons in dense ice," *Proceedings of the National Academy of Sciences of the United States of America*, vol. 110, no. 26, 10552–10556, 2013.

[95] M. Guthrie, "Future directions in high-pressure neutron diffraction," *Journal of Physics-Condensed Matter*, vol. 27, no. 15, 153201, 2015.

[96] J. Binns, K. V. Kamenev, G. J. McIntyre, S. A. Moggach, and S. Parsons, "Use of a miniature diamond-anvil cell in high-pressure single-crystal neutron Laue diffraction," *IUCrJ*, vol. 3, no. 3, 168–179, 2016.

[97] H.-K. Mao, J. Xu, V. V. Struzhkin, J. Shu, R. J. Hemley, W. Sturhahn, M. Y. Hu, E. E. Alp, L. Vocadlo, D. Alfe, G. D. Price, M. J. Gillan, M. Schwoerer-Bohning, D. Hausermann, P. Eng, G. Shen, H. Giefers, R. Lubbers, and G. Wortmann, "Phonon density of states of iron up to 153 gigapascals," *Science*, vol. 292, no. 5518, 914–916, 2001.

[98] H. Giefers, R. Lubbers, K. Rupprecht, G. Wortmann, D. Alfe, and A. I. Chumakov, "Phonon spectroscopy of oriented hcp iron," *High Pressure Research*, vol. 22, no. 2, SI, 501–506, 2002. 39th European-High-Pressure-Research-Group Meeting (EHPRG 39), Santander, Spain, Sep 16-19, 2001.

[99] R. Forman, S. Block, J. Barnett, and G. Piermari, "Pressure Measurement Made by Utilization of Ruby Sharp-line Luminescence," *Science*, vol. 176, no. 4032, 284–285, 1972.

[100] "Instrument 3 Spallation Neutron Source Fact sheet." `https://neutrons.ornl.gov/sites/default/files/Instrument_3.pdf`. Accessed: 16-06-2016.

[101] J. S. Loveday, M. I. McMahon, and R. J. Nelmes, "The effect of diffraction by the diamonds of a diamond-anvil cell on single-crystal sample intensities," *Journal of Applied Crystallography*, vol. 23, no. 5, 392–396, 1990.

[102] M. Guthrie, C. G. Pruteanu, M.-E. Donnelly, J. J. Molaison, A. M. dos Santos, J. S. Loveday, R. Boehler, and C. A. Tulk, "Radiation attenuation by single-crystal diamond windows," In preparation.

[103] C. G. Salzmann, P. G. Radaelli, B. Slater, and J. L. Finney, "The polymorphism of ice: five unresolved questions," *Physical Chemistry Chemical Physics*, vol. 13, 18468–18480, 2011.

[104] W. F. Kuhs, C. Sippel, A. Falenty, and T. C. Hansen, "Extent and relevance of stacking disorder in "ice Ic"," *Proceedings of the National Academy of Sciences*, vol. 109, 21259–21264, 2012.

[105] S.-Y. Chung, Y.-M. Kim, J.-G. Kim, and Y.-J. Kim, "Multiphase transformation and Ostwald's rule of stages during crystallization of a metal phosphate," *Nature Physics*, vol. 5, 68–73, 2009.

[106] D. Cavallo, D. Mileva, G. Portale, L. Zhang, L. Balzano, G. C. Alfonso, and R. Androsch, "Mesophase-mediated crystallization of poly(butylene-2,6-naphthalate): An example of Ostwalds Rule of Stages," *ACS Macro Letters*, vol. 1, no. 8, 1051–1055, 2012.

[107] C. G. Salzmann, E. Mayer, and A. Hallbrucker, "Effect of heating rate and pressure on the crystallization kinetics of high-density amorphous ice on isobaric heating between 0.2 and 1.9 GPa," *Physical Chemistry Chemical Physics*, vol. 6, 5156–5165, 2004.

[108] A. Boultif and D. Louër, "Powder pattern indexing with the dichotomy method," *Journal of Applied Crystallography*, vol. 37, 724–731, 2004.

[109] T. Hahn editor, *International Tables for Crystallography - Volume A Space-group Symmetry*. Springer, 2005. 5th edition.

[110] C. Donnerer, T. Scheler, and E. Gregoryanz, "High-pressure synthesis of noble metal hydrides," *Journal of Chemical Physics*, vol. 138, no. 13, 134507, 2013.

[111] C. M. B. Line and R. W. Whitworth, "A high resolution neutron powder diffraction study of D_2O ice XI," *Journal of Chemical Physics*, vol. 104, no. 24, 10008, 1996.

[112] D. Londono, J. L. Finney, and W. F. Kuhs, "Formation, Stability, and structure of helium hydrate at high-pressure," *Journal of Chemical Physics*, vol. 97, no. 1, 547–552, 1992.

[113] M. Donnelly, C. L. Bull, R. J. Husband, A. D. Frantzana, S. Klotz, and J. S. Loveday, "Urea and deuterium mixtures at high pressures," *Journal of Chemical Physics*, vol. 142, no. 12, 124503, 2015.

[114] R. J. Angel, J. Gonzalez-Platas, and M. Alvaro, "EosFit7c and a Fortran module (library) for equation of state calculations," *Zeitschrift fur Kristallographie*, vol. 229, no. 5, 405–419, 2014.

[115] L. Bezacier, J. Baptiste, J.-P. Perrillat, H. Cardon, M. Hanfland, and I. Daniel, "Equations of state of ice VI and ice VII at high pressure and high temperature," *Journal of Chemical Physics*, vol. 141, 104505, 2014.

[116] M. Somayazulu, J. Shu, C.-s. Zha, A. F. Goncharov, O. Tschauner, H.-k. Mao, and R. J. Hemley, "In situ high-pressure x-ray diffraction study of H_2O ice VII," *Journal of Chemical Physics*, vol. 128, no. 6, 064510, 2008.

[117] R. J. Hemley, A. P. Jephcoat, H.-K. Mao, C. S. Zha, L. W. Finger, and D. E. Cox, "Static compression of H_2O - ice to 128 GPa (1.28 MBar)," *Nature*, vol. 330, no. 6150, 737–740, 1987.

[118] A. D. Fortes, I. G. Wood, M. G. Tucker, and W. G. Marshall, "The PVT equation of state of D_2O ice VI determined by neutron powder diffraction in the range $0 < P < 2.6$ GPa and $120 < T < 330$ K, and the isothermal equation of state of D_2O ice VII from 2 to 7 GPa at room temperature," *Journal of Applied Crystallography*, vol. 45, 523–534, 2012.

[119] L. Liu, "Compression of ice-VII tp 500 kbar," *Earth and Planetary Science Letters*, vol. 61, no. 2, 359–364, 1982.

On the stability of the disordered molecular alloy phase of ammonia hemihydrate

C. W. Wilson,[1,2] C. L. Bull,[2,3] G. W. Stinton,[2] D. M. Amos,[2] M.-E. Donnelly,[2] and J. S. Loveday[2]
[1]*Diamond Light Source, Ltd., Harwell, Didcot, Oxfordshire OX11 0DE, United Kingdom*
[2]*SUPA, School of Physics and Astronomy, Centre for Science at Extreme Conditions, University of Edinburgh, Edinburgh EH9 3JZ, United Kingdom*
[3]*ISIS Facility, STFC Rutherford Appleton Laboratory, Harwell, Didcot, Oxfordshire OX11 0QX, United Kingdom*

(Received 6 November 2014; accepted 16 February 2015; published online 5 March 2015)

The disordered-molecular-alloy phase (DMA) of ammonia hydrates [J. S. Loveday and R. J. Nelmes, Phys. Rev. Lett. **83**, 4329 (1999)] is unique in that it has substitutional disorder of ammonia and water over the molecular sites of a body centred cubic lattice. Whilst this structure has been observed in ammonia di- and mono-hydrate compositions, it has not been conclusively observed in the ammonia hemihydrate system. This work presents investigations of the structural behaviour of ammonia hemihydrate as a function of P and T. The indications of earlier studies [Ma *et al.* RSC Adv. **2**, 4290 (2012)] that the DMA structure could be produced by compression of ammonia hemihydrate above 20 GPa at ambient temperature are confirmed. In addition, the DMA structure was found to form reversibly both from the melt, and on warming of ammonia hemihydrate phase-II, in the pressure range between 4 and 8 GPa. The route used to make the DMA structure from ammonia mono- and di-hydrates—compression at 170 K to 6 GPa followed by warming to ambient temperature—was found not to produce the DMA structure for ammonia hemihydrate. These results provide the first strong evidence that DMA is a thermodynamically stable form. A high-pressure phase diagram for ammonia hemihydrate is proposed which has importance for planetary modelling. © *2015 AIP Publishing LLC.* [http://dx.doi.org/10.1063/1.4913684]

I. INTRODUCTION

Ammonia and water are two of the most abundant molecules in the outer solar system and make up a significant fraction of the interiors of the ice giants Uranus and Neptune[1] and icy satellites such as Titan and Triton.[2] An in-depth understanding of how these molecules behave at high pressure is thus of great importance to models of the formation and internal dynamics of these planets and moons. Information on the different structural phases that form in this binary system and on how the two components speciate over the pressure and temperature (P-T) region relevant to planetary interiors (from 2-6 GPa for icy satellites[3] and up to 800 GPa for the ice giants[4]), would allow more accurate models to be constructed. Additionally, the ammonia-water system is one of the simplest systems to contain mixed (N–H···O and O–H···N) hydrogen bonds. Such bonds are widely found in biology and, for example, along with unmixed O–H···O bonds they are responsible for the base pairings in DNA.[5] High-pressure studies of ammonia hydrates provide information about the effect of compression on the geometry and strength of mixed H-bonds over a wide range of densities.

Ammonia and water are readily miscible and solidify into three stoichiometric forms; ammonia dihydrate (ADH, $NH_3{\cdot}2H_2O$), ammonia monohydrate (AMH, $NH_3{\cdot}H_2O$), and ammonia hemihydrate (AHH, $2NH_3{\cdot}H_2O$). During the formation of the solar system, the abundance of ammonia is thought to be ~15% of the nebula (the gas and dust that the sun and planets were formed from) in the outer solar system.[6] In contrast, the abundance of water is thought to be ~45%[7] and it is for this reason more effort has been made to investigate the structures and phase transitions on the water-rich side of the ammonia-water composition diagram and hence to focus on AMH and ADH. However, we have recently shown by x-ray and neutron diffraction studies that at 290 K 1:1 ammonia:water composition mixtures crystallise at ~3.5 GPa to form a mixture of AHH phase-II and water ice.[8] This would suggest that AHH may be more important to planetary models than had previously been thought since the conditions within the interiors of planets are well above this pressure. AHH-II has a monoclinic structure with space group $P2_1/c$ and lattice parameters a = 3.3584(5) Å, b = 9.215(1) Å, c = 8.933(1) Å, and β = 94.331(8)° at 3.5 GPa. This structure, shown in Figure 1, has full orientational order of all molecules and although weak evidence exists for substitutional disorder (water occupying ammonia sites and vice versa),[8] this substitutional disorder is small (at a level less than 10%). The molecular packing where the water and ammonia molecules form a series of crowned hexagonal hydrogen-bonded layers is similar to that found in ice VII—and also the disordered molecular alloy (DMA) structure described below.[8] However, the hydrogen bonding of AHH-II is significantly different from that of ice VII or DMA.[8]

However, the phase diagram is complicated by the fact that ammonia and water have been observed to form a molecular

0021-9606/2015/142(9)/094707/10/$30.00 © 2015 AIP Publishing LLC

This article is copyrighted as indicated in the article. Reuse of AIP content is subject to the terms at: http://scitation.aip.org/termsconditions. Downloaded to IP: 129.215.149.97 On: Sun, 08 Mar 2015 12:18:44

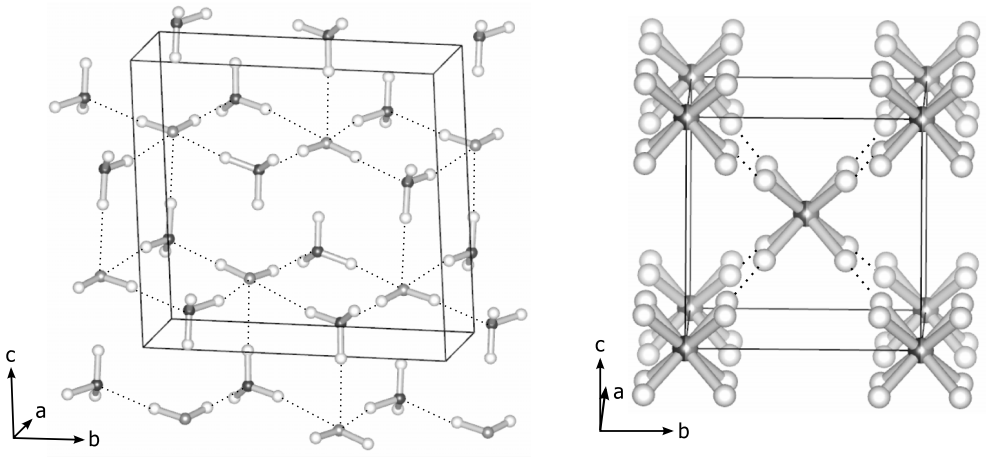

FIG. 1. The structures of AHH-II (left)[8] and DMA (right).[9] Nitrogen atoms are dark grey, oxygen atoms are light grey, hydrogen atoms are white. The light grey/dark grey atomic sites in the DMA structure show that either site can be occupied by either an oxygen or a nitrogen atom. In the DMA structure, the hydrogen sites are only partially occupied and the hydrogen sites in the ⟨110⟩ directions have been omitted for clarity. The dotted lines on both structures represent the hydrogen bonds between the molecules. Detailed descriptions of the structures can be found in Refs. 8 and 9.

alloy at high pressure.[9] This structure is unique in molecular systems in that it has full random substitutional disorder of water and ammonia on the sites of a body-centred cubic structure. It was first observed in samples of 1:1 ammonia:water composition that had been compressed to ~6 GPa and warmed to room temperature[9] and subsequently in samples of 1:2 ammonia:water composition compressed along a similar route.[10] These P-T paths are shown as dashed arrow lines on the AMH and ADH phase diagrams in Figure 2. The same cubic structure can accommodate both compositions (1:1 and 1:2) because of the substitutional disorder and the two forms differ simply in the probability of a given bcc site being occupied by a water or an ammonia molecule. The DMA structure is cubic with space group $Im\bar{3}m$ and has a lattice parameter a = 3.2727(2) Å for a 1:1 composition at 5.5 GPa[9] and 3.3141(6) Å for a 1:2 composition at 5.5-6 GPa.[10] Figure 1 shows the DMA structure along with the AHH-II structure for comparison. It has been suggested that, because of this substitutional disorder, the DMA structure could accommodate a wide range of non-stoichiometric hydrate compositions and thus be the ultimate high-pressure form of a wide range of hydrate compositions.[9] However, the situation remains unclear since both 1:1 and 1:2 compositions when compressed at room temperature solidify to form mixtures of AHH-II and ice VII.[8] Recent x-ray diffraction, Raman and infra-red spectroscopic studies by Ma *et al.* also explored the behaviour of a 2:1 composition up to ~40 GPa.[11] They concluded that the sample crystallised to an orthorhombic structure at 3.5 GPa which subsequently transformed to DMA at 19 GPa and then underwent a further transition at 25 GPa where a new reflection appears at ~1.875 Å. These conclusions are somewhat surprising. They disagree with our conclusions—based

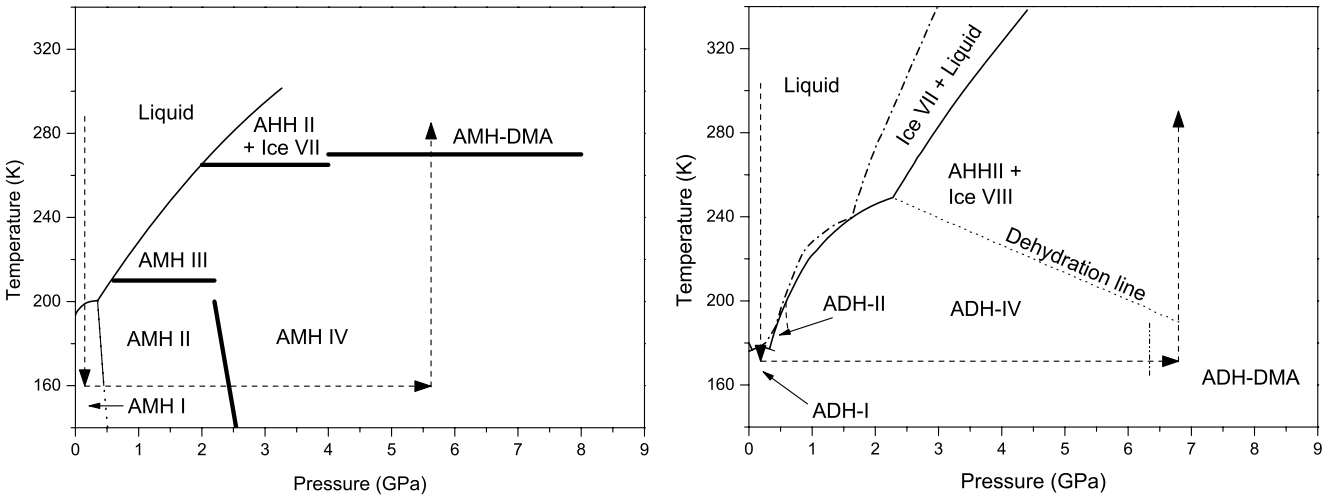

FIG. 2. The phase diagrams of both AMH (left)[14] and ADH (right),[24] respectively. The thick black lines on the AMH phase diagram show the approximate positions of phase transition lines. The dotted-dashed line on the ADH phase diagram denotes the liquidus, where solid ice forms co-exist with a fluid richer in ammonia.[24] The dotted line on the ADH phase diagram shows the dehydration boundary where solid ADH structures break down into a mixture of solid ice and AHH.[8,24] The dashed arrows show the P-T path taken to form the DMA phase in both compositions in Refs. 9, 10, and 24. The P-T path begins at room temperature where the samples are cooled until they solidify and are then compressed to a pressure of 5 GPa or above before being warmed to room temperature where the sample transforms to the DMA phase. For ADH, the sample must first be an amorphous solid formed by flash freezing the sample and can transform to the DMA phase at low temperatures upon compression, unlike AMH-DMA which only forms while being warmed to room temperature.

This article is copyrighted as indicated in the article. Reuse of AIP content is subject to the terms at: http://scitation.aip.org/termsconditions. Downloaded to IP: 129.215.149.97 On: Sun, 08 Mar 2015 12:18:44

partially on single-crystal data—on the structure of AHH-II. And although they report a transition to DMA at 19 GPa, they observe two reflections in their diffraction data—one at 2.275 Å and the other at 2.15 Å—where only one reflection would be expected.[9]

In addition to the doubt over the structure of the crystalline phase produced on compression through the melting line at room temperature, it is unclear whether DMA is ever the phase with the lowest free energy. At room temperature, compression of all compositions richer in water than 2:1 ammonia:water—compositions richer in ammonia than 2:1 have not been studied—produces AHH-II and ice VII, and this configuration is stable—in the sense that it does not change with time on a timescale of weeks—up to at least 9 GPa.[9,10] In contrast, low-temperature compression and warming to room temperature above 6 GPa produces the DMA structure (in both 1:1 and 1:2 compositions) which also does not decompose with time on the same timescale. Further complicating this picture are the aforementioned observations of Ma *et al.* at 19 GPa and 25 GPa, and additionally the absence of diffraction studies above ambient temperature. In this paper, we report the results of synchrotron x-ray and neutron diffraction studies up to 530 K and 30 GPa which explore the relationships between AHH-II and DMA and assist in the resolution as to what the stable structures are in this complicated and planetary relevant system.

II. EXPERIMENTAL

The work described here has been performed using neutron diffraction techniques for deuterated samples in Paris-Edinburgh (P-E) presses[12] and complimentary x-ray diffraction studies using both hydrogenous and deuterated samples in diamond anvil cells (DACs) at the Diamond Light Source synchrotron. Neutrons offer the advantages of improved contrast between nitrogen and oxygen—whose x-ray cross sections are very similar—and the fact that the deuterium atoms contribute much more strongly to the neutron diffraction pattern than they do to the x-ray pattern. However, x-ray studies are able to explore the pressure and temperature range beyond that currently achievable by neutron diffraction in a P-E press.[13]

A. Sample preparation

The sample preparation technique has been described in detail elsewhere[8,14] and will only be described in brief here. A small mass of ammonia is condensed into an empty container at 80 K. A corresponding mass of water (to form the desired molar ratio of ammonia:water) is placed in a second vessel and cooled to liquid nitrogen temperatures. The ammonia is then condensed into the water-containing vessel to form the ammonia hydrate.

B. Neutron diffraction experiments

Neutron diffraction data were collected using the PEARL instrument at the ISIS pulsed-neutron source at the Rutherford-Appleton Laboratory in the UK. The PEARL instrument is dedicated to performing high-pressure experiments using the P-E press which allows large volume samples to be taken up to approximately 30 GPa.[13] To load the samples, an assembly composed of the anvils (made from tungsten carbide or sintered diamond), a clamping mechanism, and the TiZr (null scattering) encapsulated gasket[15] was cooled to liquid nitrogen temperatures. The ammonia hydrate solution (held at ~240 K) was poured into the sample chamber of the gasket. The assembly was put together and immersed in liquid nitrogen. The assembly was then transferred to a pre-cooled V4 P-E press (held at 170 K in a cryostat) and a sealing load of ~5 tonnes applied. The cryostat and press were placed on the PEARL instrument and data collected using the 90° detector bank. The data were corrected for the effects of anvil attenuation.[16] The corrected data were analysed by Rietveld profile refinement using the GSAS suite of programs.[17,18]

C. X-ray diffraction experiments

Synchrotron x-ray diffraction data were collected at the I15 Extreme Conditions beamline of the Diamond Light Source in DACs. Two types of DAC were used, Merrill-Bassett (M-B) cells[19] were used in heating experiments, and a Diacell Bragg-(S) DAC (Almax-Easylab) (DXR)[20] was used to explore the highest pressure ranges as this type of cell offers improved anvil alignment compared to that available for M-B cells. X-ray data were collected on a Mar345 image plate detector with an x-ray wavelength of 0.4254(1) Å determined by calibration with a silicon standard sample. All samples were loaded under the same conditions used for the P-E press experiments. The gaskets used for the compression experiments in the DXR cells were made of 200 μm thick tungsten, pre-indented to a thickness of ~50 μm with 125 μm diameter gasket holes. In the heating experiments, rhenium gaskets were used, as steel gaskets are known to react with ammonia and water samples at elevated temperatures,[6,21] and it was found that tungsten also reacted with the samples when heated. The rhenium gaskets prepared for the M-B cells were 270 μm thick, pre-indented to a thickness of ~30μm, and had 100 μm diameter gasket holes. In all x-ray samples, a small ruby sphere was included in the sample chamber for use as a pressure calibrant.[22] The x-ray beam was 50 μm in diameter and the diffractometer constants were determined by calibration with a silicon standard. The 2-D images were processed and integrated with the Fit2D software[23] before being exported for Rietveld refinement using the GSAS suite of programs.[17,18]

III. RESULTS AND DISCUSSION

In the work by Ma *et al.*,[11] a 2:1 ammonia:water solution first crystallises at room temperature on compression between 3.1 and 4.3 GPa as expected. At ~19.2 GPa, Ma *et al.* reported that the sample formed the AHH-DMA phase.[11] This pressure is much higher than the pressure of 5.5 GPa required to produce AMH-DMA and ADH-DMA, respectively, in samples with 1:1 and 1:2 composition when compressed at low temperature and then warmed to room temperature. In this work, we have attempted to form AHH-DMA at lower pressures; by following this low-T compression path, by decompressing AHH-DMA formed through compression at room temperature

This article is copyrighted as indicated in the article. Reuse of AIP content is subject to the terms at: http://scitation.aip.org/termsconditions. Downloaded to IP: 129.215.149.97 On: Sun, 08 Mar 2015 12:18:44

and finally by heating a 2:1 sample at pressure. In the interests of presenting these results in the clearest way possible, the results have been grouped together by the initial as-prepared sample composition (ammonia:water ratio), and we describe the solid phases that are observed to form within each of these different sample compositions.

A. Compression study of deuterated 1:2 samples using neutron and x-ray diffraction

A 1:2 ammonia:water ratio solution was prepared and loaded using the neutron powder diffraction technique described in Sec. II using double toroidal anvils[13] allowing access to pressures in excess of 19.2 GPa required for the transition to AHH-DMA.[11] As described previously[8] by loading a 1:2 solution at room temperature and compressing, the sample solidifies into a mixture of AHH-II and ice VII, allowing the ice VII to be used as a pressure marker. Figure 3 shows the series of patterns collected on the deuterated 1:2 sample as load was increased. The sample first solidifies into a mixture of AHH-II and ice VII as is expected. Two features become clear from the patterns. Comparison of the observed d-spacings (including those of ice VII) with those observed by Ma *et al.*[11] reveals that the samples have similar diffraction patterns and that the orthorhombic AHH phase of Ma *et al.* is in fact a mixture of AHH-II[8] and ice VII. This of course implies that the sample of Ma *et al.* did not have exactly the 2:1 ammonia water ratio claimed but was in fact richer in water than this composition. It also is quite clear from Figure 3 that no transformation to the bcc AHH-DMA phase is observed for AHH-II up to the maximum pressure of 26.6 GPa, although it is possible that a transformation to the DMA phase has begun at this pressure, since, the relative intensities of the three most intense reflections of AHH-II ($(12\bar{1})$, (102), and (023)) have begun to change in this pattern. It is therefore clear, at least for deuterated samples, that the AHH-II to DMA transition occurs at a significantly higher pressure than previously reported, if at all.

To determine if the changing intensities observed in the last diffraction pattern in Figure 3 are the first sign of a transition from AHH-II to the AHH-DMA phase, a deuterated sample must be taken to pressures beyond those which are currently achievable in a P-E press. For this reason, a set of deuterated samples were studied on the I15 beamline at the Diamond Light Source in DACs, where pressures in excess of 30 GPa can be reached. The x-ray powder diffraction data collected from a deuterated 1:2 sample compressed at room temperature are shown on the right of Figure 4. The behaviour of this deuterated sample was very different from the deuterated 1:2 sample studied in the neutron powder diffraction experiment (summarised in Figure 3). In this x-ray experiment, ice VII forms first in the sample at 2.5(1) GPa as expected,[24] and after further compression to 7.6(1) GPa one singular peak forms at ~2.38 Å, consistent with the (110) bcc reflection for AHH-DMA. The reason for this unexpected behaviour of the 1:2 x-ray sample could be a result of the rapid compression from 2.5(1) to 7.6(1) GPa, compared to all the other samples studied, where the AHH-II phase was formed close to the crystallising pressure (3.5(1) GPa[8]). Another possible explanation for the difference could be the presence of ice VII in the sample, which has a crystal structure very similar to that of the DMA phase,[8] and could potentially act as a seed crystal to the DMA phase allowing it to form more readily; however, the presence of ice VII does not seem to have affected the 1:2 sample studied by neutron powder diffraction.

B. Compression study of a deuterated 1:1 sample using X-ray diffraction

Figure 4 also shows the x-ray powder diffraction data collected for a 1:1 deuterated ammonia:water sample (left

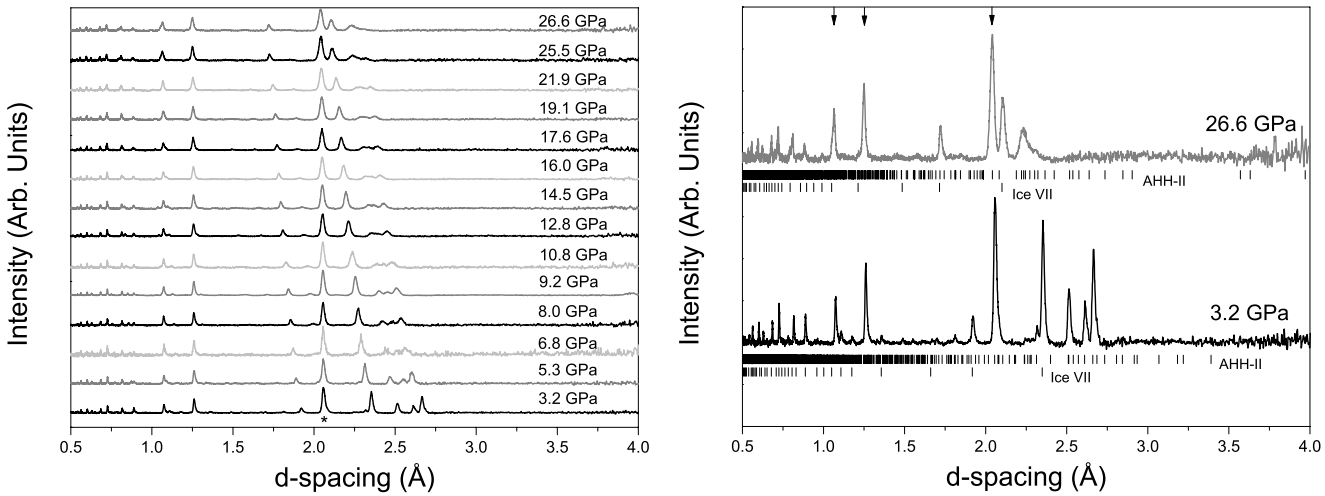

FIG. 3. Neutron powder diffraction data collected on a 1:2 deuterated ammonia:water sample. The asterisk (*) shows the most prominent reflection in the patterns caused by the sintered diamond anvils. The change in the relative intensities of the $(12\bar{1})$, (102), and (023) peaks in the sample between the lowest and the highest pressures appears to suggest that there is a phase transition in the very last pattern at 26.6(1) GPa, the emerging phase cannot be confirmed to be AHH-DMA because the transition is not complete and there is a large overlap with the $(12\bar{1})$, (102), and (023) reflections of AHH-II. The pressures shown in this figure were calculated from the equation of state of ice VII.[26] Since each powder pattern was collected over differing lengths of time, they have been rescaled so that the diamond peaks are of comparable size to one another. The first and last neutron powder diffraction patterns have been reproduced in the right hand figure for ease of comparison. The tick marks for the peaks associated with AHH-II and ice VII are shown for both plots.

This article is copyrighted as indicated in the article. Reuse of AIP content is subject to the terms at: http://scitation.aip.org/termsconditions. Downloaded to IP: 129.215.149.97 On: Sun, 08 Mar 2015 12:18:44

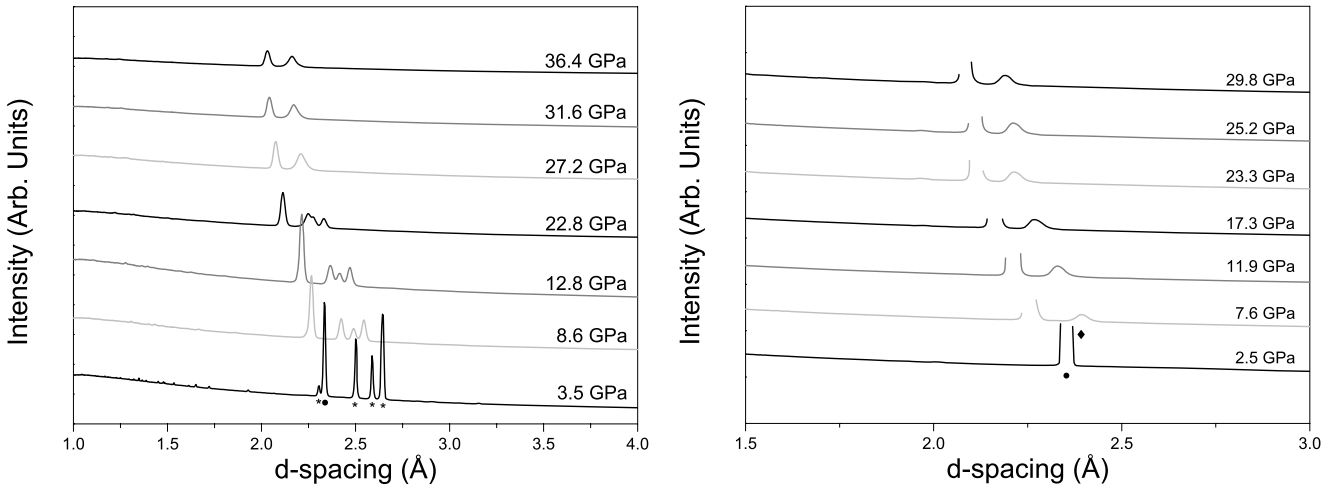

FIG. 4. X-ray powder diffraction patterns of a deuterated 1:1 ammonia:water sample (left) and a deuterated 1:2 sample (right). The pressures were measured using the ruby fluorescence method.[22] The behaviour and patterns in the 1:1 sample are very similar to that observed in the data presented in Figure 5. A structural transition is observed between 22.8(3) and 27.2(2) GPa where the three prominent AHH-II ($12\bar{1}$), (102), and (023) reflections are again replaced with a single AHH-DMA (110) reflection consistent with Figure 5. Note that the (110) reflection in the patterns associated with ice VII, marked with the filled circles (•) are several times larger than in the 2:1 sample in Figure 5. The 1:2 x-ray powder sample data show different behaviour from the neutron powder sample in Figure 3, forming AHH-DMA and ice VII without forming the AHH-II phase, see text for details. The asterisks (*) show the ($12\bar{1}$), (102), (023), and (040) reflections associated with the AHH-II phase, the full circle (•) shows the (110) reflection associated with ice VII. The diamond (♦) shows the AHH-DMA (110) reflection where it first forms in the 1:2 sample. Note that in the 1:2 sample data, the ice VII(110) reflection has been truncated for clarity.

hand figure). The 1:1 sample first solidifies as a mixture of AHH-II and ice VII at 3.5 GPa as expected[8] and again shows a marked resemblance to the x-ray patterns reported by Ma *et al.* with a much larger contribution from excess water ice, as would be expected. A transition to a phase that is consistent with the AHH-DMA structure can be seen at a pressure of 27.2(1) GPa, 8 GPa higher than that reported by Ma *et al.*;[11] however, this appears to be consistent with the 1:2 neutron powder diffraction experiment summarised in Figure 3 and described above where in a deuterated sample, the transition to the AHH-DMA phase was not observed up to a maximum pressure of 26.6 GPa.

C. High-pressure behaviour of 2:1 ammonia:water samples

This section describes the behaviour of two deuterated and one hydrogenous 2:1 ammonia:water samples. One deuterated sample was compressed in a DAC and subsequently decompressed and studied with x-ray powder diffraction, similar to the route used by Ma *et al.*[11] The other deuterated 2:1 sample was compressed at 170 K before subsequently being warmed to room temperature and studied with neutron powder diffraction, similar to the route used to form AMH-DMA and ADH-DMA.[9,10] The hydrogenous sample was heated at high-pressure and studied using x-ray powder diffraction to explore the potential of new methods for entering the AHH-DMA phase.

Figure 5 shows the x-ray powder diffraction data collected on compression of the 2:1 deuterated ammonia:water sample. Starting at a pressure of 3.8(2) GPa, the sample can be fitted with the AHH-II phase with a small excess of water present as ice VII, again as expected.[8] As was seen in the 1:1 deuterated sample (see above), beyond 26.5(2) GPa there is a change in the sample which is consistent with a phase transition to the AHH-DMA structure. The sample was compressed without further change to 41.0(5) GPa and no evidence was seen of the second transition reported by Ma *et al.*[11] From this maximum pressure of 41.0(5) GPa, the sample pressure was then decompressed in steps. As Figure 5 shows the DMA phase persisted down to the lowest measured pressure of 9.5(4) GPa, after which the sample was accidentally lowered to a pressure of 1.1(1) GPa and became liquid once more. However, starting at 19.2(1) GPa, a new feature can be observed at a d-spacing of ~2.37 Å (highlighted in Figure 5 with asterisks) along with the (110) bcc reflection of the DMA phase at ~2.27 Å (denoted by the filled circles in Figure 5). This new feature may be an evidence of the onset of the reverse DMA to AHH-II transition since it appears at the expected position of the ($12\bar{1}$) AHH-II reflection, but this cannot be confirmed from the data presented here. However, it is clear that there is hysteresis of at least 8 GPa in the pressure of the AHH-II to DMA transition, and there is evidence that this transition is very sluggish on decompression.

As has been stated in Sec. I, in both 1:1 and 1:2 ammonia:water compositions, the transition to a DMA phase is observed when the sample is compressed at ~170 K to ~60 tonnes of applied load—which corresponds to a generated sample pressure of 5-6 GPa—and then warmed to room temperature[9,10] (see Figure 2). A neutron diffraction experiment was conducted using very similar methods to those used in Refs. 9 and 10 on a 2:1 sample to establish if the same P-T path could be used to form the AHH-DMA phase.

Once the sample had been prepared and loaded into the P-E press as described in Sec. II, the applied load on the P-E press piston was increased in 10 tonnes steps up to a maximum of 55 tonnes at 170 K (the observed powder patterns are shown in Figure 6). The left hand figure of Figure 6 shows the neutron powder pattern of a 2:1 ammonia:water sample at 170 K and a sealing load of 5 tonnes along with a Rietveld refinement of

This article is copyrighted as indicated in the article. Reuse of AIP content is subject to the terms at: http://scitation.aip.org/termsconditions. Downloaded to IP: 129.215.149.97 On: Sun, 08 Mar 2015 12:18:44

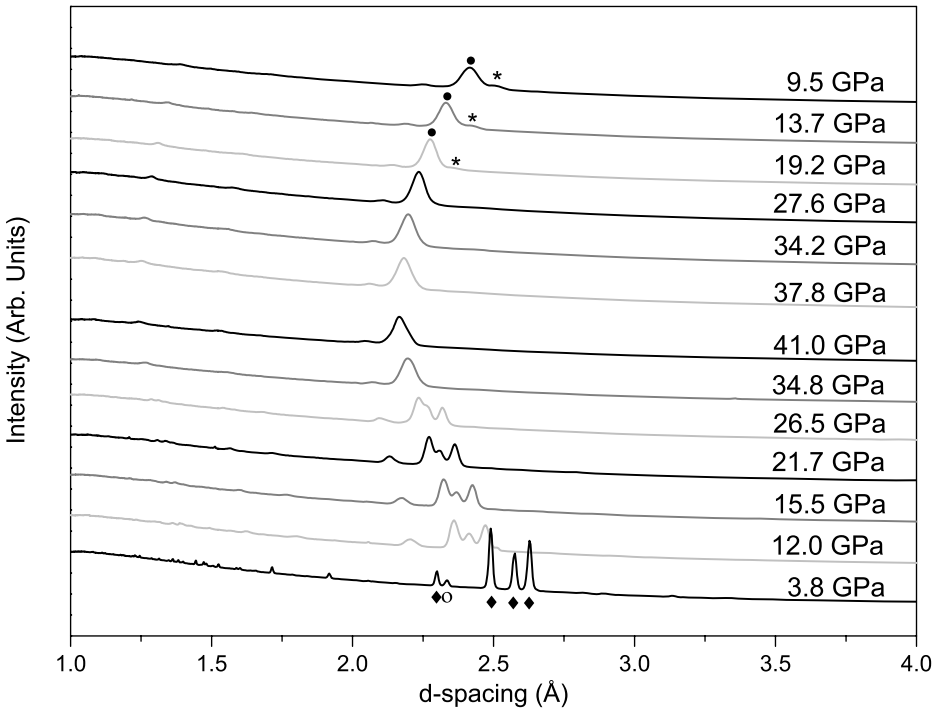

FIG. 5. X-ray powder patterns of a deuterated 2:1 ammonia:water sample as a function of pressure. The sample was compressed from 3.8(2) GPa to 41.0(5) GPa before being slowly decompressed to 9.5(4) GPa. The pressures were measured with the ruby fluorescence method.[22] The peaks highlighted with the filled diamonds (⧫) belong to the AHH-II phase, the hollow circle (○) highlights an ice VII (110) reflection showing a slight excess of ice in the sample. The filled circles (●) show the peak associated with the AHH-DMA (110) reflection, and the asterisks (*) highlight the unidentified peak that emerges when decompressing at 19.2(1) GPa and below, which could identify transitioning back to AHH-II. A change in structure, where the three prominent AHH-II ($12\bar{1}$), (102), and (023) reflections are replaced with a single AHH-DMA (110) reflection, is observed to occur between 26.5(2) GPa and 34.8(1) GPa. Upon decompression, this phase remained stable to 9.5(4) GPa.

the pattern using the orthorhombic (Pbnm) AHH-I structure[14] and the difference curve between the observed and calculated intensities. The fit in this figure is to the AHH-I structure and accounts for the majority of the diffraction peaks observed in the pattern, the remainder can be accounted for by contributions from the sintered diamond anvils and a small amount of ammonia-I in the sample. The small contribution in the powder pattern from ammonia-I suggests that there was a slight excess of ammonia in the sample. Upon compression to 55 tonnes, the sample appears to go through 2 phase transitions, from AHH-I to an intermediate phase at a load of 15 tonnes, before entering a phase that shows several overlapping peaks at a d-spacing of approximately 2.6 Å shown in Figure 6.

Once at an applied load of 55 tonnes, the sample was slowly warmed to room temperature at constant applied load, during which no change in the powder pattern were observed, which can be seen in Figure 7. It is quite clear from Figure 6 that the pattern observed is not what is expected from a bcc structure. The expected reflection positions are shown by the tick marks of bcc AMH-DMA (the nearest comparable structure) in Figure 7.

Two other samples were also used in this experiment, but contained excess water. This was evident from the relative ammonia and water weights during the sample preparation process (these samples were calculated to have ammonia:water ratios of 1.94(1):1 and 1.92(2):1 compared to the third sam-

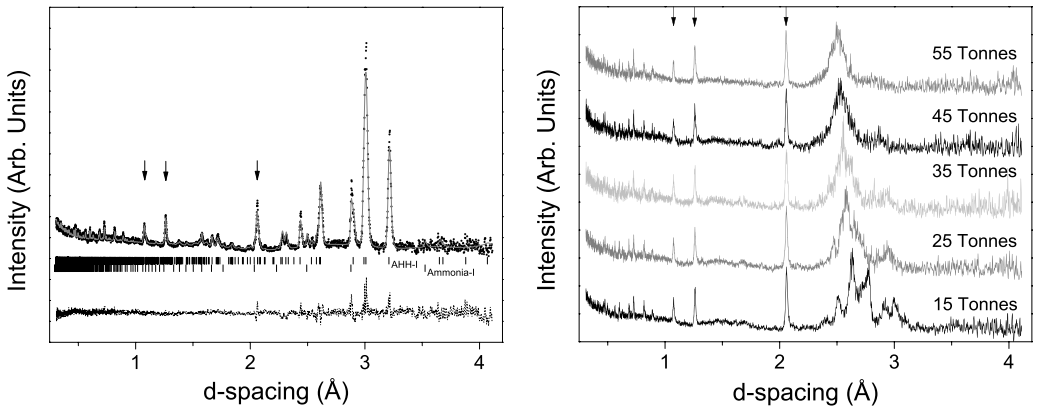

FIG. 6. The neutron powder diffraction data recorded on a 2:1 sample following the same P-T path used to produce both AMH-DMA and ADH-DMA, as described in the text. The left hand figure shows the result of the Rietveld refinement of the AHH sample at 170 K as loaded at the sealing load of 5 tonnes. The dots are the data points, the solid line shows the calculated pattern, and the dashed line below is the difference between the observed and calculated pattern. The arrows show the three most prominent peaks from the sintered diamond anvils. The upper tick marks show the peak positions from the AHH-I structure and the lower tick marks show the peak positions for the ammonia-I structure. The right hand figure shows the powder patterns observed upon slow compression of the sample to the applied load of 55 tonnes in 10 tonnes steps, equivalent to a change in pressure of (0.5-1 GPa). The arrows show the location of the three most prominent diffraction peaks in the pattern from the sintered diamond anvils. It is clear that there is a transition to an intermediate structure upon increasing the load to 15 tonnes, as seen by the change in the diffraction pattern from that shown in the left hand figure, and that the phase obtained at a load of 55 tonnes is not a cubic DMA phase.

This article is copyrighted as indicated in the article. Reuse of AIP content is subject to the terms at: http://scitation.aip.org/termsconditions. Downloaded to IP: 129.215.149.97 On: Sun, 08 Mar 2015 12:18:44

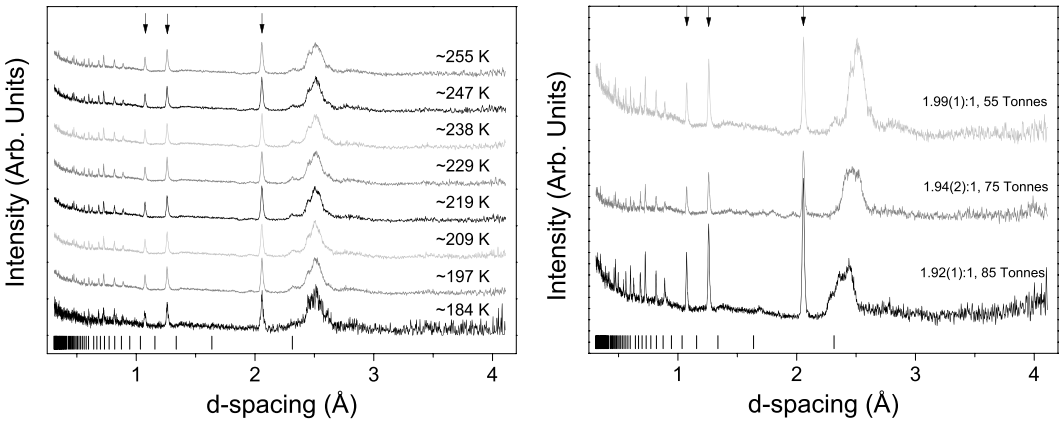

FIG. 7. The left hand figure shows neutron diffraction data collected on a sample loaded with an ammonia:water ratio closest to the ideal 2:1 ratio warmed to room temperature at an applied load of 55 tonnes. The arrows show the three most prominent peaks in the patterns caused by the sintered diamond anvils. The tick marks at the bottom of powder patterns show the expected positions of DMA phase peaks based on the structure of AMH VI. The right hand figure shows three different loadings of an AHH sample with different ammonia:water ratios that were warmed to room temperature at pressure. The top most powder pattern on the right hand figure corresponds to the top most plot of the left hand figure. Again the arrows show the three most prominent peaks in the patterns caused by the sintered diamond anvils and the tick marks show the expected peak positions of AMH VI at ~5 GPa (55 tonnes load).

ple's 1.99(1):1) and from the low-temperature powder patterns, which contained peaks identified as AMH-I as well as AHH-I. These samples were compressed to a maximum load of 75 and 85 tonnes, respectively, both at a temperature of 170 K before being gradually warmed back to room temperature at constant load. The patterns collected from the compressed samples once recovered to room temperature are shown in Figure 7, where the powder diffraction patterns of all three samples can easily be distinguished from one another, as the relative intensities of the most prominent sample peaks differ in each pattern and do not appear at the correct d-spacings to be accounted for by the bcc DMA structure.

We have also explored the high-temperature behaviour of the phase diagram using x-ray diffraction at the I15 station at the Diamond Light Source. A hydrogenous 2:1 ammonia:water ratio solution was loaded into a Merrill-Bassett DAC with a rhenium gasket using the process described in Sec. II. The cell was heated by a ring heater in thermal contact with the outside of the cell and the temperature was measured with a K-type thermocouple on the back of one of the diamond anvils. Once solidified (by compression at room temperature), the sample was heated. A hydrogenous sample with a 2:1 composition was explored over two heating cycles at two different initial pressures. The first heating cycle is shown in Figure 8 beginning at 4.0(1) GPa and 61(2) °C. In this pattern and those up to the pattern collected at 4.0(2) GPa and 80(3) °C, peaks of both AHH-II and bcc DMA (marked respectively with (*) and (•) symbols in Figure 8) are apparent. On compression and warming, to 87(2) °C and 4.7(1) GPa, the sample transformed completely to DMA. The sample was heated to 95(1) °C and although the (110) reflection disappeared, this appears to be the result of the reorientation of crystallites in the rather poorly averaged powder rather than melting because the (400) reflection remained visible. When the sample was compressed to 5.9(1) GPa at 95(3) °C, it showed evidence of transforming back to AHH-II and peaks of both AHH-II and DMA are visible. On warming and compression to 6.0(1) GPa and 105(1) °C, the transformation had reversed and only peaks from DMA are visible. On further compression and warming, the peaks from DMA disappeared between 6.6(1) GPa and 185(2) °C and 5.7(2) GPa and 214(4) °C leaving only a diffuse liquid halo. The sample was left to cool overnight and the second cycle of heating was started at 7.5(1) GPa and 20 °C (room temperature) where the sample showed only peaks from AHH-II (Figure 9). On warming the sample transformed to DMA between 7.0(1) GPa and 108(2) °C and 7.3(1) GPa and 118(2) °C. Further changes in temperature and pressure located melting of DMA between 6.2(1) GPa and 208(2) °C and 5.8(1) GPa and 209(2) °C, freezing of liquid to DMA between 6.5(1) and 7.4(2) at 209(3) °C and melting of DMA between 6.4(2) GPa and 257(5) °C and 6.6(2) GPa and 252(5) °C. Additionally, the lattice parameter for the AHH-DMA phase at 4.8 GPa and 89 °C is a = 3.578(2) Å calculated from the d-spacing of the (110) reflection. This is the most comparable pressure and temperature to that reported for AMH-DMA and ADH-DMA (5.5 GPa and room temperature[9,10]) and is again comparable in magnitude, although larger than both as a result of the lower pressure and higher temperature. Taken together with the lattice parameter calculated for 9.5(4) GPa of a = 3.296(4) Å, this would suggest that AHH-DMA has a lattice parameter ~3% larger than those of both AMH-DMA and ADH-DMA whose lattice parameters appear not to depend strongly on composition[9,10] at the same pressure and temperature.

D. Discussion

As we have seen, our results are consistent with the result of Ma *et al.*[11] below 25 GPa once it is recognised that the sample of Ma *et al.* contained more water than the claimed 2:1 ammonia:water ratio and hence contains ice. Our studies confirm an AHH-II to DMA transformation at high pressure and room temperature and reveal an 8 GPa increase in the upstroke transition pressure on deuteration. This is a large isotope substitution effect. We find no evidence for the second transition reported by Ma *et al.* at 25 GPa[11] in an hydrogenous sample since we find that DMA persists unchanged up to 41.0(5) GPa in a deuterated sample. This difference could of course be an even larger (15 GPa) deuteration effect but we

This article is copyrighted as indicated in the article. Reuse of AIP content is subject to the terms at: http://scitation.aip.org/termsconditions. Downloaded to IP: 129.215.149.97 On: Sun, 08 Mar 2015 12:18:44

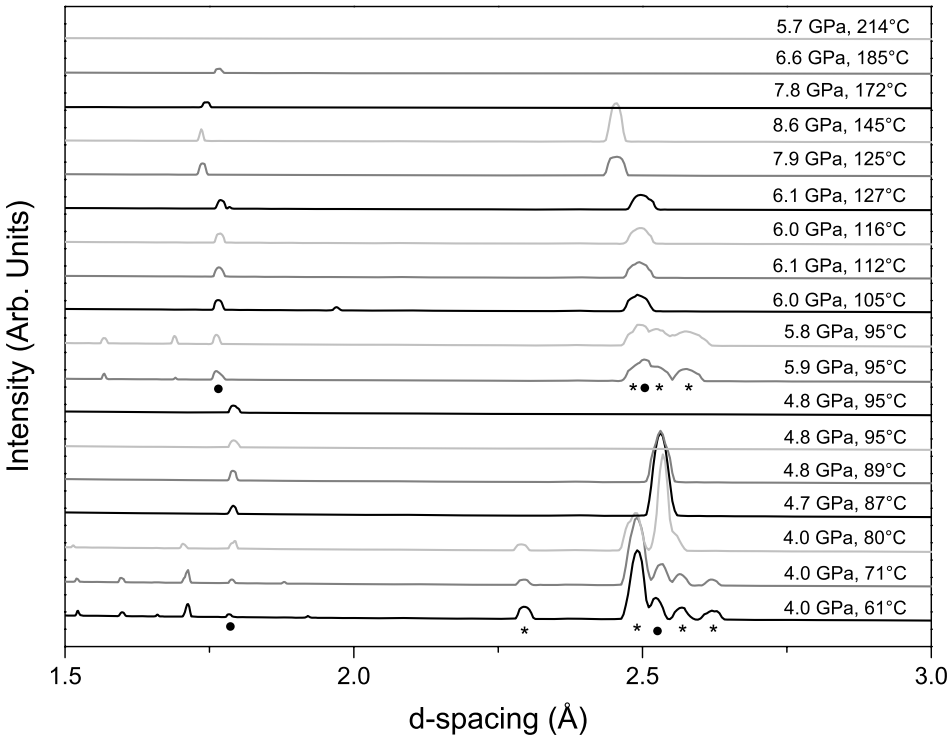

FIG. 8. X-ray powder diffraction data of a hydrogenous 2:1 ammonia:water sample as it was heated over its first heating cycle from 4.0(2) GPa at 61(2)°C to 5.7(2) GPa at 214(4)°C. The pressures were measured with the ruby fluorescence method and temperatures measured from the back of the diamond anvils. Several transitions from the AHH-II phase to the bcc DMA phase are observed along with a transition from the DMA phase to the liquid phase which is preceded by the disappearance of the most intense diffraction peak and a broad "halo" of a liquid pattern observable in the diffraction image once through the transition, this is not observable in the 1D diffraction patterns as the feature is very broad and has much less intensity than the crystallographic reflections. Asterisks (*) show the peaks associated with AHH-II, filled circles (•) show those associated with AHH-DMA. The poor peak shapes are attributed to the highly textured nature of the sample.

argue that it is not the case. We note that the evidence for this transition in the data of Ma *et al.* comes from the diffraction data and there is no evidence for the transition in the Raman data.[11] Furthermore, in the data of Ma *et al.*, the transition is signalled by strong changes in the intensity of a peak at ~2.1 Å—this peak is in fact a reflection from ice VII that appears to become overlapped with a new emerging reflection—and the appearance of a second new peak at ~1.9 Å. These

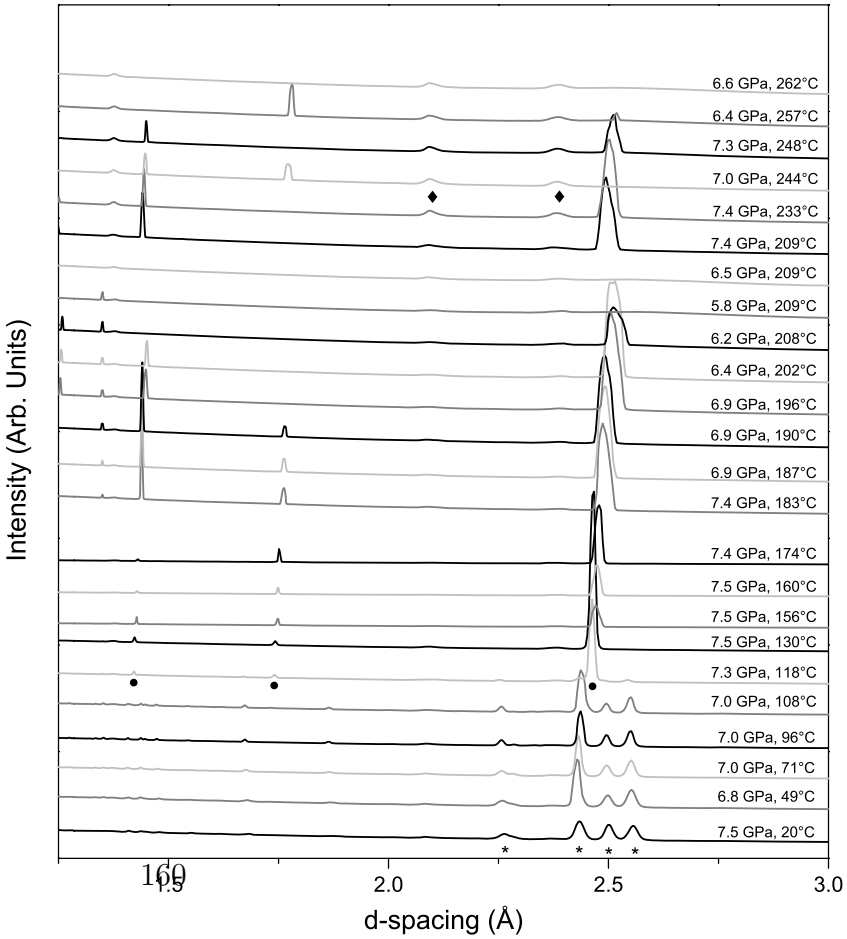

FIG. 9. X-ray powder diffraction data of a hydrogenous 2:1 ammonia:water sample as it was heated over its second heating cycle. Reflections associated with AHH-II are shown with asterisks (*), those associated with AHH-DMA are highlighted with filled circles (•), and diffraction peaks that belong to the rhenium gaskets are highlighted with filled diamonds (♦). Along with a clear transition to a bcc phase at 7.3(1) GPa at 118(2)°C, this phase can also be observed melting, at 6.5(1) GPa and 209(2)°C, and re-entering the bcc phase from the melt at 7.4(2) GPa and 209(2)°C. The irregular peak profiles are caused by the highly textured appearance of the sample.

This article is copyrighted as indicated in the article. Reuse of AIP content is subject to the terms at: http://scitation.aip.org/termsconditions. Downloaded to IP: 129.215.149.97 On: Sun, 08 Mar 2015 12:18:44

new peaks have essentially pressure independent positions above 25 GPa. It thus may be that they are either peaks from the gasket material or the product of a reaction between that sample and the gasket, further studies are needed to confirm this hypothesis.

From the cold compression experiments, it appears that AHH-DMA does not form by following the same path used to form both AMH-DMA and ADH-DMA. From the collected neutron powder data, a new intermediate phase has been observed in a 2:1 ammonia:water ratio sample, this is the bottom pattern on the right hand side of Figure 6 at a load of 15 tonnes and a temperature of 170 K. The exact nature of this complicated pattern (mixed phase, decomposition of sample, new structural phase, etc.) has not been determined in this work, but the pattern is clearly distinct from the AHH-I pattern shown in the left hand figure of Figure 6. Additionally, as three separate loadings with minor differences in their ammonia:water ratios (1.92(2):1, 1.94(1):1, and 1.99(1):1) were all recovered to room temperature, but exhibited differing powder patterns, this appears to suggest that the recovered samples are a mixed phase (the end products of these three samples are shown in the right hand figure of Figure 7).

These results of the heating experiment are summarised in Figure 10 along with tentative phase boundaries for the liquid to AHH-DMA and AHH-DMA to AHH-II transitions. The fact that both of these boundaries can be crossed reversibly provides the first direct evidence that (at least for the 2:1 ammonia:water composition) DMA is a thermodynamically stable phase and not a metastable form with frozen in disorder. Previously, most of the observations of DMA had been made in samples compressed at low temperature and warmed and hence the question of metastability was open. This has important potential consequences for planetary modelling since in any planet or satellite where the P-T profile crosses the AHH melting line above ~4 GPa (the lowest pressure at which we observed DMA), the solid phase formed will be DMA and not AHH-II. This has effects for the modelling of the heat produced by freezing, since DMA will have a lower latent heat of fusion than AHH-II because it has a higher entropy. The fact that DMA forms directly from the melt may also have consequences for chemical differentiation in planetary bodies whose ammonia:water mixtures are generally richer in water than 2:1. We have now shown that the DMA structure exists for 2:1, 1:1, and 1:2 ammonia:water compositions. It thus is possible that, above 4 GPa, compositions richer in water than 2:1 form a DMA whose composition is the same as the liquid from which they form; that is, that DMA forms without precipitating ice VII. Below this pressure, our earlier work shows that liquids richer in water than 2:1 freeze to form AHH-II and ice VII. This possibility needs to be explored experimentally.

The conclusion that DMA is thermodynamically stable implies that the AHH-II to DMA transition is an order-disorder transition. As we have shown,[8] the molecular packings of AHH-II and DMA are very similar. The two phases differ in that AHH-II has long-range order of both the molecular orientations and of the species occupying each molecular site and at the transition to DMA these long-range features are lost. Thus, AHH-II provides a basis for a local snapshot of the disordered arrangement which fluctuates spatially and with time to give an average which is the DMA structure in a similar way to the way that ordered ice VIII provides basis for models of the local structure of disordered ice VII.[25] It should be noted that in our earlier work we found evidence for a low (10%) level of substitutional disorder in AHH-II.[8] This provides evidence to support the view that energy cost of disordering the AHH-II structure is low.

From the mixed AHH-II/DMA diffraction patterns, it is possible to estimate the volume difference between AHH-II and DMA. The values vary somewhat, but are always positive and lie in the range 1%-3%. The positive volume change is consistent with the observed increase in the critical temperature for the AHH-II to DMA transition and combined with a Clapeyron slope of 0.14 $GPaK^{-1}$ give a ΔS for the AHH-II to DMA transition of between 50-150 $JK^{-1}mol^{-1}$. If this entropy change is attributed entirely to configurational disorder, it corresponds to between 7.5 and 413 configurations for each molecular site in the DMA structure. The lower value

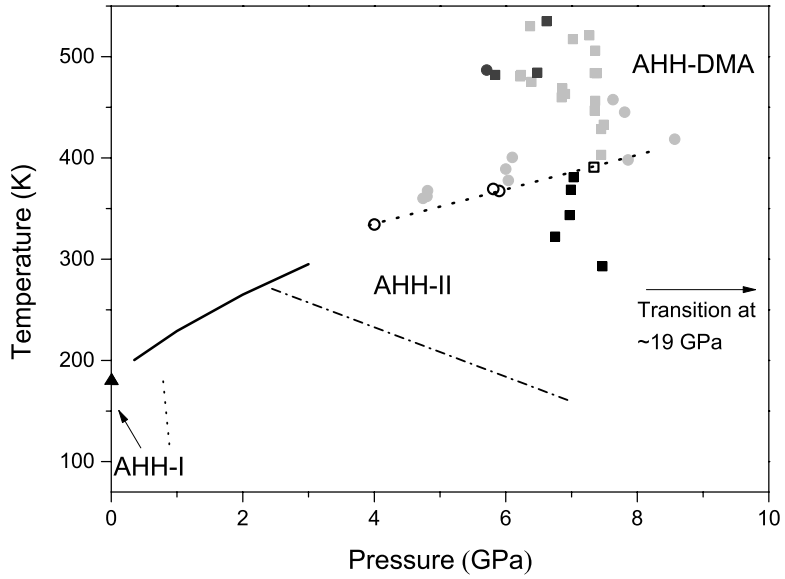

FIG. 10. Proposed phase diagram for hydrogenous AHH based upon the data collected in the heating experiment presented in Figures 8 and 9. The black symbols denote the P and T's where AHH-II was observed, the light grey where AHH-DMA phase was seen, and the dark grey show where the sample was fully molten. The open symbols show the P and T at which both AHH-II and AHH-DMA were observed. The different shapes show which points are from the patterns shown in Figure 8 (circle •) and Figure 9 (square ■). The open symbols show patterns that contained contributions from both AHH-II and the AHH-DMA phases. The dashed-dotted line shows the approximate area of the dehydration line where water rich samples break down into AHH-II and ice VII/VIII (see Figure 2) where AHH-II has yet to be observed experimentally. The dotted line shows the phase boundary estimated from the pressure at which the 2:1 neutron sample started to transform (see Figure 6). The triangle (▲) is where deuterated AHH is observed to freeze in the solid AHH-I phase at ambient pressure[14] and the solid line shows the melting curve of AMH as determined by Hogenboom *et al.*[27]

This article is copyrighted as indicated in the article. Reuse of AIP content is subject to the terms at: http://scitation.aip.org/termsconditions. Downloaded to IP: 129.215.149.97 On: Sun, 08 Mar 2015 12:18:44

is plausible for a disordered structure given that in addition to the N/O substitutional disorder, there is also orientational disorder of the molecules. The higher value seems too large to be plausible, hence, it appears that the volume difference between AHH-II and DMA is closer to 1% than 3%. Clearly, more accurate measurements of this quantity are needed. The fact that a transition between AHH-II and DMA is observed at room temperature at much higher pressures (25-30 GPa) implies that the transition temperature must have a maximum somewhere between 7.5 GPa and 25 GPa and further work is required to locate the maximum. Finally, although we observed melting in our samples, the data do not provide sufficient information to extend the melting line. There is thus a clear need to make measurements of the melting lines of all three compositions of ammonia hydrates in the pressure range above 3 GPa.

Finally, it is worth noting the 3% difference in lattice parameters between DMA with compositions of 2:1 and 1:1 and 1:2. At ambient pressure, the volume per-molecule of ammonia hydrates is almost composition-independent.[8] The fact that at 6 GPa we estimate the volume per molecule to be 9% larger in 2:1 DMA than the other two compositions suggests some profound difference which would benefit further investigation.

IV. CONCLUSIONS

As we have seen, our results provide the first evidence of transitions from the AHH-II phase to and from the DMA structure, as well as direct transformation from the DMA phase to the liquid phase. They thus provide the first evidence that this unique structure is indeed a thermodynamically stable phase. They also provide new information on the boundaries and transition behaviour of the 2:1 ammonia:water composition. We have been unable to produce the DMA structure in this composition by the low temperature compression and warming route that produces DMA in the 1:1 and 1:2 compositions. We have also confirmed the direct compression transformation from AHH-II to DMA observed by Ma *et al.*[11] and shown that this transition has a large (8 GPa) deuteration effect.

ACKNOWLEDGMENTS

The authors would like to thank both the EPSRC and STFC for both funding and provision of beam time at both the Diamond Light Source and the ISIS Pulsed-Neutron Source. Thanks also to the I15 team (Heribert Wilhelm, Annette Kleppe, Dominic Daisenberger, and Allan Ross) for their help in collecting the x-ray data and providing their scientific and technical support while on experiment. Thanks also to Andy Chamberlin and Chris Goodway from ISIS for their technical support on our neutron experiments.

[1]R. Helled, J. D. Anderson, M. Podolak, and G. Schubert, Astrophys. J. **726**, 15 (2011).
[2]G. Tobie, O. Grasset, J. I. Lunine, A. Mocquet, and C. Sotin, Icarus **175**, 496 (2005).
[3]J. S. Loveday and R. J. Nelmes, High Pressure Res. **23**, 41 (2003).
[4]T. Guillot, Annu. Rev. Earth Planet. Sci. **33**, 493 (2005).
[5]G. A. Jeffrey, *An Introduction to Hydrogen Bonding* (Oxford University Press, 1997), Chap. 10.
[6]H. C. Cynn, S. Boone, A. Koumvakalis, M. Nicol, and D. J. Stevenson, in *Proceedings of the 19th Lunar and Planetary Science Conference* (Cambridge University Press/Lunar and Planetary Institute, 1989), Vol. 1, p. 433.
[7]J. I. Lunine and D. J. Stevenson, Icarus **70**, 61 (1987).
[8]C. W. Wilson, C. L. Bull, G. Stinton, and J. S. Loveday, J. Chem. Phys. **136**, 094506 (2012).
[9]J. S. Loveday and R. J. Nelmes, Phys. Rev. Lett. **83**, 4329 (1999).
[10]J. S. Loveday, R. J. Nelmes, C. L. Bull, H. E. Maynard-Casely, and M. Guthrie, High Pressure Res. **29**, 396 (2009).
[11]C. Ma, F. Li, Q. Zhou, F. Huang, J. Wang, M. Zhang, Z. Wang, and Q. Cui, RSC Adv. **2**, 4920 (2012).
[12]J. M. Besson, R. J. Nelmes, G. Hamel, J. S. Loveday, G. Weill, and S. Hull, Physica B **181**, 907 (1992).
[13]S. Klotz, J. M. Besson, G. Hamel, R. J. Nelmes, and J. S. Loveday, Appl. Phys. Lett. **66**, 1735 (1995).
[14]J. S. Loveday and R. J. Nelmes, High Pressure Res. **24**, 45 (2004).
[15]W. Marshall and D. Francis, J. Appl. Crystallogr. **35**, 122 (2002).
[16]R. M. Wilson, J. S. Loveday, R. J. Nelmes, S. Klotz, and W. G. Marshall, Nucl. Instrum. Methods Phys. Res., Sect. A **354**, 145 (1995).
[17]A. C. Larson and R. B. Von Dreele, Los Alamos National Laboratory Report No. 86, 2004.
[18]B. H. Toby, J. Appl. Crystallogr. **34**, 210 (2001).
[19]L. Merrill and W. A. Bassett, Rev. Sci. Instrum. **45**, 290 (1974).
[20]Almax-Easylab, Diacell bragg-(s) product page, 2014.
[21]S. Boone and M. F. Nicol, in *Proceedings of the Lunar and Planetary Science Conference* (Lunar and Planetary Institute, 1991), Vol. 21, p. 603.
[22]R. A. Forman, G. J. Piermarini, J. D. Barnett, and S. Block, Science **176**, 284 (1972).
[23]A. P. Hammersley, "FIT2D: An introduction and overview," Tech. Rep., ESRF Internal Report No. ESRF97HA02T, 1997.
[24]A. D. Fortes, I. G. Wood, M. Alfredsson, L. Vočadlo, K. S. Knight, W. G. Marshall, M. G. Tucker, and F. Fernandez-Alonso, High Pressure Res. **27**, 201 (2007).
[25]R. Nelmes, J. Loveday, W. Marshall, G. Hamel, J. M. Besson, and S. Klotz, Phys. Rev. Lett. **81**, 2719 (1998).
[26]R. J. Hemley, A. P. Jephcoat, H. K. Mao, C. S. Zha, L. W. Finger, and D. E. Cox, Nature **330**, 737 (1987).
[27]D. Hogenboom, Icarus **128**, 171 (1997).

This article is copyrighted as indicated in the article. Reuse of AIP content is subject to the terms at: http://scitation.aip.org/termsconditions. Downloaded to IP: 129.215.149.97 On: Sun, 08 Mar 2015 12:18:44

Urea and deuterium mixtures at high pressures

M. Donnelly,[1,a)] C. L. Bull,[2] R. J. Husband,[1] A. D. Frantzana,[1] S. Klotz,[3] and J. S. Loveday[1]
[1]*Centre for Science at Extreme Conditions and School of Physics and Astronomy, The University of Edinburgh, Erskine Williamson Building, Peter Guthrie Tait Road, The King's Buildings, Edinburgh EH9 3FD, United Kingdom*
[2]*ISIS, Rutherford Appleton Laboratory, Oxford Harwell, Didcot OX11 0QX, United Kingdom*
[3]*IMPMC, CNRS UMR 7590, Université P & M Curie, 4 Place Jussieu, 75252 Paris, France*

(Received 9 December 2014; accepted 9 March 2015; published online 24 March 2015)

Urea, like many network forming compounds, has long been known to form inclusion (guest-host) compounds. Unlike other network formers like water, urea is not known to form such inclusion compounds with simple molecules like hydrogen. Such compounds if they existed would be of interest both for the fundamental insight they provide into molecular bonding and as potential gas storage systems. Urea has been proposed as a potential hydrogen storage material [T. A. Strobel *et al.*, Chem. Phys. Lett. **478**, 97 (2009)]. Here, we report the results of high-pressure neutron diffraction studies of urea and D_2 mixtures that indicate no inclusion compound forms up to 3.7 GPa. © *2015 AIP Publishing LLC.* [http://dx.doi.org/10.1063/1.4915523]

I. INTRODUCTION

Inclusion or guest-host compounds are an important and interesting group of materials. They consist of a network forming host which contains voids or channels which are capable of incorporating a guest species.[1] The presence of the guest obviously has strong effects on the host, and its bonding and inclusion compounds often access network configurations not adopted by the network former alone. For example, the clathrate hydrate structures are not adopted by water in the absence of a host and hence have no stable ice analogues.[1] Inclusion compounds also have wide applications as storage and filter systems. Under appropriate conditions, they can incorporate significant amounts of guest and by a change of thermodynamic conditions can be induced to release unchanged guest molecules.[2] Often the conditions required to produce a particular inclusion compound can be used to separate different guest species. For example, the proposed use of carbon dioxide hydrates to remove carbon dioxide from flue gas.[3]

Whilst network formers like silica, water, and metal organic framework compounds have been very widely studied for their ability to take up guest species, urea, a simple hydrogen bonded organic network former has been less widely studied. It is known to form inclusion compounds with long-chain hydrocarbons[4,5] but currently, little is known about its ability to take up simple gases (for example, methane, hydrogen, and nitrogen) all of which form several different inclusion structures when mixed with water. Urea however is a potentially valuable inclusion compound former. It is readily available in nature as a major component of *Avian Stercore* and hence is cheap. It is relatively environmentally benign and is widely used as a deicer in situations where rock-salt cannot be used. Finally, its structure at ambient pressure which is tetragonal (space group $P\text{-}42_1m$, $a = b = 5.589$ Å, $c = 4.680$ Å) has square channels formed from hydrogen bonded planar urea molecules running along the tetragonal c-axis (see Figure 1). These channels, which are 5.6 Å across, are large enough to accommodate a simple molecule.[6–8] Furthermore, neutron and x-ray diffraction studies of pure urea have identified three high-pressures phases at room temperature.[6–8] The ambient pressure form transforms to an orthorhombic structure above 0.5 GPa known as phase III ($P2_12_12_1$, $a = 8.272$ Å, $b = 3.624$ Å, $c = 8.844$ Å). At around 2.8 GPa, phase III of urea transforms to another orthorhombic structure known as phase IV ($P2_12_12$, $a = 3.414$ Å, $b = 7.360$ Å, $c = 4.606$ Å) and then transforms above 7.2 GPa into a further orthorhombic phase V ($Pmcn$). These transformations indicate that pressure has strong effects on the network bonding and thus may access new inclusion compounds.

Similarly, hydrogen is a good guest species as it is the smallest diatomic gas and diffuses readily through most liquids and solids. It readily forms inclusion compounds with water and to date four different hydrate structures have been identified at different pressures and temperatures with a fifth predicted but not yet confirmed experimentally.[9–11] Hydrogen inclusion compounds have the added technological benefit that if their hydrogen content is high enough, they may form the basis of a hydrogen storage system.[12] Such a storage system is one of the principal hurdles to be overcome in the development of hydrogen based energy economy. Hydrogen-urea has been suggested as such a potential system.[12] However, to date, there have been no searches for hydrogen-urea inclusion compounds. In this paper, we present the first results from neutron diffraction experiments on mixtures of urea and deuterium[13] at high pressures. Our results suggest that urea does not form clathrates with deuterium within the pressure and temperature range studied.

II. EXPERIMENT

Below 0.3 GPa, an aluminium gas cell was used with a preformed Bridgeman seal for the neutron diffraction studies

a)Author to whom correspondence should be addressed. Electronic mail: m.donnelly-2@sms.ed.ac.uk.

 © 2015 AIP Publishing LLC

This article is copyrighted as indicated in the article. Reuse of AIP content is subject to the terms at: http://scitation.aip.org/termsconditions. Downloaded to IP: 129.215.149.97 On: Thu, 30 Apr 2015 15:48:03

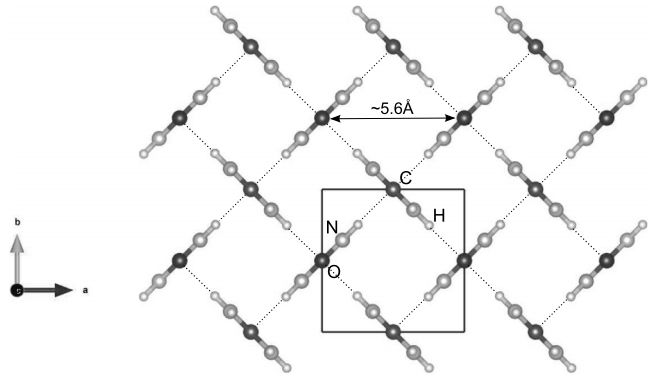

FIG. 1. The crystal structure of the tetragonal phase I of urea (P-42$_1m$) showing the channels running along the c direction. Dotted lines mark the hydrogen bonds between the urea molecules.

of urea and deuterium. Powdered deuterated urea was placed in the gas cell. The cell was then pressurised using D_2 gas; the pressure of which was carefully controlled by an in-house control panel and Hi-Pro capstan 0.3 GPa pump suitable for use with deuterium. The gas cell was mounted on the PEARL instrument at the ISIS neutron facility, UK. Time-of-fight (t-o-f) diffraction data were collected in 90° scattering geometry at room temperature at a series of gas pressures up to 0.3 GPa.

For the higher pressure neutron diffraction experiments above 0.3 GPa, a Paris-Edinburgh (PE) press was used to generate pressure on a mixture of deuterium and urea. Powdered urea was placed in a deuterium-proof encapsulated copper beryllium gasket (modified from the standard titanium-zirconium alloy encapsulated gasket[8]) between a pair of standard tungsten-carbide anvils with a toroidal profile.[14] The anvils are part of a specially designed clamp that allows high-density gases to be loaded into the sample chamber formed by the gasket assembly and then sealed by the application of load to the anvils. The clamp is placed in a specialised deuterium gas loading pressure vessel and charged with 0.2 GPa of D_2 gas. The clamp is then sealed so as to retain the high density D_2 gas in the sample volume. This process has been fully described elsewhere.[15] The sealed clamp is then placed in a VX3 variant Paris-Edinburgh press[16] and mounted on the PEARL instrument. Diffraction patterns were obtained in the 90° scattering geometry with increasing applied hydraulic load to increase the sample pressure. Each diffraction pattern was collected over approximately 3-4 h.

For both experiments, data were reduced using the Mantid software suite[17] and the resulting diffraction patterns were analysed by Rietveld profile refinement using the GSAS software suite.[18] Although the data were analysed by Rietveld refinement, the relatively small proportion of urea in the sample volume that was necessary for the deuterium loading procedure resulted in a low signal level which prevented refinement of the atomic fractional co-ordinates.

III. RESULTS

Figure 2(a) shows a neutron diffraction pattern of the as-loaded deuterated urea sample at 293 K in the aluminium gas cell. The diffraction peaks can be assigned to the known tetragonal phase I of urea and the aluminium of the gas cell. To check whether there is any filling of the voids of the urea structures by deuterium, the lattice parameters of the unit cell can be followed as a function of pressure. If there were some inclusion of the D_2 into the structure, this would be expected to be manifested in anomalies in the lattice parameters and changes in the relative intensities of the reflections.

Upon pressurisation of the sample with D_2 gas, the reflections move to lower d-spacing as expected with increasing pressure as shown in Figure 2. The refined lattice parameters as determined by Rietveld analysis of the patterns shown in Figure 2(a) are shown in Figure 2(b). No anomalies are observed in the unit cell parameters on compression suggesting that no deuterium has entered the phase I structure and that normal compression behaviour of the sample is being observed. Based on the gas cell data, the bulk modulus of the sample in the range 0–0.3 GPa was determined to be 10.4(2) GPa using a Murnaghan equation of state.[19] At pressures up to 0.3 GPa, the diffraction patterns can all be fitted by the known structure of tetragonal phase I of urea, and there is no obvious transition to a new inclusion phase.

At pressures above 0.3 GPa, the Paris-Edinburgh press was used to compress a mixture of deuterium and deuterated urea. A neutron diffraction pattern of the as-loaded sample

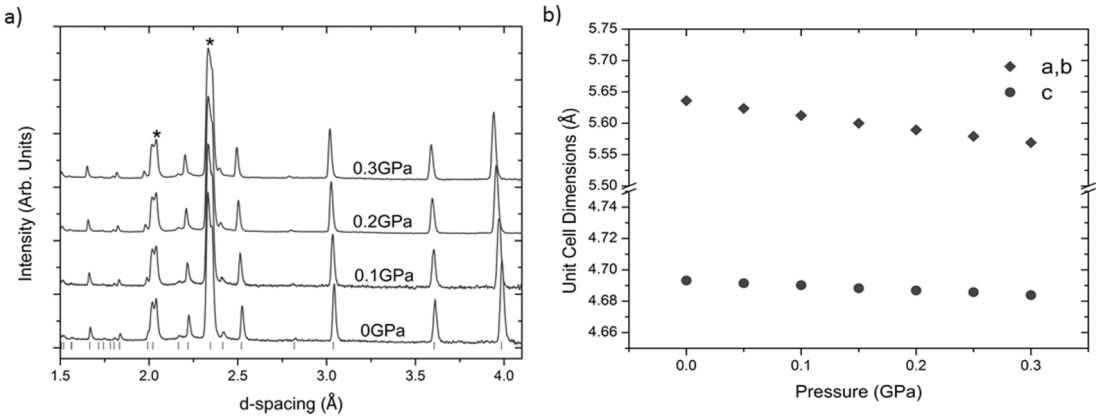

FIG. 2. The neutron diffraction patterns of urea compressed with D_2 gas and the refined unit cell parameters as a function of pressure below 0.3 GPa. Figure (a) shows the diffraction patterns from urea compressed with D_2 gas between 0 and 0.3 GPa. Asterisks mark contaminant reflections from the gas cell and the ticks mark reflections from the tetragonal phase I of urea. Figure (b) shows the lattice parameters obtained from Rietveld refinement of phase I of urea to the diffraction patterns shown in (a).

This article is copyrighted as indicated in the article. Reuse of AIP content is subject to the terms at: http://scitation.aip.org/termsconditions. Downloaded to IP: 129.215.149.97 On: Thu, 30 Apr 2015 15:48:03

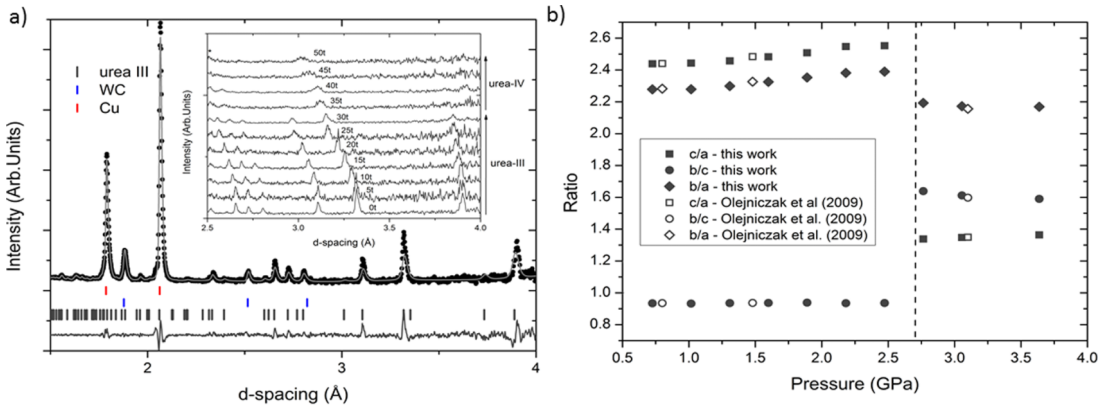

FIG. 3. Neutron diffraction data and refined unit cell parameters of urea and D_2 at pressures above 0.3 GPa. Figure (a) shows a Rietveld refinement of the urea phase III structure to the profile of the as-loaded urea sample. The inset shows diffraction patterns at increasing load applied to the Paris-Edinburgh press showing the transition from phase III to phase IV of urea. The top tick marks mark the position of reflections from copper (the gasket), the middle from tungsten carbide (the anvils), and the bottom ticks show the positions of reflections of urea III. Figure (b) shows the ratios of the unit cell parameters obtained from Rietveld refinements of the diffraction data shown in the inset of (a). Squares, circles, and diamonds show the c/a, b/c, and b/a ratios, respectively, and the filled symbols show the data from this study while the open symbols represent data measured by Olejniczak *et al.*[7] The dotted line at approximately 2.75 GPa marks the phase boundary between the orthorhombic phase III ($P2_12_12_1$) and the orthorhombic phase IV ($P2_12_12$) of urea. Estimated uncertainties were smaller than symbol sizes and so have not been included.

(with no load applied on the PE press) is shown in Figure 3(a). Rietveld refinements (Figure 3(a)) of these data showed that all peaks can be explained by orthorhombic urea phase-III, or the gasket and anvil material surrounding the sample and that the sample pressure (all pressures above 0.3 GPa were determined by comparison of the unit cell volumes of the urea from our Rietveld refinements with those found by a previous study by Olejniczak *et al.*[7]) was 0.8 GPa. This high pressure of the as-loaded sample is a result of the load applied to the clamp that is required to seal the D_2 gas into the sample chamber combined with the 0.2 GPa pressure at which the gas was loaded. The pressure of 0.8 GPa is quite high given the relatively small applied load of 12 tonnes. This provides a clear indication that a full charge of deuterium had been sealed. The amount of urea loaded into the sample chamber filled less than half of the available volume and so had no gas been loaded when the clamp was sealed, the pressure would have been close to ambient. Furthermore as the load was increased, the pressure rose at a rate that indicated the sample chamber was filled. And, in phase III, there is no evidence of peak broadening indicating that the sample is under near-hydrostatic conditions. Experience suggests that urea peaks broaden considerably without a hydrostatic medium such as deuterium.[6] These observations are important because they confirm indirectly the presence of deuterium which is a fluid at these pressures and temperatures and so cannot be observed directly in the diffraction signal. The pressure dependence of the axial ratios (c/a, b/a, b/c) are shown in Figure 3(b). At an applied load of 35 tonnes (Figure 3(a) inset), corresponding to a sample pressure of approximately 2.75 GPa, a clear change in the diffraction pattern was observed. The diffraction peaks from the sample can be indexed as the orthorhombic phase IV of urea and this can be seen from the change in the axial ratios in Figure 3(b). Up to the maximum pressure of almost 4 GPa, no evidence was found of any peaks which could not be explained by either a known phase of urea or the gasket (beryllium copper) or anvil (tungsten carbide with nickel binder) materials.

The ratios of the refined lattice parameters (c/a, b/a, b/c) are shown as a function of pressure alongside data from a previous x-ray diffraction study on pure urea by Olejniczak *et al.*[7] in Figure 3(b). Although we have used the unit cell volume to determine the pressure, it is extremely unlikely that formation of an inclusion compound would give a unit cell whose shape and size were identical to those of pure urea. Hence, the fact that the unit cell shapes (the c/a, b/a, b/c ratios) shown in Figure 3(b) are the same as those of pure urea[7] for a given pressure (or unit cell volume) indicates that there is no measureable deuterium uptake in the pressure range studied.

Thus, the behaviour of the urea sample conforms to that reported for pure urea.[6–8] No evidence is seen of any new phases in the diffraction signal and all transitions occur at the expected unit cell volumes and hence pressures as the transition pressures found for pure urea.[6–8] Furthermore, the axial ratios of the various unit cells are again within error of those observed in pure urea for the same unit cell volume (or pressure).[7] The absence of any new unexplained phase, or anomalies in the transition pressures and unit cell dimensions of the high pressure phases, indicates that there is no incorporation of deuterium into the urea lattice and that urea-deuterium clathrates do not form. This conclusion has been reached on the basis of experiments carried out with solid urea at room temperature. It might appear that formation of inclusion compounds under these conditions is kinetically inhibited because deuterium is unable to enter the bulk material. However, deuterium is found to be extremely diffusive at high pressure and will penetrate solid metals,[20] and even diamond. For this reason, it appears that the absence of inclusion compound formation we report here represents the true thermodynamic behaviour.

IV. CONCLUSIONS

We have investigated the possibility of forming a urea-deuterium gas clathrate at high pressure as previously suggested.[7] However, our high-pressure neutron-diffraction exper-

This article is copyrighted as indicated in the article. Reuse of AIP content is subject to the terms at: http://scitation.aip.org/termsconditions. Downloaded to IP: 129.215.149.97 On: Thu, 30 Apr 2015 15:48:03

iments from 0 GPa to above 3 GPa show only compression behaviour as expected from the pure urea phases and no anomalies are observed in the lattice parameters with increasing hydrostatic pressure. This suggests that at room temperature, urea does not form any inclusion compounds with deuterium and is not a candidate for a hydrogen storage material.

ACKNOWLEDGMENTS

We wish to thank Philip Hawkins, Chris Goodway, and Mark Kibble (ISIS) for their invaluable technical assistance on the PEARL instrument. We would also like to thank Bill Marshall (ISIS) for helpful scientific discussions. We also acknowledge the ISIS Facility of the STFC for access to the PEARL instrument.

[1]J. S. Loveday and R. J. Nelmes, Phys. Chem. Chem. Phys. **10**, 913 (2008).
[2]M. Nandi and H. Uyama, Chem. Rec. **14**, 1134 (2014).
[3]B. Chazallon, M. Ziskind, Y. Carpentier, and C. Focsa, J. Phys. Chem. B **118**, 13440 (2014).
[4]A. E. Smith, Acta Crystallogr. **5**, 224 (1952).
[5]W. Schlenk, Justus Liebigs Ann. Chem. **565**, 204 (1949).
[6]W. G. Marshall and D. Francis, J. Appl. Crystallogr. **35**, 122 (2002).
[7]A. Olejniczak, K. Ostrowska, and A. Katrusiak, J. Phys. Chem. C **113**, 15761 (2009).
[8]H. P. Weber, W. G. Marshall, and V. Dmitriev, Acta Crystallogr., Sect. A: Found. Crystallogr. **58**(s1), c174 (2002).
[9]W. L. Vos, L. W. Finger, R. J. Hemley, and H. K. Mao, Phys. Rev. Lett. **71**, 3150 (1993).
[10]W. L. Mao, H. K. Mao, A. F. Goncharov, V. V. Struzhkin, Q. Z. Guo, J. Z. Hu, J. F. Shu, R. J. Hemley, M. Somayazulu, and Y. S. Zhao, Science **297**, 2247 (2002).
[11]V. S. Efimchenko, M. A. Kuzovnikov, V. K. Fedotov, M. K. Sakharov, S. V. Simonov, and M. Tkacz, J. Alloys Compd. **509**, S860 (2011).
[12]T. A. Strobel, K. C. Hester, C. A. Koh, A. K. Sum, and E. D. Sloan, Jr., Chem. Phys. Lett. **478**, 97 (2009).
[13]Deuterated samples were used to avoid the high background scattering caused by the large incoherent neutron cross section of hydrogen.
[14]J. M. Besson, R. J. Nelmes, G. Hamel, J. S. Loveday, G. Weill, and S. Hull, Physica B **180**, 907 (1992).
[15]S. Klotz, J. Philippe, C. L. Bull, J. S. Loveday, and R. J. Nelmes, High Pressure Res. **33**, 214 (2013).
[16]S. Klotz, G. Hamel, and J. Frelat, High Pressure Res. **24**, 219 (2004).
[17]O. Arnold, J. C. Bilheux, J. M. Borreguero, A. Buts, S. I. Campbell, L. Chapon, M. Doucet, N. Draper, R. F. Leal, M. A. Gigg, V. E. Lynch, A. Markvardsen, D. J. Mikkelson, R. L. Mikkelson, R. Miller, K. Palmen, P. Parker, G. Passos, T. G. Perring, P. F. Peterson, S. Ren, M. A. Reuter, A. T. Savici, J. W. Taylor, R. J. Taylor, R. Tolchenov, W. Zhou, and J. Zikovsky, Nucl. Instrum. Methods Phys. Res., Sect. A **764**, 156 (2014).
[18]A. C. Larson and R. B. Von Dreele, Los Alamos National Laboratory Report LAUR 86, 1994.
[19]R. J. Angel, M. Alvaro, and J. Gonzalez-Platas, Z. Kristallogr. **229**, 405 (2014).
[20]C. Donnerer, T. Scheler, and E. Gregoryanz, J. Chem. Phys. **138**, 134507 (2013).

This article is copyrighted as indicated in the article. Reuse of AIP content is subject to the terms at: http://scitation.aip.org/termsconditions. Downloaded to IP: 129.215.149.97 On: Thu, 30 Apr 2015 15:48:03